

Removal of Perchlorate, Pharmaceutical Compounds, Artificial Sweeteners, and Perfluoroalkyl Substances from Water Using Photocatalytic and Passive Treatment Systems

by

YingYing Liu

A thesis

presented to the University of Waterloo

in fulfillment of the

thesis requirement for the degree of

Doctor of Philosophy

in

Earth Sciences

Waterloo, Ontario, Canada, 2017

© YingYing Liu 2017

Examining Committee Membership

The following served on the Examining Committee for this thesis. The decision of the Examining Committee is by majority vote.

External Examiner

Paul Helm

Senior Research Scientist

Supervisor

Carol Ptacek

Professor

Internal Member

David Blowes

Professor

Internal-external Member

Frank Gu

Associate Professor

Other Member

Doug Gould

Adjunct Professor

Author's Declaration

This thesis consists of material all of which I authored or co-authored: see Statement of Contributions included in the thesis. This is a true copy of the thesis, including any required final revisions, as accepted by my examiners.

I understand that my thesis may be made electronically available to the public.

Statement of Contributions

Chapter 2 was reproduced with permission from: Liu, Y.Y., Ptacek, C.J., Blowes, D.W., 2014. Treatment of dissolved perchlorate, nitrate, and sulfate using zero-valent iron and organic carbon. *J. Environ. Qual.* 43(3), 842-850. Copyright ©2014 by the American Society of Agronomy, Crop Science Society of America, and Soil Science Society of America, Inc., License Number 4065480445068. Editorial and formatting changes have been made to accommodate reproduction in this thesis.

Chapter 3 was reproduced with permission from Liu, Y. Y., Blowes, D. W., Groza, L., Sabourin, M. J., Ptacek, C. J., 2014. Acesulfame-K and pharmaceuticals as co-tracers of municipal wastewater in a receiving river. *Environ. Sci.: Processes Impacts.* 16(12), 2789-2795. Copyright ©2014 by the Royal Society of Chemistry. Editorial and formatting changes have been made to accommodate reproduction in this thesis.

In Chapter 4 (Ultraviolet Light Photo(catalytic) Treatment of Acesulfame-K and Pharmaceuticals Using Magnetically Recoverable TiO₂ Nanoparticles), the data of UV photolysis and photocatalysis of caffeine (CAF) and carbamazepine (CBZ) using P25 and GO TiO₂ nanoparticles (presented in Figure 4.4) were reproduced with permission from Linley, S., Liu, Y., Ptacek, C. J., Blowes, D. W., Gu, F. X., 2014. Recyclable graphene oxide-supported titanium dioxide photocatalysts with tunable properties. *ACS Appl. Mater. Interfaces.* 6(7), 4658-4668. Copyright ©2014 by the American Chemical Society. Editorial and formatting changes have been made to accommodate reproduction in this thesis.

Abstract

The persistence and widespread occurrence of emerging contaminants (ECs) such as perchlorate (ClO_4^-), pharmaceutical compounds, artificial sweeteners, and perfluoroalkyl substances in the environment has received increasing attention due to the adverse effects on human health and aquatic ecosystems they may cause. Conventional wastewater treatment plants (WWTPs) collect household sewage which contains various types of ECs. Emerging contaminants are consequently released to the environment due to incomplete removal of the ECs in the WWTPs. These ECs have been widely found in treated wastewater, surface water, groundwater, and even drinking water at concentrations ranging from ng L^{-1} to $\mu\text{g L}^{-1}$. This thesis describes laboratory experiments for evaluating the effectiveness of passive treatment systems and photocatalytic technologies for removing these ECs from water. In addition, a field investigation is described for tracking wastewater downstream of WWTPs using potential tracers in a receiving river.

Laboratory column experiments were performed to evaluate the effectiveness of reactive media zero-valent iron (ZVI), organic carbon (OC, wood chips), and a mixture of (ZVI + OC) for simultaneous removal of NO_3^- , SO_4^{2-} , and ClO_4^- from contaminated water associated with mining and blasting sites. Input NO_3^- ($\sim 10.8 \text{ mg L}^{-1} \text{ NO}_3\text{-N}$) was effectively removed through NO_3^- reduction to NH_4^+ in Column ZVI, through denitrification in Column OC, and through the combination of NO_3^- reduction by ZVI and denitrification by OC in Column (ZVI + OC). Input SO_4^{2-} ($\sim 24.5 \text{ mg L}^{-1}$) was partially removed (up to 71%) in Column OC through biologically mediated SO_4^{2-}

reduction coupled to OC oxidation. Biological degradation of ClO_4^- (input concentration: $\sim 860 \mu\text{g L}^{-1}$) to Cl^- was observed in the columns containing OC, but not ZVI. Removals of NO_3^- , SO_4^{2-} , and ClO_4^- within three treatment columns was enhanced as a result of a decrease in flow rate from 0.5 to 0.1 pore volume (PV) d^{-1} . Addition of ZVI to OC reduced the inhibition of ClO_4^- removal by NO_3^- ($\text{NO}_3\text{-N} > 2 \text{ mg L}^{-1}$), but sulfate did not inhibit ClO_4^- removal in any treatment column.

Environmentally relevant EC contamination is frequently derived from WWTP discharge. Two-year water sampling was conducted to identify potential tracers to track wastewater downstream from two WWTPs over a 31 km stretch of the Grand River in southwestern Ontario, Canada. The results indicate that elevated concentrations of Cl^- , $\text{NH}_3\text{-N}$, NO_2^- , and ECs including the artificial sweetener acesulfame-K (ACE-K), and pharmaceuticals carbamazepine (CBZ), caffeine (CAF), sulfamethoxazole (SMX), ibuprofen (IBU), gemfibrozil (GEM), and naproxen (NAP) were observed near the two WWTPs, and their concentrations decreased over distance downstream. A Spearman Rank correlation analysis shows strong correlation among ACE-K, CBZ, GEM, NAP, and Cl^- , suggesting the potential use of these contaminants as co-tracers to track wastewater in the study area. However, Cl^- was less reliable due to other sources of contamination such as road salt applications in winter.

Laboratory batch experiments were conducted to evaluate the ultraviolet light (UV) photocatalytic treatment of artificial sweetener ACE-K and pharmaceuticals CBZ, CAF, SMX, 3,4-methylenedioxyamphetamine (MDA), 3,4-methylenedioxymethamphetamine (MDMA), IBU, GEM, and NAP using two types of catalyst, magnetically separable TiO_2 (MST) recoverable nanoparticles ($\gamma\text{-Fe}_2\text{O}_3@\text{SiO}_2@\text{TiO}_2$ colloidal

nanospheres) and graphene oxide supported TiO₂ (GO TiO₂) recoverable nanoparticles (GO/TiO₂/CSA nanocomposites) compared to commercial P25 TiO₂. The synthesized GO TiO₂ exhibited comparable or greater photocatalytic ability compared to P25 TiO₂ in terms of intrinsic reaction rate constants for removal of ACE-K (> 99% removed from 10 µg L⁻¹) and eight pharmaceuticals (> 92% removed from 1 µg L⁻¹) from water. Photocatalytic ability of MST nanoparticles was lower compared to GO and P25 TiO₂ nanoparticles. The non-recoverable P25 nanoparticles have been reported to have adverse impact on human health and ecological systems when released to the environment after use. The GO TiO₂ nanoparticles could potentially be used as a substitute for P25 nanoparticles in water treatment due to its competitive photocatalytic ability and high magnetic recovery.

Laboratory column experiments were conducted to evaluate the removal of pharmaceuticals, artificial sweeteners, and perfluoroalkyl substances using ZVI, biochar (BC), and a mixture of (ZVI + BC). The results show that input pharmaceuticals CBZ, CAF, SMX, MDA, MDMA, IBU, GEM, and NAP at ~9 µg L⁻¹ were almost completely removed (> 97%) in Columns ZVI, BC, and (ZVI + BC). About 80–99% of input artificial sweetener sucralose (SCL) (~110 µg L⁻¹) was removed in three treatment columns. However, artificial sweeteners ACE-K and saccharin (SAC) were partially removed; cyclamate (CYC) was not removed in any column. About 60–99% of input perfluorooctane sulfonic acid (PFOS) (24.0–89.6 µg L⁻¹) was removed in Columns BC and (ZVI + BC); less of input PFOS was removed in Column ZVI compared to the columns containing BC. Partial removal of input perfluorooctanoic acid (PFOA) (~45 µg L⁻¹) was observed in Columns BC and (ZVI + BC), but less in Column ZVI. The removal

rates of target contaminants within three treatment columns were not enhanced after column flow rates were decreased from 0.3 to 0.1 PV d⁻¹, except for ACE-K.

Laboratory batch experiments were conducted to investigate the removal mechanisms of PFOA and PFOS by ZVI and a mixture of (ZVI + BC). The results show ~20% and ~60% of input PFOA (~20,000 µg L⁻¹) were removed by ZVI and (ZVI + BC); ~90% and ~94% of input PFOS (~20,000 µg L⁻¹) were removed by ZVI and (ZVI + BC). However, only ~17% of input short chain perfluoroalkyl carboxylic acid (PFCA) perfluoroheptanoic acid (PFHpA, C7-PFCA) (26 µg L⁻¹) was removed by ZVI alone and (ZVI + BC); the input PFCA perfluorohexanoic acid (PFHxA, C6-PFCA) (0.8 µg L⁻¹) was not removed by ZVI and (ZVI + BC). Similarly, the input short chain perfluoroalkyl sulfonic acids (PFSAs) including 330 µg L⁻¹ of perfluoroheptane sulfonic acid (PFHpS, C7-PFSA), 13 µg L⁻¹ of perfluorohexane sulfonic acid (PFHxS, C6-PFSA), and 6 µg L⁻¹ perfluorobutane sulfonic acid (PFBS, C4-PFSA) were less effectively removed by ZVI and (ZVI + BC) compared to PFOS. About 57–70% of input PFHpS, 30–40% of input PFHxS, and 20% of input PFBS were removed by ZVI alone and (ZVI + BC). The removal efficiency of short chain PFCAs and PFSAs by ZVI and (ZVI + BC) decreased with a decrease in chain length. Sorption and reductive defluorination likely contributed to the removal of PFOA and PFOS by ZVI and (ZVI + BC). Fluoride (F⁻) is the indicative by-product of defluorination of PFOA and PFOS; increasing concentrations of F⁻ were observed in the supernatants of (PFOA + ZVI) and (PFOS + ZVI) samples. The defluorination efficiencies of PFOA and PFOS were back-calculated based on the observed F⁻ concentrations. About 10% of input PFOA and 5% of input PFOS (~20,000 µg L⁻¹) were partially defluorinated (2F defluorinated from 15F of PFOA and 17F of

PFOS) by ZVI alone, but not by the mixture of (ZVI + BC). The defluorination efficiency of PFOA and PFOS by (ZVI + BC) were likely underestimated due to sorption of F⁻ by the reactive media.

This study demonstrates that ZVI, wood chips, and biochar are promising and cost-effective reactive media which can potentially be used in permeable reactive barriers or flow-through reactors for effective removal (> 97%) of perchlorate and pharmaceuticals (CBZ, CAF, SMX, MDA, MDMA, IBU, GEM, and NAP); for moderate removal of artificial sweeteners ACE-K and SCL and perfluoroalkyl substance PFOS; for some removal of artificial sweetener SAC and perfluoroalkyl substance PFOA; and for no removal of artificial sweetener CYC from contaminated water under ambient environmental conditions.

Acknowledgements

First and foremost, I would like to express my sincerest gratitude to my supervisor Dr. Carol J. Ptacek for her constant patience, motivation, guidance and support throughout the course of this degree. I appreciate all her contributions of time, ideas, and funding to make my Ph.D. experience productive and stimulating. Without her precious support, this work would not have been possible.

I thank my committee members Dr. David W. Blowes and Dr. Doug W. Gould for their insightful comments, discussions and encouragement over the years. I thank Dr. Frank X. Gu, who illuminated me in the field of nanotechnology and provided me opportunities to access his laboratory and research facilities. My sincere thanks also go to my external examiner Dr. Paul Helm for his valuable comments and helpful suggestions for improving this thesis.

Thank you to all of the laboratory technicians, graduate students and co-op students who helped me in the field and laboratory. Thank you to Laura Groza for your continuous support with the analyses of the emerging contaminants. Thank you to Syed Ismail Hussain, Krista Paulson, Rachel Baldwin, Janice Cooper, Maria Digaletos, Julia Jamieson-Hanes, and Dr. Peng Liu for your assistance with laboratory experimental sampling and sample preparations. Thank you to Michelle Sabourin, Emily Saurette, Ellie Owens, Amy Kenwell, and Sara Fellin for assisting with the Grand River sampling (Chapter 3). I also would like to thank Timothy Leshuk, Stuart Linley, and Perry Everett for their help with the synthesis and characterization of nanoparticles (sections 4.3.1 and 4.3.2 in Chapter 4) as well as their contributions to the writing of these two sections.

I thank Dr. Rich Amos for his valuable discussions and suggestions regarding the feasibility of modeling perchlorate removals in this thesis. I also want to thank Joy Hu, Jeff Bain, Jing Ma, Jeff Sparks, Alana Ou Wang, Corina McDonald, Dr. Matt Lindsay, Dr. Blair Gibson, and Dr. Brenda Bailey for their help in the laboratory. I am grateful to all the colleagues and friends in the Department of Earth and Environmental Sciences for making my life at the University of Waterloo a pleasant learning experience. My thanks also go to Ms. Gillian Binsted (BSc, MASc, Member of the Editors Association of Canada) for her English editing and technical comments in Chapters 2, 3 and 4.

Funding for this study was provided by the Natural Sciences and Engineering Research Council of Canada and the Ontario Ministry of Research and Innovation–Ontario Research Excellence Fund.

I would like to extend my sincere thanks to my family for all their love and encouragement. I thank my parents Guizhen Sun and Jiayou Liu for giving birth to me, raising me with love and their spiritual support throughout my life. I also thank my parents-in-law for their help with my young child over these busy days.

Finally, I am sincerely grateful to my husband Peng Liu for his love, support, encouragement, understanding, and patience. I also thank my lovely daughter Christina Yuan Liu, who made my life enjoyable and full of sunlight.

Dedication

This thesis is dedicated to my parents, Guizhen Sun and Jiayou Liu, my husband Peng Liu and my lovely daughter Christina Yuan Liu for all of their love, support, and patience over the years.

Table of Contents

Examining Committee Membership	ii
Author’s Declaration	iii
Statement of Contributions.....	iv
Abstract.....	v
Acknowledgements	x
Dedication	xii
List of Tables	xvi
List of Figures.....	xviii
List of Abbreviations	xxiv
Chapter 1: <i>Introduction</i>	1
1.1 Background.....	2
1.1.1 Occurrences and Environmental Fate of Emerging Contaminants .	2
1.1.2 Occurrence, Fate and Treatment Technologies of Emerging Contaminant, Perchlorate.....	3
1.1.3 Occurrence, Fate, and Treatment Technologies of Emerging Contaminants, Pharmaceutical Compounds	7
1.1.4 Occurrence, Fate, and Treatment Technologies of Emerging Contaminants, Artificial Sweeteners	11
1.1.5 Occurrence, Fate, and Treatment Technologies of Emerging Contaminants, Perfluoroalkyl Substances	15
1.1.6 Why Use Zero-valent Iron, Biochar, Magnetically Recoverable Nano-TiO ₂ Nanoparticles, and Passive Treatment Systems?	19
1.2 Research Hypotheses and Objectives	22
1.2.1 Research Hypotheses.....	22
1.2.2 Research Objectives	24
1.3 Thesis Organization.....	25
Chapter 2: <i>Treatment of Dissolved Perchlorate, Nitrate, and Sulfate Using Zero- Valent Iron and Organic Carbon</i>	27
2.1 Executive Summary.....	28
2.2 Introduction.....	29
2.3 Material and Methods	31
2.3.1 Column Design and Experimental Setup.....	31
2.3.2 Sample Collection and Analytical Methods	33
2.4 Results and Discussion	34
2.4.1 Conservative Tracer Test and Control Column Results	34
2.4.2 Geochemistry Conditions of Columns	35
2.4.3 Removal of Nitrate, Sulfate, and Perchlorate in Columns	36
2.4.4 Removal Rates of Nitrate and Perchlorate within Columns.....	40

2.4.5 Effect of Nitrate and Sulfate on Perchlorate Removal Rate	43
2.5 Conclusions.....	45
Chapter 3: <i>Artificial Sweeteners and Pharmaceuticals as Co-tracers of Municipal Wastewater in a Receiving River</i>	57
3.1 Executive Summary	58
3.2 Introduction.....	59
3.3 Materials and Methods	61
3.3.1 Water Sampling and Field Analyses	61
3.3.2 Analysis of Water Samples	62
3.4 Results and Discussion	67
3.4.1 Grand River Sampling Results	67
3.4.2 Mechanisms Affecting the Transport of the Target Compounds ..	71
3.4.3 Acesulfame-K and Pharmaceuticals as Co-tracers in the Grand River.....	73
3.5 Conclusions.....	74
Chapter 4: <i>Ultraviolet Light Photo(catalytic) Treatment of Acesulfame-K and Pharmaceuticals Using Magnetically Recoverable TiO₂ Nanoparticles</i>.....	81
4.1 Executive Summary.....	82
4.2 Introduction.....	83
4.3 Material and Methods	86
4.3.1 Nanoparticle Synthesis	86
4.3.2 Characterization of Particles.....	87
4.3.3 Batch Experimental Procedures.....	88
4.3.4 Analytical Procedures.....	89
4.3.5 Magnetic Separation	91
4.4 Results and Discussion	92
4.4.1 Particle Characterization	92
4.4.2 Control and Dark Adsorption Samples.....	93
4.4.3 UV Photo(catalytic) Treatment Results and Rate Calculations....	94
4.4.4 Magnetic Separation Results	102
4.5 Conclusions.....	104
Chapter 5: <i>Removal of Pharmaceutical Compounds, Artificial Sweeteners, and Perfluoroalkyl Substances from Water Using Zero-valent Iron and Biochar</i>	114
5.1 Executive Summary.....	115
5.2 Introduction.....	117
5.3 Material and Methods	123
5.3.1 Column Design and Experimental Setup.....	123
5.3.2 Sample Collection and Analytical Methods	125
5.4 Results and Discussion	129
5.4.1 Column Geochemistry.....	129
5.4.2 Removal of Pharmaceutical Compounds in Columns.....	131
5.4.3 Removal of Artificial Sweeteners in Columns	140
5.4.4 Removal of PFOA and PFOS in Columns	145
5.5 Conclusions.....	151

Chapter 6: Removal of Perfluoroalkyl Carboxylic and Sulfonic Acids from Water Using Zero-valent Iron and Biochar	172
6.1 Executive Summary.....	173
6.2 Introduction.....	175
6.3 Materials and Methods	180
6.3.1 Batch Experiments for Removal of Perfluoroalkyl Carboxylic Acids (PFCAs) and Perfluoroalkyl Sulfonic Acids (PFSA) Using ZVI and Mixture of ZVI and BC	180
6.3.2 Batch Experiments for Evaluating Sorption of F ⁻ by Reactive Media	183
6.3.3 Analysis of Water Samples and Solid-Phase Extracts.....	183
6.4 Results and Discussion	188
6.4.1 Removal of Perfluoroalkyl Carboxylic Acids (PFCAs) and Perfluoroalkyl Sulfonic Acids (PFSA) Using ZVI and Mixture of ZVI and BC.....	188
6.4.2 Sorption of F ⁻ by Reactive Media ZVI and Mixture of ZVI and BC	191
6.4.3 Correction of Defluorination Efficiency.....	192
6.4.4 Possible Removal Mechanisms of PFCAs and PFSA by ZVI and BC	193
6.4.5 Mass Balance of PFOA (PFCAs) and PFOS (PFSA) in Treatment Samples	197
6.5 Conclusions.....	199
Chapter 7: Conclusions	211
7.1 Summary of Findings and Comparison of Contaminant Removals Using Photocatalytic and Passive Treatment Systems.....	212
7.1.1 Summary of Findings	212
7.1.2 Comparison of Contaminant Removals Using Photocatalytic and Passive Treatment Systems.....	217
7.2 Scientific Contributions	218
7.3 Recommendations.....	220
7.4 Future Research	224
References	237
Appendix A: Supplementary Information in Chapter 2	263
Appendix B: Supplementary Information in Chapter 3	266
Appendix C: Supplementary Information in Chapter 4	271
Appendix D: Supplementary Information in Chapter 5	275
Appendix E: Supplementary Information in Chapter 6	290

List of Tables

Table 1.1 Selected properties for target pharmaceuticals.	7
Table 1.2 Selected properties for target artificial sweeteners.	12
Table 1.3 Selected properties for target perfluoroalkyl carboxylic acids (PFCAs) and perfluoroalkyl sulfonic acids (PFSAs).	16
Table 2.1 Physical characteristics of the columns used in this study, including a control and columns containing zero-valent Fe (ZVI), organic C (OC) or both.	46
Table 2.2 Nitrate and ClO_4^- removal rates calculated using least-squares regression during two experimental stages.	47
Table 3.1 Spearman rank correlation coefficients (ρ) [†] of the target compounds and Cl ⁻ over the sampling distance in the Grand River in August 2012.	75
Table 3.2 Spearman rank correlation coefficients (ρ) [†] of the target compounds and Cl ⁻ over the sampling distance in the Grand River in July 2013.	76
Table 4.1 Nanocrystal size, BET surface area, and hydrodynamic (DLS) diameter of the particle samples used in this study.	105
Table 4.2 Selected properties of acesulfame-K (ACE-K), sulfamethoxazole (SMX), 3,4-methylenedioxyamphetamine (MDA), and 3,4-methylenedioxymethamphetamine (MDMA), first order rate constants (k), correlation coefficient (R^2), mass normalized rate constants (k_M), and surface-area normalized rate constants (k_{SA}) during (photo)catalytic treatment.	106
Table 4.3 Selected properties of ibuprofen (IBU), gemfibrozil (GEM), naproxen (NAP), caffeine (CAF), and carbamazepine (CBZ), first order rate constants (k), correlation coefficient (R^2), mass normalized rate constants (k_M), and surface-area normalized rate constants (k_{SA}) during (photo)catalytic treatment.	108
Table 5.1 Physical characteristics of the columns used in this study, including a control and columns containing zero-valent Fe (ZVI), organic C (BC), and both.	153
Table 5.2 Selected properties of target pharmaceuticals and potential interaction (removal mechanisms) between target pharmaceutical compounds and reactive media. N: Neutral; (+): Positive charged; (-): Negative charged.	154
Table 5.3 Selected properties of target artificial sweeteners and potential interaction (removal mechanisms) between target artificial sweeteners and reactive media. N: Neutral; (+): Positive charged; (-): Negative charged.	158

Table 5.4 Selected properties of target perfluoroalkyl substances and potential interaction (removal mechanisms) between target perfluoroalkyl substances and reactive media. N: Neutral; (+): Positive charged; (-): Negative charged.	160
Table 6.1 Batch experimental setup.	201
Table 6.2 Selected properties for target perfluoroalkyl carboxylic acids (PFCAs) and perfluoroalkyl sulfonic acids (PFSAs).	202
Table 7.1 Comparison of average surface area normalized rate constants (K_{SA} , $L m^{-2} d^{-1}$), average removal efficiencies, and potential removal mechanisms of target contaminants during UV photocatalytic treatment using GO TiO ₂ nanoparticles (Chapter 4) and passive treatment using ZVI and BC (Chapter 5).	227
Table 7.2 Comparison of removal efficiency and removal rate (surface area normalized rate constant, K_{SA} , $L m^{-2} d^{-1}$), treatment conditions, energy consumption, and required catalysts/reactive media during photocatalytic and passive treatment systems for removing ACE-K and eight pharmaceuticals.	229

List of Figures

- Figure 2.1** Concentrations of $\text{NO}_2\text{-N}$, $\text{NH}_3\text{-N}$, $\text{NO}_3\text{-N}$, SO_4^{2-} , and ClO_4^- as a function of pore volumes in effluent from columns containing zero-valent Fe (ZVI), organic C (OC), or both; the dashed lines indicate a change in flow rate in each column, dividing the experiment into two stages. 48
- Figure 2.2** Values of pH, Eh, and concentrations of alkalinity as a function of distance along flow direction within the columns containing zero-valent Fe (ZVI), organic C (OC), or both. Blue circle symbols represent data collected during the first stage of the experiment, while orange square and green triangle symbols represent data collected during the second stage of the experiments, given in terms of pore volumes (PV). 49
- Figure 2.3** Values of pH, Eh, and concentrations of alkalinity as a function of pore volumes in effluent from columns containing zero-valent Fe (ZVI), organic C (OC), or both; the dashed lines indicate a change in flow rate in each column, dividing the experiment into two stages. 50
- Figure 2.4** Concentrations of Cl^- , ClO_4^- , and total Cl^- (sum of Cl^- and ClO_4^-) as a function of pore volumes in effluent from columns containing zero-valent Fe (ZVI), organic C (OC), or both; the dashed lines indicate a change in flow rate in each column, dividing the experiment into two stages. 51
- Figure 2.5** Suggested pathway for biological degradation of ClO_4^- (Rikken et al., 1996). 52
- Figure 2.6** Concentrations of $\text{NO}_3\text{-N}$, $\text{NH}_3\text{-N}$, $\text{NO}_2\text{-N}$, SO_4^{2-} , H_2S , ClO_4^- , and Cl^- as a function of distance along flow direction within the columns containing zero-valent Fe (ZVI), organic C (OC), or both. Blue circle symbols represent data collected during the first stage of the experiment, while orange square and green triangle symbols represent data collected during the second stage of the experiments, given in terms of pore volumes (PV). 54
- Figure 2.7** Regression fits of $\text{NO}_3\text{-N}$ removal as a function of residence time in columns containing zero-valent Fe (ZVI), organic C (OC), or both. 55
- Figure 2.8** Regression fits of ClO_4^- removal as a function of residence time in columns containing organic C (OC) and both zero-valent Fe (ZVI) and OC. 56
- Figure 3.1** Sampling locations along the Grand River, southwestern Ontario, Canada. . 77
- Figure 3.2** Concentrations of pH, Eh, alkalinity, electrical conductivity (EC), Cl^- , NO_3^- , NO_2^- , $\text{NH}_3\text{-N}$, SO_4^{2-} , and $\text{PO}_4\text{-P}$ as a function of sampling distance. 78

- Figure 3.3** Concentrations of acesulfame-K (ACE-K), caffeine (CAF), sulfamethoxazole (SMX), carbamazepine (CBZ), ibuprofen (IBU), gemfibrozil (GEM), and naproxen (NAP) as a function of sampling distance. The method detection limits of ACE-K and CAF were too low to appear in the figure. 79
- Figure 3.4** Concentrations of acesulfame-K (ACE-K), caffeine (CAF), sulfamethoxazole (SMX), carbamazepine (CBZ), ibuprofen (IBU), gemfibrozil (GEM), and naproxen (NAP) as a function of Cl⁻ concentration. The method detection limits of ACE-K and CAF were too low to appear in the figure. 80
- Figure 4.1** TEM images of MST particles. 110
- Figure 4.2** XRD patterns of the MST particles and P25 as indicated. Peaks labelled with A match anatase phase TiO₂ (JCPDS No. 21-1272), R matches rutile phase TiO₂ (JCPDS No.21-1276), and those labeled with M match maghemite (γ-Fe₂O₃) iron oxide (JCPDS No. 89-3850). 111
- Figure 4.3** Concentrations of acesulfame-K (ACE-K), sulfamethoxazole (SMX), 3,4-methylenedioxyamphetamine (MDA), and 3,4-methylenedioxymethamphetamine (MDMA) as a function of reaction time during UV photo(catalytic) treatment. Group 1: Easily photo- and photocatalytically degradable compounds ACE and SMX. Group 2: Easily photocatalytically degradable compounds MDA and MDMA. 112
- Figure 4.4** Concentrations of ibuprofen (IBU), gemfibrozil (GEM), naproxen (NAP), caffeine (CAF), and carbamazepine (CBZ) as a function of reaction time during UV photo(catalytic) treatment. Group 3: Moderately photo- and photocatalytically degradable compounds IBU, GEM, and NAP. Group 4: Recalcitrant photo- and photocatalytically degradable compounds CAF and CBZ. The data of UV photolysis and photocatalysis of CAF and CBZ using P25 and GO TiO₂ nanoparticles were reproduced with permission from Linley et al. (2014). 113
- Figure 5.1** Values of pH, Eh, and concentrations of alkalinity as a function of distance along flow direction within control column and columns containing zero-valent Fe (ZVI), biochar (BC), and both. Blue circle, orange square, and green triangle symbols represent data collected during the first stage of the experiment (flow rate = 0.3 PV/d), while grey diamond symbols represent data collected during the second stage of the experiment (flow rate = 0.1 PV/d), given in terms of pore volumes (PV). 161
- Figure 5.2** Values of pH, Eh, and concentrations of alkalinity as a function of pore volumes (PV) in effluent from control column and columns containing zero-valent Fe (ZVI), biochar (BC), and both; dash lines indicate a decrease in flow rate in each column, dividing the experiment into two stages. 162

- Figure 5.3** Concentrations of neutral pharmaceutical carbamazepine (CBZ) and basic pharmaceuticals caffeine (CAF), 3,4-methylenedioxyamphetamine (MDA), and 3,4-methylenedioxymethamphetamine (MDMA) as a function of pore volumes (PV) in effluent from control column and columns containing zero-valent Fe (ZVI), biochar (BC), and both; dash lines indicate a decrease in flow rate in each column, dividing the experiment into two stages. 163
- Figure 5.4** Concentrations of acidic pharmaceuticals sulfamethoxazole (SMX), ibuprofen (IBU), gemfibrozil (GEM), and naproxen (NAP) as a function of pore volumes (PV) in effluent from control column and columns containing zero-valent Fe (ZVI), biochar (BC), and both; dash lines indicate a decrease in flow rate in each column, dividing the experiment into two stages. 164
- Figure 5.5** pK_a values of target contaminants plotted on the pH scale. The pH range in Column ZVI is between 7.5–9.5; the pH range in Column BC is between 7.0–8.3; the pH range in Column (ZVI + BC) is between 7.9–8.9. 165
- Figure 5.6** Concentrations of neutral pharmaceutical carbamazepine (CBZ) and basic pharmaceuticals caffeine (CAF), sulfamethoxazole (SMX), 3,4-methylenedioxyamphetamine (MDA), and 3,4-methylenedioxymethamphetamine (MDMA) as a function of distance along flow direction within control column and columns containing zero-valent Fe (ZVI), biochar (BC), and both. Blue circle, orange square, and green triangle symbols represent data collected during the first stage of the experiment (flow rate = 0.3 PV/d), while grey diamond symbols represent data collected during the second stage of the experiment (flow rate = 0.1 PV/d), given in terms of pore volumes (PV). 166
- Figure 5.7** Concentrations of acidic pharmaceuticals sulfamethoxazole (SMX), ibuprofen (IBU), gemfibrozil (GEM), and naproxen (NAP) as a function of distance along flow direction within control column and columns containing zero-valent Fe (ZVI), biochar (BC), and both. Blue circle, orange square, and green triangle symbols represent data collected during the first stage of the experiment (flow rate = 0.3 PV/d), while grey diamond symbols represent data collected during the second stage of the experiment (flow rate = 0.1 PV/d), given in terms of pore volumes (PV). 167
- Figure 5.8** Concentrations of acefulfame-K (ACE-K), cyclamate (CYC), saccharine (SAC), and sucralose (SCL) as a function of pore volumes (PV) in effluent from control column and columns containing zero-valent Fe (ZVI), biochar (BC), and both; dash lines indicate a decrease in flow rate in each column, dividing the experiment into two stages. 168
- Figure 5.9** Concentrations of acefulfame-K (ACE-K), cyclamate (CYC), saccharine (SAC), and sucralose (SCL) as a function of distance along flow direction within control column and columns containing zero-valent Fe (ZVI), biochar

(BC), and both. Blue circle, orange square, and green triangle symbols represent data collected during the first stage of the experiment (flow rate = 0.3 PV/d), while grey diamond symbols represent data collected during the second stage of the experiment (flow rate = 0.1 PV/d), given in terms of pore volumes (PV). 169

Figure 5.10 Concentrations of perfluorooctanoic acid (PFOA) and perfluorooctane sulfonic acid (PFOS) as a function of pore volumes (PV) in effluent from control column and columns containing zero-valent Fe (ZVI), biochar (BC), and both; dash lines indicate a decrease in flow rate in each column, dividing the experiment into two stages. 170

Figure 5.11 Concentrations of perfluorooctanoic acid (PFOA) and perfluorooctane sulfonic acid (PFOS) as a function of distance along flow direction within control column and columns containing zero-valent Fe (ZVI), biochar (BC), and both. Blue circle, orange square, and green triangle symbols represent data collected during the first stage of the experiment (flow rate = 0.3 PV/d), while grey diamond symbols represent data collected during the second stage of the experiment (flow rate = 0.1 PV/d), given in terms of pore volumes (PV). 171

Figure 6.1 Values of pH, Eh, and concentrations of alkalinity as a function of reaction time in the supernatant samples of batch experiment for removal of PFOA and PFOS using zero-valent Fe (ZVI) alone and a 1:4 (v/v) mixture of ZVI and biochar (ZVI + BC). 203

Figure 6.2 Concentrations of perfluorooctanoic acid (PFOA) and perfluorooctane sulfonic acid (PFOS) as a function of reaction time in the supernatant samples of batch experiment for removal of PFOA and PFOS using zero-valent Fe (ZVI) alone and a 1:4 (v/v) mixture of ZVI and biochar (ZVI + BC). Duplicate samples were prepared at Days 40, 90, and 120 where were indicated with error bars. The method detection limits (MDLs) of PFOA and PFOS were 45 and 110 ng L⁻¹, which were too low to appear in the figure. 204

Figure 6.3 Concentrations of perfluoroheptanoic acid (PFHpA, C7-PFCA) and perfluorohexanoic acid (PFHxA, C6-PFCA) as a function of reaction time in the supernatant samples of batch experiment for removal of PFOA and PFOS using zero-valent Fe (ZVI) alone and a 1:4 (v/v) mixture of ZVI and biochar (ZVI + BC). Duplicate samples were prepared at Days 40, 90, and 120 where were indicated with error bars. The instrument limits of quantification (LOQ) of PFHpA and PFHxA were 0.5 µg L⁻¹. The LOQ of PFHpA was too low to appear in the figure..... 205

Figure 6.4 Concentrations of perfluoroheptane sulfonic acid (PFHpS, C7-PFSA), perfluorohexane sulfonic acid (PFHxS, C6-PFSA), and perfluorobutane sulfonic acid (PFBS, C4-PFSA) as a function of reaction time in the

supernatant samples of batch experiment for removal of PFOA and PFOS using zero-valent Fe (ZVI) alone and a 1:4 (v/v) mixture of ZVI and biochar (ZVI + BC). Duplicate samples were prepared at Days 40, 90, and 120 where were indicated with error bars. The instrument limit of quantification (LOQ) of PFHpS was $0.5 \mu\text{g L}^{-1}$; the LOQ of PFHxS and PFBS was $0.2 \mu\text{g L}^{-1}$. The LOQ of PFHpS, PFHxS, and PFBS were too low to appear in the figure... 206

Figure 6.5 Concentrations of F^- as a function of reaction time in the supernatant samples of batch experiment for removal of PFOA and PFOS using zero-valent Fe (ZVI) alone and a 1:4 (v/v) mixture of ZVI and biochar (ZVI + BC). The concentrations of F^- in the supernatant samples PFOA/PFOS + (ZVI +BC) were below the method detection limits. Duplicate samples were prepared at Days 40, 90, and 120 where were indicated with error bars. 207

Figure 6.6 Percentage of F^- remaining in the supernatant samples of F^- sorption test as a function of reaction time. 208

Figure 6.7 Proposed defluorination mechanisms of PFOA by ZVI (Reproduced from Song et al., 2003). The defluorination of PFOA was initiated by the cleavage of α -position C–F bond by e^- transfer from ZVI. 209

Figure 6.8 Mass balances for PFOA and PFOS in batch experiments as a function of reaction time. Because the concentrations of PFOA and PFOS were two to four orders of magnitude higher than that of the short chain PFCAs and PFSAs in both supernatant samples and aqueous samples extracted from reactive media, this figure also represents the mass balances of total perfluoroalkyl carboxylic acids (PFCAs, including PFOA, PFHpA, and PFHxA) and total perfluoroalkyl sulfonic acids (PFSAs, including PFOS, PFHpS, PFHxS, and PFBS) in the batch experiments as a function of reaction time. Partial defluorination percentages were stoichiometrically back-calculated based on the observed F^- concentrations in the supernatant, assuming 2F defluorinated from 15F atoms of PFOA and 2F defluorinated from 17F atoms of PFOS. 210

Figure 7.1 Schematic cross-section showing application of reactive mixture of zero-valent iron (ZVI) and organic carbon (OC) as a horizontal reactive layer underneath the septic drain tiles. The reactive layer is expected to remove NO_3^- , SO_4^{2-} and emerging contaminants from wastewater before it reaches groundwater. 230

Figure 7.2 Schematic cross-section showing application of reactive mixture of zero-valent iron (ZVI) and organic carbon (OC) in a reactor attached to the effluent pipe derived from the primary treatment unit of the facility. The reactor is expected to remove NO_3^- , SO_4^{2-} and emerging contaminants in the sewage wastewater after primary treatment. 231

- Figure 7.3** Schematic cross-section showing application of reactive mixture of zero-valent iron (ZVI) and organic carbon (OC) in a vertical permeable reactive barrier (PRB). The reactive mixture in the PRB is expected to remove NO_3^- , SO_4^{2-} and emerging contaminants in the plume before it discharges to surface water. 232
- Figure 7.4** Schematic areal map showing in-line reactor containing reactive mixture of zero-valent iron (ZVI) and organic carbon (OC) to remove NO_3^- , SO_4^{2-} and emerging contaminants from water collected from the tile drainage system before it discharges to receiving water body..... 233
- Figure 7.5** Schematic cross-section showing application of reactive mixture of zero-valent iron (ZVI) and organic carbon (OC) in a horizontal reactive layer underneath the recharge basin of a soil aquifer treatment. The reactive layer is expected to remove NO_3^- , SO_4^{2-} and emerging contaminants in the wastewater before it infiltrates to groundwater..... 234
- Figure 7.6** Schematic cross-section showing application of reactive mixture of zero-valent iron (ZVI) and organic carbon (OC) in a permeable reactive barrier (PRB) installed between the river and the production well in a river bank filtration process. The reactive mixture packed in the PRB is expected to remove NO_3^- , SO_4^{2-} and emerging contaminants in the recovery river water before end uses. 235
- Figure 7.7** Schematic diagram showing application of reactive mixture of zero-valent iron (ZVI) and organic carbon (OC) or UV photocatalytic treatment using recoverable GO TiO_2 nanoparticles in a polishing cell (reactor) attached to the effluent of a wastewater treatment plant (WWTP). The emerging contaminants which cannot be removed in WWTPs are expected to be removed in the reactor before entering the receiving river. 236

List of Abbreviations

AC	Activated carbon
ACE-K	Acesulfame-K
AOPs	Advanced oxidation processes
BC	Biochar
CAF	Caffeine
CBZ	Carbamazepine
CYC	Cyclamate
DBPs	Disinfection by-products
DLS	Dynamic light scattering
DOC	Dissolved organic carbon
EDCs	Endocrine disrupting compounds
ESI	Electrospray ionization
GAC	Granular activated carbon
GEM	Gemfibrozil
GO TiO ₂	Graphene oxide-supported TiO ₂
HPLC	High performance liquid chromatography
IBU	Ibuprofen
LOECs	Lowest observed effect concentrations
LOD	Limits of detection
LOQ	Limits of quantification
MDA	3,4-methylenedioxyamphetamine
MDMA	3,4-methylenedioxymethamphetamine

MDL	Method detection limits
MST	Magnetically separable TiO ₂
NAP	Naproxen
NOM	Natural organic matter
NSAID	Nonsteroidal anti-inflammatory drug
OC	Organic carbon
PAC	Powder activated carbon
PFASs	Polyfluoroalkyl and perfluoroalkyl substances
PFBA	Perfluorobutanoic acid
PFBS	Perfluorobutane sulfonic acid
PFCAs	Perfluoroalkyl carboxylic acids
PFCs	Perfluorinated compounds
PFHpA	Perfluoroheptanoic acid
PFHpS	Perfluoroheptane sulfonic acid
PFHxA	Perfluorohexanoic acid
PFHxS	Perfluorohexane sulfonic acid
PFOA	Perfluorooctanoic acid
PFOS	Perfluorooctane sulfonic acid
PFPeA	Perfluoropentanoic acid
PFSA	Perfluoroalkyl sulfonic acids
PPCPs	Pharmaceuticals and personal care products
PRBs	Permeable reactive barriers
PV	Pore volumes

SAC	Saccharine
SCL	Sucralose
SMX	Sulfamethoxazole
SPE	Solid-phase extraction
SS	Silica sand
STPs	Sewage treatment plants
TEM	Transmission electron microscopy
TOC	Total organic carbon
USGS	United States Geological Survey
UV	Ultraviolet light
VOCs	Volatile organic compounds
WWTP	Wastewater Treatment Plant
XRD	X-ray diffraction
ZVI	Zero-valent iron

Chapter 1: *Introduction*

1.1 Background

1.1.1 Occurrences and Environmental Fate of Emerging Contaminants

Water pollution, and the associated ecosystem and public health effects is a major environmental problem (Schwarzenbach et al., 2006). Conventional contaminants, such as organic contaminants (VOCs, PCBs, TCE, etc.) and inorganic contaminants (heavy metals, arsenic, nitrate, etc.), have drawn great attention of public and environmental researchers due to their high ecotoxicity. The corresponding remedial technologies for these contaminants also have been extensively studied and developed. However, there are inadequate studies about the occurrence, fate and treatment of emerging contaminants in aquatic systems.

The United States Geological Survey (USGS) defines emerging contaminants as “any synthetic or naturally occurring chemical or any microorganism that is not commonly monitored in the environment but has the potential to enter the environment and cause known or suspected adverse ecological and (or) human health effects”. A contaminant could also be “emerging” due to a lack of published health standards or an evolving standard, or the discovery of a new source, a new pathway to humans, or the development of a new detection method or technology, even though the contaminant likely has been in existence in the environment for a long time (Daughton, 2005; Murnyak et al., 2011). Emerging contaminants encompass a diverse group of compounds and include nanomaterials, perfluorinated compounds (PFCs), pharmaceuticals and personal care products (PPCPs), steroids and hormones, surfactants, drinking water disinfection byproducts (DBPs), sunscreens/UV filters, brominated flame retardants (polybrominated diphenyl ethers), benzotriazoles, naphthenic acids, antimony, siloxanes,

musks, algal toxins, perchlorate, dioxane, pesticide transformation products and microorganisms, veterinary products as well as food additives such as artificial sweeteners (ASs) (acesulfame-K and sucralose) (Lapworth et al., 2012; Richardson & Ternes, 2011).

Emerging contaminants are commonly derived from municipal, agricultural, and industrial wastewater sources. Wastewater treatment plant (WWTP) effluents are the primary contributions to many environmentally-relevant emerging contaminants due to the persistence of the parent compound or their intermediate byproducts, many of which cannot be removed using conventional treatment approaches. Terrestrial run-off (from roofs, pavements, roads and agricultural land) and atmospheric deposition account for secondary sources of emerging contaminants (Farré et al., 2008). Once released into the environment, emerging contaminants are likely to be transported and become widely distributed in aquatic systems, especially in surface water and groundwater. Therefore, extensive studies are currently underway that focus on technologies for removing these contaminants from environmental waters through advanced oxidation, photolysis, adsorption, microbial degradation and other processes (Andreozzi et al., 2004; Kim & Tanaka, 2009; Kim et al., 2009b; Onesios & Bouwer, 2012).

1.1.2 Occurrence, Fate and Treatment Technologies of Emerging Contaminant, Perchlorate

Perchlorate anion (ClO_4^-) consists of four tetrahedral oxygen atoms around a central chlorine atom. Perchlorate is found both naturally and anthropogenically. The naturally occurring perchlorate is mainly associated with extreme arid environments, such as the Chilean nitrate deposits in the Atacama Desert (Srinivasan & Sorial, 2009; Urbansky et

al., 2001). Perchlorate also can occur naturally in nitrate fertilizers and be produced naturally by atmospheric deposition (Rajagopalan et al., 2006; Srinivasan & Viraraghavan, 2009). The main anthropogenic source of perchlorate is the manufacture of perchlorate containing salts, such as ammonium perchlorate, potassium perchlorate, and sodium perchlorate. The perchlorate salts are strong oxidizers (redox potential = +1.38 V) based on the central chlorine atom in its highest oxidation state (+7); they are widely used in rocket propellants, military munitions, blasting agents, fireworks, explosives, and some consumer products (Urbansky, 2002).

The major source of perchlorate contamination has been attributed to the manufacture or use of perchlorate salts in military activities, rocket propellant, fireworks, blasting agents, and military munitions (Bailey et al., 2013; Gullick et al., 2001; Smith et al., 2015; Tikkanen, 2006; Wilkin et al., 2007). Perchlorate is highly soluble, mobile, stable in water and adsorbs poorly to soil (Xu et al., 2003b), which results in its widespread occurrence and persistence in the environment. Perchlorate is widely detected in surface water (Wilkin et al., 2007), raw and treated drinking water (Gullick et al., 2001; Kim et al., 2009a), groundwater (Izbicki et al., 2015), bottled water (Iannece et al., 2013) at concentrations ranging from 5 ng L⁻¹ to 200 µg L⁻¹, and in human breast milk and baby formulas at 1.49–33.3 µg kg⁻¹ (Her et al., 2010). Perchlorate has been reported to inhibit the iodide uptake in animals and humans and causes decreased thyroid hormone production, resulting in mental retardation and hearing and speech degradation (Vandenberg et al., 2012; Wolff, 1998). The EPA established a chronic oral reference dose (RfD) of 0.0007 mg kg⁻¹ d⁻¹ for perchlorate (US EPA, 2005). Thyroid hormone is very important for growth, development, and metabolism in the human body, especially for

pregnant women and fetuses (Melse-Boonstra & Jaiswal, 2010; Mendez et al., 2010). Due to its toxicity, perchlorate has been listed by the US EPA in the drinking water contaminant candidate list (US EPA, 2006). The California Department of Health Services has established the action level of perchlorate at $6 \mu\text{g L}^{-1}$ in drinking water (California Department of Health Services (CDHS), 2004). The EPA established an Interim Lifetime Drinking Water Health Advisory of perchlorate at $15 \mu\text{g L}^{-1}$ (US EPA, 2009b; US EPA, 2012). Health Canada suggested a guidance value of $6 \mu\text{g L}^{-1}$ for perchlorate in drinking water (Health Canada, 2005).

The treatment technologies for perchlorate include physical separation (adsorption, membrane filtration, ion exchange), chemical and electrochemical reduction, and biological or biochemical reduction (Sijimol et al., 2015). Granular activated carbon (GAC) sorption and anion exchange are the most common methods for removing perchlorate from water. It has been reported that the sorption of perchlorate by GAC are through specific chemical interactions between perchlorate and surface functional groups and electrostatic forces (Mahmudov & Huang, 2010). The virgin GAC is not a very effective adsorbent for removing perchlorate; however, the GAC after appropriate surface modification such as ammonia-tailoring (Chen et al., 2005) and pre-adsorption of cationic surfactants (Lin et al., 2013) shows competitive removals of perchlorate compared to ion exchange and biological treatment. Ion-exchange is the most effective and commonly used method for removing perchlorate from drinking water; however, the high cost, disposal of the spent resins and brine makes this technology less feasible and economically sustainable (Srinivasan & Sorial, 2009; Ye et al., 2012). Chemical reduction is a destructive method in which perchlorate is completely reduced to non-toxic Cl^- . The

high activation energy (120 kJ mol^{-1}) kinetically limits the rate of perchlorate reduction (Yang et al., 2016); however, the applications of metallic catalysts (Hurley & Shapley, 2007; Zhang et al., 2011) and catalytic electrodes (Rusanova et al., 2006) greatly enhance perchlorate reductive kinetics during the catalytic and electrochemical reduction. The deactivation and fouling of catalysts and electrode by natural water constituents and the high cost and toxicity of the catalysts and electrodes challenge the application of these technologies (Yang et al., 2016).

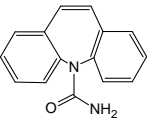
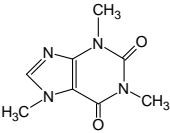
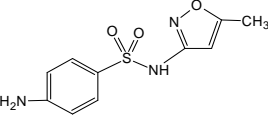
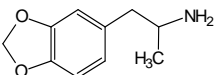
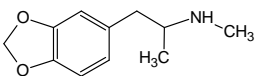
Biological reduction of perchlorate to environmentally innocuous Cl^- is identified as one of the most effective and cost-efficient technology and has shown promise for large scale applications (Srinivasan & Sorial, 2009). Perchlorate reducing microorganisms are ubiquitous in the environment; they can use different types of organic and inorganic substrates as electron donors (Okeke & Frankenberger Jr., 2005; Xu et al., 2003b). Effective biological reduction of perchlorate from $5\text{--}8 \text{ mg L}^{-1}$ to $< 0.5 \text{ mg L}^{-1}$ has been reported using elemental sulfur (Sahu et al., 2009). A full-scale in-situ biological permeable reactive barrier (PRB) containing a mixture of gravel (70%), mushroom compost (20%), and soybean oil-soaked woodchips (10%) was used to biologically degrade perchlorate in ground water at the Naval Weapons Industrial Reserve Plant McGregor in 2002. Perchlorate was removed from an average input concentration of $13,000 \text{ } \mu\text{g L}^{-1}$ to an undetectable level upon exiting the PRB (US EPA website: <https://clu-in.org/products/newsletters/tnandt/view.cfm?issue=0204.cfm#2>). A full-scale fluidized bed reactor (FBR) system containing GAC (fluidization media), ethanol (an electron donor), and inorganic N and P (nutrients for supporting microbial growth) was used to treat perchlorate from influent concentration of $6\text{--}8 \text{ mg L}^{-1}$ to below practical

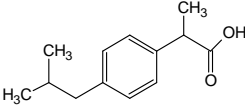
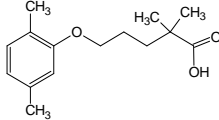
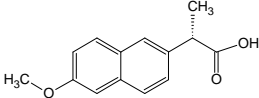
quantitation limits (0.004 mg L^{-1}) at a water flow of $4,000 \text{ gal min}^{-1}$ for more than 8 months in California (Hatzinger et al., 2000).

1.1.3 Occurrence, Fate, and Treatment Technologies of Emerging Contaminants, Pharmaceutical Compounds

Pharmaceuticals and personal care products (PPCPs) represent one of the largest and most important groups of emerging contaminants. It is reported that nearly 3000 different substances commonly are used as pharmaceutical ingredients, including painkillers, antibiotics, antidiabetics, betablockers, contraceptives, lipid regulators, antidepressants and impotence drugs (Richardson & Ternes, 2011). The structures and uses of target pharmaceuticals evaluated in this thesis are shown in Table 1.1.

Table 1.1 Selected properties for target pharmaceuticals.

Compound (CAS#)	Structure	pKa	Log Kow	Therapeutic uses
Carbamazepine (CBZ) (298-46-4)		-0.49 ^a	2.25	Anti-depressant, antiepileptic
Caffeine (CAF) (58-08-2)		10.4 ^b	-0.07	Stimulant
Sulfamethoxazole (SMX) (723-46-6)		1.7, 5.6	0.89	Antibiotic
3,4-methylenedioxy-amphetamine (MDA) (4764-17-4)		9.7	1.64	Psychedelic drug
3,4-methylenedioxy-methamphetamine (MDMA) (42542-10-9)		9.9	2.28	Ecstasy

Ibuprofen (IBU) (15687-27-1)		4.5	3.5	Anti-inflammatory drug
Gemfibrozil (GEM) (25812-30-0)		4.8	4.3	Lipid regulator
Naproxen (NAP) (22204-53-1)		4.2	2.8	Anti-inflammatory drug

^a From Schaffer et al. (2012). ^b From Martínez-Hernández et al. (2014).

Pharmaceutical compounds, such as ibuprofen, naproxen, carbamazepine, caffeine, and gemfibrozil, are widely detected in aquatic systems and treated wastewater effluents (Kolpin et al., 2002; Martín et al., 2011; Rahman et al., 2010; Ternes, 1998). Environmentally-relevant contamination of surface water (Kolpin et al., 2002; Ternes, 1998) and groundwater (Carrara et al., 2008; Heberer, 2002; Hirsch et al., 1999) is mainly associated with sewage effluents. After ingestion and subsequent excretion, human pharmaceuticals end up in wastewater treatment plants (WWTPs) in the form of the non-metabolized parent compounds or metabolites (Farré et al., 2008). Due to the inefficiency of conventional WWTPs and some advanced technologies for removing these compounds from wastewaters, pharmaceuticals can enter aquatic systems, and thus become widely distributed in surface water, groundwater and even in drinking water (Grover et al., 2011; Jones et al., 2005; Kleywegt et al., 2011; Metcalfe et al., 2003a; Stackelberg et al., 2007). Besides human pharmaceuticals, veterinary drugs used for livestock, poultry, and fish farming to treat and prevent diseases account for another important source of pharmaceutical contamination to the environment, as liquid manure is used as a fertilizer

in agricultural fields from which pharmaceuticals are transported to surface waters and groundwater with run-off and infiltration (Farré et al., 2008).

The presence of pharmaceuticals in aquatic systems has received growing attention because of their frequent detection in environmental waters and the ecotoxicological effects that they may cause. Pharmaceuticals are usually found at low concentrations of ng L^{-1} to $\mu\text{g L}^{-1}$ in the environment, which are unlikely to induce acute effects; however, continuous low-dose exposure to these compounds, especially at sensitive life stages, may cause chronic effects or even lethal effects on sensitive organisms (Caliman & Gavrilescu, 2009; Fent et al., 2006; Oaks et al., 2004). A number of pharmaceuticals have been reported to have adverse impacts on reproduction and development of biota in the environment: carbamazepine (CBZ) ($2.0\text{--}20\text{ mg L}^{-1}$), an antiepileptic drug, can induce enzymatic and oxidative stress in common carp (*Cyprinus carpio*) (Li et al., 2010b; Malarvizhi et al., 2012); gemfibrozil (GEM), a lipid regulator, bioconcentrates and reduces testosterone in goldfish (*Carassius auratus*), leading to potential endocrine disruption at concentration ranging from $1.5\text{ }\mu\text{g L}^{-1}$ to 10 mg L^{-1} (Mimeault et al., 2005); naproxen (NAP), a non-steroidal anti-inflammatory drug (NSAID), noticeably inhibits the growth rate of some plankton species at acute toxicity concentration (LC_{50}) of $56\text{--}78\text{ mg L}^{-1}$ (El-Bassat et al., 2012). Gillis et al. (2017) report the decreasing population and species of freshwater mussel downstream a wastewater treatment plant affected by various emerging contaminants. The environmental concentrations of most pharmaceuticals are generally below the lowest observed effect concentrations (LOECs), with the exception of some pharmaceuticals, such as salicylic acid, diclofenac, propranolol, clofibrac acid, carbamazepine, and fluoxetine. The chronic

toxic LOECs of these compounds are close to environmental levels. Besides the ecotoxicology of the pharmaceuticals, another important concern for pharmaceuticals is the creation of “Super Bugs”, the development of bacterial resistance due to widespread distribution of antibiotics (Richardson & Ternes, 2011).

Treatment technologies for removing pharmaceuticals from water include physical adsorption, biological degradation, chemical advanced oxidation, and combined chemical and biological methods (Wang & Wang, 2016). The sorbents used in physical adsorption for removing pharmaceutical compounds include activated carbon (AC), graphene and graphene oxide, and carbon nanotubes. Ek et al. (2014) demonstrate effective removal (90–98%) of seven pharmaceutical residues from sewage treatment plant effluents using AC filtration as an additional polishing technique. Yang and Tang (2016) report variable removals of pharmaceuticals acetaminophen (43%), caffeine (84%), cephalexin (81%), and sulfamethoxazole (34%) using graphene. Jung et al. (2015c) summarize the high potential adsorption capacities of various types of carbon nanotubes in removal of different endocrine-disrupting compounds and pharmaceutical compounds and their removal mechanisms. Biological degradation is an important removal mechanism of pharmaceuticals in the environment involving various microorganism communities; however, the removal efficiency varies greatly for different pharmaceuticals (Wang & Wang, 2016). Joss et al. (2005) report > 90% of ibuprofen, but < 10% of carbamazepine are removed in biological WWTP.

Advanced oxidation processes (AOPs) are considered very effective technologies for degradation of toxic and recalcitrant organic contaminants in water, which include ozonation (Tay & Madehi, 2015), UV/H₂O₂ (Kim et al., 2009b), UV/O₃ (Kim et al.,

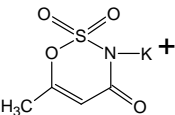
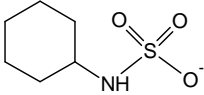
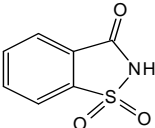
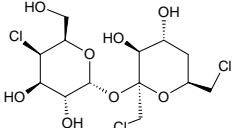
2009c), UV photolysis and photocatalysis using TiO₂ (Calisto et al., 2011; Rosal et al., 2008), Fenton and Fenton-like oxidation (Ganzenko et al., 2015; Segura et al., 2014), gamma radiation (Liu & Wang, 2013), sonolysis (Naddeo et al., 2015), and electrochemical oxidation (Moreira et al., 2016). Biological technologies cannot completely degrade some recalcitrant pharmaceuticals due to their persistence and toxicity to microorganisms. The AOPs often require high operating costs and the intermediate products of some organic compounds are perhaps more toxic and recalcitrant to oxidation. However, the combined AOPs and biological methods can first degrade the persistent large molecule contaminants to biodegradable small molecule intermediates during AOPs, and then the intermediates can be degraded during biological treatment (Wang & Wang, 2016). Keen et al. (2012) report carbamazepine as one of the most recalcitrant pharmaceuticals, but its UV/H₂O₂ oxidation byproducts can be completely mineralized by a mixed bacterial inoculum. In addition, the AOPs can also be used as a polishing post-treatment process to enhance the overall removal efficiency of bio-recalcitrant pharmaceuticals (Ghatak, 2014; José et al., 2010). Other treatment technologies, such as soil aquifer treatment (Onesios & Bouwer, 2012) and constructed wetland (Verlicchi & Zambello, 2014) have also been investigated for removing pharmaceuticals from water.

1.1.4 Occurrence, Fate, and Treatment Technologies of Emerging Contaminants, Artificial Sweeteners

Artificial sweeteners, such as acesulfame-K (potassium), cyclamate, saccharin, sucralose and aspartame, have been used worldwide for decades as food and drink additives. The highly intense sweetness of these artificial sweeteners can greatly reduce sugar intake by

using them in food manufacturing. Moreover, artificial sweeteners can help to reduce the risk of tooth decay as they are not metabolized like sugar, and do not provide significant energy following ingestion making them suitable for diabetics and dietetics (Kroger et al., 2006). The target artificial sweeteners evaluated in this study are listed in Table 1.2.

Table 1.2 Selected properties for target artificial sweeteners.

Compound (CAS#)	Structure	pKa	Log Kow	Uses/Trade names
Acesulfame-K (ACE-K) (55589-62-3)		2.0	-1.33	200 times sweeter than sugar/Sunett and Sweet One
Cyclamate (CYC) (45951-45-9)		1.7	-2.63	30–50 times sweeter than sugar/Sweet'N Low and Sugar Twin
Saccharin (SAC) (81-07-2)		2.0	0.91	Benzoic sulfilimine
Sucralose (SCL) (56038-13-2)		11.8	-1.00	600 times sweet as sugar/Splenda, Sukrana, SucraPlus, Candys, Cukren and Nevella

Artificial sweeteners pass through human bodies with little metabolic breakdown after ingestion and are excreted via urine and feces, and therefore end up in wastewater virtually unchanged (Buerge et al., 2009). Studies also indicate that some of these artificial sweeteners reach receiving surface waters and groundwater due to incomplete removal in WWTPs. The prevalence and widespread occurrence of artificial sweeteners in the aquatic environment has recently been reported (Buerge et al., 2009; Buerge et al., 2011; Lubick, 2008; Scheurer et al., 2009; Scheurer et al., 2010; Scheurer et al., 2011). An investigation on the occurrence of four artificial sweeteners at eight urban sites in

Canada showed that acesulfame-K, the most prevalent artificial sweetener, was detected in all eight investigated sites, including groundwater and surface water, at high concentrations of several $\mu\text{g L}^{-1}$, and tend to be a good tracer of wastewater; saccharin, sucralose, and cyclamate were also detected at some investigated sites (Van Stempvoort et al., 2011).

Acesulfame-K is quite persistent in surface waters and groundwater. In Switzerland, it was detected at concentrations of 12–46 $\mu\text{g L}^{-1}$ in untreated and treated water from WWTPs, in most investigated surface water samples and 65% of groundwater samples. It was detected in tap water samples at concentrations up to 2.6 $\mu\text{g L}^{-1}$. Sucralose was also found to be quite persistent in wastewater with no degradation observed during a 7 h residence time in a WWTP. In contrast, cyclamate and saccharin were readily biodegraded with removals of 99% and 90% from untreated wastewater, respectively (Buerge et al., 2009). In Germany, acesulfame-K was also the predominant artificial sweetener in surface waters with concentrations exceeding 2 $\mu\text{g L}^{-1}$ (Scheurer et al., 2009), and was the only artificial sweetener detected at concentrations up to several hundred ng L^{-1} in finished drinking water after treatment with granular activated carbon (GAC) filters (Scheurer et al., 2010). Similarly, little sucralose was removed in sewage treatment plants (STPs). However, more than 94% of saccharin and cyclamate were eliminated in STPs (Scheurer et al., 2009). Aspartame and saccharin are likely biodegraded easily in the sewage treatment system (Ferrer & Thurman, 2010).

Artificial sweeteners acesulfame-K and sucralose have been used as tracers to track the contamination of environmental waters by domestic wastewater, because they are primarily present in wastewater and recalcitrant to natural attenuation processes such as

biological degradation (Buerge et al., 2009; Van Stempvoort et al., 2011). Sucralose has been used as indicator compound for anthropogenic influence on finished drinking water as well as the presence of other recalcitrant contaminants in finished drinking water (Mawhinney et al., 2011). The ecotoxicity of artificial sweeteners is controversial and a cause for concern, because the long-term health effects resulting from chronic exposure to low levels of these compounds are still to a great extent unknown (Kroger et al., 2006). Sang et al. (2014a) report that the photo-induced transformation by-products of acesulfame-K are >500 times more toxic than the parent compound and may impact aquatic ecosystems. In addition, the accumulation of artificial sweeteners in drinking water due to incomplete removal of these artificial sweeteners in WWTPs and drinking water treatment plants (DWTPs) is a quality concern especially in water shortage and reuse areas (Mawhinney et al., 2011).

Therefore, remedial technologies for removing artificial sweeteners from water supplies are consequently being developed. Besides WWTPs and biological degradation, many technologies have been studied for removing artificial sweeteners from water, such as physical adsorption using AC and chemical oxidation (Sharma et al., 2012). Scheurer et al. (2010) and Mailler et al. (2014) report effective removal of saccharin and sucralose using GAC filtration, but poor removals for acesulfame-K and cyclamate. Recently, advanced oxidation processes have been extensively investigated for removing artificial sweeteners from water, and include photochemical and electrochemical oxidation (Lin et al., 2016; Perkola et al., 2016), UV/H₂O₂ photo-oxidation (Keen & Linden, 2013), ozonation (Scheurer et al., 2012), ferrate (VI) and radicals based oxidation (Lin et al., 2016; Sharma et al., 2012). Sharma et al. (2014) provide a review on the advanced



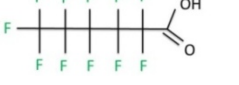
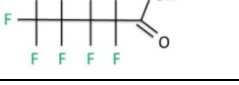

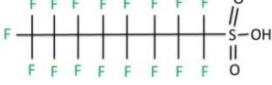
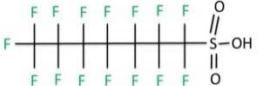
oxidation processes (AOPs) for removing sucralose from water using ozonation, $\cdot\text{OH}$ radical, $\text{UV}/\text{H}_2\text{O}_2$, and ferrate. The highly strong oxidizing agent hydroxyl radicals ($\cdot\text{OH}$) generated during these AOPs effectively degrade sucralose in water. Toth et al. (2012) demonstrate effective degradation of five artificial sweeteners acesulfame-K, aspartame, rebaudioside, saccharin, and sucralose by $\cdot\text{OH}$ and $\text{SO}_4\cdot^-$ radicals. In addition, other technologies have been studied for removing artificial sweeteners from water, such as soil aquifer treatment (Scheurer et al., 2009; Scheurer et al., 2011), conventional multi-barrier treatment (including bank filtration, artificial recharge, flocculation, ozonation, activated carbon filtration, and disinfection) (Scheurer et al., 2010), and constructed wetlands (Vymazal & Dvořáková Březinová, 2016).

1.1.5 Occurrence, Fate, and Treatment Technologies of Emerging Contaminants, Perfluoroalkyl Substances

Polyfluoroalkyl and perfluoroalkyl substances (PFASs) are a recent class of Persistent Organic Pollutants that have an aliphatic carbon backbone in which hydrogen atoms are partially (poly-) or completely (per-) replaced by fluorine (F) (Rahman et al., 2014). Due to the unique structure of C-F bond, PFASs present high surface activity, and high thermal and chemical stability. Therefore, they have been widely used in numerous industrial and consumer products such as firefighting foams, food packing, waterproof breathable fabrics, non-stick cookware, semiconductors, and photographic films. The perfluoroalkyl acids (PFAAs) are one class of PFASs which have received the most attention to date. The two important sub-classes of PFAAs are perfluoroalkyl carboxylic acids (PFCAs) and perfluoroalkyl sulfonic acids (PFSAs). The most commonly used and frequently detected PFCAs and PFSAs are perfluorooctanoic acid (PFOA) and

perfluorooctane sulfonic acid (PFOS), respectively. Both PFOA and PFOS have eight C atoms in their structure; PFOA consists of a hydrophobic perfluorinated carbon (C₇F₁₅) tail and a hydrophilic carboxylic (–COOH) ionic head, PFOS consists of a hydrophobic perfluorinated carbon (C₈F₁₇) tail and a hydrophilic sulfonic (–SO₃H) ionic head (Table 1.3). The target PFCAs and PFSAAs in this study are summarized in Table 1.3. As the C chain length increases, the water solubility and vapour pressure of PFCAs and PFSAAs decrease; however, the soil organic carbon-water partitioning coefficient (log *K_{oc}*) and acid dissociation constant (p*K_a*) increase with increasing carbon chain length (Rahman et al., 2014; Rayne & Forest, 2009).

Table 1.3 Selected properties for target perfluoroalkyl carboxylic acids (PFCAs) and perfluoroalkyl sulfonic acids (PFSAAs).

	Compound (CAS#)	Acronym	Molecular Formula	Structure
PFCAs	Perfluorooctanoic acid (335-67-1)	PFOA	C ₈ HF ₁₅ O ₂	
	Perfluoroheptanoic acid (375-85-9)	PFHpA	C ₇ HF ₁₃ O ₂	
	Perfluorohexanoic acid (307-24-4)	PFHxA	C ₆ HF ₁₁ O ₂	
	Perfluoropentanoic acid (2706-90-3)	PFPeA	C ₅ HF ₉ O ₂	
	Perfluorobutanoic acid (375-22-4)	PFBA	C ₄ HF ₇ O ₂	
PFSAAs	Perfluorooctane sulfonate acid (2795-39-3)	PFOS	C ₈ HF ₁₇ O ₃ S	
	Perfluoroheptane sulfonic acid (375-92-8)	PFHpS	C ₇ HF ₁₅ O ₃ S	

Perfluorohexane sulfonic acid (355-46-4)	PFHxS	$C_6HF_{13}O_3S$	
Perfluorobutane sulfonic acid (375-73-5)	PFBS	$C_4HF_9O_3S$	

The high stability of PFASs results in their environmental persistence and widespread occurrences. The PFASs are detected in numerous worldwide jurisdictions in wastewater (D'Eon et al., 2009; Rayne & Forest, 2009), surface water (Müller et al., 2011; Scott et al., 2009), groundwater (Lin et al., 2015b; Schaidler et al., 2014), drinking water (Pan et al., 2016; Post et al., 2013) at reported concentrations that range from $\mu\text{g L}^{-1}$ to pg L^{-1} levels and in soils at reported concentrations that range from 29 to 14,300 pg g^{-1} (Rankin et al., 2016), and even human serum and milk at reported concentrations ranging from 0.07 to 27 $\mu\text{g L}^{-1}$ (Von Ehrenstein et al., 2009). PFASs can have adverse effects on human reproductive and development systems (Goudarzi et al., 2016; Lopez-Espinosa et al., 2011). PFOA is reported to be associated with human kidney and testicular cancer near a PFAS chemical manufacturing plant (Barry et al., 2013). In addition, PFASs are endocrine disruptors; the longer chain PFASs ($> C_8$) are bioaccumulative in wild life and humans, the shorter chains are less bioaccumulative (Conder et al., 2008; Martin et al., 2003). US EPA recommends drinking water advisory levels for PFOA and PFOS of 400 and 200 ng L^{-1} (US EPA, 2009a).

Treatment technologies for removing PFASs from water have been extensively investigated, and include advanced oxidation (electrochemical oxidation, photolysis, and photocatalysis) (Cho, 2011; Liu et al., 2015c), advanced reduction (by nanoscale ZVI, iodide, dithionite) (Arvaniti et al., 2015; Park et al., 2011; Vellanki et al., 2013), sorption

(by activated carbon, resins and other sorbents) (Deng et al., 2012; Zhang et al., 2016), and microbial treatment (Liu & Liu, 2016; Ochoa-Herrera et al., 2016). During advanced oxidation processes, strong oxidizing and non-selective radicals ($\cdot\text{OH}$, $\text{SO}_4^{\cdot-}$, and $\text{O}_2^{\cdot-}$) are generated to attack and cleave the contaminant. However, F is the most electronegative element; C-F bond is one of the strongest bonds, and the bond becomes stronger with an increased number of C-F. This unique saturated C-F structure makes PFASs resistant to oxidation, even using O_3 and $\cdot\text{OH}$ (Rahman et al., 2014).

The extreme laboratory conditions such as high temperature, low pH, and high pressure greatly enhance the oxidative degradation of PFASs. Zhang et al. (2015) report the removal (24–52%) of eleven PFASs using an electrochemical oxidation reactor within 30 min. Yin et al. (2016) report effective degradation (90%) and defluorination (24%) of PFOA (initial concentration: 20 μM) using activated persulfate oxidation at pH of 2.0 and a temperature of 50 $^\circ\text{C}$. Ochiai et al. (2011) report efficient decomposition of PFCAs in aqueous suspensions using a TiO_2 photocatalyst.

During the advanced reduction of PFASs, the highly reactive, non-selective reducing hydrated electrons are the main nucleophiles attributed to the reductive defluorination of PFASs. Song et al. (2013) demonstrate reductive defluorination of PFOA (88.5%) after 24 h by hydrated electrons generated from a sulfite-mediated UV photochemical system. Park et al. (2011) report reductive degradation of six PFASs, PFCAs, and PFSAs using hydrated electrons generated from photolysis of iodide at 254 nm. Sorption of PFASs by different sorbents and environmental matrices occur mainly through hydrophobic interaction and electrostatic forces (Merino et al., 2016). Effective sorption of PFOA, PFOS, and PFHpA has been reported using granular activated carbon

(GAC) (Zhang et al., 2016). Due to the high stability of C-F bond, the microbial degradation of PFASs is only likely for polyfluoroalkyl substances (containing C-H), but less likely for perfluoroalkyl substances (containing C-F) (Liu & Mejia Avendaño, 2013; Merino et al., 2016). Liu and Liu (2016) observe the microbial transformation of polyfluoroalkyl phosphate esters (PAPs) into PFCAs in activated sludge and soil.

1.1.6 Why Use Zero-valent Iron, Biochar, Magnetically Recoverable Nano-TiO₂ Nanoparticles, and Passive Treatment Systems?

Permeable reactive barriers (PRBs), efficient, cost-effective, long-term stable passive treatment technologies, have been extensively used to remediate contaminated groundwater and soil (Blowes et al., 2000). Zero valent iron (ZVI) is a strong reducing agent extensively used in permeable reactive barriers (PRBs) to remove a large number of inorganic contaminants, including As, Cd, Cr, Cu, Hg, U, V, NO₃, and SO₄ (Blowes et al., 2000; Blowes et al., 1997; Robertson et al., 2000), and organic contaminants, such as halogenated compounds (TCE, DCE, PCE), nitroaromatics, dyes, and phenolic compounds from contaminated wastewater, groundwater and soil (Bell et al., 2003; Cundy et al., 2008; Gillham & O'Hannesin, 1994; Jeon et al., 2006; Orth & Gillham, 1996; Scherer et al., 2000). ZVI is abundant in the environment and easy to access. As a remediation tool, ZVI can act as a reductant, sorbent, and coagulant to treat a wide range of contaminants (Crawford et al., 1993; Matheson & Tratnyek, 1994; Odziemkowski & Simpraga, 2004). The high reductive capacity, environmental sustainability, and non-toxic iron by-products after treatment make ZVI a promising technology for treating a range of pollutants in wastewater and groundwater (Sun et al., 2016).

Biochar is a carbon rich material produced from the pyrolysis of biomass, such as wood, manure or leaves under low oxygen conditions (Lehmann & Joseph, 2009). Its high porosity, low density, large surface area and cation exchange capacity, and cost-effectiveness make biochar practical and effective for stabilizing organic and inorganic contaminants in soils (Beesley et al., 2011), and removing various contaminants, such as organic compounds, heavy metals from water (Chen et al., 2011a; Xu et al., 2012). Inyang and Dickenson (2015) report a review of the use of biochar for removal of a wide range of organic contaminants include volatile organic compounds (VOCs), natural organic matter (NOM), disinfection by-products (DBPs), perfluoroalkyl acids (PFAAs), pesticides, pharmaceutical and personal care products (PPCPs) as well as the associated removal mechanisms. Ahmad et al. (2012) report equivalent or stronger sorption capacity of BC compared to AC for removing TCE from water. In addition, it has been reported that the estimated break-even price for biochar is \$246/ton, but \$1500/ton for activated carbon (Lehmann & Joseph, 2009). Biochar can be a potential substitute sorbent to AC due to its competitive or enhanced sorption efficiency and lower production costs compared to AC.

Ultraviolet light (UV) photodegradation catalyzed by nanoTiO₂ particles has been studied as an effective advanced oxidation process for removing a wide range of emerging contaminants from water such as pharmaceuticals (Choina et al., 2010), artificial sweeteners (Calza et al., 2013), perchlorate (Ye et al., 2013), and perfluoroalkyl substances (Cho, 2011). TiO₂ is the most widely studied heterogeneous photocatalyst due to its cost effectiveness, inert nature and photo-stability (Gaya & Abdullah, 2008). However, nano-TiO₂ particles themselves are also emerging contaminants which can

cause adverse toxic effects to various aquatic organisms and even humans (Hund-Rinke & Simon, 2006; Sharifi et al., 2012); they tend to enter the environment after use if they are not properly recovered. Magnetically recoverable nano-TiO₂ particles can be a substitute for commercial nano-TiO₂ particles used in photocatalytic treatment to minimize the risk of releasing nano-TiO₂ into the environment (Makovec et al., 2011). Linley et al. (2014) demonstrate enhanced removal of pharmaceuticals carbamazepine and caffeine using a recyclable graphene oxide-supported TiO₂ photocatalyst compared to commercial P25 TiO₂. Similarly, comparable catalytic activity of synthesized magnetic TiO₂ to P25 TiO₂ nanoparticles has been reported in the removal of acetaminophen and four PPCPs (Álvarez et al., 2010).

Passive treatment systems were proposed and used to remove metals and neutralize pH of acid mine drainage (Blowes et al., 1995; Blowes et al., 1991; Kleinmann & Hedin, 1993). Passive treatment systems are different from active systems (such as water treatment plants) which commonly use power and hazardous chemicals (such as hydrated lime and ammonia). Successful passive treatment systems can achieve competitive treatment results compared to active treatment systems, but are often less expensive than active treatment systems because of lower use of resources and maintenance. Active treatment systems require continuous inputs of resources and maintenance (Ford, 2003). Passive treatment systems include wetlands, bioreactors, and permeable reactive barriers (Benner et al., 1997; Blowes et al., 1995; Blowes et al., 1994; Johnson & Hallberg, 2005).

1.2 Research Hypotheses and Objectives

1.2.1 Research Hypotheses

Five main research hypotheses are proposed in this thesis; each hypothesis corresponds to the research study from Chapters 2 to 6:

Hypothesis One (for Chapter 2):

Passive treatment systems containing ZVI and wood chips are an effective approach for simultaneously removing nitrate, sulfate, and perchlorate from water under dynamic flow conditions.

- Nitrate is removed by zero-valent iron through reduction and removed by wood chips (organic carbon, OC) through denitrification.
- Sulfate and perchlorate are removed by OC through biological reduction of sulfate to sulfide and of perchlorate to chloride.

Hypothesis Two (for Chapter 3):

Effluents from WWTPs are the primary sources of the emerging contaminants (ECs) in the study area. The ECs are correlated with each other and can be used as potential co-tracers of municipal wastewater in a receiving river.

Hypothesis Three (for Chapter 4):

UV photocatalysis using laboratory-synthesized magnetically recoverable TiO₂ and commercial P25 TiO₂ nanoparticles are effective for removing artificial sweetener acesulfame-K and pharmaceuticals from water.

- Target ECs are removed to varying extents during UV photocatalysis due to their different chemical structures (functional groups).
- Magnetically recoverable TiO₂ can be removed from water through magnetic separation.

Hypothesis Four (for Chapter 5):

Passive treatment systems containing ZVI, biochar, and a mixture of ZVI and biochar are an effective approach for simultaneously removing pharmaceuticals, artificial sweeteners, and perfluoroalkyl substances from water under dynamic flow conditions.

- Target ECs are removed to differing degrees and removal mechanisms are likely related to their different physiochemical properties (*pKa* and $\log K_{ow}$) and chemical structures (functional groups).
- Target ECs with redox sensitive and halogen functional groups are removed by ZVI through reduction and dehalogenation.
- Target ECs are more effectively removed by the combination of ZVI and biochar (through both reduction and sorption) than by ZVI alone or biochar alone.

Hypothesis Five (for Chapter 6):

Removal of perfluoroalkyl substances PFOA and PFOS by ZVI is through reductive defluorination. The hydrophobicity of C-F bonds in PFOA and PFOS might result in efficient removal of PFOA and PFOS by biochar through hydrophobic interaction.

1.2.2 Research Objectives

The primary objectives of this research are to evaluate the effectiveness of passive treatment systems using ZVI and organic carbon (wood chips and biochar) and UV photocatalytic treatment technology for removing emerging contaminants, perchlorate, pharmaceutical compounds, artificial sweeteners, and perfluoroalkyl substances (PFASs) from water. In addition, the use of artificial sweeteners and pharmaceutical compounds as co-tracers of municipal wastewater was investigated in a receiving river. The target pharmaceutical compounds include carbamazepine (CBZ), caffeine (CAF), sulfamethoxazole (SMX), 3,4-methylenedioxyamphetamine (MDA), 3,4-methylenedioxymethamphetamine (MDMA), ibuprofen (IBU), gemfibrozil (GEM), and naproxen (NAP). The target artificial sweeteners include acesulfame-K (ACE-K), cyclamate (CYC), saccharin (SAC), and sucralose (SCL). The target PFASs include PFCAs perfluorooctanoic acid (PFOA, C8-PFCA), perfluoroheptanoic acid (PFHpA, C7-PFCA), perfluorohexanoic acid (PFHxA, C6-PFCA) and PFASs perfluorooctane sulfonic acid (PFOS, C8-PFSA), perfluoroheptane sulfonic acid (PFHpS, C7-PFSA), perfluorohexane sulfonic acid (PFHxS, C6-PFSA), and perfluorobutane sulfonic acid (PFBS, C4-PFSA). These emerging contaminants were selected because of their widespread occurrence and persistence in the environment and limited information is available regarding their treatability. These compounds were also selected to represent different types of emerging contaminants due to their varying physiochemical properties such as pK_a , $\log K_{ow}$, and type of functional groups. Specific research objectives are as follows:

- Evaluate the effectiveness of a passive treatment system composed of ZVI and wood chips for removing perchlorate, nitrate, and sulfate under dynamic flow conditions.
- Track the emerging contaminants artificial sweetener acesulfame-K and a suite of pharmaceutical compounds downstream from two WWTPs and assess the potential use of these compounds as co-tracers of municipal wastewater in a receiving river.
- Evaluate the effectiveness of UV photocatalytic treatment using recoverable TiO₂ nanoparticles for removing artificial sweetener acesulfame-K and a suite of pharmaceutical compounds from water compared to commercial P25 TiO₂ nanoparticles.
- Evaluate the effectiveness of a passive treatment system composed of ZVI and biochar for removing pharmaceutical compounds, artificial sweeteners, and perfluoroalkyl substances from water under dynamic flow conditions.
- Investigate the removal mechanisms of perfluoroalkyl substances PFOA and PFOS by reactive media ZVI and BC.

1.3 Thesis Organization

This thesis is composed of seven chapters. Chapter 1 presents an overall research introduction and objectives. Chapters 2, 3, 4, 5 and 6 are five main research papers for publication in international peer-reviewed journals that are related to the objectives outlined in the previous section. Chapter 2 describes four column experiments conducted

to evaluate the effectiveness of ZVI, organic C (OC), and a mixture of (ZVI + OC) for removing perchlorate, nitrate, and sulfate from water. Chapter 3 investigates the transport of emerging contaminants artificial sweetener acesulfame-K and pharmaceutical compounds downstream from two WWTPs effluents and assesses the potential use of these compounds as co-tracers of municipal wastewater in a receiving river. Chapter 4 describes a series of laboratory batch experiments conducted to evaluate the UV photocatalytic treatment using recoverable TiO₂ nanoparticles (MST and GO TiO₂ nanoparticles) for removing artificial sweetener acesulfame-K and pharmaceutical compounds from water compared to commercial P25 TiO₂ nanoparticles. Chapter 5 describes four column experiments conducted to evaluate the potential of ZVI, biochar (BC), and a mixture of (ZVI + OC) for simultaneous removal of pharmaceutical compounds, artificial sweeteners, and perfluoroalkyl substances from water. Chapter 6 describes a series of batch experiments conducted to investigate the removal mechanisms of perfluoroalkyl substances PFOA and PFOS by ZVI and BC. Chapter 7 summarizes the main findings and scientific contributions of the above five research papers and gives recommendations for future work. Supplementary information related to Chapter 2, 3, 4, 5 and 6 are included in the Appendices A, B, C, D, E.

Chapter 2: *Treatment of Dissolved
Perchlorate, Nitrate, and Sulfate Using
Zero-Valent Iron and Organic Carbon*

2.1 Executive Summary

Waters containing ClO_4^- and dissolved NO_3^- , derived from detonated explosives and solid propellants, often also contain elevated concentrations of other dissolved constituents, including SO_4^{2-} . Four column experiments, containing mixtures of silica sand, zero-valent Fe (ZVI) and organic C (OC) were conducted to evaluate the potential for simultaneous removal of NO_3^- , SO_4^{2-} and ClO_4^- . Initially, the flow rate was maintained at 0.5 pore volume (PV) d^{-1} , and then decreased to 0.1 PV d^{-1} after 100 PV of flow. Nitrate concentrations decreased from 10.8 mg L^{-1} ($\text{NO}_3\text{-N}$) to trace levels through NO_3^- reduction to NH_4^+ using ZVI alone, and through denitrification using OC. Observations from the mixture of ZVI and OC suggest a combination of nitrate reduction and denitrification. Up to 71% of input SO_4^{2-} ($24.5 \pm 3.5 \text{ mg L}^{-1}$) was removed in the column containing OC and more than 99.7% of the input perchlorate ($857 \pm 63 \text{ } \mu\text{g L}^{-1}$) was removed by the OC- and (ZVI + OC)-containing columns as the flow rate was maintained at 0.1 PV d^{-1} . Nitrate and ClO_4^- removal followed first-order and zero-order rates, respectively. Nitrate $> 2 \text{ mg L}^{-1}$ $\text{NO}_3\text{-N}$ inhibited ClO_4^- removal in the OC-containing column but not in the (ZVI + OC)-containing column. Sulfate did not inhibit ClO_4^- degradation within any of the columns.

2.2 Introduction

Perchlorate (ClO_4^-) is a common contaminant in groundwater and surface water. Approximately 90% of perchlorate salts are manufactured as NH_4ClO_4 , which is widely used in large volumes of solid propellants for rockets, missiles, explosives, and pyrotechnics. A variety of non-military sources, such as the use and manufacture of road flares, HClO_4 and HClO_3 , fireworks displays, and blasting agents used in mining and construction, can also cause widespread, low concentration ClO_4^- contamination in water. In addition to these anthropogenic sources, naturally-occurring ClO_4^- generated via atmospheric processes and contained in NO_3 fertilizers and some natural minerals also contributes low levels of ClO_4^- in some parts of the world (Ward, 2008).

Perchlorate is highly soluble, mobile, and recalcitrant in the environment. It is potentially toxic to various forms of life, with low concentrations inhibiting iodide uptake in human thyroid and animal thyroid glands (Leung et al., 2010). Due to these health impacts, the US EPA adopted the National Research Council (NRC) recommended reference dose of $0.0007 \text{ mg kg}^{-1}$ per day for perchlorate as an interim health limit in 2005, which translates to a drinking water equivalent level (DWEL) of $24.5 \mu\text{g L}^{-1}$.

Physical-chemical treatment technologies, such as ion exchange, C adsorption, and advanced oxidation are effective for treating a range of contaminants, but are less cost-efficient and effective for removing ClO_4^- from water (Srinivasan & Sorial, 2009). Ion-exchange, a widely accepted water treatment technology, can effectively remove ClO_4^- from water; however, the highly saline (7–12%) brine generated during the ion-exchange process requires costly management before disposal (Okeke et al., 2002). Microbial

reduction of perchlorate is an area of intense interest because this strategy is relatively cost effective, environmentally compatible, and has shown promise for large scale applications (Gal et al., 2008; Okeke & Frankenberger Jr., 2005). The hazardous ClO_4^- is converted into two innocuous compounds— Cl^- and O_2 —catalyzed by at least two separate enzymes (Xu et al., 2003a).

Perchlorate and nitrate are often found as co-contaminants in water, as a large number of propellants, blasting agents, and explosives contain perchlorate as well as nitrogen-containing compounds. Moreover, NO_3^- -containing compounds, such as KNO_3 and NaNO_3 , are widely used in agriculture and ClO_4^- -containing pyrotechnics. High concentrations of SO_4^{2-} , derived from S^{2-} oxidation at some mining sites, also require management. Because ClO_4^- and NO_3^- -containing blasting agents and explosives are used at mine sites, water containing co-mingled ClO_4^- , NO_3^- , and SO_4^{2-} can develop (Bailey et al., 2013; Ward, 2008). Bioremediation of ClO_4^- and NO_3^- -contaminated water has been widely studied using various electron donors, such as H_2 or ethyl acetate gases (Evans & Trute, 2006), edible oil (Borden, 2007; Hunter, 2002), compost and mulch mixtures (Wang et al., 2013), and wood particle media (Robertson et al., 2007). The purpose of this study was to identify an effective, economical, and feasible technology to remediate ClO_4^- , NO_3^- , and SO_4^{2-} -contaminated waters associated with mining and blasting sites. A series of column experiments was conducted using mixtures of zero-valent Fe (ZVI) and wood chips (OC) as reactive media to remove co-mingled ClO_4^- , NO_3^- , and SO_4^{2-} in simulated groundwater.

2.3 Material and Methods

2.3.1 Column Design and Experimental Setup

Four acrylic columns were used, each 30 cm in length with an internal diameter of 5 cm. Influent ports were located at the base of each column, and effluent ports were located at the top of each column for discharge of the effluent solution and for sample collection. In addition, 13 equally spaced sampling ports were installed at approximately 2.1-cm intervals along the length of the columns. Both the bottom and top layers of the four columns were packed with a 1.0 cm thick layer of silica sand as a non-reactive material to separate the reactive mixture from the influent and effluent end ports.

Column 1 was packed with 100% silica sand (SS) as a control. Column packings were composed of 50% (v/v) granular ZVI with the balance as SS (Column 2), 50% (v/v) wood chips (OC) with the balance as SS (Column 3), and a mixture of 10% (v/v) ZVI and 40% (v/v) OC adjusted with 50% (v/v) SS (Column 4). The granular ZVI (0.17–1.41 mm) was obtained from Connelly-GPM, Inc. (Chicago, USA). The silica sand (0.6–0.8 mm) was obtained from the Silica Company (Ottawa, USA). The wood chips (~1–9.5 mm, deciduous hardwood) were obtained from a lumber producer in Waterloo, ON. Before initiating the experiments, all four columns were placed in an anaerobic glove box (COY, Ltd., Grass Lake, USA) that contained 5% H₂ and 95% N₂. The columns were flushed with CO_{2(g)}, which is more soluble in water than N₂ and O₂, for 24 h to displace atmospheric gases from the void pore space of the column packing and enhance saturation of the packing material. The columns were then wet with simulated groundwater, composed of CaCO₃ saturated water, over a 48-h period.

A conservative tracer test was performed to determine the flow and transport

characteristics of each column. The computer code CXTFIT 2.0 (Toride et al., 1995), a series of analytical solutions to the one-dimensional advection-dispersion equation with non-linear, least-squares parameter optimization, was used to determine the average linear velocities and dispersion coefficients from the column effluent concentration data. The flow rates of the column experiments were approximately 0.5 pore volumes (PV) d⁻¹ during the conservative tracer test.

The input solution was prepared by adding NO₃⁻, SO₄²⁻, and ClO₄⁻ to the CaCO₃ saturated water as Na salts to obtain concentrations of 10.8 ± 0.3 mg L⁻¹ NO₃-N, 24.5 ± 3.5 mg L⁻¹ SO₄²⁻, and 857 ± 63 µg L⁻¹ ClO₄⁻. The ratios of concentrations were based on measurements of effluent from test-scale waste-rock piles (Bailey et al., 2013). The purpose of using CaCO₃ saturated water as the input solution is to simulate the presence of HCO₃⁻ and CO₃²⁻, which are common in natural surface water and groundwater. Before introducing the input solution, Columns 3 (OC) and 4 (ZVI + OC) were saturated with a solution containing 5% (v/v) sodium lactate for 3 d to promote the growth of microorganisms (Lindsay et al., 2011). The input solution initially was displaced through the four columns from the bottom to the top at a flow rate of 0.5 PV d⁻¹ during the first stage of the experiment. During the second stage of the experiment, the flow rates were decreased to 0.1 PV d⁻¹ (after 99 PV in Column 2, 112 PV in Column 3, and 110 PV in Column 4) to evaluate the effect of residence time on contaminant removal. The selected flow rates resulted in a range of average groundwater velocities that are typical of shallow aquifers. Three profiles were collected along the columns during the course of the experiments: after 95.4, 115, and 129 PV of flow passed through Column 2 (ZVI); after 108, 132, and 151 PV of flow through Column 3 (OC); and after 106, 128, and 144

PV of flow through Column 4 (ZVI + OC). During the experiment, there were no obvious signs of clogging or changes in hydraulic conductivity.

2.3.2 Sample Collection and Analytical Methods

Water samples were collected using 30-mL glass syringes attached directly to the ports along the length of the columns and to the effluent ports so that the syringes were filled at the same rate as the input solution being introduced to the columns. Except where noted, all samples were passed through 0.45- μm cellulose acetate filters prior to measurement. The pH, Eh, and alkalinity were determined immediately after sampling. All other samples were kept chilled ($< 4^{\circ}\text{C}$) until analysis within 1 mo of collection.

Values of pH and Eh were measured on unfiltered samples in sealed cells to minimize O_2 exposure. The pH measurements were made using a Ross combination glass electrode (Orion 815600) calibrated using standard pH 4.0 and 7.0 buffers and then checked against a pH 10.0 buffer. The Eh measurements were made using a Pt-billeted Ag/AgCl combination electrode (Orion 9678BNWP). The performance of the electrode was checked using Zobell's (Nordstrom, 1977) and Light's (Light, 1972) solutions before and after each measurement. Measurements were corrected to the standard H_2 electrode (SHE). Alkalinity was determined using a Hach digital titrator with bromocresol green/methyl red indicator and $0.08 \text{ mol L}^{-1} \text{H}_2\text{SO}_4$.

The concentrations of major anions (Br^- , NO_3^- , NO_2^- , Cl^- and SO_4^{2-}) were determined by ion chromatography (IC; DX600, Dionex, Sunnyvale, USA). Ammonia ($\text{NH}_3\text{-N}$) concentrations were determined using a Hach spectrophotometer DR/8400 following the salicylate method (APHA, 2005a). Dissolved H_2S was determined using the methylene blue spectrophotometric method (Lindsay & Baedecker, 1988).

Filtered 20-mL samples were collected separately in 30-mL polyethylene bottles for ClO_4^- analysis. A headspace was maintained in these sample bottles to minimize the possibility of anaerobic conditions developing during storage. Perchlorate was analyzed following the method described by Snyder et al. (2005) with the addition of equal aliquots of isotopically enriched sodium perchlorate ($\text{NaCl}^{18}\text{O}_4$, Cambridge Isotope Laboratories, Andover, USA) to all the samples and calibration standards as an internal standard (IS). All water samples were prepared by elution through one OnGuard-II Ba cartridge and one OnGuard-II H cartridge (Dionex, Sunnyvale, USA) in series to remove SO_4^{2-} and CO_3^{2-} , respectively. Perchlorate was analyzed by high performance liquid chromatography (Agilent 1100, Agilent Technologies) followed by electrospray tandem mass spectrometry (4000 Q TRAP, Applied Biosystems) and detected by negative electrospray ionization mass spectrometry using multiple reaction monitoring detection. The instrument and practical detection limits were 0.02 and 0.05 $\mu\text{g L}^{-1}$, respectively. Quality assurance/quality control results showed that relative method recovery over the entire standard curve (0.5–100 $\mu\text{g L}^{-1}$) fell into the range of 98 to 110%, and the relative internal standard recovery for unknown samples was 71 to 118%.

2.4 Results and Discussion

2.4.1 Conservative Tracer Test and Control Column Results

The transport model CXTFIT 2.0 was used to determine the velocity and dispersion coefficient for each column during the first stage of the experiments. The fitted velocities estimated by CXTFIT using the Br^- breakthrough curve data ranged from 40.3 to 54.3 m yr^{-1} for the four columns. These values were in agreement with the average linear velocities calculated from porosity and flow volume measurements, which ranged from

49.1 to 59.6 m yr⁻¹, with the exception of Column 2 (ZVI). The dispersion coefficients ranged from 0.1 to 1.2 m² yr⁻¹ for the four columns (Table 2.1). Measurements made on the control column indicated that transport of ClO₄⁻, NO₃⁻ and SO₄²⁻ was conservative (Figure 2.1)

2.4.2 Geochemistry Conditions of Columns

The three pH profiles within Columns 2-4 measured at different times almost overlapped, exhibiting similar values with distance (Figure 2.2). The influent water pH value was 8.3 throughout the experiments. The average pH value within Column 2 (ZVI) was 9.7. The increase in pH was due to the reduction of water by ZVI. The average pH in Column 4 (ZVI + OC) was slightly lower at 8.6. The pH of Column 3 (OC), which did not contain ZVI, was much lower at pH 7.4. Similarly, the average pH of the column effluent was 9.7 in Column 2 and 7.2 in Column 3, remaining within 0.5 pH units throughout the entire experiment (Figure 2.3). The effluent pH of Column 4 increased quickly from below 7 to about 9.5 during the first 10 PVs and then decreased to about 8.6 for the remainder of the first stage of the experiment.

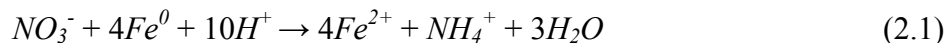
The three alkalinity profiles for each of Columns 2, 3, and 4 indicated similar average values and changing trends, with slight increases as the input solution advanced through the columns (Figure 2.2). Total alkalinities with an average value of 96 mg L⁻¹ (as CaCO₃) were generated in Column 2 (ZVI) effluent; in the effluent of the columns containing OC, slightly higher alkalinity values of 119 mg L⁻¹ (as CaCO₃) in Column 3 (OC) and 113 mg L⁻¹ (as CaCO₃) in Column 4 (ZVI + OC) were observed (Figure 2.3).

The values of Eh in Columns 2, 3, and 4 ranged from moderately oxidizing to

moderately reducing conditions over the course of the experiments, with lower values observed during the second stage of the experiments when the flow rates were lower (Figure 2.2). Higher average Eh values of ~ 300 mV were observed within Column 3 (OC) relative to the values observed in the middle distances in Columns 2 (ZVI, -200 mV) and 4 (ZVI + OC, -400 mV). Addition of the lactate solution to Columns 3 and 4 likely resulted in the relatively low Eh and high alkalinity values in the column effluent at the beginning of the first stage of the experiment compared to Column 2 (Figure 2.3). In the effluent of Columns 2 and 4 (Figure 2.3), the Eh values were relatively constant throughout the experiment. The Eh values in the effluent of Column 3 gradually increased from approximately 40 mV at the 35 PV to 460 mV at 110 PV in the first stage of the experiment, and then decreased to the average value of 200 mV in the second stage of the experiment. These decreases in Eh values were likely due to the decrease in flow rate from 0.5 PV d⁻¹ in the first stage of the experiment to 0.1 PV d⁻¹ in the second stage of the experiment.

2.4.3 Removal of Nitrate, Sulfate, and Perchlorate in Columns

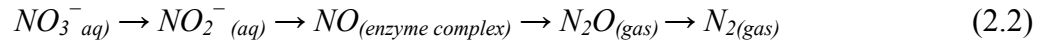
Reduction of NO₃⁻ by ZVI has been observed to proceed rapidly through NO₂⁻ to NH₄⁺. The proposed pathway for the overall reaction is (Rahman & Agrawal, 1997):



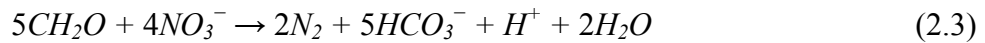
Nitrate was almost completely removed in the column containing ZVI (Column 2) from the average input concentration of 10.8 mg L⁻¹ (NO₃-N) to a trace concentration. Nitrite concentrations remained < 0.02 mg L⁻¹ (NO₂-N) and the average NH₄⁺ concentration was 10.7 mg L⁻¹ (NH₃-N) indicating that NH₄⁺ was the principal byproduct throughout the course of the experiment (Figure 2.1). The concentrations of total N (sum

of NO₃-N, NO₂-N, and NH₃-N) in Column 2 (ZVI) effluent were consistent with the input NO₃⁻ concentrations, indicating complete conversion of NO₃⁻ to NH₄⁺.

Bacterially mediated denitrification by OC such as wood waste as a C source is thermodynamically favored and leads to the stepwise reduction of NO₃⁻ to form N₂ gas:



The overall reaction can be expressed as (Appelo & Postma, 2005):

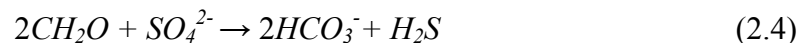


The removal of NO₃⁻ in Column 3 containing OC was variable (Figure 2.1). In the first stage of the experiment (108 PV) at a flow rate of 0.5 PV d⁻¹, up to 2.6 mg L⁻¹ NO₃-N remained in the effluent. In addition, up to 2.4 mg L⁻¹ NO₂-N, an intermediate reaction product, was observed in the effluent in the first stage of the experiment. However, NO₃⁻ was more completely removed in the second stage of the experiment when the flow rate decreased to 0.1 PV d⁻¹, from an average input concentration of 10.8 to < 0.02 mg L⁻¹ (NO₃-N) without measurable NO₂⁻ observed. A trace of NH₃ (average value 0.1 mg L⁻¹ NH₃-N) was observed in Column 3 effluent samples, perhaps due to the decomposition of OC. In the first stage of the experiment, the total N concentrations in the Column 3 (OC) effluent progressively rose from 0.1 to 5.2 mg L⁻¹. The increase in total N concentrations is predominantly due to an increase in the concentrations of NO₃⁻ and NO₂⁻, indicating that the increase in total N was due to incomplete denitrification, possibly due to a depletion of labile OC. In the second stage of the experiment the total N concentration decreased to as low as 0.7 mg L⁻¹ N, suggesting that the rate of OC consumption was sufficient to result in complete denitrification during this stage.

The mixture of ZVI + OC in Column 4 resulted in extensive removal of NO₃⁻, no

detectable release of NO_2^- , and the release of 9.5 mg L^{-1} of $\text{NH}_3\text{-N}$ at the beginning of the experiment that gradually decreased to 6.6 mg L^{-1} at 100 PV (Figure 2.1). This decreasing trend suggests that NO_3^- reduction by ZVI predominated early in the experiment and that denitrification became established, resulting in partial conversion of NO_3^- to $\text{N}_{2(\text{g})}$. In stage 2 the average total N concentration was 5.5 mg L^{-1} , almost exclusively as NH_4^+ , indicating an increase in the extent of denitrification as the residence time increased, resulting in approximately equal removal by NO_3^- reduction and denitrification. Less NH_4^+ is observed when ZVI was used in conjunction with a microbial consortia to reduce NO_3^- (Till et al., 1998).

Effluent SO_4^{2-} concentrations did not decrease in the columns containing ZVI (Column 2) or the mixture of ZVI + OC (Column 4) during the experiment (Figure 2.1). Sulfate was observed to break through Column 3 (OC) in the first stage of the experiment; however, effluent SO_4^{2-} concentrations in Column 3 decreased from 24.7 mg L^{-1} after 108 PV in the first stage of the experiment to 7.1 mg L^{-1} after 132 PV in the second stage of the experiment (when the flow rate slowed), with approximately 71% of the input SO_4^{2-} (24.5 mg L^{-1}) removed. The effluent SO_4^{2-} concentration then increased to 15.0 mg L^{-1} after 151 PV in the second stage of the experiment. This SO_4^{2-} removal is attributed to the onset of biologically mediated SO_4^{2-} reduction coupled to OC oxidation (Blowes et al., 2000):



The decrease in the rate of SO_4^{2-} removal over time was probably due to depletion of labile OC (C, N, and P source for microbial growth) over the long-term operation of the experiment. The inhibition of SO_4^{2-} reduction observed in Column 4 (ZVI + OC) might

be attributed to the higher pH conditions developed in this column compared to Column 3 (OC) (Figures 2.2 and 2.3).

Although reduction of ClO_4^- by ZVI is thermodynamically favored, with $\Delta G^\circ = -596.27 \text{ kcal mol}^{-1}$, ClO_4^- was not removed by ZVI in Column 2 throughout the experiment; this is likely due to the high activation energy required for ClO_4^- reduction (Yu et al., 2006). The effluent ClO_4^- concentration was $857 \pm 63 \mu\text{g L}^{-1}$, similar to the input concentration (Figure 2.1). The total effluent Cl concentrations (sum of ClO_4^- and Cl in $\mu\text{mol L}^{-1}$) in Column 2 (ZVI) were much higher than the input ClO_4^- concentrations, this difference may be due to the release of Cl initially present on the ZVI (Figure 2.4). The presence of Cl in the first pore volumes of flow likely represented residual from the ZVI manufacturing processes.

The effluent concentrations of ClO_4^- in Column 3 decreased from $547 \mu\text{g L}^{-1}$ after 108 PV in the first stage of the experiment to $28 \mu\text{g L}^{-1}$ after 151 PV in the second stage of the experiment (Figure 2.1). Similarly, in the second stage of the experiment when the flow rate was lowered, OC combined with ZVI exhibited more uniform removal of ClO_4^- in Column 4 than Column 3. The concentration of ClO_4^- in the effluent of Column 4 decreased from $679 \mu\text{g L}^{-1}$ after 106 PV in the first stage of the experiment to $1.37 \mu\text{g L}^{-1}$ after 144 PV in the second stage of the experiment. Previous studies have suggested the pathway for biological degradation of ClO_4^- (Rikken et al., 1996) as shown in Figure 2.5.

The first two reactions are catalyzed by (per)chlorate reductase. Chlorite dismutase catalyzes the disproportionation of ClO_2^- into Cl^- and O_2 (Okeke & Frankenberger Jr., 2003). The OC probably provided sufficient C and N for microbial degradation of ClO_4^- in Columns 3 (OC) and 4 (ZVI + OC); however, complete removal

of ClO_4^- was not consistently observed until the second stage of the experiment (Figure 2.1). Extensive removal of ClO_4^- initially was observed in Column 3, but the rate of ClO_4^- removal declined after 30 PVs. After the flow rate decreased, complete removal of ClO_4^- was observed. Initially, little ClO_4^- removal was observed in Column 4. More extensive removal was observed after 10 PVs, suggesting a period of acclimation was required before ClO_4^- reduction was established. After 60 PVs, the rate of ClO_4^- removal declined, suggesting depletion of labile OC. During stage 2 of the experiment, complete removal of ClO_4^- was observed, suggesting that the rate of OC fermentation was sufficient to provide labile OC (C, N, and P source for microbial growth) for sustained biological ClO_4^- reduction.

Chloride, the final potential product of ClO_4^- biological degradation, should be released at an amount equivalent to the moles of ClO_4^- removed. In contrast to Column 2 (ZVI), the concentrations of Cl in the first 2 PVs effluents of Columns 3 (OC) and 4 (ZVI + OC) were below the detection limit (0.01 mg L^{-1}), likely due to the flushing and saturation of the columns prior to the experiment and the small fraction (10% v/v) of ZVI in Column 4 (ZVI + OC) compared to that of ZVI (50% v/v) in Column 2 (ZVI). The changes in Cl^- concentrations in both Columns 3 (OC) and 4 (ZVI + OC) effluent were inversely correlated to ClO_4^- concentrations. Very consistent concentrations of total effluent Cl (sum of ClO_4^- and Cl^- in $\mu\text{mol L}^{-1}$) relative to the input ClO_4^- concentrations for these columns indicated that the expected mass of Cl was accounted for in both Columns 3 and 4 (Figure 2.4).

2.4.4 Removal Rates of Nitrate and Perchlorate within Columns

The two NO_3^- and ClO_4^- profiles collected for each of Columns 2, 3, and 4 in the second

stage of the experiment were similar (Figure 2.6). Therefore, only the profiles measured in the first stage of the experiment (95.4 PV for Column 2; 108 PV for Column 3, and 106 PV for Column 4) and one of the profiles measured in the second stage of the experiment (115 PV for Column 2; 132 PV for Column 3; and 128 PV for Column 4) were used for calculation of removal rate parameters.

Nitrate removal rates within Columns 2, 3, and 4 were consistent with a first-order rate model (Figure 2.7) as reported in other studies (Appelo & Postma, 2005; Tan et al., 2004):

$$C = C_0 \exp(-k_1 t) \quad (2.5)$$

$$R_N = k_1 C \quad (2.6)$$

where C is the NO_3^- concentration (mg L^{-1}), C_0 is the initial NO_3^- concentration (mg L^{-1} or mmol L^{-1}), k_1 is a first-order rate constant (d^{-1}), t is the residence time (d), and R_N is the reaction rate (removal rate) of nitrate ($\text{mg L}^{-1} \text{d}^{-1}$ or $\text{mmol L}^{-1} \text{d}^{-1}$). The best-fit NO_3^- degradation equation based on calculated residuals for each column (SigmaPlot, SPSS Inc.) was selected from the two first-order expressions derived from the two stages of the experiment.

Nitrate removal by ZVI within Column 2 (ZVI) followed a first order removal model, with removal rates of $R_{N,2} = 0.015C \text{ mmol L}^{-1} \text{d}^{-1}$ in the first stage of the experiment and $R_{N,2} = 0.011C \text{ mmol L}^{-1} \text{d}^{-1}$ in the second stage of the experiment (Table 2.2; Figure 2.7); however, neither of these equations could adequately describe the degradation curves in both experimental stages. An average first-order removal rate of $R_{N,2} = 0.013C \text{ mmol L}^{-1} \text{d}^{-1}$, which fell between the first and second stage data sets, is recommended to best describe the NO_3^- removal within Column 2 (ZVI).

The denitrification rate within Column 3 (OC) can be described by: $R_{N,3} = 0.010C$ mmol L⁻¹ d⁻¹ (Table 2.2; Figure 2.7). Both zero-order and first-order rate expressions have been observed to provide reasonable descriptions of the rate of denitrification ($R^2 > 0.86$) (Tan et al., 2004). Similar findings were observed in this study: NO₃⁻ removal by ZVI and OC in Column 4 in both first and second stages of the experiment were consistent with both the first-order and zero-order rate equations in terms of $R^2 (> 0.94)$ (Table 2.2 and Figure 2.7). However, to maintain consistency between the NO₃⁻ removal rates for Column 4 (ZVI + OC) and those for Column 2 (ZVI) and Column 3 (OC), $R_{N,4} = 0.025C$ mmol L⁻¹ d⁻¹ was used to describe the rates of NO₃⁻ removal in Column 4 throughout the experiment. Given the same initial concentration, NO₃⁻ was removed much more rapidly in Column 4 than in Columns 2 or 3 (Figure 2.6).

Perchlorate removal in some bioreactors has been observed to follow first-order reaction rates with respect to ClO₄⁻ concentration (Min et al., 2004). However, in this study, ClO₄⁻ removal in Columns 3 (OC) and 4 (ZVI + OC) followed zero-order rate equations (Figure 2.8):

$$C = -k_0 t \quad (2.7)$$

where C is the ClO₄⁻ concentration (μg L⁻¹ or μmol L⁻¹), t is the residence time (d), and k₀ is a zero-order rate constant for ClO₄⁻ removal (μg L⁻¹ d⁻¹ or μmol L⁻¹ d⁻¹). The best fit equation for ClO₄⁻ removal, based on least squares regression, was also obtained using a zero-order rate expression derived from the two stages of the experiment. The ClO₄⁻ removal rate within Column 3 (OC) was $R_{P,3} = 0.61 \mu\text{mol L}^{-1} \text{d}^{-1}$ for $0 < x < 2.9$ d (derived from the distance between the column input and the sampling point) and NO₃⁻ concentration $> 2 \text{ mg L}^{-1}$ (NO₃-N). The ClO₄⁻ removal rates were $R_{P,3} = 1.95 \mu\text{mol L}^{-1} \text{d}^{-1}$

in the first stage of the experiment and $R_{P,3} = 1.84 \mu\text{mol L}^{-1} \text{d}^{-1}$ in the second stage of the experiment, where $2.9 < t < 6.7 \text{ d}$ (for a NO_3^- concentration $< 2 \text{ mg L}^{-1} \text{NO}_3\text{-N}$). Neither of these removal rates adequately described the observations from both experimental stages. An average zeroth-order removal rate of $R_{P,3} = 1.89 \mu\text{mol L}^{-1} \text{d}^{-1}$ was selected to describe the ClO_4^- removal rate within Column 3 (OC) for $2.9 < t < 6.7 \text{ d}$ and $\text{NO}_3^- < 2 \text{ mg L}^{-1} \text{NO}_3\text{-N}$. The overall ClO_4^- removal rate within Column 4 (ZVI + OC) was $R_{P,4} = 1.14 \mu\text{mol L}^{-1} \text{d}^{-1}$ (Table 2.2; Figures 2.6 and 2.8). The ClO_4^- removal rate for the second stage of the Column 4 experiment was $R_{P,4} = 0.94 \mu\text{mol L}^{-1} \text{d}^{-1}$ for $0 < t < 2.0 \text{ d}$ and NO_3^- concentration $> 2 \text{ mg L}^{-1} \text{NO}_3\text{-N}$. A statistical comparison of the ClO_4^- removal rates for Columns 3 (OC) and 4 (ZVI + OC) indicated that ClO_4^- was removed more rapidly in Column 4 (ZVI + OC) than in Column 3 (OC) for $\text{NO}_3^- > 2 \text{ mg L}^{-1} (\text{NO}_3\text{-N})$ in the second stage of the experiment (Figures 2.6 and 2.8), but more rapidly in Column 3 for $\text{NO}_3^- < 2 \text{ mg L}^{-1} \text{NO}_3\text{-N}$.

2.4.5 Effect of Nitrate and Sulfate on Perchlorate Removal Rate

The impact of NO_3^- on ClO_4^- reduction is important because NO_3^- is a common co-contaminant in ClO_4^- -contaminated water (Xu et al., 2003a). Most ClO_4^- reducing bacteria (PRB) are also denitrifiers, and the simultaneous removal of NO_3^- and ClO_4^- from contaminated waters has been observed (Logan & LaPoint, 2002; Min et al., 2004). Likewise, the NO_3^- and ClO_4^- within Columns 3 (OC) and 4 (ZVI + OC) were removed simultaneously. However, the overall NO_3^- removal within both Columns 3 and 4 occurred at a more rapid rate than ClO_4^- removal (Figure 2.6), which may have been due to competition for common electron donors (organic matter) between the two removal processes (Chung et al., 2010). The selection of electron acceptors by microorganisms is

competitive to maximize the energy yield in a redox reaction. Nitrate reduction was found more thermodynamically favored over ClO_4^- reduction due to the lower electron transfer requirement for NO_3^- reduction compared to that for ClO_4^- reduction (Chung et al., 2010). The ClO_4^- reducing bacteria in preference of O_2 or NO_3^- over ClO_4^- was also reported (Roldan et al., 1994). Moreover, if the same enzyme in a microorganism was used for both NO_3^- and ClO_4^- reductions, NO_3^- were likely to inhibit ClO_4^- reduction and ClO_4^- also likely to inhibit NO_3^- reduction, depending on the initial concentrations of NO_3^- and ClO_4^- (Giblin & Frankenberger W.T, 2001). Complete NO_3^- removal within Columns 3 and 4 was observed prior to complete ClO_4^- removal (Figure 2.6), which is similar to other studies (Min et al., 2004).

Nitrate has different effects on ClO_4^- removal rates. Nitrate was found to inhibit the ClO_4^- reduction rate in some studies (Brown et al., 2002; Xu et al., 2003a) but not others (Giblin et al., 2000). In this study, the inhibition of ClO_4^- removal by NO_3^- was observed within Column 3 (OC) but not Column 4 (ZVI + OC). The inhibiting effects of NO_3^- on ClO_4^- removal occurred at NO_3^- concentrations $> 2 \text{ mg L}^{-1} \text{ NO}_3\text{-N}$ within Column 3 (OC) during the second stage of the experiment when flow rate was maintained at 0.1 PV d^{-1} . Moreover, rapid ClO_4^- degradation did not proceed until NO_3^- concentrations were reduced to relatively low levels (normally $< 2 \text{ mg L}^{-1} \text{ NO}_3\text{-N}$), which is consistent with previous findings (Tan et al., 2004). However, the presence of NO_3^- within Column 4 (ZVI + OC) did not inhibit ClO_4^- removal (Figure 2.6), which followed similar linear rates in the presence and absence of NO_3^- . These results suggest that adding ZVI to wood chips can potentially reduce the inhibition of $\text{NO}_3^- (> 2 \text{ mg L}^{-1} \text{ NO}_3\text{-N})$ on ClO_4^- removal when flow rate was maintained at 0.1 PV d^{-1} . The presence of SO_4^{2-} did not inhibit ClO_4^-

removal in Column 3 (OC) or 4 (ZVI + OC) (Figure 2.6), as is consistent with previous reports (Chung et al., 2010).

2.5 Conclusions

Reactive media containing OC or a mixture of ZVI + OC were found effective for removing NO_3^- and ClO_4^- from water. The removal of NO_3^- and ClO_4^- followed first-order and zero-order rates in these column experiments, respectively. Nitrate and ClO_4^- were removed simultaneously within the columns; however, complete NO_3^- removal occurred prior to complete ClO_4^- removal. Addition of ZVI to wood chips reduced the inhibition of NO_3^- ($> 2 \text{ mg L}^{-1} \text{ NO}_3\text{-N}$) on ClO_4^- degradation when flow rate was maintained at 0.1 PV d^{-1} . Decreasing the flow rate from 0.5 to 0.1 PV d^{-1} resulted in more complete removal of NO_3^- , SO_4^{2-} , and ClO_4^- . These results suggest that permeable reactive barriers and bioreactors containing OC or mixtures of OC and ZVI may be suitable for treating NO_3^- , ClO_4^- and SO_4^{2-} at mining and blasting sites.

Table 2.1 Physical characteristics of the columns used in this study, including a control and columns containing zero-valent Fe (ZVI), organic C (OC) or both.

	Column 1 Control	Column 2 ZVI	Column 3 OC	Column 4 ZVI + OC
Bulk density (g cm ⁻³)	1.73	2.27	1.34	1.59
Porosity	0.35	0.40	0.45	0.41
Pore volume (cm ³)	219	248	273	246
Average linear velocity (m yr ⁻¹)	59.6	51.7	50.8	49.1
Fitted velocity (m yr ⁻¹)	54.3	40.3	49.1	46.4
Dispersion coefficient (m ² yr ⁻¹)	0.07	1.16	0.94	0.46
<i>R</i> ²	0.999	0.989	0.995	0.997
Residence time (d)	2.02	2.72	2.23	2.36

Table 2.2 Nitrate and ClO₄⁻ removal rates calculated using least-squares regression during two experimental stages.

Contaminant	Column	Stage†	Removal rate‡, mmol L ⁻¹ d ⁻¹	Recommended fit§	Half- life, d	R ²
			(NO ₃ -N) μmol L ⁻¹ d ⁻¹ (ClO ₄ ⁻)			
NO ₃ -N	2	1	0.015×C		0.7	0.983
		2	0.011×C		1.0	0.999
		avg.	0.013×C	§	0.8	—¶
	3	1	0.010×C	§	1.1	0.993
		2	0.010×C		1.1	0.997
	4	1	0.025×C	§	0.4	0.947
		2	0.017×C		0.7	0.985
	ClO ₄ ⁻		1	1.41		3.1
2			1.36	§	3.2	0.950
3		1	1.21 (0–12.9cm)		3.6	0.833
		2	0.61 (0–12.9cm)	§	7.0	0.999
		1	1.95 (12.9–30cm)		2.2	0.882
		2	1.84 (12.9–30cm)		2.3	0.991
		avg.	1.89 (12.9–30cm)	§	2.3	—
4		1	0.93		4.6	0.945
	2	1.14	§	3.8	0.968	

† Removal rates were calculated for either Stage 1 or 2 of the experiment or the average of the stages, where indicated.

‡ C is the input NO₃-N concentrations; the reported rates were calculated for the entire length of the columns, except where the column distance range is provided. The distance 0–12.9 cm corresponds to NO₃-N concentrations > 2 mg L⁻¹ and the distance 12.9–30 cm corresponds to NO₃-N concentrations < 2 mg L⁻¹.

§ Recommended rates that provide the best fits for both stages of the experiments.

¶ Not applicable.

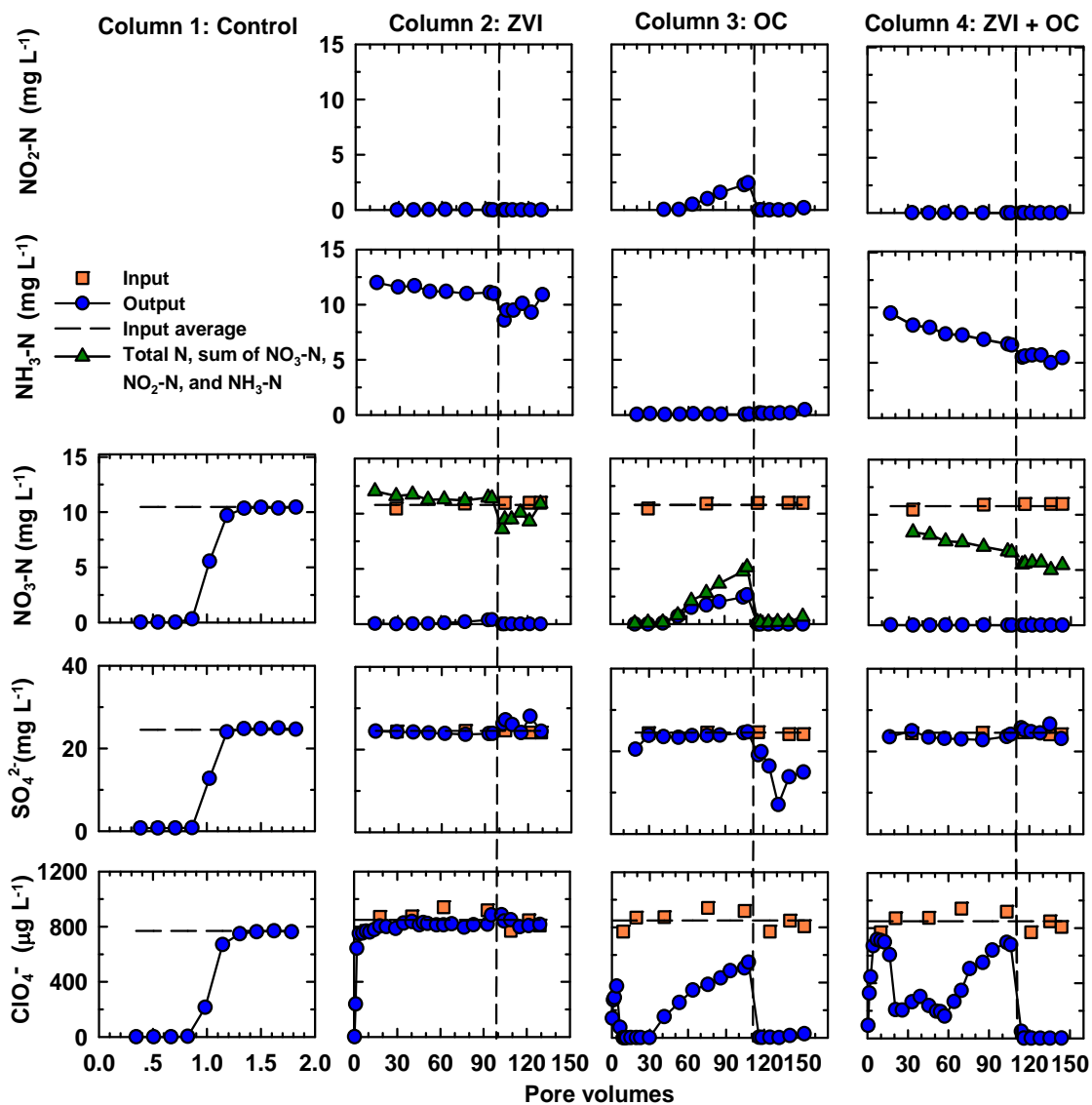


Figure 2.1 Concentrations of NO₂-N, NH₃-N, NO₃-N, SO₄²⁻, and ClO₄⁻ as a function of pore volumes in effluent from columns containing zero-valent Fe (ZVI), organic C (OC), or both; the dashed lines indicate a change in flow rate in each column, dividing the experiment into two stages.

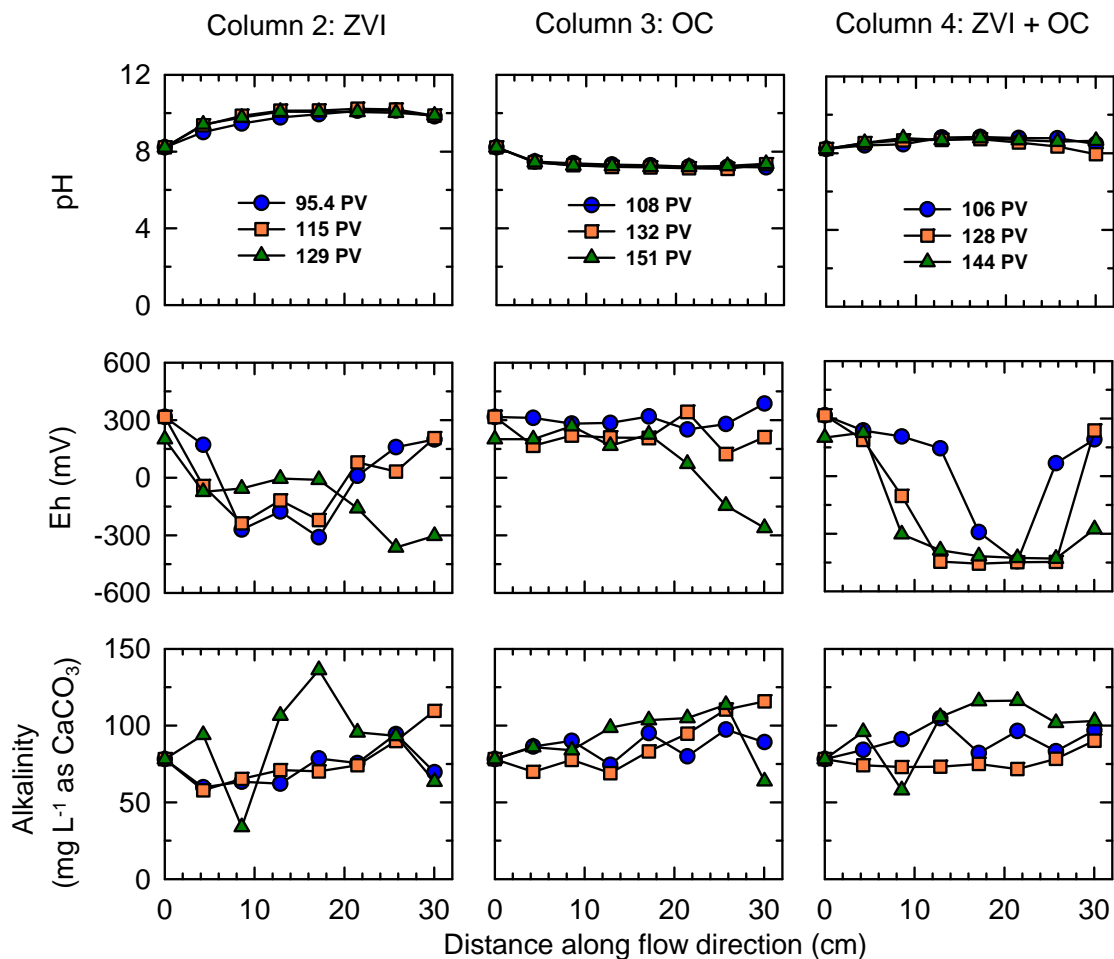


Figure 2.2 Values of pH, Eh, and concentrations of alkalinity as a function of distance along flow direction within the columns containing zero-valent Fe (ZVI), organic C (OC), or both. Blue circle symbols represent data collected during the first stage of the experiment, while orange square and green triangle symbols represent data collected during the second stage of the experiments, given in terms of pore volumes (PV).

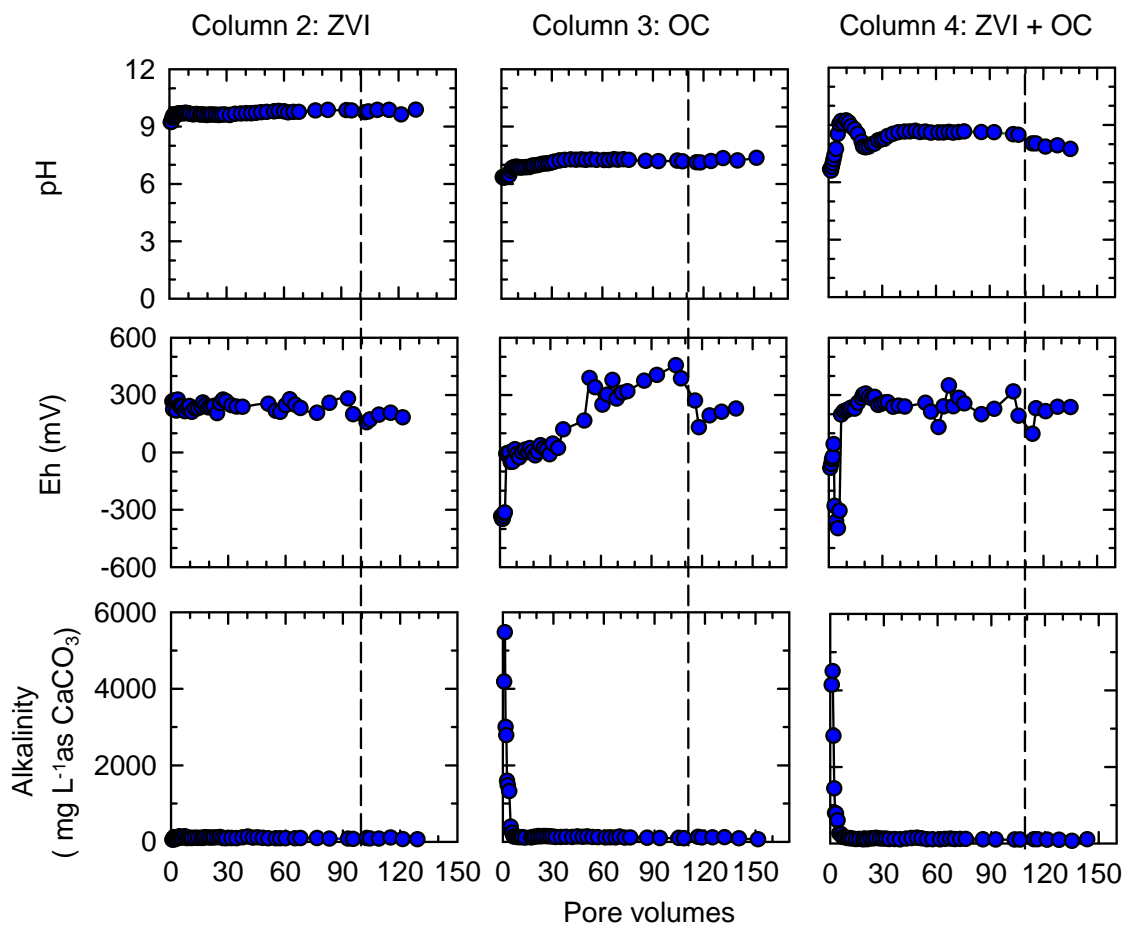


Figure 2.3 Values of pH, Eh, and concentrations of alkalinity as a function of pore volumes in effluent from columns containing zero-valent Fe (ZVI), organic C (OC), or both; the dashed lines indicate a change in flow rate in each column, dividing the experiment into two stages.

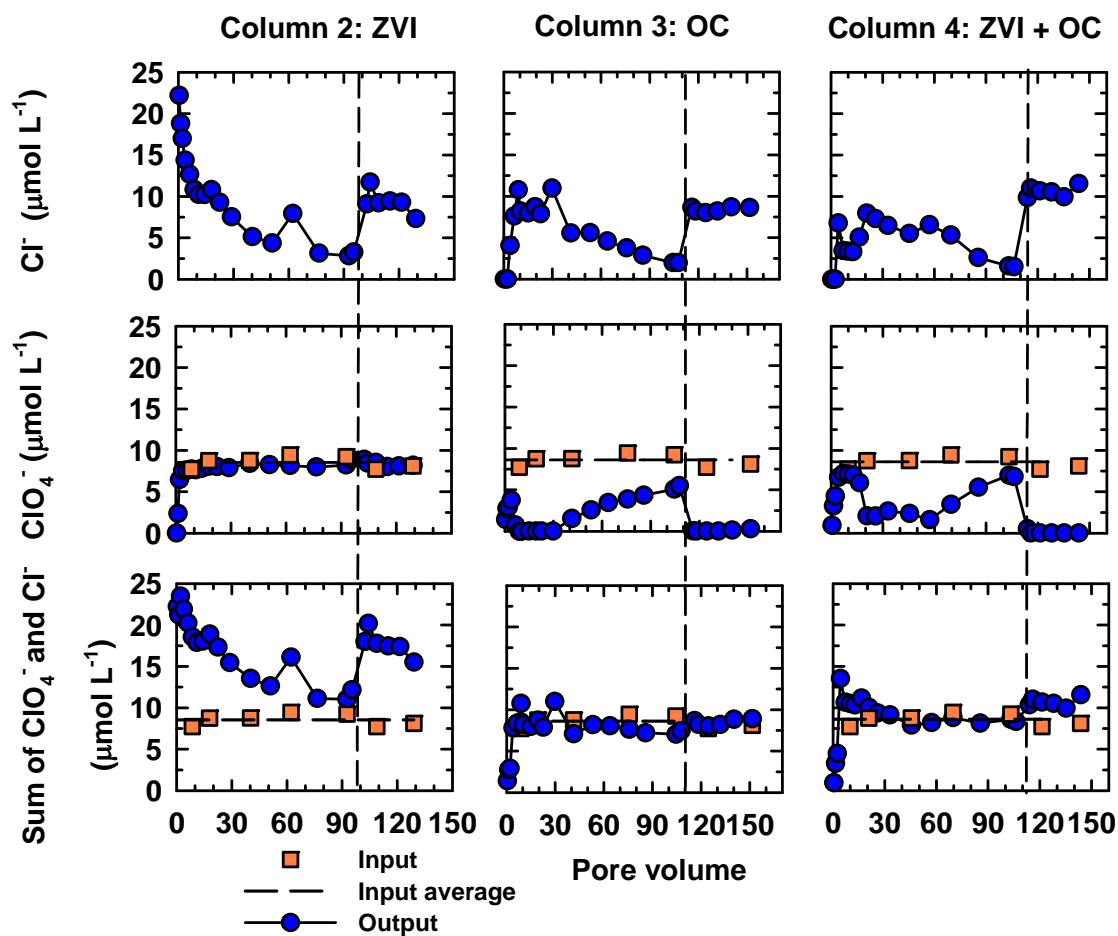


Figure 2.4 Concentrations of Cl^- , ClO_4^- , and total Cl^- (sum of Cl^- and ClO_4^-) as a function of pore volumes in effluent from columns containing zero-valent Fe (ZVI), organic C (OC), or both; the dashed lines indicate a change in flow rate in each column, dividing the experiment into two stages.

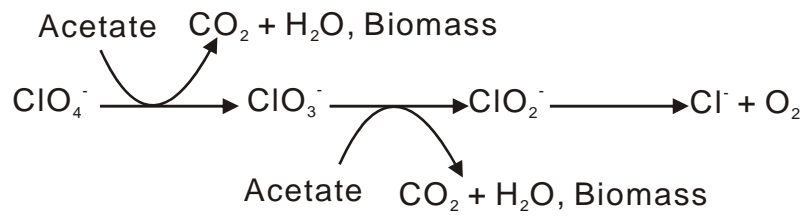


Figure 2.5 Suggested pathway for biological degradation of ClO_4^- (Rikken et al., 1996).

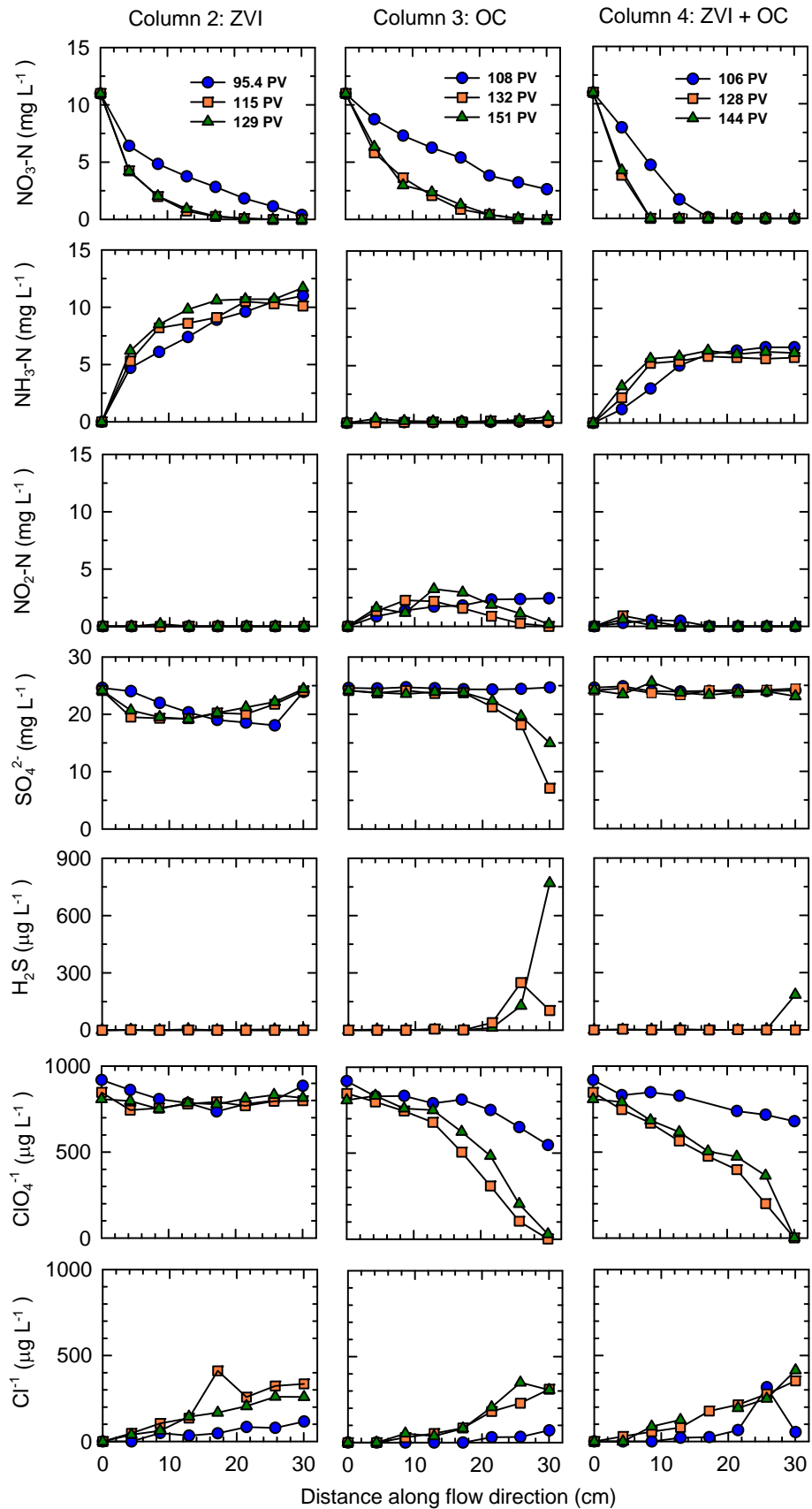


Figure 2.6 Concentrations of $\text{NO}_3\text{-N}$, $\text{NH}_3\text{-N}$, $\text{NO}_2\text{-N}$, SO_4^{2-} , H_2S , ClO_4^- , and Cl^- as a function of distance along flow direction within the columns containing zero-valent Fe (ZVI), organic C (OC), or both. Blue circle symbols represent data collected during the first stage of the experiment, while orange square and green triangle symbols represent data collected during the second stage of the experiments, given in terms of pore volumes (PV).

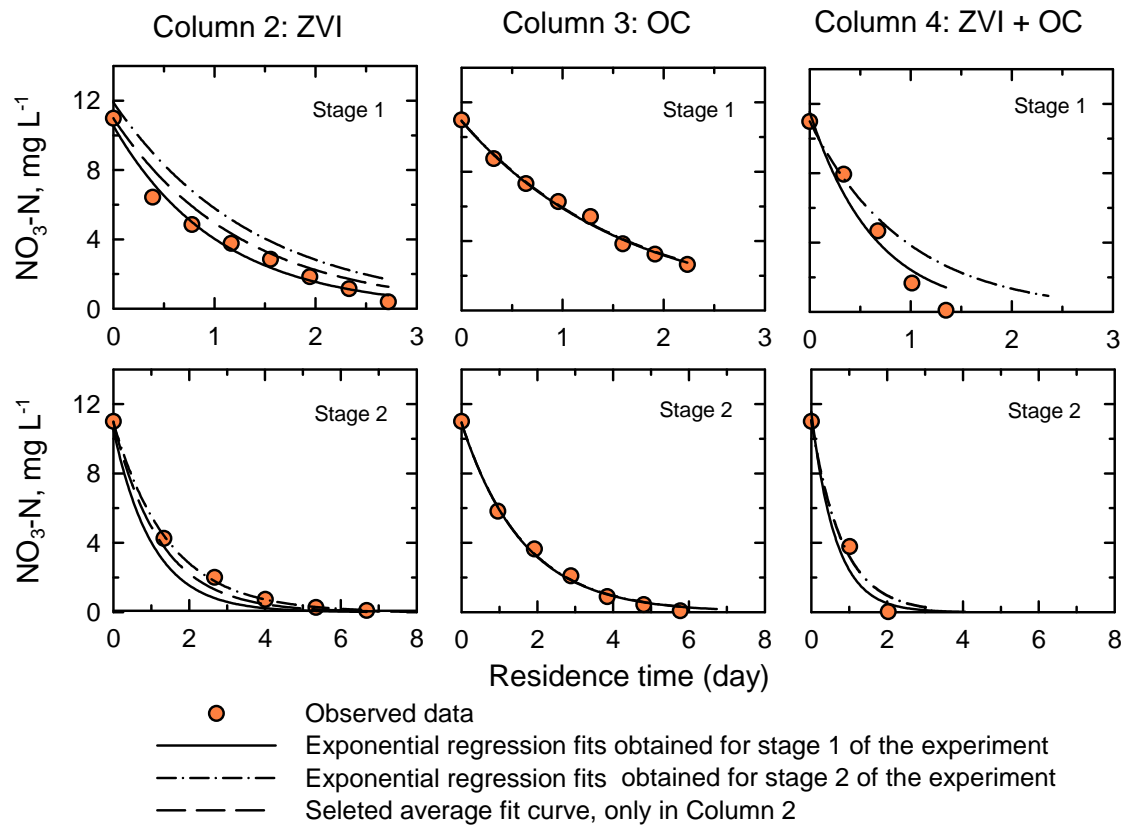


Figure 2.7 Regression fits of NO₃-N removal as a function of residence time in columns containing zero-valent Fe (ZVI), organic C (OC), or both.

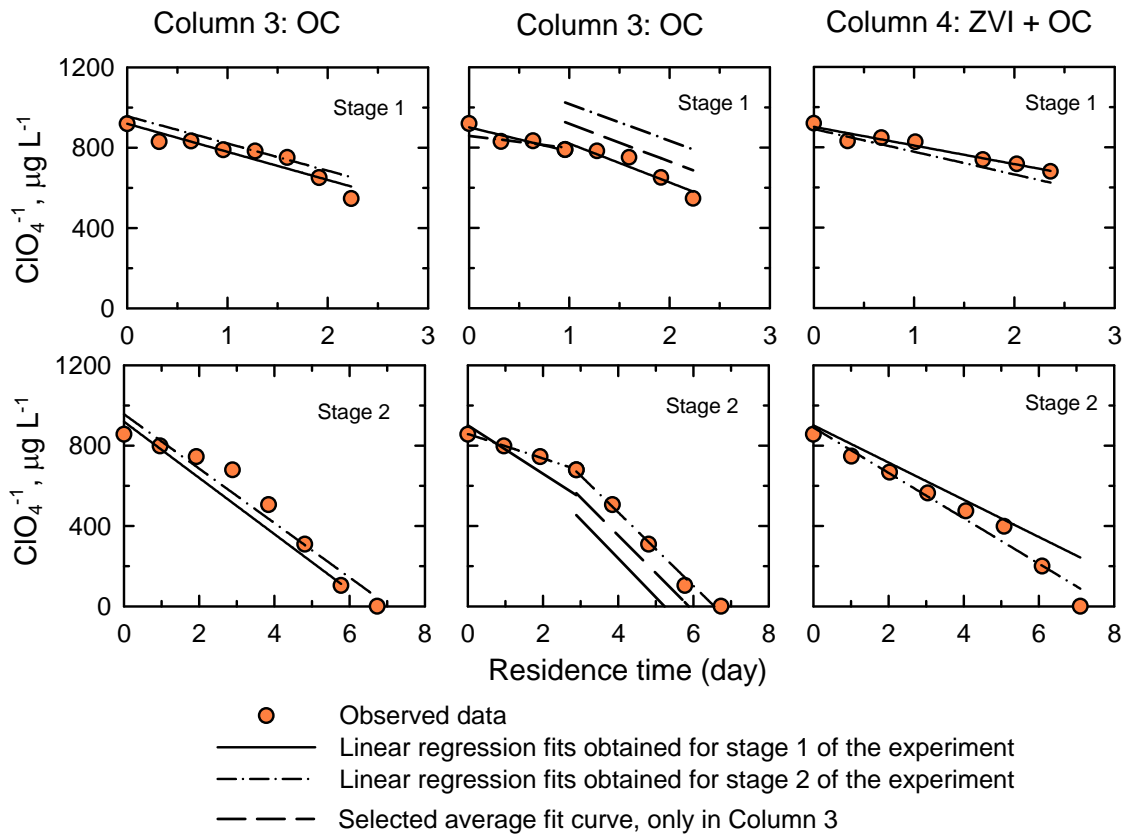


Figure 2.8 Regression fits of ClO_4^- removal as a function of residence time in columns containing organic C (OC) and both zero-valent Fe (ZVI) and OC.

Chapter 3: *Artificial Sweeteners and
Pharmaceuticals as Co-tracers of Municipal
Wastewater in a Receiving River*

3.1 Executive Summary

Wastewater treatment plant (WWTP) effluents are important sources of emerging contaminants at environmentally-relevant concentrations. In this study, water samples were collected from a river downstream of two WWTPs to identify practical tracers for tracking wastewater. The results of the study indicate elevated concentrations of Cl^- , nutrients ($\text{NH}_3\text{-N}$ and NO_2^-), the artificial sweetener acesulfame-K (ACE-K), and the pharmaceuticals carbamazepine (CBZ), caffeine (CAF), sulfamethoxazole (SMX), ibuprofen (IBU), gemfibrozil (GEM), and naproxen (NAP) in the river close to the WWTPs that decreased with distance downstream. A correlation analysis using the Spearman Rank method showed that ACE-K, CBZ, GEM, NAP, and Cl^- were strongly correlated with each other over a 31 km stretch of the river in the study area. The strong correlations of these target compounds indicate that the artificial sweetener ACE-K and the pharmaceuticals CBZ, GEM, and NAP can potentially be used as co-tracers to track wastewater.

3.2 Introduction

Domestic sewage is collected and treated in wastewater treatment plants (WWTPs) where contaminant removal occurs through a series of physical, chemical, and biological processes. However, due to the persistence of some emerging contaminants (ECs) and their metabolites, they cannot be completely removed in WWTPs and become widely distributed in environmental waters (Bueno et al., 2012). Emerging contaminants and their metabolites accumulated in the aquatic environment may cause adverse effects on aquatic ecosystems, such as interference with reproduction and development systems of biota in the environment and development of bacterial resistance (Fent et al., 2006; Morley, 2009; Santos et al., 2010). It is important to track the transport, and monitor the widespread occurrence, of ECs in the aquatic environment using proper tracers.

Chemical tracers for wastewater contamination should be conservative and present in most wastewaters, and ideally be derived only from wastewater. In addition, the concentrations of tracers should be well above analytical detection limits and not vary greatly over time (Kasprzyk-Hordern et al., 2009; Van Stempvoort et al., 2013). Chloride and nutrients have been used as conventional tracers of wastewater contamination; however, other anthropogenic sources, such as road salts and fertilizer, can contribute to loadings in surface and ground waters thus making these constituents potentially less reliable as tracers.

Artificial sweeteners such as acesulfame-K (ACE-K) and sucralose are particularly widespread and persistent in surface water and groundwater, and therefore have been suggested as ideal tracers of domestic wastewater in the

environment (Buerge et al., 2009; Lubick, 2009; Scheurer et al., 2009). In addition, some pharmaceuticals, such as carbamazepine (CBZ) and caffeine (CAF), have been proposed as indicators of wastewater contamination in the environment (Andreozzi et al., 2002; Clara et al., 2004; Kurissery et al., 2012). However, CBZ and naproxen (NAP) can adsorb to sediment (Chefetz et al., 2008; Durán-álvarez et al., 2012) and CAF tends to biodegrade (Buerge et al., 2003). These natural attenuation processes make these pharmaceuticals less ideal as wastewater tracers. Therefore, the use of multiple tracers would greatly increase the confidence of identifying wastewater in aquatic environments (Van Stempvoort et al., 2013; Williams et al., 2013). The purpose of this study is to evaluate the potential use of ECs as co-tracers to track wastewater in receiving water bodies.

In this study, samples of river water were collected and analyzed for several potential tracers to track wastewater from two WWTPs in the Grand River watershed. The Grand River is the largest watershed in southwestern Ontario, Canada, flowing 300 km through a number of municipalities before discharging to Lake Erie. The persistence of several target compounds—ACE-K, CBZ, CAF, NAP, sulfamethoxazole (SMX), 3,4-methylenedioxyamphetamine (MDA), 3,4-methylenedioxymethamphetamine (MDMA), ibuprofen (IBU), and gemfibrozil (GEM)—was compared to conventional wastewater parameters to determine the potential use of these compounds as tracers.

3.3 Materials and Methods

3.3.1 Water Sampling and Field Analyses

Samples of river water were collected at 10 locations over a distance of 32.1 km along the Grand River near the cities of Waterloo and Kitchener (southwestern Ontario, Canada) in August 2012 and July 2013. Winter samples were collected in December 2014; sampling results are updated in Appendix B (Table B.1 and Figures B.1-B.3). The 10 sampling locations are labeled GR 1 to GR 10 (Figure 3.1). GR 8 and GR 1 are upstream of GR 2 (the location of the first WWTP; WWTP-1), then GR 3, 9, 10, 4, 5, 6, 7 are located sequentially downstream. GR 5 is located at the intake of a Water Treatment Plant-1 (WTP-1) where Grand River water is treated to provide a drinking water supply, and GR 6 is located 0.1 km downstream of the effluent of WWTP-2. The average discharge of the Grand River measured at a gauge station near GR 6 (Grand River near DOON, station number 02GA048) (Environment Canada, 2013) was $9.8 \text{ m}^3 \text{ s}^{-1}$ for the sampling dates in 2012 (August 9–10) and $56.7 \text{ m}^3 \text{ s}^{-1}$ for the sampling dates in 2013 (July 8–9, during a rain event).

All river water samples were collected in a consistent manner 5 m away from the river bank on the side of the river into which WWTP-1 and WWTP-2 effluents are discharged. Additional samples were collected directly from the effluent discharge pipe from the wastewater treatment plant (WWTP-1), and from the water treatment plant (WTP-1) influent reservoir. Duplicate samples were collected at the two WWTPs. These locations were selected to provide samples most representative of the WWTP-1 effluent and of the intake of WTP-1. Samples were obtained using Teflon tubing (6.5 m in length)

connected to a peristaltic pump (MasterFlex, Cole-Parmer Instrument Company, CA). All samples, except those for pH, Eh, and electrical conductivity (EC) measurements, were filtered through 0.45 μm Thermopor membrane filters to determine alkalinity and concentrations of Cl^- , SO_4^{2-} , NO_3^- , NO_2^- , $\text{NH}_3\text{-N}$, $\text{PO}_4\text{-P}$, and the target pharmaceuticals and artificial sweetener. Determination of pH, Eh, alkalinity, and EC was performed on site immediately after sample collection. The sampling program included: collection of 2 L river water in two 1 L amber glass bottles for pharmaceutical and ACE-K analysis; 30 mL river water in a 35 mL polypropylene bottle for $\text{NH}_3\text{-N}$ and $\text{PO}_4\text{-P}$ analysis; and 10 mL river water in a 15 mL polypropylene bottle for anion analysis. The samples for $\text{NH}_3\text{-N}$, $\text{PO}_4\text{-P}$, pharmaceuticals, and artificial sweetener were acidified on site with H_2SO_4 to $\text{pH} < 2$ while samples for anions (Cl^- , SO_4^{2-} , NO_3^- , NO_2^-) were not. All samples were stored at 4 $^\circ\text{C}$ and analyzed within one month of collection, except for pharmaceuticals and ACE-K samples which were analyzed within three days after collection.

3.3.2 Analysis of Water Samples

3.3.2.1 Primary Wastewater Parameters

Values of pH were determined using a pH electrode (Ross combination, Orion 815600) calibrated with standard pH 7.0 and pH 10.0 buffers prior to each measurement, and checked with a pH 7.0 buffer after each measurement. Values of Eh were determined using an Eh electrode (Pt-billeted Ag/AgCl combination, Orion 9678BNWP) checked using Zobell's (Nordstrom, 1977) solution before and after each measurement. Electrical conductivity was measured using an Orion 013005MD conductivity cell. The performance of the electrical conductivity cell was checked with a 0.01M KCl solution prior to each measurement. Alkalinity

values were determined using standardized H₂SO₄ and a Hach digital titrator following Titration Method 2320 B (APHA, 1992).

Anion (Cl⁻, SO₄²⁻, NO₃⁻, NO₂⁻) concentrations were determined by ion chromatography (Dionex ICS-5000+, Mississauga, CA). Ammonia (NH₃-N) and ortho-phosphate (PO₄-P) concentrations were determined using a Hach spectrophotometer DR/8400 following the salicylate method (4500-NH₃)(APHA, 2005a) and ascorbic acid method (4500-P: E) (APHA, 2005b), respectively.

3.3.2.2 Trace Wastewater Parameters

ACE-K and the eight pharmaceutical compounds were analyzed using solid-phase extraction and high-performance liquid chromatography (HPLC) followed by tandem mass spectrometry using previously published methods (Scheurer et al., 2009; Stafiej et al., 2007; Vanderford & Snyder, 2006), with slight modifications such as inclusion of isotope dilution techniques for each study compound and optimization of instrument operating conditions. Native compounds were supplied by Sigma-Aldrich (Oakville, Canada) with the exception of ACE-K obtained from Toronto Research Chemicals Inc. (Toronto, Canada). Isotope-labeled standards, including ACE-K-d4 and SMX-d4 (Toronto Research Chemicals Inc., Toronto, Canada), MDA-d5 and MDMA-d5 (Cerilliant Inc., Texas, USA), and CBZ-d10, CAF-d3, IBU-d3, GEM-d6, and [¹³C]-NAP (Cambridge Isotope Laboratory Inc., Cambridge, USA) were obtained as dry powders. Standard stock solutions of ~1000 µg L⁻¹ were prepared by dissolving each compound in methanol. Working standard solutions containing all analytes were prepared by serial dilution in methanol:water 50:50 vol:vol. HPLC-grade ammonium acetate and formic acid

were obtained from Sigma-Aldrich (Oakville, Canada). Ultrapure (Type 1) water was generated using a MilliQ A10 water system (18.2 M Ω .cm @ 25 °C).

Prior to analysis, 600 mL aliquots of aqueous samples were spiked with a consistent amount of internal standard mixture. These samples were passed through solid-phase extraction (SPE) cartridges (Oasis HLB 6 mL glass cartridges; Waters Corp., Mississauga, Canada) pre-conditioned with 3 \times 2 mL methanol and then equilibrated with 3 \times 2 mL ultrapure water. After loading the 600 mL samples, the cartridges were washed using 3 \times 2 mL 5 vol. % methanol then eluted with 3 \times 2 mL methanol. The eluate was collected in an amber glass vial and stored at 4 °C until analysis.

The extracts were analyzed using an Agilent 1100 HPLC (Agilent Technologies, Mississauga, Canada) followed by electrospray tandem mass spectrometry (MS/MS; 4000 Q TRAP, Applied Biosystems, Foster City, USA). Caffeine, SMX, CBZ, MDA, and MDMA were analyzed in electrospray ionization positive (ESI+) mode, while IBU, GEM, NAP, and ACE-K were analyzed in ESI negative (ESI-) mode. The gradient and mobile phases were changed from previous methods based on the HPLC analytical columns and mass spectrometer (MS) requirements. The compound and source-dependent parameters of the MS were modified to obtain an optimum signal response. The mobile phases for analysis in ESI+ mode consisted of 0.1% formic acid and 5 mM ammonium acetate in water (phase A) and 99.9% MeOH with 0.1% formic acid (phase B). A gradient elution started at 10% B for 3 min, increased to 90% B in 10 min, and then held at 90% B min for 10 min. The flow rate was 1000 μ L min⁻¹ and the

injection volume was 15 μL . The mobile phases for analysis in ESI- mode consisted of 6.9 mM acetic acid in 300 mL acetonitrile and 700 mL water (phase A) and 100% acetonitrile (phase B). A gradient elution started at 12% B, then increased linearly to 40% in 10 min and held at 40% for 10 min. The injection volume was 10 μL and the flow rate was 1000 $\mu\text{L min}^{-1}$. For ACE-K analyzed in ESI- mode, the mobile phases consisted of 20 mM ammonium acetate in water (phase A) and 20 mM ammonium acetate in methanol (phase B). The gradient elution started at 2% B, then increased linearly to 75% in 8 min and held at 75% for 8 min. The injection volume was 10 μL and the flow rate was 1000 $\mu\text{L min}^{-1}$.

A mixed standard containing ACE-K, CBZ, CAF, SMX, IBU, NAP, and GEM was used for method calibration. The same amount of isotope-labeled compounds was added to the calibration standards, method standards, and unknown samples. The recovery of the isotope-labeled compounds was used to correct the response of the instrument to each compound. Nine-point calibration curves from 5 to 10,000 ng L^{-1} were established by analysis of standard mixtures prepared in 50% methanol: 50% water. Tap water samples spiked with the analyte mixtures and internal standards and extracted following the same procedure as the unknown samples were used to evaluate the addition of the SPE step to the method. The limits of detection (LOD) and quantification (LOQ) were calculated at three and 10 times the signal-to-noise values, respectively. The method detection limits (MDL) were determined by extracting 14 deionized water samples fortified with labeled analytes at concentrations three to five times the LOD, depending on the expected MDL and internal standard at the same concentration level used in the method. The

MDL was calculated by multiplying the standard deviation of the replicate measurements by the Student's t value for n-1 degrees of freedom. The MDLs determined were 41.9 ng L⁻¹ for ACE-K, 99 ng L⁻¹ for CAF, 10.4 ng L⁻¹ for SMX, 17.1 ng L⁻¹ for CBZ, 38.8 ng L⁻¹ for MDA, 3.9 ng L⁻¹ for MDMA, 29.6 ng L⁻¹ for IBU, 3.1 ng L⁻¹ for GEM, and 9.7 ng L⁻¹ for NAP. The LOQs determined were four to 230 times lower than MDL values.

Methanol:water samples (continuous calibration verification samples) were analyzed at initial instrument calibration and after every 10 unknown samples. Quality assurance/quality control results showed that the concentrations of all target compounds in the calibration standard blanks and method standard blanks were consistently below detection limits. The absolute analyte and internal standard recovery for continuous calibration verification samples ranged from 84 to 116%. Relative method recovery for ACE-K ranged from 94 to 118% across the standard curve from 0.1 to 100 µg L⁻¹. The relative internal standard recovery of ACE-K for unknown samples ranged from 71 to 95%. Relative method recovery for CAF, SMX, CBZ, MDA, and MDMA ranged from 84 to 120% across the standard curve (0.01–10 µg L⁻¹ for SMX and MDMA, 0.05–10 µg L⁻¹ for CBZ and MDA, 1–10 µg L⁻¹ for CAF). Relative internal standard recovery of CAF, SMX, CBZ, MDA, and MDMA for unknown samples ranged from 70 to 109%; CBZ had the best absolute internal standard recovery (84 – 97%) for unknown samples. Relative method recovery for IBU, GEM, and NAP ranged from 91 to 110% across the standard curve (0.02 – 10 µg L⁻¹); the corresponding relative internal

standard recovery for unknown samples was 94 – 119%. The recovery of duplicated, spiked, and repeated samples was 75–121%.

3.4 Results and Discussion

3.4.1 Grand River Sampling Results

The average pH of the river water samples was ~7.9 during the 2012 and 2013 sampling events, with lower values of 7.6 – 7.8 observed near the effluent of WWTP-1. Eh varied over the sampling distance of the river in 2012, with lower values observed near the effluents of both WWTP-1 and WWTP-2; however, values were relatively constant (~350 mV) in 2013 likely due to the larger discharge of the river at the time of sampling. The highest alkalinity and electrical conductivity values over the sampling distance in both 2012 and 2013 were observed near the effluent of WWTP-1, and higher values were observed in 2013 (alkalinity, ~330 as CaCO₃ mg L⁻¹; EC, ~870 μS cm⁻¹) than in 2012 (Figure 3.2).

Chloride (Cl⁻) reached its highest concentration of ~150 mg L⁻¹ near the effluent of WWTP-1 in both 2012 and 2013, and reached a second peak concentration (~87 mg L⁻¹) near the effluent of WWTP-2 in 2012. Elevated concentrations of SO₄²⁻ and PO₄-P were observed near the effluents of both WWTPs in 2012, but the concentrations of SO₄²⁻ and PO₄-P were less variable in 2013 compared to 2012 likely due to the much larger river discharge in 2013. Incomplete removal of nitrogen (nitrification and denitrification) by WWTP-1 likely resulted in the generally low observed concentrations of NO₃⁻ and higher concentrations of NO₂⁻ and NH₃-N in the effluent. Concentrations of NO₃⁻ decreased from a background concentration of ~15 to 8.5 mg L⁻¹ at the effluent of WWTP-1, where the highest

concentrations of NO_2^- (4.6 mg L^{-1}) and $\text{NH}_3\text{-N}$ (3.0 mg L^{-1}) were observed in July 2013 (Figure 3.2). In addition, small increases in the concentrations of NO_2^- and $\text{NH}_3\text{-N}$ were observed near the effluent of WWTP-2. Elevated concentrations of $\text{NH}_3\text{-N}$ near WWTPs have also been observed in other studies (Sonthiphand et al., 2013).

The concentrations of ACE-K and the target pharmaceuticals were observed to follow a similar trend over the sampling distance, with the highest concentrations observed near the effluent of WWTP-1 in both 2012 and 2013; this is consistent with other studies of pharmaceutical compounds in southwestern Ontario rivers (Spoelstra et al., 2013). The concentrations of the target compounds downstream of WWTP-1 decreased gradually with distance and, when discharge from WWTP-2 entered the river, a secondary concentration peak of target compounds was noted, especially in 2012 (Figure 3.3). The concentrations of target compounds 10 km downstream of WWTP-1 were at least one order of magnitude lower than those observed at the effluent of WWTP-1, likely as a result of dilution and dispersion and other natural attenuation processes such as biodegradation and photolysis (Carrara et al., 2008; Fono et al., 2006).

Concentrations of ACE-K ($\sim 6500 \text{ ng L}^{-1}$ in 2012 and $\sim 4000 \text{ ng L}^{-1}$ in 2013) were consistent with those observed at the effluent of WWTP-1 in 2007–2009 (Spoelstra et al., 2013). ACE-K is particularly conservative and recalcitrant, and has been proposed as an ideal marker for wastewater in the environment (Buerge et al., 2009; Robertson et al., 2013). Furthermore, observed ACE-K concentrations were well above the MDL ($\sim 40 \text{ ng L}^{-1}$), and were one or two orders of magnitude

higher in concentration than other target pharmaceuticals (Figure 3.3). Its conservative behavior and high detectable concentrations suggest that ACE-K may be a suitable tracer of wastewater in river systems.

Concentrations of CAF at the effluent of WWTP-1 in 2012 were $\sim 3300 \text{ ng L}^{-1}$, which is one order of magnitude larger than observed in 2013 ($\sim 280 \text{ ng L}^{-1}$). Caffeine is extensively ingested in food, beverage, and drugs, and has been reported as a stable compound under variable environmental conditions. Caffeine has been widely used as an anthropogenic indicator of domestic wastewater contamination (Buerge et al., 2003; Kurissery et al., 2012; Seiler et al., 1999). Metcalfe et al. (2003b) report that CAF is detectable in most sewage treatment plants and surface waters in Lake Ontario and Lake Erie in Canada. Buerge et al. (2003) observe CAF concentrations of up to $9.5 \mu\text{g L}^{-1}$ in WWTP effluents in Switzerland, and up to 250 ng L^{-1} in downstream lakes and rivers.

Illicit amphetamine compounds, including MDA and MDMA, are used as recreational and empathogenic drugs. The concentrations of MDA and MDMA in the study area over the entire sampling distance were below the MDLs in both 2012 and 2013. However, these compounds have been widely detected in wastewaters at ng L^{-1} levels, with MDMA observed to exhibit relatively higher detectable concentrations and frequencies than MDA (Lai et al., 2013; Nefau et al., 2013; Van Nuijs et al., 2011). In addition, Metcalfe et al. (2010a) report MDMA at concentrations up to 35 ng L^{-1} , but MDA at concentrations below the detection limit in treated and untreated wastewaters from three Canadian cities.

Sulfamethoxazole (SMX), a sulfonamide antibiotic, has been widely used in human and veterinary medicine. The highest concentration of SMX ($\sim 37 \text{ ng L}^{-1}$) was observed near WWTP-1 in 2012 with a somewhat lower concentration ($\sim 20 \text{ ng L}^{-1}$) observed in 2013. Sulfamethoxazole has been frequently detected in environmental water samples (Karthikeyan & Meyer, 2006; Miao et al., 2004; Milić et al., 2013; Watts et al., 1983). Yargeau et al. (2007) report up to 578 ng L^{-1} of SMX downstream of a WWTP in the Yamaska River, Quebec, Canada.

Carbamazepine (CBZ), an antiepileptic drug, was observed near WWTP-1 in the Grand River at a concentration of $\sim 146 \text{ ng L}^{-1}$; this is similar to concentrations observed in another Canadian river (Yargeau et al., 2007). Carbamazepine has been found to be recalcitrant in conventional and biological WWTPs (Clara et al., 2005; Joss et al., 2005) and is widespread in the environment. Miao et al. (2005) report the ubiquitous and persistent nature of CBZ and its five metabolites through different stages of treatment in a Canadian WWTP.

Ibuprofen (IBU) and naproxen (NAP) are two common non-steroidal anti-inflammatory drugs, and gemfibrozil (GEM) is widely used as a lipid regulator. The highest concentrations of IBU (160 ng L^{-1}), GEM (29 ng L^{-1}), and NAP (506 ng L^{-1}) were observed near the effluent of WWTP-1 in 2012; lower concentrations were observed in 2013. Widespread distribution of IBU, GEM, and NAP in wastewater and downstream river water at ng L^{-1} concentrations has been reported since 1998 and attributed to their variable removal (IBU, $> 90\%$; NAP, $\sim 80\%$; GEM, $\sim 55\%$) by conventional WWTPs (Huang et al., 2011; Lishman et al., 2006;

Ternes, 1998). IBU, GEM, and NAP have also been observed to persist in a subsurface receiving aquifer (Carrara et al., 2008).

Concentrations of ACE-K and most of the target pharmaceuticals were lower in 2013 than in 2012. Secondary concentration peaks of ACE-K, SMX, CBZ, IBU, GEM, and NAP observed near the effluent of WWTP-2 in 2012 were also not as apparent in 2013. This is likely due to either the larger discharge when sampling was conducted in 2013 vs. 2012 and/or implementation of a new ultraviolet (UV) facility at WWTP-2 in 2013 that enhanced effluent disinfection but also likely removed some target contaminants through UV photolysis (Coiffard et al., 1999; De la Cruz et al., 2012; Gagnon et al., 2008; Ngouyap Mouamfon et al., 2010).

3.4.2 Mechanisms Affecting the Transport of the Target Compounds

Natural attenuation processes account for a significant decrease in concentrations of wastewater-derived contaminants in surface water bodies (Fono et al., 2006) and groundwater (Carrara et al., 2008). During transport from WWTPs to downstream areas, the concentrations of the seven target compounds considered in this study can be affected by physical processes, primarily dilution and dispersion. Other chemical and biological natural attenuation processes, such as sorption, hydrolysis, biotransformation, and photolysis (Schwarzenbach et al., 2002) also may affect the transport of target compounds, but likely have a limited influence due to the relatively short travel time of target compounds in the study area. However, it remains important to determine the relative influence of these processes on contaminant transport in the Grand River and other rivers.

ACE-K has been reported to undergo photo-degradation in aqueous systems, following first-order rates of removal (Coiffard et al., 1999). Benotti and Brownawell (2009) report that CAF is biodegradable in estuarine and coastal waters, with an average half-life of 5.4 days. The antibiotic SMX has been reported to undergo biotransformation (Larcher & Yargeau, 2012) and direct photolysis (Periša et al., 2013) in aqueous systems. In addition, direct photolysis is an important process for removing SMX from surface water (Lam & Mabury, 2005). CBZ is reported to be resistant to biodegradation but may undergo indirect photo-degradation (Matamoros et al., 2009) and adsorption reactions (Williams & Adamsen, 2006). The indirect photo-degradation rate of CBZ is limited ($t_{1/2} = 8\text{--}39$ h), however, and strongly dependent on the dissolved organic carbon (DOC) concentration in solution (Matamoros et al., 2009).

Removal of NAP through natural attenuation processes is more variable. Approximately 40% of NAP present in surface water during daylight hours has been reported to be removed through photolysis ($t_{1/2} = 1.7$ h), with the remainder most likely removed via sorption (Lin et al., 2006). Strong sorption of NAP to soils also has been observed (Lin & Gan, 2011). Biotransformation reactions can be an important attenuating process for IBU and GEM in river water, with half lives of 5.4 h and 2.7 h respectively (Fono et al., 2006; Lin et al., 2006). IBU and GEM exhibit relatively longer photodegradation half-lives of ~ 15 h (Lin & Reinhard, 2005).

3.4.3 Acesulfame-K and Pharmaceuticals as Co-tracers in the Grand River

The concentrations of the target compounds exhibited similar changes over the sampling distance, with a primary peak in concentrations observed at the effluent of WWTP-1 and a secondary peak near WWTP-2 (Figure 3.3). Correlation analysis using Spearman Rank correlation coefficients (ρ) of the target compounds and Cl^- indicated that ACE-K and CBZ were very strongly correlated with Cl^- over the sampling distance downstream of WWTP-1, with ρ values ranging from 0.95 to 1.00 in both 2012 and 2013; GEM and NAP were strongly correlated with ACE-K, CBZ, and Cl^- with ρ values ranging from 0.69 to 0.89 in both 2012 and 2013; and CAF, SMX, and IBU were moderately correlated with ACE-K, CBZ, and Cl^- (Tables 3.1 and 3.2, Figure 3.4). Concentrations of MDA and MDMA were below the MDLs in both 2012 and 2013, therefore no correlations could be determined. Similarly, the Spearman Rank correlation for SMX in 2012 was not calculated due to the low concentrations ($< \text{MDL}$) observed.

The artificial sweetener ACE-K and pharmaceuticals CBZ, IBU, GEM, and NAP exhibited strong correlations over the sampling distance downstream of WWTP-1 in 2013, but weaker correlations in 2012. The pharmaceuticals CAF and SMX exhibited moderate correlations with other target compounds (Tables 3.1 and 3.2). This analysis indicates that ACE-K, CBZ, GEM, and NAP can potentially be used as co-tracers of the wastewater over the sampling distance considered. The very strong correlation between ACE-K, CBZ and Cl^- , however, suggests that Cl^- may also be used as a waste-water indicator. However, previous studies have

indicated that Cl^- may be affected by other sources, including road salt application (Cooke, 2006). Alkalinity and electrical conductivity were weakly or moderately correlated with target contaminants in 2012, and moderately or strongly correlated with target contaminants in 2013. Due to this inconsistency, alkalinity and electrical conductivity are not considered to be effective co-tracers of wastewater.

3.5 Conclusions

This study indicates that the decline in concentrations of bulk wastewater constituents, ACE-K, and a suite of pharmaceutical compounds downstream from two WWTPs is due to dilution and, for some compounds, other attenuation mechanisms. Of the compounds studied, the artificial sweetener ACE-K and three pharmaceutical compounds (CBZ, GEM, and NAP) had the greatest persistence. These compounds dissipated at the same rate as the conservative anion Cl^- , indicating that declines in concentration were primarily controlled by dilution alone. The use of multiple tracers, such as artificial sweeteners combined with pharmaceutical compounds, would greatly increase confidence when tracking wastewater in aquatic environments throughout the year.

Table 3.1 Spearman rank correlation coefficients (ρ)[†] of the target compounds and Cl⁻ over the sampling distance in the Grand River in August 2012.

	CAF	CBZ	IBU	GEM	NAP	Cl ⁻
ACE	0.36	0.98	0.45	0.69	0.69	0.98
CAF		0.40	0.93	0.64	0.64	0.40
CBZ			0.52	0.71	0.71	1.00
IBU				0.79	0.79	0.52
GEM					1.00	0.71
NAP						0.71

Note: [†] Positive values were interpreted as follows: 0.8-1.0 = very strong; 0.6-0.8 = strong; 0.4-0.6 = moderate; 0.2-0.4 = weak; 0.0-0.2 = weak or no relationship.

Table 3.2 Spearman rank correlation coefficients (ρ)[†] of the target compounds and Cl⁻ over the sampling distance in the Grand River in July 2013.

	CAF	SMX	CBZ	IBU	GEM	NAP	Cl ⁻
ACE	0.71	0.59	0.90	0.71	0.89	0.74	0.98
CAF		0.84	0.62	0.71	0.85	0.64	0.62
SMX			0.54	0.64	0.73	0.59	0.56
CBZ				0.90	0.92	0.93	0.95
IBU					0.92	0.98	0.76
GEM						0.92	0.89
NAP							0.81

Note: [†] Positive values were interpreted as follows: 0.8-1.0 = very strong; 0.6-0.8 = strong; 0.4-0.6 = moderate; 0.2-0.4 = weak; 0.0-0.2 = weak or no relationship.

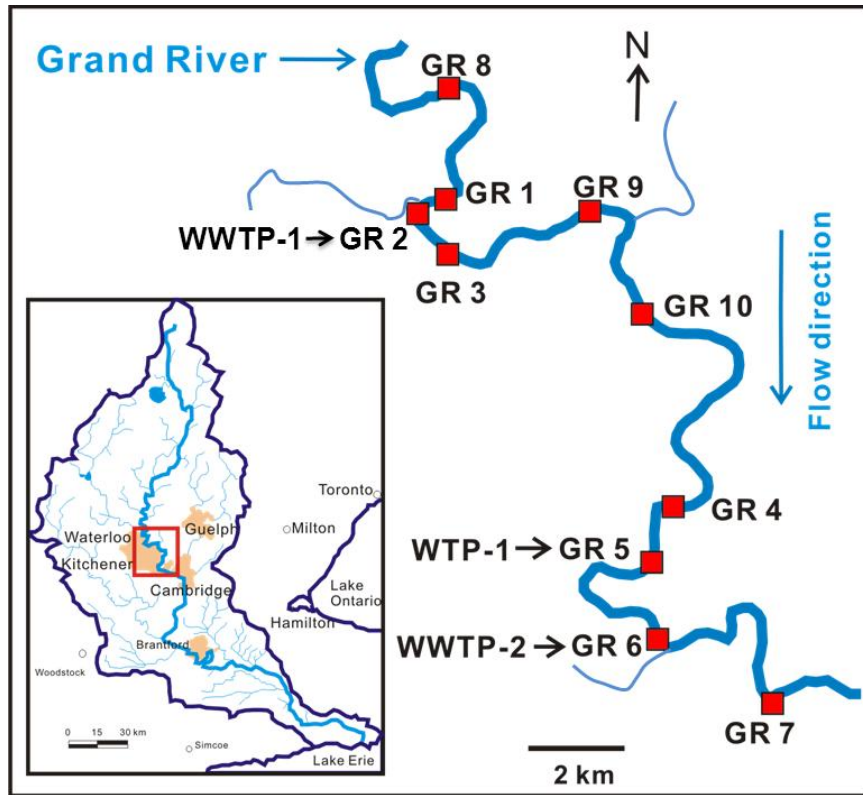


Figure 3.1 Sampling locations along the Grand River, southwestern Ontario, Canada.

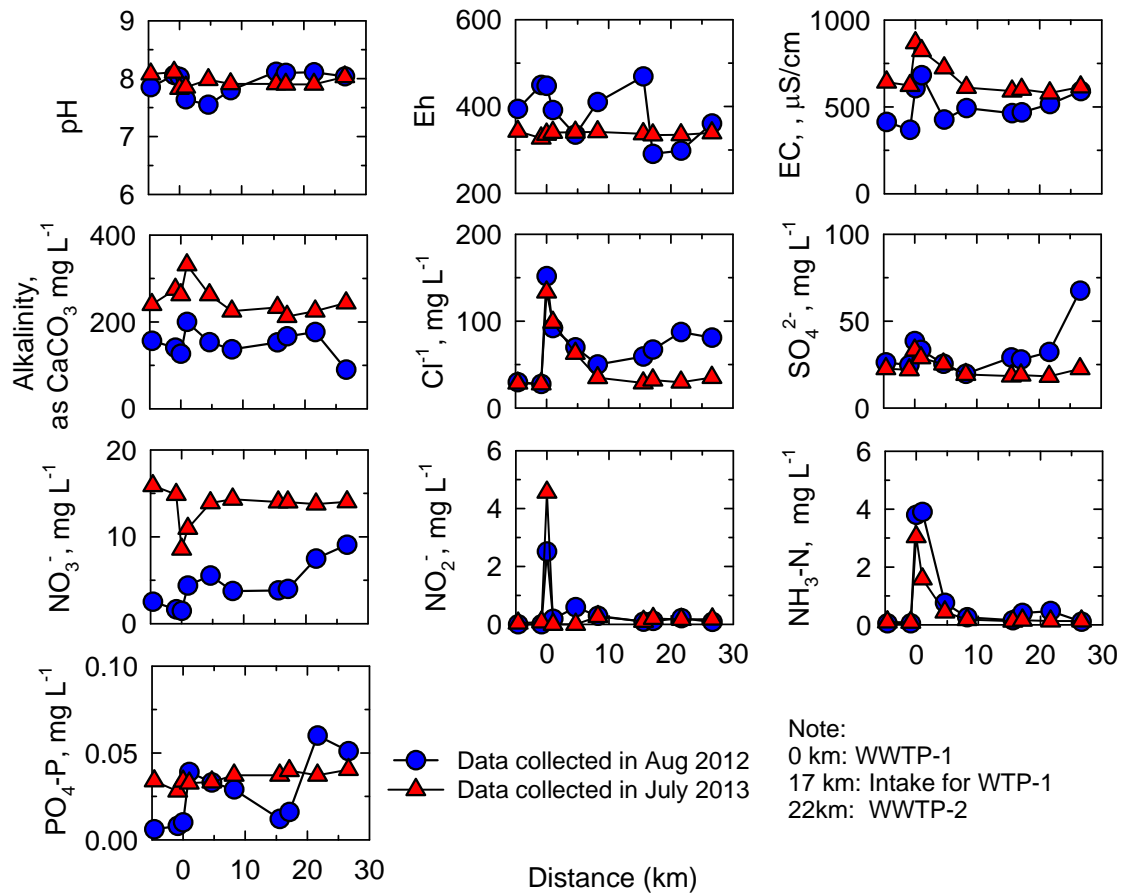


Figure 3.2 Concentrations of pH, Eh, alkalinity, electrical conductivity (EC), Cl^- , NO_3^- , NO_2^- , $\text{NH}_3\text{-N}$, SO_4^{2-} , and $\text{PO}_4\text{-P}$ as a function of sampling distance.

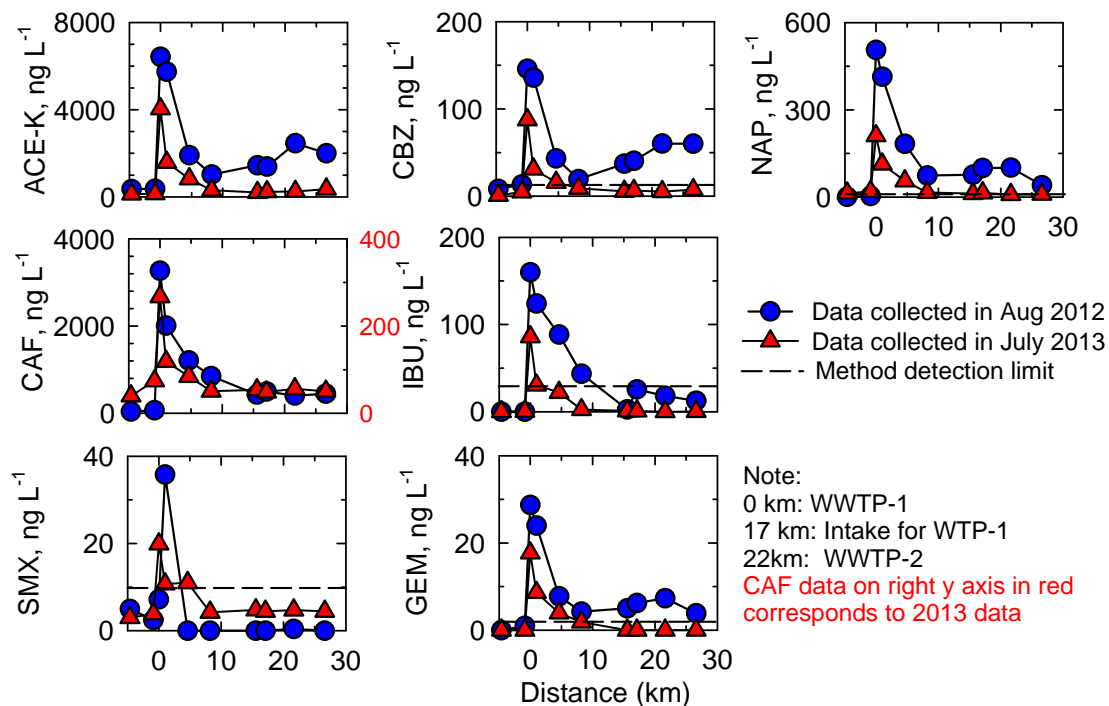


Figure 3.3 Concentrations of acesulfame-K (ACE-K), caffeine (CAF), sulfamethoxazole (SMX), carbamazepine (CBZ), ibuprofen (IBU), gemfibrozil (GEM), and naproxen (NAP) as a function of sampling distance. The method detection limits of ACE-K and CAF were too low to appear in the figure.

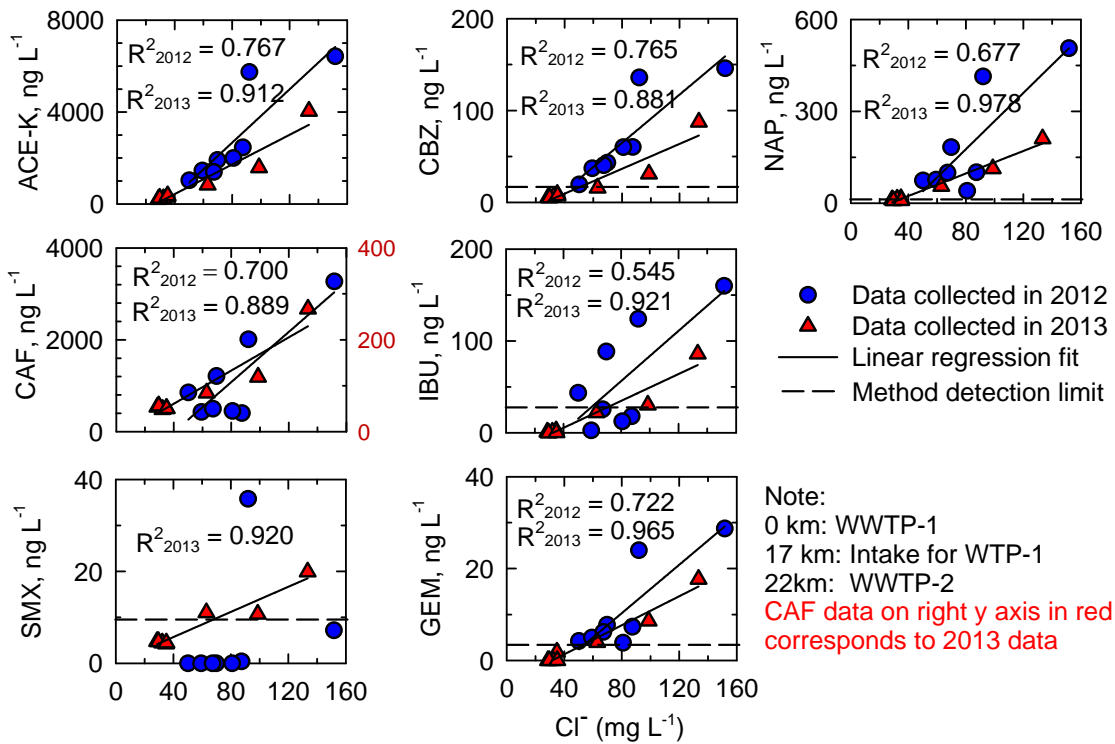


Figure 3.4 Concentrations of acesulfame-K (ACE-K), caffeine (CAF), sulfamethoxazole (SMX), carbamazepine (CBZ), ibuprofen (IBU), gemfibrozil (GEM), and naproxen (NAP) as a function of Cl⁻ concentration. The method detection limits of ACE-K and CAF were too low to appear in the figure.

Chapter 4: *Ultraviolet Light*

*Photo(catalytic) Treatment of Acesulfame-K
and Pharmaceuticals Using Magnetically
Recoverable TiO₂ Nanoparticles*

4.1 Executive Summary

Ultraviolet light (UV) photocatalysis by TiO₂ nanoparticles is an effective process for removing contaminants from drinking water and wastewater; however, non-recoverable TiO₂ nanoparticles also may become contaminants when released to the environment. In this study, two types of catalysts—magnetically separable TiO₂ (MST) recoverable nanoparticles (γ -Fe₂O₃/SiO₂/TiO₂ colloidal nanospheres) and graphene oxide-supported TiO₂ (GO TiO₂) recoverable nanoparticles (GO/TiO₂/CSA nanocomposites)—were evaluated for their effectiveness relative to commercial P25 TiO₂ for photocatalysis of an artificial sweetener and a suite of pharmaceutical compounds at environmental concentrations. The results show that over 99% of the artificial sweetener (acesulfame-K) and over 92% of the pharmaceuticals (sulfamethoxazole, 3,4-methylenedioxyamphetamine, 3,4-methylenedioxymethamphetamine, ibuprofen, gemfibrozil, naproxen, caffeine and carbamazepine) were removed within 60 min of UV (wavelength: 254 nm) photocatalysis using both P25 and GO TiO₂ nanoparticles. The UV photocatalysis of target contaminants followed a pseudo-first-order rate. The synthesized GO TiO₂ exhibited comparable or greater catalytic ability in assisting photocatalytic treatment of the target compounds by factors of up to 4.1 when comparing their intrinsic reaction rate constants. The MST particles were less effective in photocatalysis of contaminants compared to P25 and GO TiO₂ particles. The greater catalytic ability and high magnetic recovery makes the GO TiO₂ nanoparticles a potential alternative for commercial P25 nanoparticles used in water treatment.

4.2 Introduction

Emerging contaminants, including food additives such as artificial sweeteners, pharmaceuticals and personal care products, nanomaterials, steroids and hormones, surfactants, and microorganisms have been found to be widely distributed in the environment. Artificial sweeteners, including acesulfame-K (potassium), cyclamate, saccharin, sucralose, and aspartame, have been used worldwide for decades in considerable quantities as sugar substitutes in foods, diet beverages, pharmaceuticals, and some personal care products (Kroger et al., 2006). Artificial sweeteners pass through the digestive system with little metabolic breakdown and are excreted, therefore ending up in wastewater virtually unchanged. Acesulfame-K and sucralose are particularly widespread and persistent in the aquatic environment, making them ideal markers for tracing pollution from domestic wastewater into natural waters, particularly groundwater (Buerge et al., 2009; Scheurer et al., 2009). Pharmaceutical compounds also pass through the digestive system and are widely detected in the environment (Kolpin et al., 2002; Ternes, 1998).

Sewage effluents are considered to be the major source of pharmaceutical compounds in surface water (Bendz et al., 2005; Focazio et al., 2008), groundwater (Barnes et al., 2008; Carrara et al., 2008), and drinking water (Jones et al., 2005; Kleywegt et al., 2011) where they may cause toxicological effects (Fent et al., 2006) and, in the case of antibiotics, bacterial resistance (Richardson & Ternes, 2011). Adverse impacts of pharmaceuticals on ecosystem health have been generally acknowledged; however, ingestion of pharmaceuticals in drinking-water (ng L^{-1}) is not considered to result in appreciable adverse risks to human health (the WHO information sheet: Pharmaceuticals

in drinking-water). The concentrations of pharmaceuticals detected in drinking-water are typically several orders of magnitude lower than minimum therapeutic doses. The issue of health impacts of artificial sweeteners on humans is still controversial (Safe, 2000; Sharpe & Irvine, 2004; Sumpter, 2005).

Remedial technologies for removing artificial sweeteners from water supplies, including soil aquifer treatment (Scheurer et al., 2009) and chemical oxidation (Sharma et al., 2012), have recently been evaluated. Due to the ecotoxicity of pharmaceutical compounds, more extensive studies have been performed on the elimination of these compounds from environmental waters, including advanced oxidation, such as photo(catalytic) degradation using ultraviolet light (UV) and TiO₂ (Achilleos et al., 2010), UV/H₂O₂ (Rosario-Ortiz et al., 2010), (catalytic)ozonation (Beltrán et al., 2009), ultrasonic irradiation (Naddeo et al., 2009), and gamma irradiation (Zheng et al., 2011). Other methods studied include adsorption by activated carbon (Grover et al., 2011), biological activated carbon filtration (Reungoat et al., 2012), and constructed wetlands (Conkle et al., 2008).

Photocatalysis by means of illuminated TiO₂ is a promising technology for the degradation and removal of a wide range of emerging contaminants (Doll & Frimmel, 2005; Sturini et al., 2012). As a catalyst, TiO₂ can theoretically be reused indefinitely for continuous water purification. The high surface area afforded by nanostructuring enhances the catalytic efficiency (Ismail & Bahnemann, 2011; Xiang et al., 2012); however, fine TiO₂ nanoparticles are impractical to deploy in water treatment applications due to the difficulty of their recovery from the treated water after the photocatalytic decontamination process and the concern that residual TiO₂ nanocrystals

may be released to the environment (Chong et al., 2010; Malato et al., 2009). The presence of nano-TiO₂ particles can have adverse toxic effects on various organisms in environmental waters and soils (Klaine et al., 2008) and humans (Hsiao & Huang, 2011); however, the use of magnetically recoverable TiO₂ nanoparticles in water treatment would minimize the risk of releasing nano-TiO₂ into the environment.

Magnetic separation technology is widely used in industry, and is being explored for water treatment (Ambashta & Sillanpää, 2010; Yavuz et al., 2009). Extensive studies are being performed on the synthesis of different types of magnetically recoverable nanoparticles. The photocatalytic ability of these synthesized nanoparticles was usually tested in the decolouration of common model organic compounds, such as methylene blue dyes (Harraz et al., 2014), phenol (Feng et al., 2014; Mu et al., 2010), and formic acid (Makovec et al., 2011) under UV light. However, it is more impactful and attractive to test the synthesized recoverable nanoparticles in photodegradation of environmentally relevant contaminants, such as emerging contaminants under UV light. Álvarez et al. (2010) reported comparable ability of TiO₂/SiO₂/Fe₃O₄ nanoparticles in photodegradation of five pharmaceutical and personal care products (PPCPs) compared to Degussa P25 TiO₂. Linley et al. (2014) reported the enhanced photocatalytic ability of recyclable graphene oxide-supported TiO₂ nanoparticles in photodegradation of the pharmaceutical compounds caffeine and carbamazepine.

The photocatalytic ability of two types of laboratory-synthesized catalysts in removing emerging contaminants under UV light was evaluated through a series of batch experiments. The two types of laboratory-synthesized magnetically recoverable catalysts— magnetically separable TiO₂ (MST particles, γ -Fe₂O₃/SiO₂/TiO₂ colloidal

nanospheres and reduced graphene oxide-supported TiO₂ nanoparticles (GO TiO₂ particles, GO/TiO₂/CSA (Controlled SPION, Superparamagnetic Iron Oxide Nanoparticle, Aggregates) nanocomposites)—were compared with respect to photocatalytic efficiency relative to commercial P25 TiO₂ nanoparticles. Target pollutants for photocatalytic treatment included acesulfame-potassium (ACE-K) and eight pharmaceutical compounds: sulfamethoxazole (SMX), 3,4-methylenedioxyamphetamine (MDA), 3,4-methylenedioxymethamphetamine (MDMA), ibuprofen (IBU), gemfibrozil (GEM), naproxen (NAP), caffeine (CAF), and carbamazepine (CBZ). These compounds were selected because they are frequently detected in the environment due to their recalcitrance or they are emerging compounds with little available data on potential treatability. The concentrations of target contaminants were set at environmental levels (10 µg L⁻¹ of ACE-K and 1 µg L⁻¹ of pharmaceuticals) according to their reported occurrences in natural waters (Lapworth et al., 2012; Liu et al., 2014b; Metcalfe et al., 2010b; Yargeau et al., 2007).

4.3 Material and Methods

4.3.1 Nanoparticle Synthesis

Mesoporous, superparamagnetic, core-shell γ -Fe₂O₃/SiO₂/TiO₂ colloidal nanospheres (MST particles) were prepared using a stepwise synthesis method (Leshuk et al., 2013). The inner core maghemite spheres were prepared using a one-pot hydrothermal reaction (Cheng et al., 2010; Wang et al., 2012). These were then coated with silica following a modified Stöber process (Stöber et al., 1968) to preserve the photocatalytic activity of the TiO₂ by minimizing electrical contact with the inner core iron oxide (Watson et al., 2005). An outer titania coating was added using a sol-gel reaction employing titanium (IV)

butoxide as a precursor and hydroxypropyl cellulose as a surfactant (Lee et al., 2007; Linley et al., 2013). The resulting particles were hydrothermally treated in a polytetrafluoroethylene (PTFE)-lined stainless steel pressure vessel (Parr, Moline, IL, USA) at 100 °C for 2 h, followed by drying and calcination at 500 °C for 2 h.

The GO/TiO₂/CSA (1:12.5 GO/TiO₂, 1:1 TiO₂/CSAs as weight ratio) nanocomposites used in this study were prepared following a modular synthesis process allowing for tuning the ratio of GO and TiO₂ loading on GO to achieve efficient photocatalytic ability and magnetic separability (Linley et al., 2014). The synthesized magnetic CSA (Controlled SPION Aggregates) cores were first coated with a silicon dioxide shell to form silica-coated CSAs (SiO₂/CSAs). The SiO₂/CSAs and P25 underwent amine functionalization to be positively charged, and then were mixed with GO in solution and electrostatically attached to the surface of GO sheets. The composites were hydrothermally treated to reduce GO and bind the SiO₂/CSAs and P25 to the reduced GO. P25 TiO₂ Aeroxide powder was obtained from Acros Organics (New Jersey, US).

4.3.2 Characterization of Particles

The size and surface morphology of the catalyst particles were analyzed with transmission electron microscopy (TEM, Philips CM-10, 60 keV). The hydrodynamic diameters of the particles suspended in deionized water were measured with dynamic light scattering (DLS, Brookhaven 90Plus Particle Size Analyzer, MSD number-weighted mean diameter). The crystallinity of the powdered samples was analyzed through X-ray diffraction (XRD, Bruker D8 Focus, 1.542 Å Cu K α radiation). The surface area of the particles (pre-dried at 300 °C in N₂) was calculated from the Brunauer-Emmett-Teller

(BET) equation with data from N₂ adsorption isotherms obtained at 77 K (Micrometrics Gemini VII 2390 Surface Area Analyzer).

4.3.3 Batch Experimental Procedures

A concentrated stock solution was prepared by adding the target compounds in aqueous solutions containing a trace amount (< 0.01%) of methanol, resulting in about 1000 µg L⁻¹ ACE-K (Toronto Research Chemicals Inc., Toronto, Canada) and 100 µg L⁻¹ of the pharmaceuticals SMX, IBU, GEM, NAP, CAF, and CBZ (Sigma-Aldrich, Oakville, Canada), and MDA and MDMA (Cerilliant Inc., Texas, USA). A second, more dilute stock solution was prepared by adding 10 mL of the concentrated stock solution to 490 mL Nanopure water to obtain approximately 20 µg L⁻¹ ACE-K and 2 µg L⁻¹ of the pharmaceuticals.

The reaction solutions for the UV photolytic treatment (no catalysts) and control samples were prepared by adding 25 mL of the second stock solution and 25 mL Nanopure water into reaction bottles, yielding approximately 10 µg L⁻¹ ACE-K and 1 µg L⁻¹ of the pharmaceuticals. The reaction solutions for UV photocatalytic treatment and dark adsorption test samples were prepared by mixing 25 mL of the second stock solution, 24 mL Nanopure water, and 1 mL of 5 g L⁻¹ photocatalyst suspended solutions into reaction bottles with the catalysts at concentrations of 0.1 g L⁻¹. The concentrations of ACE-K and pharmaceuticals in the reaction solutions for the photo(catalytic) treatment experiments, control samples, and dark adsorption samples were about 10 and 1 µg L⁻¹. The reaction bottles used for the photo(catalytic) treatment experiments were transparent, clear glass bottles (9 cm in height, 7 cm inner diameter). Reaction bottles for the control

and dark adsorption test samples were wrapped with aluminum foil and placed in the dark during the experiments.

For the UV treatment experiments, reaction bottles with solutions were placed in a UV reactor (UVP CL-1000 Ultraviolet Crosslinker at 254 nm wavelength, energy: $\times 100 \mu\text{J}/\text{cm}^2$; UV intensity: $66.7 \text{ W}/\text{m}^2 = 6.7 \text{ mW}/\text{cm}^2$ or $24,012 \text{ mJ}/\text{cm}^2$) (UVP, Upland, CA, USA) and sampled at 0, 10, 30, and 60 min. During the 60 min UV irradiation, three control and three dark adsorption test samples were collected at 0, 30, and 60 min intervals. All samples were mixed manually every 10 min to avoid aggregation of the photocatalysts during UV irradiation, and then centrifuged at 10,000 rpm for 30 min to remove the catalysts from solution. The supernatants were transferred to amber glass bottles, acidified with H_2SO_4 to $\text{pH} < 2$, and stored at $4 \text{ }^\circ\text{C}$ until analysis. The experiments were performed at room temperature ($23 \text{ }^\circ\text{C}$) and the initial pH of the solutions was around 6.3.

4.3.4 Analytical Procedures

The target compounds were separated from the aqueous phase using solid-phase extraction (SPE). Prior to the extraction step, 10 mL samples were spiked with a mixture of isotope-labeled internal standards containing ACE-K-d4 and SMX-d4 (Toronto Research Chemicals Inc., Toronto, Canada), MDA-d5 and MDMA-d5 (Cerilliant Inc., Texas, USA), GEM-d6, IBU-d3, CAF-d3 and CBZ-d10 (CDN isotopes Inc., Quebec, Canada), and [^{13}C]-NAP (Cambridge Isotope Laboratory Inc., Cambridge, USA). The concentration of ACE-K-d4 and isotope labeled pharmaceuticals were 10 and $1 \mu\text{g L}^{-1}$ in 10 mL samples. SPE was performed using Oasis HLB 3 mL glass cartridges (Waters Corp., Mississauga, Canada). The cartridges were conditioned with $2 \times 1 \text{ mL}$ of HPLC

grade methanol and then equilibrated with 2×1 mL Nanopure water. After loading with 10 mL samples, the cartridges were washed using 2×1 mL 5 vol. % methanol, and then eluted with 2×1 mL methanol. The eluate was collected in an amber glass vial and stored at 4 °C until analysis.

The extracts were analyzed using an Agilent 1100 (Palo Alto, CA) high performance liquid chromatography system (HPLC) and detected by an API triple quadrupole tandem mass spectrometer with a turbo electrospray ion source (ESI) (4000 Q Trap; Applied Biosystems, Concord, Canada). The pharmaceuticals SMX, MDA, MDMA, CAF, and CBZ were analyzed in electrospray ionization positive (ESI+) mode, while ACE-K, IBU, GEM, and NAP were analyzed in electrospray ionization negative (ESI-) mode. A mixture of standards containing each of the non-labeled target compounds was used for instrument calibration and the response corrected by comparison to the recovery of the isotope-labeled internal standards.

Analytical procedures were modified slightly from published methods to optimize for separation and detector response (Stafiej et al., 2007; Vanderford et al., 2003). For pharmaceuticals analyzed in ESI+ mode, the mobile phase consisted of 0.1% formic acid and 5 mM ammonium acetate in Nanopure water (phase A) and 100% MeOH with 0.1% formic acid (phase B). The chromatographic separation used a gradient elution that started at 10 % B for 3 min, increased to 90% B over 10 min, and then held at 90% B min for 10 min. The flow rate was $1000 \mu\text{L min}^{-1}$ and the injection volume was 15 μL . For pharmaceuticals analyzed in ESI- mode, the mobile phase consisted of 6.9 mM acetic acid in 300 mL acetonitrile and 700 mL water (phase A) and 100% acetonitrile (phase B). A binary gradient was used: B increased linearly from 12% to 40% over 10 min and held

at 40% for 10 min. The injection volume was 10 μL and the flow rate was 1000 $\mu\text{L min}^{-1}$. For ACE-K analyzed in ESI- mode, the mobile phase consisted of 20 mM ammonium acetate in water (phase A) and 20 mM ammonium acetate in methanol (phase B). The gradient used for ACE-K was as follows: B increased linearly from 2% to 75% over 8 min and held at 75% for 8 min. The injection volume was 10 μL and the flow rate was 1000 $\mu\text{L min}^{-1}$. The relative internal standard (IS) recovery of ACE-K was between 72% and 118%. The absolute IS recovery of pharmaceuticals was between 85% and 118%. The method detection limits (MDLs) were 60 ng L^{-1} for ACE-K, 10 ng L^{-1} for SMX, 30 ng L^{-1} for MDA, 5 ng L^{-1} for MDMA, 30 ng L^{-1} for IBU, 5 ng L^{-1} for GEM, 20 ng L^{-1} for NAP, 100 ng L^{-1} for CAF, and 20 ng L^{-1} for CBZ.

4.3.5 Magnetic Separation

Magnetic separation tests to evaluate the MST particles recovery were performed by placing a glass vial containing 20 mL of MST nanoparticles suspended in solution on a permanent magnet for 15 min. Prior to magnetic separation, 2 mL of MST suspended solution was collected from the glass vial as a control. After 15 min magnetic separation, 15 mL of supernatant were extracted using a syringe and 15 mL of Nanopure water were added back to the glass vial. The MST solution was then re-suspended for further sampling as another control. Samples were acidified with HNO_3 to $\text{pH} < 2$ and stored at 4 $^\circ\text{C}$ for Fe and Ti analysis. The concentrations of total Fe and Ti, including dissolved and fine particulate fractions, were determined by inductively coupled plasma optical emission spectrometry (ICP-OES, iCAP 6000 Series, Thermo Scientific, Mississauga, Canada).

4.4 Results and Discussion

4.4.1 Particle Characterization

The synthesized MST particles were spherical and relatively monodispersed, with minimal interparticle aggregation (Figure 4.1). The MST particles were ~640 nm in diameter, with a ~50 nm thick nanocrystalline TiO₂ outer shell (measured by TEM). The observable rough surface texture of the MST particles results from the mesoporosity of the TiO₂ coating, indicating controllable uniform MST particles were successfully prepared as intended. The MST particles (in a powder form or dispersed in water) were strongly attracted towards a permanent magnet placed nearby. The TEM of GO/TiO₂/CSA nanoparticles were reported previously (Linley et al., 2014) (Figure C.1; Appendix C).

The hydrodynamic diameters of the MST particles in aqueous suspension, measured by DLS, were similar to diameters obtained using TEM (Table 4.1), indicating minimal aggregation of the particles in deionized (DI) water. This result was indicative of superparamagnetic behavior, as extensive solution phase aggregation would be observed if the particles possessed permanent magnetic moments. The colloidal stability of the synthesized particles differed from P25, a benchmark photocatalyst, which is well known to form extensive micron-scale aggregates in aqueous suspension (Table 4.1) that partially diminish the advantages of using nanocrystals. Aggregation is undesirable, because it reduces the accessible catalytic surface area available for reaction. The mean diameter of silica coated CSAs used for synthesizing GO TiO₂ particles is ~477 nm (Linley et al., 2014), which is relatively smaller than the MST particles.

XRD results indicate the TiO₂ in MST particles was present as well-crystallized anatase, which is one of the most photocatalytically active phases of TiO₂ (Figure 4.2). As expected, the MST sample also exhibited peaks corresponding to maghemite in its pattern, indicating that the iron oxide core did not transform to another iron oxide phase during synthesis; this is also consistent with the strong magnetic response. P25 is well known to consist of mixed anatase- and rutile-phase TiO₂ (Figure 4.2), with a primary nanocrystal size of ~20 nm (Table 4.1). The TiO₂ crystal sizes of the MST samples were notably smaller than P25 and much smaller than the composite spheres as a whole. The XRD analysis shows the presence of anatase, rutile, and magnetite in GO TiO₂ particles (Figure C.2), indicating both P25 and magnetite are preserved through hydrothermal treatment (Linley et al., 2014).

The specific surface area of the MST particles was double that of P25 (Table 4.1), likely due to the finer crystallite sizes in the synthesized MST samples as compared to P25. In addition, the hydrothermal processing employed during MST synthesis allows for the formation of a disordered mesoporous TiO₂ shell, comprised of small interaggregated nanocrystallites, and resulting in very high specific surface areas despite the relatively large dimensions of the composite spheres as a whole.

4.4.2 Control and Dark Adsorption Samples

The concentrations of ACE-K and pharmaceuticals in the control samples remained constant or decreased slightly relative to initial concentrations of 11000 ng L⁻¹ for ACE-K and 1200 ng L⁻¹ for pharmaceuticals. A small fraction of initial ACE-K (< 3%), SMX (< 4%), MDA (< 5%), MDMA (< 9%), IBU (< 5%), GEM (< 4%), NAP (< 10%), CAF (<

7%), and CBZ (< 10%) were lost in the control samples during 60 min of dark storage (Figures 4.3 and 4.4).

During 60 min dark adsorption, a portion of the target compounds was lost compared to the control samples. Less than 3.8% of input ACE-K, < 7.5% of input SMX, < 9.8% of input IBU, < 11.1% of input GEM, < 11.1% of input NAP, < 8.9% of input CAF, and < 11.4% of input CBZ were lost in the input solution with P25 and MST nanoparticles (Figure C.3). The differences in concentration of target compounds between the control and dark adsorption samples were likely due to the adsorption of contaminants onto the nanoparticles. Greater loss associated with the MST nanoparticles compared to P25 was likely due to their larger surface area (Table 4.1). Adsorption of a pharmaceutical (ibuprofen) on photocatalyst TiO₂ nanoparticles (< 5%) has been reported for pH > 5 solutions (Tungudomwongsa et al., 2006). The adsorption of target contaminants on GO TiO₂ particles was not tested in this study; however, GO TiO₂ particles exhibit enhanced adsorption of methylene blue compared to P25 (Linley et al., 2014).

4.4.3 UV Photo(catalytic) Treatment Results and Rate Calculations

The artificial sweetener ACE-K and pharmaceutical SMX were almost completely removed during a 60 min UV irradiation alone and during photocatalysis using P25, MST, and GO TiO₂ nanoparticles. Pharmaceuticals MDA, MDMA, IBU, GEM, NAP, CAF, and CBZ were either not removed or partially removed during 60 min UV irradiation alone; however, more rapid and complete removals of these compounds were observed during photocatalysis using P25 and GO TiO₂ particles. The MST particles were less effective in photocatalysis of the contaminants compared to P25 and GO TiO₂.

Common degradation pathways for drugs during direct UV photolysis include decarboxylation, isomerization, aromatization, dehalogenation, cyclization, elimination, dimerization, and polymerization (Min, 2012). Heterogeneous photocatalysis by TiO₂ is initiated by the excitation of the semiconductor (TiO₂) by UV irradiation to generate a positive hole-electron pair. Hydroxyl radicals are generated through a series of oxidation and reduction reactions on the surface of TiO₂. These hydroxyl radicals are highly reactive, non-selective, and very efficient oxidizers of adsorbed pollutants (Khetan & Collins, 2007).

Langmuir-Hinshelwood (L-H) kinetics is the most common kinetic expression used to represent the rate of heterogeneous photocatalysis of organic compounds by illuminated TiO₂ particles. L-H kinetic model can be described as $-dC/dt = kKC/(1+KC)$, where dC/dt is the rate of degradation; k is the apparent reaction rate constant; K is the adsorption coefficient of the substance to be degraded; and C is the concentration of the substance. The L-H model is surface-area dependent; the reaction rate is proportional to the fraction of surface covered by the organic compounds. The L-H kinetic model is valid for the four possible situations: (i) reaction occurs between the adsorbed radicals and organic compounds; (ii) reaction occurs between the radicals in water and adsorbed organic compounds; (iii) reaction occurs between the radicals on the surface and organic compounds in water; and (iv) reaction occurs with both radicals and organic compounds in water (Chong et al., 2010; Konstantinou & Albanis, 2004).

When the extent of adsorption and/or substance concentration is low (i.e., $KC \ll 1$), the L-H equation can be simplified to a pseudo-first-order kinetic equation: $-dc/dt = kC$ or $C_t = C_0 e^{-kt}$, where k is the pseudo-first-order rate constant (Dimitrakopoulou et al., 2012;

Doll & Frimmel, 2004). In this study, the concentrations of target contaminant concentrations were very low (at environmental levels) and their adsorption onto the photocatalysts was relatively weak. Therefore, a simplified pseudo-first-order kinetic approach was used to represent the photocatalytic removal of ACE-K, SMX, MDA, MDMA, IBU, GEM, NAP, CAF and CBZ. The first-order rate constant (k) of each contaminant was calculated by SigmaPlot (SPSS Inc.) based on least squares regression ($R^2 > 0.989$ for all contaminants). To explore the intrinsic photoreactivity of the catalysts, k was normalized to the mass and specific surface area of TiO_2 . The mass normalized rate constant (k_M) was calculated following $k_M = k/\rho$ and the surface area normalized rate constant (k_{SA} , intrinsic rate constant) was calculated as $k_{SA} = k/(\rho A_S)$, where k_M is the mass normalized rate constant ($\text{L g}^{-1} \text{min}^{-1}$), k is the first order rate constant (min^{-1}), ρ is the mass concentration (g L^{-1}), and A_S is the surface area of the particle ($\text{m}^2 \text{g}^{-1}$). The calculated values of k , k_M , and k_{SA} for each contaminant during the photo(catalytic) treatment are provided in Tables 4.2 and 4.3. The target contaminants were divided into four groups based on the extent of their removability during 60 min photo- and photocatalytic treatment.

4.4.3.1 Group 1: Easily Photo- and Photocatalytically Degradable Compounds ACE and SMX

Containing the same functional group sulfonamide, artificial sweetener ACE-K and pharmaceutical SMX were almost completely removed under both UV alone and UV with catalysts (Figure 4.3).

The concentration of ACE-K decreased from approximately 11000 ng L^{-1} to $< \text{MDL}$ (60 ng L^{-1}) during 60 min UV irradiation without catalysts, representing a removal $>$

99.7%. Relatively faster and complete removals of ACE-K were observed during UV photolysis than UV photocatalysis (Figure 4.3 and Table 4.2), likely due to the shielding effect of the catalysts with respect to the UV penetrating light. The removal rate constant (k , $2.3 \times 10^{-1} \text{ min}^{-1}$) of ACE-K under UV photolysis was similar to the rate constants (pH independent between 5 and 10) reported by Scheurer et al. (2014), but was one order of magnitude larger than a previously reported rate constant (pH dependent at 3, 9 and 12) which was likely due to the higher UV intensity used in this study (Coiffard et al., 1999). The concentrations of ACE-K decreased from 11000 ng L^{-1} to 146 ng L^{-1} after a 60 min photocatalysis using P25 nanoparticles (98.7% removed), decreased to 65 ng L^{-1} (99.4% removal) using MST nanoparticles, and decreased to $< \text{MDL}$ (60 ng L^{-1}) ($> 99.7\%$ removal) using GO TiO₂ nanoparticles.

The pharmaceutical SMX was almost completely removed, falling from initial concentrations of 1200 ng L^{-1} to $< \text{MDL}$ ($< 10 \text{ ng L}^{-1}$) during a 60 min UV photo(catalytic) treatment (up to 99.9% removal). However, SMX was removed much more rapidly during the first 10 min of UV photolysis without catalyst (Figure 4.3 and Table 4.2). The rate constant (k) of UV photolysis of SMX in Table 4.2 was three times to one order of magnitude larger than previously reported (Fukahori et al., 2012; Ngouyap Mouamfon et al., 2011). The greater rate constant observed was likely due to the higher UV intensity used in this study. The synthesized GO TiO₂ nanoparticles exhibited a greater ability in the photocatalysis of SMX than P25 by a factor of 1.6 and MST nanoparticles by a factor of 6.1 in terms of the intrinsic rate constant (k_{SA}) (Table 4.2). The slightly larger k value observed during P25 catalyzed photocatalysis than UV photolysis is consistent with other studies (Prieto-Rodriguez et al., 2012). Fukahori et al.

(2012) report that the reaction rate constants of photocatalysis of SMX using TiO₂ nanoparticles decrease with increasing pH (pH: 6.5–9.0) due to the repulsive force between TiO₂ particles and anionic SMX.

The photo(catalytic) degradations of ACE-K and SMX were reported to follow various pathways (Gan et al., 2014; Hu et al., 2007; Li et al., 2016; Ngouyap Mouamfon et al., 2011; Scheurer et al., 2014); however, similar degradation pathways involving ring breakage or hydroxyl radicals cleavage on sulfonamide bond likely occur during photo(catalytic) degradation (Abellán et al., 2007; Sang et al., 2014b). The presence of sulfonamide likely accounted for the easy degradation of ACE and SMX during UV photolysis and photocatalysis.

4.4.3.2 Group 2: Easily Photocatalytically Degradable Compounds MDA and MDMA

As methylenedioxyphenyl compounds, MDA and MDMA followed similar removal trends during the course of a 60 min UV photolysis and photocatalysis using P25, MST and GO TiO₂ nanoparticles.

The concentrations of MDA and MDMA decreased slightly from input concentrations of 1280 and 1322 ng L⁻¹ to 1058 and 1052 ng L⁻¹, respectively, after a 60 min UV irradiation; this represents removal of 18% of the MDA and 20% of the MDMA. However, up to 99.9% of input MDA and MDMA were removed (from approximately 1200 ng L⁻¹ to undetectable concentrations) within the first 10 min of the photocatalysis by P25, MST, and GO TiO₂ nanoparticles (Figure 4.3), with k values three orders of magnitude larger than for UV photolysis (Table 4.2). The intrinsic rate constant (k_{SA}) of

photocatalysis of MDA and MDMA using GO TiO₂ were 1.1–1.4 times larger than that using P25 particle, indicating exceeding catalytic ability of GO TiO₂ compared to P25 (Table 4.2). The MST particles were less efficient in photocatalysis of MDA and MDMA compared to commercial P25 and GO TiO₂ particles.

UV photolysis of MDA and MDMA has not been studied previously. The photocatalysis of MDA and MDMA assisted by TiO₂ were likely to follow similar degradation pathway through hydroxyl radical cleavage of methylenedioxy group with catechol and formate as metabolites (Kumagai et al., 1991). This similar photocatalytic degradation pathway likely accounted for the similar photo(catalytic) characteristic of MDA and MDMA.

4.4.3.3 Group 3: Moderately Photo- and Photocatalytically Degradable Compounds IBU, GEM, and NAP

Pharmaceuticals IBU, GEM, and NAP were not effectively removed during UV photolysis with removals of up to 65%. Faster (observed k) and almost complete removals (> 98%) of these compounds were observed during photocatalysis using P25. Extensive removal of NAP by P25-assisted photocatalysis relative to photolysis has been reported during 180 min of UV irradiation (Méndez-Arriaga et al., 2008b). During photocatalysis using GO TiO₂, concentrations of IBU and NAP decreased from ~1200 ng L⁻¹ to up to 96 ng L⁻¹ and undetectable concentrations with removals of 99% and 92%, respectively. The nanoparticle GO TiO₂ exhibited comparable ability in photocatalysis of IBU and NAP with relatively smaller intrinsic rate constants (k_{SA}) observed (Table 4.3). The first order rate constant k of photocatalysis of IBU and NAP were one or two orders of magnitude larger than previous study (Méndez-Arriaga et al., 2008a). The

concentration of GEM decreased from 1100 ng L⁻¹ to undetectable concentrations during the photocatalysis using P25 and GO TiO₂. The intrinsic rate constant ($k_{SA} = 8.3 \times 10^{-2}$ L m⁻² min⁻¹) during photocatalysis of GEM using GO TiO₂ was larger than that ($k_{SA} = 6.3 \times 10^{-2}$ L m⁻² min⁻¹) using P25, indicating advanced photocatalytic ability of GO TiO₂ in removing GEM compared to P25 by a factor of 1.3. The complete mineralization of GEM were observed during photodegradation using commercial P25 with a first-order rate constant of 1.5×10^{-5} s⁻¹, which is two orders of magnitude lower than the rate constant observed in this study (Yurdakal et al., 2007).

The MST particles were less effective in photocatalysis of IBU, GEM, and NAP with k_{SA} values one order of magnitude small than that using P25 and GO TiO₂ particles (Figure 4.4 and Table 4.3). P25 and GO nanoparticles contain both anatase and rutile forms of TiO₂, whereas MST nanoparticles contain anatase alone. The enhanced photocatalytic ability of P25 and GO TiO₂ particles compared to MST particles is likely due to a synergy effect of electron transfer in the mixed anatase and rutile phases in P25 and GO TiO₂ nanoparticles. When anatase and rutile are in direct interfacial contact, the electron transfer from rutile to anatase stabilizes the charge separation and prevents rapid recombination. This electron transfer is enhanced by the small size of rutile crystallites, making the rutile/anatase interface a hot spot for photocatalysis (Hurum et al., 2003; Scanlon et al., 2013).

The pharmaceuticals IBU, GEM, and NAP have aromatic and carboxyl groups in their structures. One pathway of the photo(catalytic) degradation of IBU and NAP likely follow decarboxylation in common (Boscá et al., 2001; Méndez-Arriaga et al., 2008a; Méndez-Arriaga et al., 2008b; Yan & Song, 2014), but not for GEM. The photocatalysis

of GEM by TiO₂ likely occur through the breakage of etheral bond besides the aromatic group (Yurdakal et al., 2007). The aromatic group in the structure of IBU, GEM, and NAP likely make them less vulnerable to UV photolysis and photocatalysis by the anatase-phase TiO₂ in MST particles.

4.4.3.4 Group 4: Recalcitrant Photo- and Photocatalytically Degradable Compounds CAF and CBZ

Caffeine and CBZ are the most recalcitrant compounds during photo(catalytic) treatment in this study, and cannot be removed during UV photolysis, which is consistent with previous study (Jelic et al., 2013); however, rapid and complete removals of CAF and CBZ were observed during photocatalysis using GO TiO₂ and P25 particles (Linley et al., 2014). The GO TiO₂ particles exhibited greater ability in photocatalysis of CAF and CBZ by a factor of 4.1 and 2.7 in terms of intrinsic rate constants (k_{SA}) (Table 4.3). The first order rate constant k for photocatalysis of CAF and CBZ using P25 and GO TiO₂ particles were ~3–9 times larger than published value using P25 and other synthesized TiO₂ particles (Barndök et al., 2013; Jelic et al., 2013; Marques et al., 2013). The MST particles were less photocatalytically effective compared to P25 and GO TiO₂ particles in photocatalysis of CAF and CBZ. Results showed of ~12% of input CAF and ~27% of input CBZ were removed during photocatalysis using MST particles, with k_{SA} values ~two orders of magnitude smaller than that using P25 and GO TiO₂ particles (Figure 4.4 and Table 4.3). The relatively stable multi-rings structure in CAF and CBZ likely make them more recalcitrant to UV photolysis and photocatalysis, resulting in slower removal rates for CAF and CBZ compared to other target contaminants (Tables 4.2 and 4.3). The photocatalytic degradation of CAF is likely initiated through hydroxylation of the C4=C8

double bond and demethylation (Dalmázio et al., 2005). Doll and Frimmel (2005) and Jelic et al. (2013) report the multi-step and interconnected pathways of photocatalytic degradation of CBZ with nine intermediates identified.

4.4.4 Magnetic Separation Results

The initial concentrations of Fe and Ti in the MST suspended solution for the control sample were 2.80 and 6.72 mg L⁻¹ before magnetic separation. The concentrations of Fe and Ti in the MST suspended solution decreased slightly to 2.76 and 6.62 mg L⁻¹ after placing the control sample on a permanent magnet for 15 min and replacing the supernatant with the same volume of water. This slight decrease in Fe and Ti concentrations shows that more than 98.5% of MST nanoparticles were magnetically recovered through a 15 min magnetic separation process.

Magnetic separation efficiency of GO TiO₂ particles was previously evaluated by exposing the GO TiO₂ particle solution to a permanent magnet and reported by the UV-vis adsorption as a function of time. Results showed that more than 90% of the GO TiO₂ particles were separated from solution in 75 s (Linley et al., 2014).

The UV photocatalytic treatment results show that the GO TiO₂ nanoparticles are comparable as commercial P25 TiO₂ in inducing photocatalysis of IBU and NAP within 60 min UV irradiation; more efficient in catalyzing the photodegradation of MDA, MDMA, GEM, CAF and CBZ in terms of intrinsic rate constants (Tables 4.2 and 4.3). However, MST nanoparticles seem much less effective compared to P25 and GO TiO₂ particles, likely due the absence of rutile-phase TiO₂. The commercial P25 TiO₂ (80% anatase and 20% rutile) is more photocatalytically efficient than laboratory synthesized

MST nanoparticles (pure form anatase); this is attributed to the morphology of crystallites, efficient photogenerated charge carrier separation due to the junction between its anatase and rutile phases, and increasing photocatalytic quantum yield by limiting recombination (Kaniou et al., 2005). In addition, the activation energy with smaller band-gap enhanced the use of visible light by rutile phase TiO₂. The rutile phase TiO₂ has been reported to exhibit advanced catalytic ability in photodegradation of phenol compared to anatase phase TiO₂ (Andersson et al., 2002). The enhanced photocatalytic ability of GO TiO₂ relatively to P25 is likely attributed to improved adsorption by the π - π stacking interaction, extended light absorption range, efficient charge separation and transportation of GO TiO₂ compared to P25 (Zhang et al., 2010). GO has a large π - π bonding network acting as a sorbent for contaminants with a similar aromatic structure (i.e. compounds such as SMX, MDA, MDMA, IBU, GEM, NAP, and CBZ) through π - π interaction. GO as an electron sink accepts photogenerated electrons from TiO₂, slowing down electron-hole recombination and improving the quantum efficiency and activity of the catalyst (Du et al., 2011). In addition, P25 nanoparticles tend to aggregate, which likely reduces the accessible surface area involved in photocatalytic treatment. By attaching the TiO₂ nanoparticles to GO, aggregation is restricted and TiO₂ surface area remains accessible throughout treatment. Therefore, application of recoverable GO TiO₂ photocatalysts in the water treatment industry is expected to provide environmental benefits over the use of non-recoverable particles due to its efficient photocatalytic ability and high recovery (> 90%).

4.5 Conclusions

The laboratory synthesized recoverable magnetic graphene oxide supported TiO₂ (GO TiO₂) nanoparticles exhibit catalytic ability comparable or greater to commercial P25 TiO₂ by an average factor of 1.8 when comparing their intrinsic reaction rate constants during UV photocatalytic treatment of target contaminants at environmental levels. Up to 99% of the artificial sweetener acesulfame-K (~10 µg L⁻¹) and pharmaceuticals (~1 µg L⁻¹) sulfamethoxazole (SMX), 3,4-methylenedioxyamphetamine (MDA), 3,4-methylenedioxymethamphetamine (MDMA), ibuprofen (IBU), gemfibrozil (GEM), naproxen (NAP), caffeine (CAF) and carbamazepine (CBZ) were removed during 60 min UV photocatalysis with 0.1 g L⁻¹ of P25 and GO TiO₂ nanoparticles. The synthesized pure anatase phased MST (γ-Fe₂O₃@SiO₂@TiO₂ colloidal nanospheres) nanoparticles were less photocatalytically efficient compared to the P25 and GO TiO₂ nanoparticles. Due to its high photocatalytic efficiency and recovery, the GO TiO₂ nanoparticles could serve as an alternative to commercial P25 in the water treatment industry in terms of environmental benefits. The results reported herein contribute to existing literature by presenting results of UV photocatalytic treatment of emerging contaminants (ACE-K, SMX, MDA, MDMA, IBU, GEM, NAP, CAF, and CBZ) using magnetically recoverable GO TiO₂ nanoparticles.

Table 4.1 Nanocrystal size, BET surface area, and hydrodynamic (DLS) diameter of the particle samples used in this study.

Sample	Crystal Size (nm) ^[a]	BET Surface Area (m ² g ⁻¹)	DLS Mean Diameter (nm)	DLS Polydispersity Index
P25	27 ^[c]	57.4 ^[c]	>3000 ^[b]	n/a
MST	8.5	115.4	592.2	0.023

Note: Similar data in this table for GO TiO₂ nanoparticles are not available.

[a] As calculated from the anatase (101) peak using the Scherrer formula.

[b] Aggregate sizes were above the operating range of the instrument.

[c] Reference: (Suttiponparnit et al., 2011)

Table 4.2 Selected properties of acesulfame-K (ACE-K), sulfamethoxazole (SMX), 3,4-methylenedioxyamphetamine (MDA), and 3,4-methylenedioxymethamphetamine (MDMA), first order rate constants (k), correlation coefficient (R^2), mass normalized rate constants (k_M), and surface-area normalized rate constants (k_{SA}) during (photo)catalytic treatment.

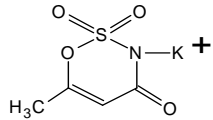
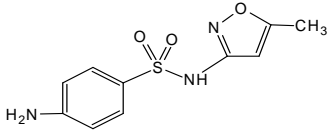
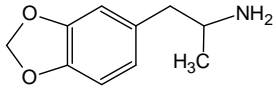
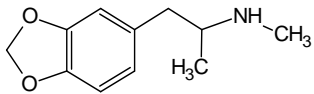
		Compound (CAS#), use, pK_a , $\log K_{ow}$, and structure	UV/ Catalyst	Catalyst concentration ^[a] , $g\ L^{-1}$	R^2	k , min^{-1}	k_M , $L\ g^{-1}\ min^{-1}$	k_{SA} ^[b] , $L\ m^{-2}\ min^{-1}$
Group 1 Easily photo- and photocatalytically degradable compounds	Acesulfame-potassium (ACE-K) (55589-62-3), artificial sweetener, $pK_a=2.0$, $\log K_{ow}=-1.3$		UV	—	0.999	2.3E-01	—	—
			P25	0.1	0.999	1.8E-01	1.8	3.1E-02
			MST	0.1	0.999	1.1E-01	1.1	9.7E-03
			GO TiO ₂	0.05	0.999	1.6E-01	3.2	7.0E-02
	Sulfamethoxazole (SMX) (723-46-6), antibiotic, $pK_{a1}=1.7$, $pK_{a2}=5.6$, $\log K_{ow}=0.9$		UV	—	1.000	3.1E-01	—	—
			P25	0.1	0.999	4.5E-01	4.5	7.9E-02
			MST	0.1	0.999	2.5E-01	2.5	2.1E-02
			GO TiO ₂	0.05	0.999	2.9E-01	6.0	1.3E-01

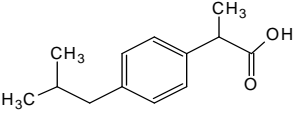
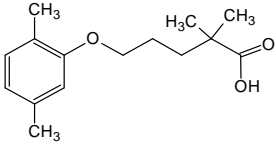
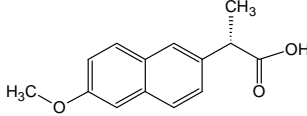
Table 4.2 Continued.

Group 2 Easily photocatalytically degradable compounds	3,4-methylenedioxyamphetamine (MDA) (4764-17-4), psychedelic and entactogenic drug, $pK_a=9.7$, $\log K_{ow}=1.6$ 	UV	—	0.499	4.0E-03	—	—
		P25	0.1	0.999	5.3E-01	5.3	9.2E-02
		MST	0.1	1.000	4.9E-01	4.9	4.3E-02
		GO TiO ₂	0.05	0.999	2.9E-01	6.0	1.3E-01
	3,4-methylenedioxymethamphetamine (MDMA) (42542-10-9), ecstasy, $pK_a=9.9$, $\log K_{ow}=2.3$ 	UV	—	0.892	3.0E-03	—	—
		P25	0.1	1.000	6.8E-01	6.8	1.2E-01
		MST	0.1	1.000	4.5E-01	4.5	3.9E-02
		GO TiO ₂	0.05	0.999	3.0E-01	6.1	1.3E-01

[a] The catalyst concentration of GO TiO₂ was normalized as TiO₂ concentration in solution based on the weight ratio of TiO₂ in GO TiO₂ (1:12.5 GO/TiO₂, 1:1 TiO₂/CSAs). The catalyst concentration of MST TiO₂ was not normalized to TiO₂ mass concentration.

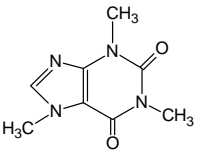
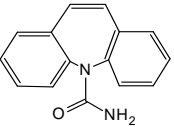
[b] The surface area of GO TiO₂ used for calculating k_{SA} was assumed to be 80% of TiO₂ surface area. The TiO₂ particles are associated on the GO sheet; the area of the TiO₂ in contact with the GO sheet is not exposed to the solution.

Table 4.3 Selected properties of ibuprofen (IBU), gemfibrozil (GEM), naproxen (NAP), caffeine (CAF), and carbamazepine (CBZ), first order rate constants (k), correlation coefficient (R^2), mass normalized rate constants (k_M), and surface-area normalized rate constants (k_{SA}) during (photo)catalytic treatment.

Compound (CAS#), use, pK_a , $\log K_{ow}$, and structure	UV/Catalyst	Catalyst concentration ^[a] , g L^{-1}	R^2	k , min^{-1}	k_M , $\text{L g}^{-1} \text{min}^{-1}$	$k_{SA}^{[b]}$, $\text{L m}^{-2} \text{min}^{-1}$
Ibuprofen (IBU) (15687-27-1), nonsteroidal anti-inflammatory drug, $pK_a=4.5$, $\log K_{ow}=3.5$ 	UV	—	0.899	6.0E-03	—	—
	P25	0.1	0.998	1.7E-01	1.7	2.9E-02
	MST	0.1	0.999	1.5E-02	1.5E-01	1.3E-03
	GO TiO ₂	0.05	0.994	5.2E-02	1.1	2.4E-02
Gemfibrozil (GEM) (25812-30-0), lipid regulator, $pK_a=4.8$, $\log K_{ow}=4.3$ 	UV	—	0.943	1.0E-02	—	—
	P25	0.1	1.000	3.6E-01	3.6	6.3E-02
	MST	0.1	0.985	1.4E-02	1.4E-01	1.2E-03
	GO TiO ₂	0.05	1.000	1.8E-01	3.8	8.3E-02
Naproxen (NAP) (22204-53-1), nonsteroidal anti-inflammatory drug, $pK_a=4.2$, $\log K_{ow}=2.8$ 	UV	—	0.992	1.8E-02	—	—
	P25	0.1	0.999	3.9E-01	3.9	6.8E-02
	MST	0.1	0.992	9.3E-02	9.3E-01	8.1E-03
	GO TiO ₂	0.05	0.999	1.4E-01	3.0	6.5E-02

Group 3
Moderately photo- and photocatalytically degradable
compounds

Table 4.3 Continued.

Group 4 Recalcitrant photo- and photocatalytically degradable compounds	Caffeine (CAF) (58-08-2), stimulant, $pK_a=10.4$, $\log K_{ow}=-0.1$	UV	—	0.348	1.0E-03	—	—
		P25	0.1	0.992	8.9E-02	8.9E-01	1.6E-02
		MST	0.1	0.836	2.0E-03	2.0E-02	1.7E-04
		GO TiO ₂	0.05	0.999	1.4E-01 ^[c]	2.9	6.3E-02
		Carbamazepine (CBZ) (298-46-4), anti-depressant, antiepileptic, $pK_a=-0.49$ ^[d] , $\log K_{ow}=2.3$	UV	—	—	—	—
		P25	0.1	0.999	5.4E-02	5.4E-01	9.4E-03
		MST	0.1	0.954	5.0E-03	5.0E-02	4.3E-04
		GO TiO ₂	0.05	0.997	5.5E-02 ^[c]	1.1	2.5E-02

[a] The catalyst concentration of GO TiO₂ was normalized as TiO₂ concentration in solution based on the weight ratio of TiO₂ in GO TiO₂. The catalyst concentration of MST TiO₂ was not normalized to TiO₂ mass concentration.

[b] The surface area of GO TiO₂ used for calculating k_{SA} was assumed to be 80% of TiO₂ surface area. The TiO₂ particles are associated on the GO sheet; the area of the TiO₂ in contact with the GO sheet is not exposed to the solution.

[c] Reference: Linley et al. (2014).

[d] Reference: Schaffer et al. (2012).

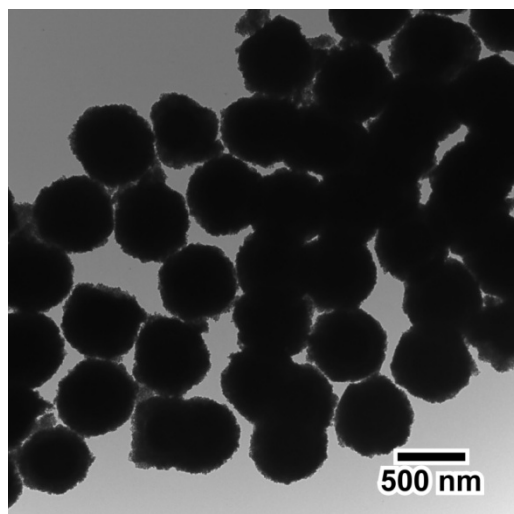


Figure 4.1 TEM images of MST particles.

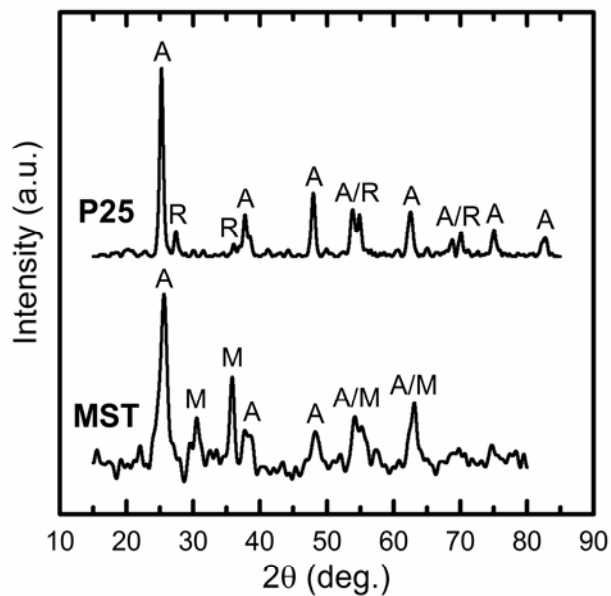


Figure 4.2 XRD patterns of the MST particles and P25 as indicated. Peaks labelled with A match anatase phase TiO_2 (JCPDS No. 21-1272), R matches rutile phase TiO_2 (JCPDS No.21-1276), and those labeled with M match maghemite ($\gamma\text{-Fe}_2\text{O}_3$) iron oxide (JCPDS No. 89-3850).

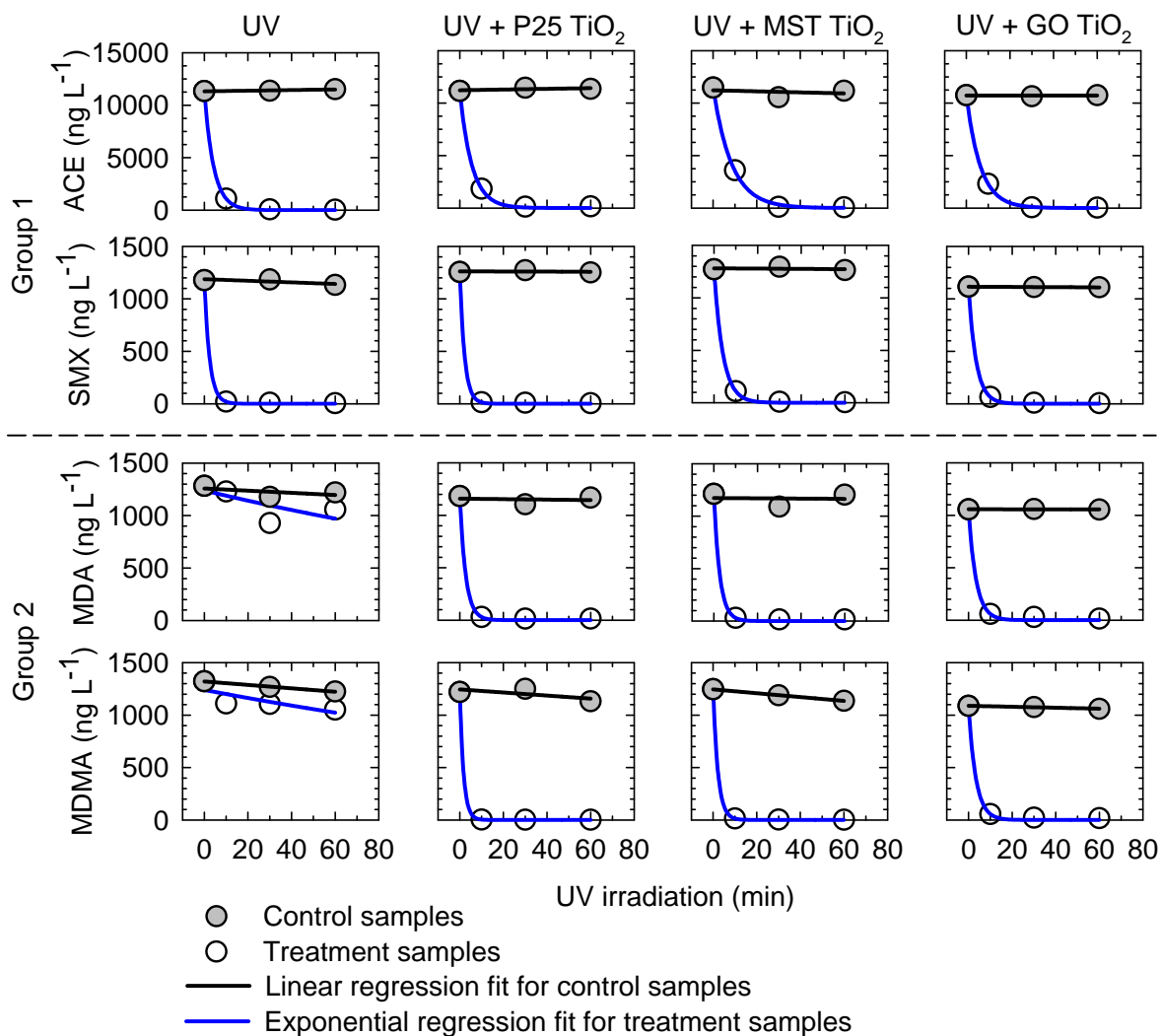


Figure 4.3 Concentrations of acesulfame-K (ACE-K), sulfamethoxazole (SMX), 3,4-methylenedioxyamphetamine (MDA), and 3,4-methylenedioxymethamphetamine (MDMA) as a function of reaction time during UV photo(catalytic) treatment. Group 1: Easily photo- and photocatalytically degradable compounds ACE and SMX. Group 2: Easily photocatalytically degradable compounds MDA and MDMA.

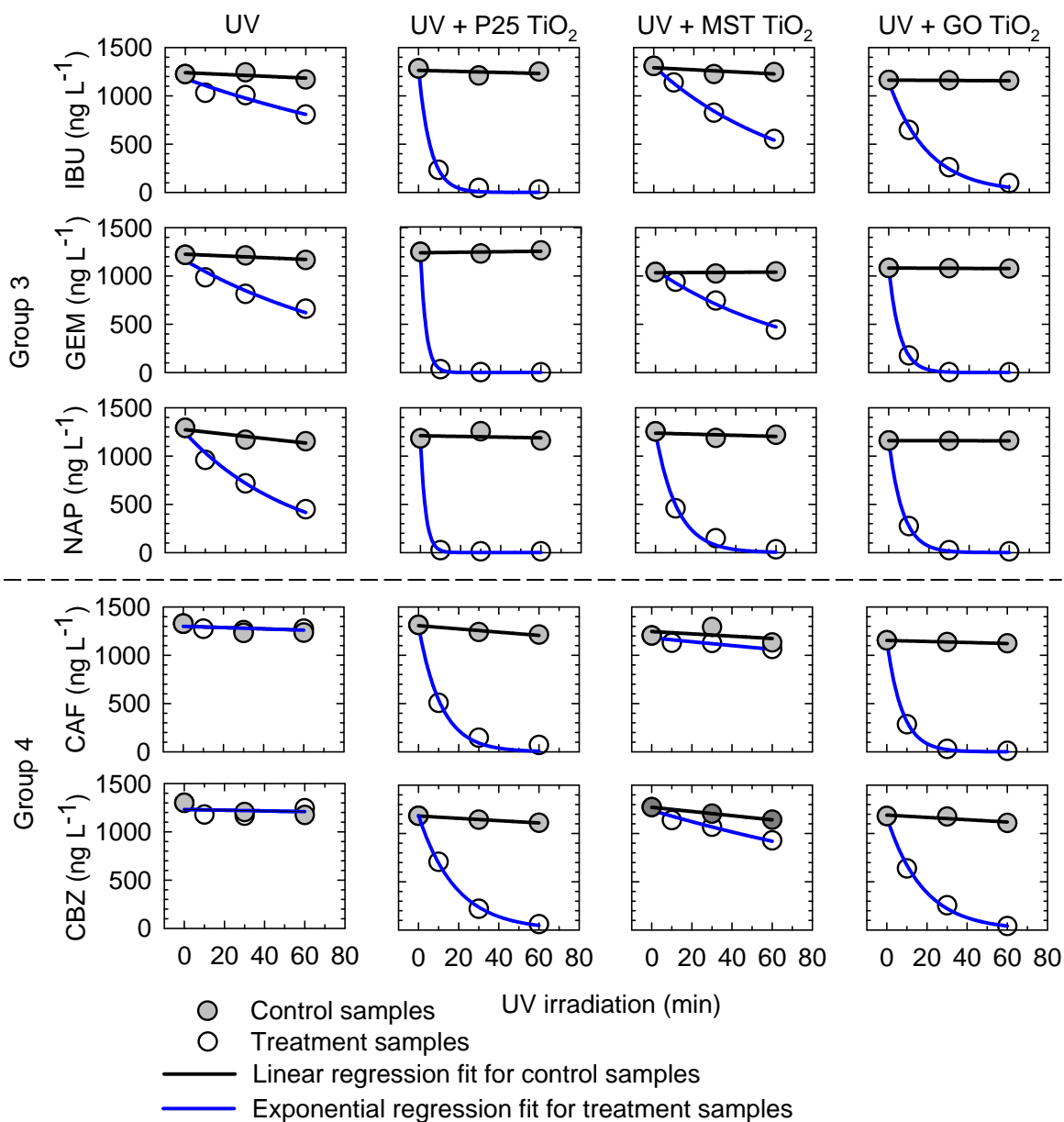


Figure 4.4 Concentrations of ibuprofen (IBU), gemfibrozil (GEM), naproxen (NAP), caffeine (CAF), and carbamazepine (CBZ) as a function of reaction time during UV photo(catalytic) treatment. Group 3: Moderately photo- and photocatalytically degradable compounds IBU, GEM, and NAP. Group 4: Recalcitrant photo- and photocatalytically degradable compounds CAF and CBZ. The data of UV photolysis and photocatalysis of CAF and CBZ using P25 and GO TiO₂ nanoparticles were reproduced with permission from Linley et al. (2014).

Chapter 5: *Removal of Pharmaceutical
Compounds, Artificial Sweeteners, and
Perfluoroalkyl Substances from Water Using
Zero-valent Iron and Biochar*

5.1 Executive Summary

Emerging contaminants such as pharmaceutical compounds, artificial sweeteners, and perfluoroalkyl substances (PFASs) are widely detected and persistent in environmental waters such as surface water, groundwater, and drinking water. Advanced oxidation processes are among the most effective and heavily studied methods for removing emerging contaminants from water; however, high energy consumption (such as ultraviolet light and ozone) greatly increases the operating costs and limits its large scale application. In this study, a passive treatment system consisting of four columns packed with mixtures of silica sand, zero-valent iron (ZVI), biochar (BC), and a mixture of (ZVI + BC) were evaluated for simultaneous removal of pharmaceuticals, artificial sweeteners, and PFASs from water. The experiment was divided into two stages; the flow rate was maintained at 0.3 pore volume (PV) d⁻¹ in the first stage of the experiment, and then decreased to 0.1 PV d⁻¹ in the second stage of the experiment. Almost complete removal (> 97%) of the pharmaceutical compounds carbamazepine (CBZ), caffeine (CAF), sulfamethoxazole (SMX), 3,4-methylenedioxyamphetamine (MDA), 3,4-methylenedioxymethamphetamine (MDMA), ibuprofen (IBU), gemfibrozil (GEM) and naproxen (NAP) from an influent of ~9 µg L⁻¹ to trace concentrations (< 0.25 µg L⁻¹) was observed in Columns ZVI, BC, and (ZVI + BC) over the complete duration of the experiment. The removal of pharmaceuticals within the treatment columns followed the first-order rate model ($R^2 > 0.93$). The artificial sweeteners acesulfame-K (ACE-K) and saccharin (SAC) (~110 µg L⁻¹) were partially removed in the treatment columns. Removal of cyclamate (CYC) was not observed in any of the columns. However, more than 76% of input sucralose (SCL) (~110 µg L⁻¹) was removed in three treatment columns. Input perfluorooctanoic acid (PFOA) (~45 µg L⁻¹) was partially removed in the columns containing BC, but not in Column ZVI. Between 10% and 80%

of input perfluorooctane sulfonic acid (PFOS) ($24.0\text{--}89.6 \mu\text{g L}^{-1}$) was removed in Column ZVI; greater removals (57–99%) of PFOS were observed in Columns BC and (ZVI + BC) compared to Column ZVI. The removal of the artificial sweeteners, PFOA, and PFOS followed the first-order or zero-order rate models or followed the first-order rate in the early stage of the experiment followed by zero-order rate in the late stage of the experiment. The removal rates of target contaminants decreased over time. The decrease in flow rate did not lead to noticeable improvements in the removals of the target compounds, except for ACE-K.

5.2 Introduction

Pharmaceuticals and artificial sweeteners are heavily consumed in our daily life. These compounds pass through human bodies and finally end up in wastewater treatment plants (WWTPs) in the forms of their unchanged parent or degradation products. However, at many locations, conventional WWTPs cannot efficiently remove these emerging contaminants from water (Joss et al., 2005; Metcalfe et al., 2003a; Scheurer et al., 2009), resulting in the ubiquitous occurrences of pharmaceuticals (such as carbamazepine, caffeine, sulfamethoxazole, 3,4-methylenedioxyamphetamine (MDA) and 3,4-methylenedioxymethamphetamine (MDMA), ibuprofen, gemfibrozil, and naproxen) and artificial sweeteners (such as acesulfame-K, cyclamate, sucralose, and saccharin) in the environment (Carrara et al., 2008; González et al., 2012; Liu et al., 2014b; Rodil et al., 2012).

Pharmaceutical carbamazepine (CBZ) is an antiepileptic drug with a carboxamide functional group attached to a benzo[b][1]benzazepine structure. The persistent behaviors of CBZ (removal < 10%) and diclofenac (removal of 21–40%) in WWTPs have been reported by Zhang et al. (2008). Caffeine (CAF) is a psychoactive substance widely consumed in beverages and drugs; CAF has two carbonyl ($-\text{C}=\text{O}-$) functional groups and three methyl side chains attached to a purine structure. Sulfamethoxazole (SMX) is a sulfonamide class antibacterial drug widely used for treating bacterial infections in humans and domesticated animals; SMX contains an amino (NH_2) and oxazole groups attached to the benzenesulfonamide. Bueno et al. (2012) report the occurrences and persistence of CBZ ($160\text{--}270\text{ ng L}^{-1}$), CAF ($8\text{--}59\text{ }\mu\text{g L}^{-1}$), SMX ($0.5\text{--}1.3\text{ }\mu\text{g L}^{-1}$), ibuprofen (IBU) ($5\text{--}14\text{ }\mu\text{g L}^{-1}$), and gemfibrozil (GEM) (up to $1\text{ }\mu\text{g L}^{-1}$) in WWTPs with removals 50–80%, except for CBZ (no removal with effluent concentration higher than

influent). MDA and MDMA are illicit psychedelic recreational drugs; they contain the same methylenedioxy (-O-CH₂-O-) group attached to the aromatic ring of amphetamine (for MDA) and methamphetamine (for MDMA) molecules. MDA and MDMA are widely detected in untreated and treated wastewater, surface water and groundwater with observed concentrations up to 600 ng L⁻¹ (Jurado et al., 2012; Metcalfe et al., 2010a; Pal et al., 2013) and reported persistent at different stages of treatment within municipal wastewater treatment plants (Nefau et al., 2013). Pharmaceuticals IBU and NAP are nonsteroidal anti-inflammatory drugs (NSAID), which are used as pain killers. IBU contains an isobutylphenyl group attached to a propanoic acid; NAP contains a methoxynaphthalene structure attached to a propanoic acid. GEM is a lipid regulating drug which contains a dimethylphenoxy attached to a 2,2-dimethylpentanoic acid. Metcalfe et al. (2003a) report the occurrences of neutral drug CBZ (1.9–2.3 µg L⁻¹) and acidic drugs IBU (24.6–75.8 µg L⁻¹), NAP (33.9–611 µg L⁻¹), and GEM (1.3–2.1 µg L⁻¹) in influent and effluent samples collected in 14 Canadian sewage treatment plants (STP) with no removal for CBZ and removals of 51% for IBU, 94% for NAP, and 38% for GEM. The widespread occurrences of pharmaceuticals IBU and NAP in surface water, treated wastewater and drinking water have also been reported previously (Boyd et al., 2003).

Acesulfame-K (ACE-K) is an artificial sweetener, which is a potassium salt of 6-methyl-1,2,3-oxathiazine-4(3*H*)-one 2,2-dioxide. Artificial sweetener cyclamate (CYC) is a sulfamic acid (NH₂SO₃H) with cyclohexane structure attached to the N atom. The artificial sweetener saccharin (SAC) is 300–400 times as sweet as sucrose or table sugar with an O-benzoic sulfimide structure. Artificial sweetener sucralose (SCL) has a disaccharide structure where three hydroxyl groups are replaced by chlorine. Due to the persistence of some pharmaceuticals and artificial sweeteners, they have been used to track anthropogenic contamination in aquatic

environments. Buerge et al. (2009) report the artificial sweeteners ACE-K and SCL are not routinely removed in WWTPs with activated sludge processes; however, SAC and CYC are biodegradable (Lange et al., 2012). Emerging contaminants such as artificial sweetener ACE-K, pharmaceuticals CAF, CBZ and IBU, and insect repellent DEET have been reported to be useful tracers of wastewater in surface water and groundwater (James et al., 2016; Liu et al., 2014b; Sorensen et al., 2015; Van Stempvoort et al., 2013). Mawhinney et al. (2011) use the artificial sweetener SCL as an indicator for the presence of other recalcitrant compounds in finished drinking water. ACE-K is also used as a population marker to assist identifying sources of perfluoroalkyl acids in surface waters (Müller et al., 2011).

Perfluoroalkyl substances (PFASs) are aliphatic hydrocarbons consisting of a hydrophobic perfluoroalkyl carbon group (H atoms have been completely replaced by F atoms) attached to a hydrophilic ionic acid (such as carboxylic acid and sulfonic acid). They are primarily used as surfactants in industrial, military, and consumer products such as polymer additives, surface treatment agents and fire retardants because of their high thermal and chemical stability (Ahrens, 2011). High water solubility, hydrophobicity/hydrophilicity, and low volatility make PFASs ubiquitous contaminants in water, wildlife, and humans (Ahrens & Bundschuh, 2014; Houde et al., 2011). These compounds are extremely persistent and resistant to physical, chemical, and biological degradation and have been reported to be transported globally (Paul et al., 2009; Rahman et al., 2014). Perfluorooctanoic acid (PFOA, $C_7F_{15}COOH$) and perfluorooctane sulfonic acid (PFOS, $C_8F_{17}SO_3^-$) are the most studied PFASs because of their frequent detection and high observed concentrations (Ahrens, 2011; Schaider et al., 2014). These contaminants have been widely found in wastewater, surface water, groundwater, and drinking water (Ahrens, 2011; Ahrens & Bundschuh, 2014; Schaider et al., 2014).

Pharmaceutical compounds and PFASs have been reported to be reproductive and development toxicants, and endocrine disruptors; moreover, PFASs are bioaccumulative and even possible carcinogens (Ding & Peijnenburg, 2013; Sanchez et al., 2011; Santos et al., 2010). Because the municipal water and wastewater treatment systems cannot efficiently remove pharmaceuticals such as CBZ, CAF, and IBU, artificial sweeteners such as ACE-K and SCL, and especially PFASs such as PFOA and PFOS from water (except for reverse osmosis and nanofiltration), different technologies such as advanced oxidation, microbial treatment, and granular activated carbon (GAC) adsorption have been extensively studied for removing these contaminants from water (Ahmed et al., 2016; Bo et al., 2015; Merino et al., 2016; Sotelo et al., 2014).

Advanced oxidation technologies such as UV photo- and photocatalytic degradation and UV/H₂O₂, ozonation have shown to effectively degrade many pharmaceuticals and artificial sweeteners (Sharma et al., 2014; Tong et al., 2012). The degradation or decomposition of PFASs is more challenging than other emerging contaminants, due to the highly stable saturated C-F bond. Efficient decomposition of PFOS has been reported using zero-valent iron (ZVI) in subcritical water (> 205 °C, high pressure at 23.3 MPa) (Hori et al., 2006). Lee et al. (2009) demonstrate that 99.3% of PFOA (254 µM) can be decomposed with 74% defluorination efficiency using microwave-induced persulfate. Effective removals of perfluoroalkyl acids (PFAAs) is observed using nanofiltration (>93%) and GAC (>80%) (Appleman et al., 2013). However, these treatment methods either require strong oxidizing radicals ($\cdot\text{OH}$ and $\text{SO}_4^{\cdot-}$) under extreme conditions such as low pH, high temperature and pressure or need to be frequently changed or renewed, which makes the treatment costly (Merino et al., 2016). In addition, the strong oxidants (such as persulfate and hydrogen peroxide) used in in-situ chemical oxidation

have been reported to be greatly decomposed by naturally occurring minerals [such as Fe(III)- and Mn(IV)-containing oxides] in groundwater and aquifer materials (Liu et al., 2014a), which also makes the advanced oxidation processes less effective in field applications.

ZVI is a strong reductant (reduction potential of -0.44 V) and has the potential to degrade environmental contaminants, such as nitro-organic compounds and chlorinated hydrocarbons (Devlin et al., 1998; Gillham & O'Hannesin, 1994; Matheson & Tratnyek, 1994; Orth & Gillham, 1996). In addition, some iron corrosion products formed on the surface of ZVI such as green rust and magnetite have been proposed as effective reductants for treating many contaminants (Agrawal et al., 2002; Elsner et al., 2004). Compared to granular ZVI, nanoscale ZVI has larger specific surface area and higher surface reactivity which results in more rapid and extensive removals of contaminants. Nanoscale and granular ZVI based advanced oxidation processes are widely studied for removing contaminants from water. Bautitz et al. (2012) report degradation (96%) and mineralization (60%) of pharmaceutical diazepam ($\sim 25 \text{ mg L}^{-1}$) after 60 min in an enhanced Fenton (ZVI/EDTA/O₂) system. Granular ZVI has also been used as a persulfate (S₂O₈²⁻) activator to facilitate chemical oxidation of pharmaceutical SMX (Liu et al., 2016b). Limited studies have been reported on the use of ZVI alone as a reducing agent for removing pharmaceuticals and PFASs from water. König et al. (2016) demonstrate reductive biotransformation of the pharmaceutical CBZ using ZVI sponge material with 20% removal. Reductive degradation (38–96% removed) of four PFASs (PFOA, PFNA, PFDA, and PFOS) has been reported using Mg-aminoclay coated nanoscale ZVI under low pH (pH = 3) conditions (Arvaniti et al., 2015).

Biochar (BC) is a porous carbon-residue derived from waste organic materials pyrolyzed under limited oxygen or anaerobic conditions. BC has a large surface area and high porosity, and

contains various functional groups such as carboxylic, aliphatic, and phenolic groups, which provide exchange sites for adsorption of cations, heavy metals, and anions. In addition, the high carbon content makes biochar an effective sorbent for nonpolar organic compounds in wastewater treatment (Scherer et al., 2000). Biochar is widely used in immobilization of organic contaminants (Kim et al., 2016; Oleszczuk et al., 2012) and heavy metals (Liu et al., 2016a; Xu et al., 2012) from contaminated water and soil. Effective sorption of pharmaceuticals CBZ, SMX, IBU, and NAP by biochar has been reported (Jung et al., 2015a; Rajapaksha et al., 2015; Williams et al., 2015).

ZVI and BC are non-toxic and cost-effective reactive materials and easy to obtain. The purpose of this study is to evaluate the potential of low-cost reactive materials for the simultaneous removal of three classes of emerging contaminants under dynamic flow conditions. Four column experiments were conducted to evaluate the removal of pharmaceuticals ($\sim 10 \mu\text{g L}^{-1}$), artificial sweeteners ($\sim 100 \mu\text{g L}^{-1}$), and perfluoroalkyl substances ($20 - 100 \mu\text{g L}^{-1}$) from simulated groundwater using ZVI, BC and a mixture of ZVI and BC. The target contaminants and their concentrations were selected and chosen according to their occurrences and concentrations found in wastewaters derived from domestic and municipal sources. Simulated groundwater ($\sim 100 \text{ mg L}^{-1} \text{ CaCO}_3$ saturated water) was used as the matrix for the influent solution to represent concentrations of dissolved Ca^{2+} , HCO_3^- , and CO_3^{2-} , which are present in natural surface water and groundwater.

5.3 Material and Methods

5.3.1 Column Design and Experimental Setup

Four acrylic columns were used, each 30 cm in length and 5 cm internal diameter. Influent and effluent ports were attached to the bottom and top of each column for introducing influent and discharging effluent solutions. Thirteen sampling ports were installed along the length of each column at 2.1 cm intervals. Column Control was packed with 100% silica sand (SS). Column ZVI was packed with 50% (v/v) granular ZVI and 50% (v/v) SS. Column BC was packed with 50% (v/v) BC and 50% (v/v) SS. Column (ZVI + BC) was packed with 10% (v/v) granular ZVI, 40% (v/v) BC, and 50% (v/v) SS. A 1 cm-thick layer of 100% SS was packed on the top and bottom ends of the columns to separate the column packing from the influent and effluent ports. The physical characteristics of the columns are provided in Table 5.1. The SS (0.6–0.8 mm) was obtained from the Silica Company (Ottawa, IL, US). The granular ZVI (0.25–1.19 mm) was obtained from Connelly-GPM, and was washed using 1.2 M HCl acid, followed by ultrapure H₂O (Type 1, 18.2 MΩ cm @ 25 °C, generated from a MilliQ A10 water system) before use. The BC (oak hard wood; 0.5–2.36 mm) was obtained from Cowboy Charcoal Co., Brentwood, TN, USA. The carbon content of the BC is 99.9% and contains hydroxyl, aliphatic, quinone, sulfate, and carbonate functional groups (Liu et al., 2015b). After packing, the columns were wrapped with aluminum foil to minimize exposure to light. The columns were purged with CO_{2(g)} for 24 hr to displace atmospheric gases in the void pore spaces of the column packing, except for the Column ZVI. The CO_{2(g)} is more soluble in water than N₂ and O₂, which enhances the saturation of the packing materials. The Column ZVI was not purged with CO_{2(g)} to avoid the formation of carbonate precipitates which can cause a decrease in reactivity of the iron (Jeen et al., 2006). The

columns were placed in an anaerobic glove box (COY Ltd.) that contained 5% H₂ and 95% N₂ and were saturated with ultrapure H₂O before introducing influent solution.

A concentrated stock solution was prepared that contained 10 mg L⁻¹ of pharmaceutical compounds carbamazepine (CBZ), caffeine (CAF), sulfamethoxazole (SMX), 3,4-methylenedioxyamphetamine (MDA), 3,4-methylenedioxymethamphetamine (MDMA), ibuprofen (IBU), gemfibrozil (GEM), and naproxen (NAP), 100 mg L⁻¹ of artificial sweeteners acesulfame-K (ACE-K), cyclamate (CYC), saccharin (SAC), and sucralose (SCL), and 50 – 100 mg L⁻¹ of perfluorooctanoic acid (PFOA) and perfluorooctane sulfonic acid (PFOS) in ultrapure water. About 9% (v/v) of methanol (HPLC grade, Sigma-Aldrich) was used in the concentrated stock solution to dissolve the dry powders in the aqueous solution. The influent solution was prepared by adding 4 mL of the concentrated stock solution to 4 L Ar-purged simulated groundwater (CaCO₃ saturated water), resulting in < 0.01% methanol. The final influent solution contained approximately 10 µg L⁻¹ of pharmaceuticals CBZ, CAF, SMX, MDA, MDMA, IBU, GEM, and NAP, 100 µg L⁻¹ of artificial sweeteners ACE-K, CYC, SAC, and SCL, and 50 µg L⁻¹ of PFOA and 20 µg L⁻¹ PFOS for the first 21 pore volumes (PV) of flow. After 21 PV of flow through the columns, the concentration of PFOS in the influent solution was increased to 50 – 100 µg L⁻¹ to match the influent PFOA concentration; the concentrations of the other target contaminants remained the same.

The experiments were divided into two stages. The influent solution was pumped through the columns from the bottom to the top at 0.3 pore volume (PV) d⁻¹ during the first stage of the experiment, and pumped at a rate of 0.1 PV d⁻¹ after 50 PV of flow during the second stage of the experiment to evaluate the effect of residence time on contaminant removals. The flow rate was set at 0.3 or 0.1 PV d⁻¹ to be representative of average groundwater velocities reported at

subsurface-wastewater disposal sites (Benner et al., 1997; Carrara et al., 2008; Robertson et al., 2000). Profile samples were collected during the experiments at four times (1, 13, 25, 53 PV of flow) along the length of the columns.

5.3.2 Sample Collection and Analytical Methods

Water samples were collected from the effluent and profile ports using 125 mL amber glass bottles except those for PFOA and PFOS analysis, which were collected using 30 mL polypropylene bottles. Samples for pH and Eh analysis were not filtered; alkalinity samples were filtered through 0.45- μm cellulose acetate membranes (Pall Corp., Canada) before measurement. Pharmaceutical samples were filtered through 0.45- μm nylon membranes (Pall Corp., Canada) and collected in 25 mL amber glass vials. Artificial sweetener samples were filtered through 0.2- μm PVDF membranes (Chromatographic Specialties Inc., Canada) and collected in 8 mL polyethylene (HDPE) bottles. Samples for PFOA and PFOS analysis were filtered through 0.45- μm polypropylene membranes (Pall Corp., Canada) and collected in 15 mL HDPE bottles before 36 PV of flow through the columns, but not filtered afterwards. The measurements of pH, Eh and alkalinity were performed immediately after sampling; all other samples were stored at 4 °C until analysis within one month of collection.

The pH values were measured using a Ross combination glass electrode (Orion 815600) calibrated using standard pH 7, 4, and 10 buffers before use and checked against pH 7 and 10 buffers between samples. The Eh values were measured using a Pt-billeted Ag-AgCl combination electrode (Orion 9678BNWP). The performance of the Eh probe was checked against A and B solutions (redox/ORP electrode user guide, Thermo Scientific, Canada) between samples. The alkalinity measurements were performed using a Hach digital titrator with bromocresol green/methyl red indicator and 0.08 mol L⁻¹ H₂SO₄.

The analysis of target compounds involved isotope dilution of each compound to track the analyte recovery, instrument variability and matrix suppression during sample analysis. The native analyte compounds of CBZ, CAF, SMX, IBU, GEM, NAP, CYC, and SAC for calibration standards and input stock solution were obtained from Sigma-Aldrich (Oakville, Canada). The isotope labeled standards CBZ-d10, CAF-d3, IBU-d3, GEM-d6, and [¹³C]-NAP were obtained from Cambridge Isotope Laboratory Inc. (Cambridge, USA); the isotope labeled standards SMX-d4, CYC-d11, and SAC-¹³C6 were obtained from Toronto Research Chemicals Inc. (Toronto, Canada). The native analytes ACE-K and SCL and isotope labeled ACE-K-d4 and SCL-d6 standards were obtained from Toronto Research Chemicals Inc. (Toronto, Canada). The native analytes MDA and MDMA and isotope labeled MDA-d5 and MDMA-d5 were obtained from Cerilliant Inc. (Texas, USA). The native analytes PFOA and PFOS and their isotope labeled standards [¹³C]-PFOA and [¹³C]-PFOS for preparation of calibration standards were obtained from Wellington Laboratories Inc. (Guelph, Canada). The analytes PFOA and PFOS dry powder for preparation of the input stock solution were obtained from Sigma-Aldrich, Canada.

Prior to analysis, 1 mL aliquots of artificial sweetener samples, 10 mL aliquots of pharmaceutical samples, and 20 mL aliquots of diluted PFOA and PFOS samples were spiked with consistent amounts of internal standards (IS). The IS spiked pharmaceutical and PFOA and PFOS samples were passed through solid-phase extraction (SPE) cartridges (Oasis HLB 3 cc glass cartridges; Waters Corp., Mississauga, Canada) preconditioned with 2 x 1 mL methanol and then washed with 2 x 1 mL ultrapure H₂O. For pharmaceutical SPE, the cartridges were loaded with 10 mL pharmaceutical sample, washed with 2 x 1 mL 5% (v/v) methanol, vacuum dried, and eluted with 2 x 1 mL methanol. The pharmaceutical extracts were collected in 7 mL amber glass vials. For PFOA and PFOS SPE, the cartridges were loaded with 20 mL PFOA and

PFOS sample, washed with 2 x 1 mL ultrapure H₂O, vacuum dried, and eluted with 2 x 1 mL methanol. The PFOA and PFOS extracts were collected in 5 mL polypropylene centrifuge tubes (Eppendorf Ltd., Canada). The extracts were kept chilled at 4 °C before analysis.

Pharmaceutical compound extracts were analyzed by high performance liquid chromatography (Agilent 1100, Agilent Technologies) followed by electrospray tandem mass spectrometry (4000 Q TRAP, Applied Biosystems, Foster City, USA) using previously described methods (Stafiej et al., 2007; Vanderford & Snyder, 2006) with some modifications to optimize for instrument operating conditions. Caffeine, SMX, CBZ, MDA, and MDMA were analyzed in electrospray ionization positive (ESI+) mode, while IBU, GEM, and NAP were analyzed in ESI negative (ESI-) mode. The mobile phase composition and gradient setup followed previously described procedures (Liu et al., 2014b). Seven to eleven point calibration curves (MDMA: 0.005–10 µg L⁻¹, CAF and SMX: 0.01–10 µg L⁻¹, CBZ and MDA: 0.1–10 µg L⁻¹, IBU, GEM and NAP: 0.05–10 µg L⁻¹) were used to quantify pharmaceutical concentrations with pharmaceutical IS mixture added to yield a concentration of 1 µg L⁻¹. Tap water samples spiked with analyte and IS following the same procedures as unknown samples (quality control, QC samples) were used to evaluate the impact of the SPE step on the analytical method. Fortified samples were prepared which consisted of the unknown samples spiked with a known amount of analyte and IS. One duplicate and one fortified sample were prepared between every ten unknown pharmaceutical samples to check the accuracy of the SPE procedures. The accuracies of pharmaceutical calibration, calibration verification (CV), and continuous calibration verification (CCV) samples were in the range of 85–120% with IS recoveries of 84–11%. The accuracies of the duplicate and fortified unknown pharmaceutical samples were 83–119%. The absolute IS recoveries of pharmaceutical quality control and unknown samples,

including duplicate and fortified samples, were in the range of 71–124%. The method detection limits (MDLs) of pharmaceutical compounds were 20 ng L⁻¹ for CBZ, 100 ng L⁻¹ for CAF, 10 ng L⁻¹ for SMX, 30 ng L⁻¹ for MDA, 5 ng L⁻¹ for MDMA, 30 ng L⁻¹ for IBU, 5 ng L⁻¹ for GEM and 20 ng L⁻¹ for NAP.

The artificial sweetener samples were analyzed by ion chromatography (Dionex ICS-5000, Thermo Scientific, Sunnyvale, USA) followed by tandem mass spectrometry (6460 QQQ, Agilent Technologies, Mississauga, Canada) in ESI- mode using a previously described method (Van Stempvoort et al., 2011). Nine point calibration curves (0.05–200 µg L⁻¹) with the IS concentration of 1 µg L⁻¹ of ACE-d4, 5 µg L⁻¹ of CYC-d11 and SAC-¹³C6, and 100 µg L⁻¹ of SCL-d6 were used for AS quantitation. The quality control samples and duplicate and fortified unknown samples were prepared followed the same procedure as for the calibration samples. The accuracies of the AS calibration, CV, and CCV samples were 82–114%. The accuracies for duplicate and fortified unknown AS samples were 80–119%. The absolute IS recoveries for CCV and unknown AS samples were in the range of 71–121%. The MDL of ACE, CYC, SAC, and SCL were 0.1 µg L⁻¹.

The PFOA and PFOS extracts were analyzed by high performance liquid chromatography (1290 HPLC, Agilent Technologies, Mississauga, Canada) followed by tandem mass spectrometry (6460 QQQ, Agilent Technologies, Mississauga, Canada) in ESI- mode using EPA Method 537 (Shoemaker, 2013) with recommended modifications (Application Note, Agilent Technology; Yamashita et al., 2004). The analytes were separated using an Agilent Zorbax Eclipse C18 4.6 × 150 mm, 5 µm i.d. (Agilent, Mississauga, Canada) at 55 °C. The mobile phase consisted of 2 mM ammonium acetate (HPLC grade, Sigma-Aldrich, Oakville,

Canada) in water (phase A) and 2 mM ammonium acetate in methanol (phase B). A gradient elution started at 6% B for 1 min, increased linearly to 95% within 7 min and held at 95% for 8 min, then decreased to 6% at 16.01 min and held at 6% until 20 min. The flow rate was 0.6 mL min⁻¹ and the injection volume was 20 µL. Eight point calibration standards (0.1–20 µg L⁻¹) with 1 µg L⁻¹ of [¹³C]-PFOA and 2 µg L⁻¹ of [¹³C]-PFOS were prepared in 96 : 4% (v/v) methanol : water for PFOA and PFOS quantitation. The accuracies of calibration, CV, and CCV sample were between 80% and 119%. One duplicate sample with two different dilution factors was prepared for every ten unknown PFOA and PFOS samples, yielding accuracies of 85–126%. One third of the unknown PFOA and PFOS samples were analyzed in duplicate or triplicate to assess the instrument variability. Tap water samples (QC samples) spiked with analyte and IS were used to track the precision of the SPE procedures. The absolute IS recoveries of the CV, CCV, QC, and unknown samples were 73–126%. The MDL of PFOA and PFOS were 45 and 110 ng L⁻¹.

5.4 Results and Discussion

5.4.1 Column Geochemistry

The four pH profiles measured at different times within the columns were highly consistent, exhibiting similar values with distance along the columns, except for those obtained within Column ZVI (Figure 5.1). The average pH values within Columns Control and BC effluents were about 8.3 during the first stage of the experiment, which was consistent with the influent pH values. During the second stage of the experiment, the pH values of the Column Control effluent gradually increased to 8.6 at 63 PV, while the pH values of the Column BC effluent gradually decreased to 6.9 at 68 PV (Figure 5.2). The pH values of the Column ZVI effluent

gradually increased from 7.8 at 5 PV to 9.4 at 25 PV until the end of the first stage of the experiment (50 PV); this increase in pH is attributed to the reduction of water by ZVI ($Fe^0 + 2H_2O \leftrightarrow Fe^{2+} + 2OH^- + H_{2(g)}$) (Wilson, 1923); however, the pH of the Column ZVI effluent then started to decrease to 8.6 at 63 PV in the second stage of the experiments as the flow rate was decreased from 0.3 to 0.1 PV d⁻¹ (Figure 5.2). This changing trend in pH for the Column ZVI effluent was consistent with the profile results (Figure 5.1). The average pH within Column (ZVI + BC) and in its effluents was constant at 8.7 through the entire experiment despite the decrease in flow rate.

The four Eh profiles within the columns exhibited similar values of < -400 mV, indicating strong reducing conditions in these columns over the course of the experiment. The average Eh values within Columns Control, ZVI, BC, and (ZVI + BC) were about -410, -450, -395 and -440 mV (Figure 5.1). The Eh of the Column Control effluent was consistent with the influent Eh (~ -410 mV). The lowest Eh values of -500 mV were observed within Column ZVI and in its effluent at around 25 PV likely due to the production of H₂ associated with ZVI corrosion (Wilson, 1923). The Eh values within Column BC and in the effluents were similar to the influent Eh during the first stage of the experiment; however, the Eh values increased from -384 mV at 53 PV to -338 mV at 69 PV during the second stage of the experiment. The Eh values of Column (ZVI + BC) were relatively constant at -440 mV throughout the entire experiment (Figures 5.1 and 5.2).

The four alkalinity profiles within each column indicated similar changing trends, with constant concentrations observed in the influent within Columns Control and BC and decreasing values with distance along the flow direction within Columns ZVI and (ZVI + BC) (Figure 5.1).

The concentrations of alkalinity in Columns Control and BC effluents were consistent with the influent alkalinity (51–94 mg L⁻¹ as CaCO₃) during the experiment. The average alkalinity concentration in Column ZVI effluent increased from 14 mg L⁻¹ (as CaCO₃) before 18 PV to 39 mg L⁻¹ (as CaCO₃) at 47 PV during the first stage of the experiment, and then decreased slightly to 27 mg L⁻¹ (as CaCO₃) at 63 PV in the second stage of the experiment. The concentrations of alkalinity in Column (ZVI + BC) effluent were slightly lower than that of Column BC, but higher than that of Column ZVI likely as a result of the mixed composition of the two reactive media (Figure 5.2).

5.4.2 Removal of Pharmaceutical Compounds in Columns

5.4.2.1 Removal of Pharmaceutical Compounds from Column Effluent

Pharmaceutical compounds CBZ, CAF, MDA, MDMA, IBU, GEM, and NAP were not removed in the Column Control with consistent concentrations between their effluent and influent, except for sulfamethoxazole (SMX). SMX was not removed in the Column Control in the early stage of the experiment; however, increasing removal of SMX in the Column Control was observed in the late stage of the experiment. In general, all eight pharmaceuticals were removed in the three treatment columns with removals ranging from 97–99% (Figures 5.3 and 5.4).

The concentrations of SMX in the Column Control effluent were consistent with the influent concentration before 14 PV; however, a gradual decrease from 8.6 µg L⁻¹ at 14 PV to 2.8 µg L⁻¹ at 47 PV was observed in the first stage of the experiment. The decrease in flow rate from 0.3 PV d⁻¹ in the first stage of the experiment to 0.1 PV d⁻¹ in the second stage of the experiment led to enhanced removal of SMX in the Column Control; the concentration of SMX then

decreased to $\sim 0.3 \mu\text{g L}^{-1}$ in the second stage of the experiment (Figure 5.4). As an antibiotic, SMX has been reported to inhibit bacterial growth at concentrations in the range of $1.3\text{--}253 \mu\text{g L}^{-1}$ (Underwood et al., 2011). However, the removal of SMX in Column Control was likely due to biodegradation and sorption of SMX to the biofilms as a result of microbial growth during the extended operating period. Removal of SMX in sand and soil matrix systems has been reported previously (Bertelkamp et al., 2014; Martínez-Hernández et al., 2016; Wunder et al., 2011).

The concentrations of pharmaceutical compounds in the Columns ZVI, BC and (ZVI + BC) effluents decreased from the average input concentration of $\sim 9 \mu\text{g L}^{-1}$ to the concentrations $< 0.25 \mu\text{g L}^{-1}$ throughout the experiment, indicating almost complete removals ($> 97\%$) of the eight target pharmaceuticals (Figures 5.3 and 5.4). The decrease in flow rate did not affect the removals of pharmaceutical compounds in the Columns ZVI, BC and (ZVI + BC).

5.4.2.2 Potential Removal Mechanisms of Pharmaceutical Compounds by ZVI and BC

Removal of contaminants using ZVI has been reported involving direct and indirect reduction of contaminants by ZVI and iron oxides, or adsorption or coprecipitation of contaminants on corrosion products (Blowes et al., 1997; Crawford et al., 1993; Lee & Batchelor, 2002; Matheson & Tratnyek, 1994; Odziemkowski & Simpraga, 2004). The corrosion of Fe^0 in natural waters (pH 4–9) produces hydrated iron oxide films on the metal surface (Wilson, 1923). The OH groups (H donors and acceptors) of iron hydroxide can interact with NH, NH_2 , and OH groups (H donors and acceptors) of target pharmaceuticals through H bonding which likely enhanced the removal of pharmaceuticals by ZVI. In this study, common products of Fe^0 corrosion and precipitation in dissolved calcium carbonate water (simulated groundwater) are iron hydroxy carbonate [$\text{Fe}_2(\text{OH})_2\text{CO}_3$] and aragonite (CaCO_3), which likely are negatively charged in the pH range of this study (pH 7.9–9.5) (Guilbaud et al., 2013); the electrostatic

interaction between negatively charged ZVI and positively charged pharmaceuticals can also contribute to the removal of pharmaceuticals by ZVI.

Removal of organic contaminants by BC is attributed to the strong sorption affinity between organic contaminants and BC, which likely involves hydrophobic interaction, $\pi - \pi$ electron donor-acceptor (EDA) interaction, $\pi - \pi$ electron coupling interaction between the graphite moieties of BC and π electron of contaminants, electrostatic interaction, and H-bonding (Inyang & Dickenson, 2015; Wang et al., 2016). The BC used in this study (pyrolyzed under high temperature ~ 700 °C) is likely a π -donor due to a high content of graphitic carbon content (99.9%) (Liu et al., 2015b), which likely interact with electron withdrawing functional groups of target pharmaceuticals through $\pi - \pi$ EDA interaction. The $-OH$ functional groups on BC (Liu et al., 2015b) can serve as both H donors and acceptors which can interact with electronegative N and O bearing functional groups (H acceptors) through H bonding. The BC was likely negatively charged under pH 7.0–9.5 (Mukherjee et al., 2011); positively charged pharmaceuticals can be adsorbed on negatively charged BC through electrostatic interaction. The potential removal mechanisms of target pharmaceuticals by ZVI and BC are summarized in Table 5.2.

The hydrophobic interaction between target pharmaceuticals and BC can be affected by the pH of the treatment system and pKa and $\log K_{ow}$ (K_{ow} : octanol-water partition coefficient) of the pharmaceuticals. $\log K_{ow}$ is used to express the hydrophobicity of a compound. A compound is considered to be hydrophilic when its $\log K_{ow} < 1$, moderately hydrophobic (transphilic) when its $1 < \log K_{ow} < 3$, and hydrophobic when its $\log K_{ow} > 3$ (Verliefde et al., 2008). The pharmaceuticals CBZ, MDA, MDMA, IBU, GEM, and NAP are moderately hydrophobic in their neutral forms ($\log K_{ow} > 1$). However, dissociation of these compounds (except for CBZ, a neutral compound) at pH=8.3 (average investigated pH) results in a decrease in hydrophobicity

compared to the neutral form. $\text{Log } D_{ow}$ (pH dependent $\text{log } K_{ow}$) is used to express the relationship among $\text{log } K_{ow}$, pH, and pKa , and was calculated using the following expression (Schwarzenbach et al., 2003).

$$\text{Log } D_{OW} = \text{Log } K_{OW} - \text{Log } \frac{1}{1+10^{\text{pH}-\text{pKa}}} \quad \text{For organic acids} \quad \text{Equation 5.1}$$

$$\text{Log } D_{OW} = \text{Log } K_{OW} - \text{Log } \frac{1}{1+10^{\text{pKa}-\text{pH}}} \quad \text{For organic bases} \quad \text{Equation 5.2}$$

The calculated $\text{log } D_{ow}$ values of target pharmaceuticals (Table 5.2) indicate that all the target pharmaceuticals (except for CBZ, moderately hydrophobic with $\text{log } D_{ow}=2.25$) were hydrophilic in this study; hydrophobic interaction between these hydrophilic pharmaceuticals and hydrophobic BC is expected to be limited.

The eight target pharmaceuticals were divided into three groups (neutral pharmaceuticals, basic pharmaceuticals, and acidic pharmaceuticals) according to their acidic (deprotonated) / basic (protonated) character of functional groups in the investigated pH range (pH: 7.0–9.5):

5.4.2.2.1 Neutral Pharmaceutical CBZ

CBZ is a basic compound due to the presence of $-\text{NH}_2$ functional group in its structure. CBZ was primarily in its neutral form in the investigated pH range due to its low pKa value ($\text{pKa} < \text{pH}$, Figure 5.5). Shirazi et al. (2013) argue that reductive degradation of CBZ by ZVI and nanoscale ZVI is unlikely; however, König et al. (2016) report that CBZ can be reduced by ZVI through reductive catalytic hydrogenation (H_2 was produced during anaerobic corrosion of ZVI by H_2O) with nine hydrogenation products identified. In addition, the H bonding between $-\text{NH}_2$ (H donor and acceptor) and O (H acceptor) of $=\text{O}$ functional groups in CBZ and $-\text{OH}$ groups (H donor and acceptor) on the surface of ZVI likely contributes to the sorption of CBZ by ZVI.

Sorption of CBZ by BC likely occurs through hydrophobic interactions (between moderately hydrophobic CBZ, $\log D_{ow}=2.25$ and hydrophobic BC) (Inyang & Dickenson, 2015), π - π interaction (between the aromatic rings of CBZ and the graphene aromatic structure of BC), and H bonding (between $-\text{NH}_2$ and $=\text{O}$ in CBZ and $-\text{OH}$ on BC). Effective stabilization of CBZ in contaminated soil and water has been reported using BC (Jung et al., 2013; Williams et al., 2015).

5.4.2.2.2 Basic (Cationic) Pharmaceuticals CAF, MDA, and MDMA

CAF, MDA, and MDMA are basic compounds because the N bearing functional groups in these compounds are protonated in the investigated pH range and in their cationic forms ($\text{pH} < \text{pKa}$) (Table 5.2 and Figure 5.5). Electrostatic interactions between positively charged CAF, MDA, and MDMA and negatively charged ZVI and BC likely contribute to the removals of these compounds from water. In addition, the N, $-\text{NH}-$, $-\text{NH}_2$, $=\text{O}$, and $-\text{O}-$ functional groups (H donor or acceptor) in CAF, MDA, and MDMA likely interacted with $-\text{OH}$ groups (H donor or acceptor) on the surfaces of ZVI and BC through H bonding (Table 5.2).

Limited studies have reported the removal of CAF, MDA, and MDMA from water using ZVI and BC. Effective decolorization (92.6%) and total organic carbon removal (60.2%) of dark brown colored coffee effluent has been reported using ZVI, its core (ZVI)-shell structure (ion oxides and hydroxides) provides electrons for reducing coffee and sites for sorption and chemical complex formation (Tomizawa et al., 2016). Effective removal of MDMA ($\sim 30 \text{ ng L}^{-1}$) to undetectable levels is achieved using a ZVI modified Fenton reaction ($\text{ZVI}/\text{H}_2\text{O}_2/\text{H}_2\text{SO}_4$) and ferrate (VI) (Mackul'ak et al., 2016).

The sorption of CAF, MDA, and MDMA by BC was likely through π - π EDA interaction, electrostatic interaction, H bonding, and π - π stacking interaction (except for CAF). The π - π EDA interaction likely formed between the electron withdrawing N, -NH-, -NH₂, =O, and -O- functional groups in CAF, MDA, and MDMA and the π -electron rich BC. The aromatic structure in MDA and MDMA also likely interacted with the graphene aromatic structure of BC through π - π stacking interaction (Table 5.2). Effective mitigation of CAF uptake in plants has been reported using a wood biochar (Hurtado et al., 2016). Sotelo et al. (2014) report the competitive adsorption of CAF and diclofenac by GAC with the sorption capacity of 190.9 mg g⁻¹ for CAF and 233.9 mg g⁻¹ for diclofenac; the relatively lower sorption capacity of CAF compared to diclofenac is likely due to the relatively high water solubility, low molecular weight and low K_{ow} value of CAF.

5.4.2.2.3 Acidic (Anionic) Pharmaceuticals SMX, IBU, GEM, and NAP

SMX is a zwitterion (with two pK_a s: 1.7 and 5.6) which contains both acidic (-NH-) and basic (-NH₂) functional groups. Due to the presence of two strong electron withdrawing groups (heterocyclic ring and sulfonamide), the sulfonamide -NH- group deprotonates at pH > 5.6. The aromatic amine -NH₂ group protonates at pH < 1.7. SMX exists predominantly as an anionic species (negatively charged) at pH > 5.6, uncharged species (neutral) at pH between 1.7 and 5.6, and cationic species (positively charged) at pH < 1.7. IBU, GEM, and NAP are acidic compounds because carboxylic groups in IBU, GEM, and NAP are deprotonated at pH > their pK_a s (4.2-4.5) (Figure 5.5). Therefore, SMX, IBU, GEM, and NAP were present as anionic (negatively charged) species in the pH range of this study (Table 5.2).

Removal of SMX, IBU, GEM, and NAP using ZVI alone has not been previously reported; however, rapid degradation of SMX has been reported within 0.5 h using a ZVI-activated persulfate-assisted mechanochemical method (a chemical oxidation process induced by mechanical forces, which accelerates the reaction due to enhanced mass transfer) (Liu et al., 2016b). The reductive degradation of aqueous IBU (10 mg L⁻¹) by ZVI nanoparticles alone has been reported by Machado et al. (2013) with removals of 54–66% observed. Similar to this study, the degradation rates of IBU by ZVI greatly decrease with increased reaction time likely due to the passivation (oxidation) of the ZVI nanoparticles surface which limits the electron transfer from the core of the ZVI particles to its surface (Li et al., 2006). Effective removal of IBU by advanced oxidation processes using ZVI as a catalyst or activator has been reported by Ziyilan and Ince (2015) and Rodriguez et al. (2016). In addition, the H bonding between –NH₂, –NH–, and N in heterocyclic ring of SMX, COOH group (H donor or acceptor) of IBU, GEM, and NAP and –OH groups (H donor or acceptor) on the ZVI surface also likely contributed to the removal of SMX, IBU, GEM, and NAP by ZVI.

The sorption of SMX, IBU, GEM, and NAP by BC has been reported through mainly hydrophobic interactions (log *K_{ow}* of these compounds ranged from 0.89–4.3) and π – π EDA interaction (Jung et al., 2015a; Jung et al., 2013; Zheng et al., 2013). However, hydrophobic interactions between SMX, IBU, GEM, NAP and BC were likely limited due to the dissociation (deprotonation) of these compounds under the investigated pH. The dissociation of these compounds resulted in much lower hydrophobicity (lower log *D_{ow}* values) (Table 5.2) compared to their neutral species. The π – π EDA interaction likely formed between electron withdrawing sulfonamide and heterocyclic ring groups in SMX, carboxyl groups in IBU, GEM, and NAP (π electron acceptors) and the π -electron rich BC (π electron donors). The π – π stacking interaction

between the aromatic rings in SMX, IBU, GEM, and NAP molecule and graphene aromatic structure of BC likely enhanced the sorption of SMX, IBU, GEM, and NAP by BC. In addition, H bonding and π -H bonding between the N, NH, or NH₂ functional groups in SMX, =O and –OH in carboxyl groups of IBU, GEM, NAP (H electron donor or acceptors) and –OH (H electron donor or acceptors), and aromatic π structure of BC also likely contributed to sorption of these compounds by BC.

Effective sorption of SMX (0–80 mg L⁻¹) has been reported using BC (produced at 300–600 °C) with a sorption capacity of 1.9–4.9 mg g⁻¹ at pH=5. The competitive adsorption of IBU by BC has been observed in the presence of other adsorption competitors diclofenac and NAP, which causes a lower binding energy (Jung et al., 2015a). Jung et al. (2015b) demonstrate that about 97.7% of input NAP (10 μ M) can be removed by 50 mg L⁻¹ BC from an aqueous solution (pH 6.5). Powder activated carbon (PAC) is a similar carbonaceous sorbent to biochar; limited removals of IBU < 21%, NAP and GEM < 50% from the input concentration of 50–80 ng L⁻¹ by PAC were reported during a simulated drinking water treatment process following a conventional (coagulation plus chlorination) treatment system (Westerhoff et al., 2005). However, Margot et al. (2013) report more effective removals of NAP (78–95% removed from input concentration of 0.5–0.7 μ g L⁻¹) and IBU (38–83% removed from input concentration of 1.6–6.6 μ g L⁻¹) from raw wastewater by PAC (10–20 mg L⁻¹).

5.4.2.3 Removal Rates of Pharmaceutical Compounds within Columns

The removal of pharmaceutical compounds within Columns ZVI, BC and (ZVI + BC) followed a first-order rate model (Figures 5.6 and 5.7) with $R^2 > 0.93$. The removal rates were calculated using least-squares regression by dividing the data into two experimental stages. The removal

rates, first order removal rate constants (k_{obs} , d^{-1}), mass normalized rate constants (k_M , $L\ g^{-1}\ d^{-1}$), and surface area normalized rate constants (k_{SA} , $L\ m^{-2}\ d^{-1}$) of target pharmaceuticals are summarized in Appendix D (Tables D.1 – D.8). K_M and K_{SA} were calculated following the expressions (Johnson et al., 1996):

$$K_M = K_{obs}/\rho_m \quad \text{Equation 5.3}$$

$$K_{SA} = K_{obs}/\rho_a = K_M/a_s \quad \text{Equation 5.4}$$

Where ρ_m is the mass concentrations of reactive media ($g\ L^{-1}$ of solution); ρ_a is the surface area concentrations of reactive media ($m^2\ L^{-1}$ of solution); and a_s is the specific surface area of reactive media ($m^2\ g^{-1}$). Specific surface areas of ZVI, BC, and (ZVI + BC) used in the experiments are 9.5, 64.5, and 33.6 $m^2\ g^{-1}$ (Jamieson-Hanes, 2012; Liu, 2016).

Overall, the pharmaceuticals were removed more rapidly in Columns ZVI and (ZVI + BC) than Column BC. The removal rates of pharmaceuticals within the treatment columns decreased by 67–99% over the experimental period. Decreases in the removal rates of pharmaceuticals by ZVI may be related to a declining reactivity of ZVI due to accumulation of secondary precipitates on the ZVI surfaces, such has been described for treatment of trichloroethylene (TCE) by ZVI (Jeen et al., 2006; Jeen et al., 2007). Decreasing removals of pharmaceuticals by BC may be due to in-filling of pores and decreasing sorption sites over time. The removal rates of pharmaceuticals within Columns ZVI and (ZVI+BC) followed the order: SMX > MDMA > MDA > CAF > CBZ > GEM > NAP > IBU (SMX > cationic compounds > neutral compound > anionic compounds or N functional group bearing compounds > carboxylic functional group bearing compounds). The removal rates of pharmaceuticals within Column BC followed the order: MDMA > MDA > CAF > CBZ > NAP > GEM > SMX > IBU (cationic compounds >

neutral compound > anionic compounds) (Appendix D, Tables D.1–D.8). Overall, removal rates of cationic pharmaceuticals (positively charged) were greater than neutral and anionic pharmaceuticals within each treatment column independent of the hydrophobicity ($\log D_{ow}$), number of aromatic rings and number of H acceptors and donors of the compounds. CBZ is the most hydrophobic (high $\log D_{ow}$ value) pharmaceutical in this study, but its removal rate was lower than for the cationic pharmaceuticals (MDMA, MDA, and CAF). Electrostatic interactions were likely more important than other removal mechanisms such as hydrophobic interactions ($\log D_{ow}$), $\pi - \pi$ EDA and stacking interactions, and H bonding in removal of target pharmaceuticals.

5.4.3 Removal of Artificial Sweeteners in Columns

5.4.3.1 Removal of Artificial Sweeteners from Column Effluent

Artificial sweeteners acesulfame-K (ACE-K), cyclamate (CYC), saccharin (SAC) and sucralose (SCL) (input concentration: 90–120 $\mu\text{g L}^{-1}$) were not removed in Column Control. ACE-K and SAC were partially removed by the three treatment columns. Artificial sweetener CYC was not removed in any treatment column throughout the experiment. More than 76% of input SCL was removed in the three treatment columns (Figure 5.8).

A small fraction of input ACE-K ($\sim 100 \mu\text{g L}^{-1}$) was removed in Columns ZVI and (ZVI + BC). The effluent ACE-K concentration was maintained at $\sim 75 \mu\text{g L}^{-1}$ ($\sim 27\%$ removed) in Column ZVI and $\sim 85 \mu\text{g L}^{-1}$ ($\sim 14\%$ removed) in Column (ZVI + BC) in the first stage of the experiment. The removals of ACE-K in Columns ZVI and (ZVI + BC) were enhanced by the decrease in flow rate from 0.3 to 0.1 PV d^{-1} . The concentrations of ACE in the effluents of Columns ZVI and (ZVI + BC) decreased to ~ 40 and $\sim 75 \mu\text{g L}^{-1}$. The removals increased to 61%

and 31% as the experiment proceeded to the second stage. No removal of ACE-K was observed in Column BC (Figure 5.8). Similarly, poor removal (~10%) of ACE-K is reported using PAC filtration (Mailler et al., 2015; Scheurer et al., 2010). CYC was not removed in this study (Figure 5.8). Similarly, poor removal of CYC is observed using GAC; CYC is minimally retarded in a GAC filter with 80% breakthrough after 3 d (Scheurer et al., 2010).

Partial removal of SAC was observed in the columns containing BC, but not Column ZVI. The removal of SAC in Column BC was slightly enhanced with the decrease in flow rate; however, the removal of SAC in Column (ZVI + BC) was not affected by the decreasing flow rate. The concentration of SAC in the Column BC effluent gradually increased from 1.1 $\mu\text{g L}^{-1}$ at 6 PV to 85.5 $\mu\text{g L}^{-1}$ at 56 PV in the first stage of the experiment, then slightly decreased to 70.3 $\mu\text{g L}^{-1}$ at 65 PV in the second stage of the experiment when the flow rate was decreased. The concentration of SAC in the Column (ZVI + BC) effluent increased from 7.3 $\mu\text{g L}^{-1}$ at 6 PV to 87.3 $\mu\text{g L}^{-1}$ at 38 PV in the first stage of the experiment, and consistent effluent concentrations of SAC were maintained during the remainder of the first stage of the experiment and the second stage of the experiment (Figure 5.8).

More than 88%, 85%, and 76% of input SCL (~110 $\mu\text{g L}^{-1}$) were removed in Column ZVI, Column BC, and Column (ZVI + BC). The concentrations of SCL in Column ZVI effluent increased from 2.6 $\mu\text{g L}^{-1}$ at 11 PV to 9.3 $\mu\text{g L}^{-1}$ at 50 PV in the first stage of the experiment, and then increased to 13.1 $\mu\text{g L}^{-1}$ at 58 PV in the second stage of the experiment. The removal of SCL in Column ZVI was not affected by the decrease in flow rate from 0.3 to 0.1 PV d^{-1} ; however, the removal of SCL in Columns BC and (ZVI + BC) was slightly enhanced with the decreasing flow rate. The concentration of SCL in the effluents of Columns BC and (ZVI + BC) increased from 7.4 and 0.9 $\mu\text{g L}^{-1}$ at 10 PV to 17.2 and 28.4 $\mu\text{g L}^{-1}$ at 53 PV in the first stage of

the experiment, then slightly decreased to 12.8 and 24.3 $\mu\text{g L}^{-1}$ at 63 PV in the second stage of the experiment (Figure 5.8).

5.4.3.2 Potential Removal Mechanisms of Artificial Sweeteners by ZVI and BC

Four artificial sweeteners were divided into two groups (acidic and neutral artificial sweeteners) according to their acidic (deprotonated) / basic (protonated) character of functional groups in the investigated pH range (pH: 7.0–9.5). The potential removal mechanisms of artificial sweeteners by ZVI and BC are summarized in Table 5.3.

5.4.3.2.1 Anionic Artificial Sweeteners ACE-K, CYC, and SAC

ACE-K, CYC, and SAC were anionic (negatively charged) in the investigated pH range (7.0–9.5) due to dissociation of these compounds at $\text{pH} > \text{p}K_{\text{as}}$ ($\text{p}K_{\text{as}}$ of ACE-K, CYC, and SAC: 1.7–2.0, Table 5.3 and Figure 5.5). The removal of ACE-K by ZVI has not been previously reported. The removal of ACE-K (30–60%) by ZVI was likely due to reduction by ZVI and H bonding between =O and N bearing groups (H acceptors) of ACE-K and –OH groups (H donors) on the surface of ZVI.

The sorption of SAC by BC was likely through $\pi - \pi$ stacking interaction between the aromatic ring in SAC and graphene aromatic structure of BC. ACE-K, CYC, and SAC are hydrophilic compounds due to their very low negative $\log D_{ow}$ values (calculated following Equation 5.1 and listed in Table 5.3); hydrophobic interactions between these artificial sweeteners and BC were likely limited. The $\pi - \pi$ EDA interaction between electron withdrawing sulfonamide and carbonyl functional groups (π electron acceptors) in SAC and the π -electron rich BC (π electron donors) also likely contributed to the sorption of SAC by BC (Inyang &

Dickenson, 2015). In addition, the H bonding between the =O and N bearing groups (H acceptors) in SAC molecule and the –OH (H donors) of BC could also contribute to sorption of SAC by BC. Similarly, Seo et al. (2016) report that the H bonding between the –NH₂ group (H donor) on modified sorbent and =O (H acceptor) in SAC molecule contributes to the adsorption removal of SAC by urea modified metal-organic frameworks. As a similar carbonaceous sorbent to BC, GAC has been used to removed SAC from contaminated water with similar removals (47–90%) compared to BC (Mailler et al., 2015; Scheurer et al., 2010).

5.4.3.2.2 Neutral Artificial Sweeteners SCL

Artificial sweetener SCL mainly exists in its neutral form at pH (7.0–9.5) < its p*K*_a (11.8) (Figure 5.5) in this study (Lange et al., 2012). The removal of SCL by ZVI was likely through the dechlorination of the chlorine atom in SCL molecule (Table 5.3) by ZVI. Reductive dehalogenation is a surface reaction involving three potential pathways: (1) direct electron transfer from Fe⁰ surface; (2) reduction by Fe²⁺ produced from Fe⁰ corrosion; and (3) reduction by H₂ formed by H₂O corrosion (Matheson & Tratnyek, 1994). In addition, the H bonding between –OH groups (H donors and acceptors) of SCL and –OH groups (H donors and acceptors) on the surface of ZVI also likely contributed to removal of SCL by ZVI.

The sorption of SCL by BC was likely through H bonding. Sucralose contains hydroxyl groups (–OH, H donor or acceptor) which might be attracted to the quinone groups (–CO–, H acceptor) and hydroxyl groups (–OH, H donor and acceptor) in BC through H bonding. Similar to ACE-K, CYC, and SAC, hydrophobic interaction between SCL and BC was likely limited due to its low log *D*_{ow} (calculated following Equation 5.1 and listed in Table 5.3). In addition, the electrostatic interaction between neutral SCL and negatively charged BC (Mukherjee et al., 2011)

was likely limited. Compared to the removal of SCL (85–99%) by BC in this study, greater removal (> 99%) of SCL by AC has been demonstrated by Minten et al. (2011); in addition, SCL is removed more efficiently by AC filtration than ozonation, advanced oxidation, and membrane bioreactors.

5.4.3.3 Removal Rates of Artificial Sweeteners within Columns

The removal rates of artificial sweeteners were calculated using least-squares regression for the two experimental stages. The removal of artificial sweeteners followed the first-order or zero-order rate models or followed the first-order rate in the early stage of the experiment followed by zero-order rate in the late stage of the experiment (Figure 5.9). The first-order and zero-order removal rates, removal rate constants (k_{obs} , d^{-1} for first-order; μmol or μg contaminant $L^{-1} d^{-1}$ for zero-order), mass normalized rate constants (k_M , $L g^{-1} d^{-1}$ for first-order; μmol or μg contaminant $d^{-1} g^{-1}$ for zero-order), and surface area normalized rate constants (k_{SA} , $L m^{-2} d^{-1}$ for first-order; μmol or μg contaminant $d^{-1} m^{-2}$ for zero-order) were calculated using Equations 5.3 and 5.4 and listed in Appendix D (Tables D.9–D.12).

ACE-K was removed more rapidly within Column ZVI (first-order model) than Column (ZVI + BC) (zero-order removal model) (Figure 5.9 and Table D.9). The average removal rate of ACE by ZVI in this study was much greater than observed by direct photolysis of ACE-K at pH of 4 in deionized water with a rate constant of $0.036 d^{-1}$ (Gan et al., 2014). The half-life of ACE-K within Column (ZVI + BC) during the first stage of the experiment was similar to the half-life (9 d) observed in surface water during summer (Gan et al., 2014).

Removal rate of SAC within three treatment columns followed the order: Column BC > Column (ZVI + BC) > Column ZVI (Figure 5.9 and Table D.11). Removal rate of SCL within

three treatment columns followed: Column ZVI > Column (ZVI + BC) > Column BC (before 13PV) and followed: Column BC = Column (ZVI + BC) > Column ZVI (after 13PV) (Figure 5.9 and Table D.12). This decrease in the removal rates of SCL by ZVI through dechlorination (discussed in section 5.4.3.2) is likely due to the declining reactivity of ZVI resulting from the formation of secondary precipitates on the ZVI surfaces. The input solution used in this study contained CaCO₃ which likely accelerated the formation of secondary precipitates resulting in further declining reactivity of ZVI. Similar decreasing removal rates of TCE by ZVI through dechlorination has been reported (Jeen et al., 2006; Jeen et al., 2007). The removal rates of ACE-K, SAC and SCL within treatment columns were lower than the rates observed using advanced oxidation technologies (Sharma et al., 2014; Toth et al., 2012).

Overall, adding ZVI to BC did not enhance the removals of artificial sweeteners ACE-K, CYC, SAC, and SCL in Column (ZVI + BC); artificial sweeteners are less effectively removed in Column (ZVI + BC) than either Column ZVI or Column BC. The removal rate of four artificial sweeteners followed: SCL > ACE-K > SAC > CYC (no removal) within Column ZVI and SCL > SAC > ACE-K and CYC (no removals) within the column containing BC.

5.4.4 Removal of PFOA and PFOS in Columns

5.4.4.1 Removal of PFOA and PFOS from Column Effluent

Perfluorooctanoic acid (PFOA) and perfluorooctane sulfonic acid (PFOS) were persistent and not removed in the Column Control. More than 89% of input PFOA (~45 µg L⁻¹) was removed in Columns ZVI, BC and (ZVI + BC) at the early first stage of the experiment (< 10 PV), the removal efficiency of PFOA in three treatment columns greatly decreased during the remainder of the experiment. About 49–98% of input PFOS (24.0–89.6 µg L⁻¹) was removed in the

columns containing BC over the experimental period, less was removed in Column ZVI (Figure 5.10).

The concentration of PFOA in the Column ZVI effluent was $< 0.5 \mu\text{g L}^{-1}$ before 10 PV with removal of 99%; then rapidly jumped to $28.1 \mu\text{g L}^{-1}$ at 11 PV and continued to increase to $51.4 \mu\text{g L}^{-1}$ (which was 10 – 25 % higher than the input PFOA) at 18 PV until the end of the first stage of the experiment, the concentration of PFOA gradually decreased to the influent PFOA level during the second stage of the experiment. Partial removal of PFOA was observed in Column BC. The concentration of PFOA in the Column BC effluent was $< 5 \mu\text{g L}^{-1}$ before 10 PV with removal of $> 89\%$, and then gradually increased to $39.3 \mu\text{g L}^{-1}$ at the end of the first stage of the experiment with removal of 13%. The removal of PFOA in Column BC was enhanced as a result of a decrease in flow rate. The concentration of PFOA in the effluent of Column BC slightly decreased from 39.3 at 53 PV to $34.3 \mu\text{g L}^{-1}$ at 65 PV at the beginning of the second stage of the experiment when the flow rate was first lowered; however, PFOA then rapidly broke through Column BC with the concentration of $50.7 \mu\text{g L}^{-1}$ at 69 PV at the end of the second stage of the experiment (Figure 5.10).

Limited removal of PFOA was observed in Column (ZVI + BC). More than 97% of input PFOA was removed in Column (ZVI + BC) from the average input concentration of $44.6 \mu\text{g L}^{-1}$ to $1.58 \mu\text{g L}^{-1}$ within the first 6 PV in the first stage of the experiment; however, the concentration of PFOA in the Column (ZVI + BC) effluent rapidly increased to $44.7 \mu\text{g L}^{-1}$ after 25 PV and continued to increase until concentrations reached $55.4 \mu\text{g L}^{-1}$ at 55 PV in the first stage of the experiment. Like in Column BC, the removal of PFOA in Column (ZVI + BC) was slightly enhanced when the flow rate was decreased. The concentration of PFOA in the effluent

of Column (ZVI + BC) slightly decreased from $55.4 \mu\text{g L}^{-1}$ to the average influent PFOA value ($45 \mu\text{g L}^{-1}$) during the second stage of the experiment (Figure 5.10).

More than 81% of input PFOS ($24.0\text{--}82.6 \mu\text{g L}^{-1}$) was removed in Column ZVI before 37 PV during the first stage of the experiment; however, as the average input PFOS concentration increased from $47.5 \mu\text{g L}^{-1}$ at 34 PV to $82.9 \mu\text{g L}^{-1}$ at 50 PV, the concentration of PFOS in Column ZVI effluent rapidly increased from $2.23 \mu\text{g L}^{-1}$ to $51.2 \mu\text{g L}^{-1}$ with removals of 25–46% during the first stage of the experiment. The concentration of PFOS in Column ZVI effluent followed the same changing trend with the influent PFOS with relatively smaller removals of 11–49% during the second stage of the experiment (Figure 5.10).

More than 82% of input PFOS (varied from 24.0 to $89.6 \mu\text{g L}^{-1}$) was removed in Column BC throughout the experiment with the effluent concentrations $< 8.6 \mu\text{g L}^{-1}$ and removal of up to 99%, except for 13–21 PV with removals of 63–94%. Relatively less removal of PFOS was observed in Column (ZVI + BC) compared to Column BC. Similarly, low concentrations of PFOS ($< 6.07 \mu\text{g L}^{-1}$) were observed in the Column (ZVI + BC) effluent before 41 PV with removal $> 88\%$, except for 15–22 PV with the smaller removals of 57–95%. As the average input PFOS concentration increased from 49.0 to $84.7 \mu\text{g L}^{-1}$ at ~ 40 PV, the effluent PFOS concentration in Column (ZVI + BC) then increased from $6.07 \mu\text{g L}^{-1}$ at 41 PV to $19.2 \mu\text{g L}^{-1}$ at 45 PV and maintained consistent at $\sim 20 \mu\text{g L}^{-1}$ with the relatively smaller removals of 56–79% (Figure 5.10). Overall, PFOA (up to 89%) and PFOS (up to 99%) were removed more effectively by high carbon content (99%) BC in this study compared to a previously reported study; Kupryianchyk et al. (2016) report little or no removal of PFOA and PFOS from top 20 cm soils

of a fire fighting training sites contaminated with PFASs attributed to the low C content (19–53%) biochars.

5.4.4.2 Potential Removal Mechanisms of PFOA and PFOS by ZVI and BC

PFOA and PFOS are acidic compounds which deprotonate and exist primarily in their anionic forms (negatively charged) at the investigated pH range (pH: 7.0–9.5 > pK_{as} ; Table 5.4 and Figure 5.5). Removal of PFOA and PFOS by ZVI during the early stage (before 18 PV) of the experiment was likely due to electrostatic interactions, and H bonding and ion-dipole interactions; however, electrostatic interactions were likely limited after 18 PV through Column ZVI. The pH of pore water in Column ZVI ranged from 7.1 to 8.2 before 18 PV (Figure 5.2); the oxides and hydroxides were likely positively charged at $pH < 8.3$ (Parks, 1965), which may have promoted sorption of negatively charged PFOA and PFOS through electrostatic interactions. Similarly, the sorption of PFOA and PFOS by ZVI oxidation products (iron oxides and hydroxides) in a low pH (3.0–6.0) aqueous solution has been reported through electrostatic interactions (Gao & Chorover, 2012). However, the pH of pore water in Column ZVI > 8.3 after 18 PV (Figure 5.2) resulted in negatively charged iron hydroxides, leading to a reduction in electrostatic interactions between negatively charged PFOA, PFOS, and the iron hydroxide surface. This pH induced decrease of electrostatic interaction possibly resulted in the desorption of PFOA from ZVI, accounting for the higher concentration of PFOA (10–25 %) in the Column ZVI effluent compared to the influent PFOA (18–50 PV) (Figure 5.10).

The H bonding between PFOA/PFOS and ZVI were likely formed between the –OH groups (H donors) on iron hydroxide surfaces and the carboxylic (–COO⁻, 2O as 2H acceptors) and sulfonic (–SO₃⁻, 3O as 3H acceptors) groups of PFOA and PFOS. The H bonding between

PFOS (3H acceptors) and ZVI was likely greater than between PFOA (2H acceptors) and ZVI; this may account for the greater removal of PFOS by ZVI than PFOA. The anionic PFOA and PFOS molecules can also develop ion-dipole interactions with the polar –OH functional groups (dipole) on the ZVI surface (Punyapalakul et al., 2013). In addition, the formation of Fe-carboxylate complexes from the ferric Fe hydroxide on the surface of ZVI and the carboxylic group in PFOA may also contribute to sorption of PFOA by ZVI (Gao & Chorover, 2012).

Fluoride, the indicative by-product of defluorination, was not observed in the treated effluent of any column in this study likely due to either lack of defluorination reactions, analytical limitations, or the removal of F⁻ by the reactive media. The sorption of F⁻ by iron hydroxide (Sujana et al., 2009) and biochars (Guan et al., 2015) has been reported previously. In addition, Ca²⁺ in the simulated groundwater used in this study may have reacted with F⁻ to form CaF₂ precipitates which can also remove F⁻ from the column effluent and pore water. Therefore, reductive defluorination of PFOA and PFOS by ZVI cannot be confirmed in this study. However, the reductive defluorination of PFOA and PFOS is demonstrated by Arvaniti et al. (2015) using Mg-aminoclay modified nanoscale ZVI. Effective reductive defluorination of PFOA has been reported using photo-generated hydrated electrons (a powerful reductant, E^o = -2.9 V) to initiate the cleavage of α-position C-F bond (Park et al., 2009; Song et al., 2013).

Removal of PFOA and PFOS by BC was likely through hydrophobic interactions between the hydrophobic perfluoroalkyl tail and hydrophobic surface of BC (Du et al., 2014), which is consistent with high log *D_{ow}* values in Table 5.4. In addition, H bonding, ion-dipole interactions may also contribute to the removal of PFOA and PFOS by BC. Greater removals of PFOS by BC compared to PFOA are attributed to the stronger hydrophobic interaction between PFOS and BC. Both PFOA and PFOS have the same carbon chain length (C8); however, PFOS

contains two additional C-F bonds compared to PFOA, which leads to stronger hydrophobicity of PFOS than PFOA (Higgins & Luthy, 2006). Similarly, H bonding between the –OH groups (H donors) in BC and the $-\text{SO}_3^-$ group (3H acceptors) in PFOS was likely greater than the H bonding between the –OH groups in BC and the $-\text{COO}^-$ group (2H acceptors) in PFOA. This stronger H bonding between BC and PFOS may have contributed to the stronger sorption of PFOS by BC compared to PFOA (Gao & Chorover, 2012). A relatively weak ion-dipole interaction between the –OH dipole groups in BC and anionic PFOA and PFOS molecules can also contribute to the sorption of PFOA and PFOS to BC (Du et al., 2014; Karoyo & Wilson, 2013). In addition, the Ca^{2+} present in simulated groundwater in this study has been reported to enhance the sorption of PFOA and PFOS to adsorbents due to the formation of a cation bridge between Ca^{2+} and negatively charged carboxyl and sulfonate groups (Wang & Shih, 2011). The electrostatic interaction between negatively charged PFOA and PFOS and negatively charged ZVI and BC (discussed in section 5.4.2.2) was likely limited at pH of 7–9.5 in this study.

5.4.4.3 Removal Rates of PFOA and PFOS within Columns

The removal rates of PFOA and PFOS were calculated using least-squares regression for the two experimental stages. The removal of PFOA and PFOS followed the first-order or zero-order rate models or followed the first-order rate in the early stage of the experiment followed by zero-order rate in the late stage of the experiment (Figure 5.11). The removal rates, removal rate constants (k_{obs}), mass normalized rate constants (k_M), and surface area normalized rate constants (k_{SA}) were calculated following Equations 5.3 and 5.4 and listed in Appendix D (Tables D.13–D.14).

The removal rate of PFOA followed: Column BC > Column (ZVI + BC) > Column ZVI (Figure 5.11 and Table D.13). The removal rate of PFOS: Column (ZVI + BC) > Column BC > Column ZVI during the first stage of the experiment and Column BC > Column (ZVI + BC) > Column ZVI during the second stage of the experiment (Figure 5.11 and Table D.14). Overall, PFOA and PFOS were removed more rapidly within the columns containing BC than Column ZVI.

The decreasing removal rates of PFOA and PFOS by BC were likely due to the competitive sorption between PFASs and other organic contaminants pharmaceuticals and artificial sweeteners, which has been reported previously (Yu et al., 2012). In addition, Du et al. (2014) demonstrate that the adsorbed negatively charged PFAS molecules on the sorbents produce a repulsive force to prevent further adsorption of negatively charged PFASs. This repulsive interaction on the surface of BC also likely decreased the sorption efficiency of PFOA and PFOS by BC over time. The removal rates of PFOA and PFOS by ZVI and BC were slower than rates reported using the iron containing material hematite (Gao & Chorover, 2012) and carbonaceous sorbent GAC (Zhang et al., 2016).

5.5 Conclusions

Simultaneous removal of emerging contaminants pharmaceutical compounds (CBZ, CAF, MDA, MDMA, SMX, IBU, GEM, and NAP with removals > 97%), artificial sweeteners (ACE-K, SAC, and SCL with partial removals), and perfluoroalkyl substances (PFOA and PFOS with partial removals) was observed in a passive treatment system (four columns) containing reactive media zero-valent iron (ZVI), biochar (BC), and a mixture of (ZVI + BC). No obvious signs of clogging or decrease in flow rates were observed over the course of the experiment. Eight

pharmaceuticals were more rapidly and completely removed in the columns containing ZVI than Column BC. In general, removal rates of pharmaceuticals within three treatment columns followed: SMX (in Column ZVI but not in the columns containing BC) > cationic (positively charged) compounds (MDMA, MDA, and CAF) > neutral compound (CBZ) > anionic (negatively charged) compounds (NAP, GEM, and IBU). The removal rates of artificial sweeteners within treatment columns followed: SCL > ACE-K and SAC > CYC (no removal). Unlike pharmaceuticals, greater and relatively more rapid removals of PFOA and PFOS were observed in the columns containing BC than Column ZVI; PFOS was more effectively removed than PFOA. Overall, target pharmaceuticals, artificial sweeteners (except for CYC with no removal), and perfluoroalkyl substances were more considerably removed using the combination of (ZVI + BC) than either ZVI alone or BC alone. These results suggest that the reactive mixture (ZVI + BC) has the potential to be an effective combination for use in large-scale field applications such as in-situ reactors and permeable reactive barriers (PRBs) for remediation of emerging contaminants. These materials are relatively low cost and when combined show considerable reactivity for ubiquitous trace organic emerging contaminants present in wastewater. However, more extensive study is required when the reactive mixture is applied to remove emerging contaminants from different wastewater streams; as the complex matrix of the wastewater such as DOC content and ionic strength may influence the removal efficiency

Table 5.1 Physical characteristics of the columns used in this study, including a control and columns containing zero-valent Fe (ZVI), organic C (BC), and both.

	Column 1	Column 2	Column 3	Column 4
	Control	ZVI	BC	(ZVI + BC)
Bulk density, g cm ⁻³	1.77	2.39	1.18	1.46
Porosity	0.39	0.32	0.59	0.40
Pore volume, cm ³	230	207	372	276

Table 5.2 Selected properties of target pharmaceuticals and potential interaction (removal mechanisms) between target pharmaceutical compounds and reactive media. N: Neutral; (+): Positive charged; (-): Negative charged.

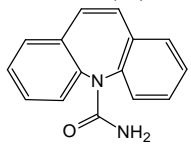
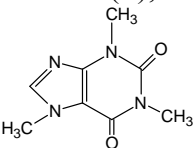
Contaminant		Reactive Media		Potential interaction between contaminant and reactive media
CAS#, therapeutic use, pKa, log K _{ow} , log D _{ow} , character (charge), and structure	Reactive functional group	Column/ Reactive media	Reactive functional group or agent	
Carbamazepine (CBZ) (298-46-4), Anti-depressant, pKa= -0.49 ^a , log K _{ow} =2.25, log D _{ow} =2.25, Base (N), 	C=C bonds	Column 2/ ZVI	H ₂	Catalytic hydrogenation ¹
	-NH ₂ , -C=O		-OH on surface of ZVI	H bonding
	Aromatic structure	Column 3/ BC	Graphene aromatic structure	Hydrophobic interaction ² π-π interaction
	-NH ₂ , -C=O		-OH	H bonding
C=C bonds, aromatic structure, -NH ₂ , -C=O	Column 4/ (ZVI +BC)	H ₂ and graphene aromatic structure	Catalytic hydrogenation ¹ , hydrophobic interaction ² , π-π interaction, H bonding	
Caffeine (CAF) (58-08-2), Stimulant, pKa=10.4 ^b , log K _{ow} = -0.07, log D _{ow} = -2.17, Base (+), 	Not reported	Column 2/ ZVI	Core ZVI-shell structure (iron oxides and hydroxides)	Reduction and adsorption ³
	N, =O		Electrostatic interaction	
	+ charged		- charged	H bonding
	N, =O	Column 3/ BC	-OH, graphene aromatic structure	H bonding, π-π EDA interaction
	+ charged		- charged	Electrostatic interaction
N, =O	Column 4/ (ZVI +BC)	Core ZVI-shell structure (iron oxides and hydroxides), -OH	Reduction and adsorption ³ , π-π EDA interaction, H bonding, electrostatic interaction	

Table 5.2 Continued.

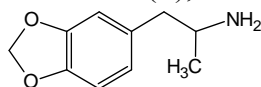
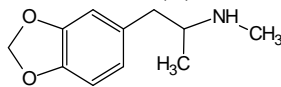
Contaminant		Reactive Media		Potential interaction between contaminant and reactive media
CAS#, therapeutic use, pK_a , $\log K_{ow}$, $\log D_{ow}$, character (charge), and structure	Reactive functional group	Column/ Reactive media	Reactive functional group or agent	
3,4-methylenedioxy-amphetamine (MDA) (4764-17-4), Psychedelic and entactogenic drug, $pK_a=9.7$, $\log K_{ow}=1.64$, $\log D_{ow}=0.22$, Base (+), 	-NH ₂ , O	Column 2/ ZVI	-OH on surface of ZVI	Electrostatic interaction
	+ charged		- charged	H bonding
	Aromatic structure	Column 3/ BC	Graphene aromatic structure	π - π stacking
	-NH ₂ , O		-OH, graphene aromatic structure	π - π EDA interaction, π -H bonding, H bonding,
	+ charged		- charged	Electrostatic interaction
-NH-, O, aromatic structure	Column 4/ (ZVI +BC)	-OH, graphene aromatic structure	Electrostatic interaction, π - π stacking, π - π EDA interaction, π -H bonding, H bonding	
3,4-methylenedioxy-methamphetamine (MDMA) (42542-10-9), Ecstasy, $pK_a=9.9$, $\log K_{ow}=2.28$, $\log D_{ow}=0.67$, Base (+), 	-NH-, O	Column 2/ ZVI	-OH on surface of ZVI	Electrostatic interaction
	+ charged		- charged	H bonding
	Aromatic structure	Column 3/ BC	Graphene aromatic structure	π - π stacking
	-NH-, O		-OH, graphene aromatic structure	H bonding, π - π EDA interaction, π -H bonding
	+ charged		- charged	Electrostatic interaction
-NH-, O, aromatic structure	Column 4/ (ZVI +BC)	-OH, graphene aromatic structure	Electrostatic interaction, π - π stacking, π - π EDA interaction, π -H bonding, H bonding	

Table 5.2 Continued.

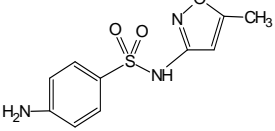
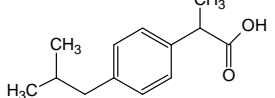
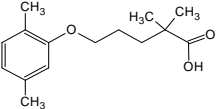
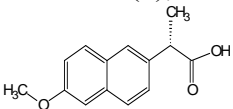
Contaminant		Reactive Media		Potential interaction between contaminant and reactive media
CAS#, therapeutic use, pK_a , $\log K_{ow}$, $\log D_{ow}$, character (charge), and structure	Reactive functional group	Column/ Reactive media	Reactive functional group or agent	
<p>Sulfamethoxazole (SMX) (723-46-6), Antibiotic, $pK_{a1}=1.7$, $pK_{a2}=5.6^b$, $\log K_{ow}=0.89$, $\log D_{ow}= -1.81$, Acid (-),</p> 	-NH ₂ , sulfonamide group, N-heterocyclic ring	Column 2/ ZVI	-OH on surface of ZVI	H bonding
	Aromatic structure	Column 3/ BC	Graphene aromatic structure	π - π stacking
	-NH ₂ , sulfonamide group, N-heterocyclic ring		-OH, graphene aromatic structure	H bonding, π - π EDA interaction ⁴ , π -H bonding
	-NH ₂ , sulfonamide group, N-heterocyclic ring, aromatic structure	Column 4/ (ZVI +BC)	-OH, graphene aromatic structure	H bonding, π - π stacking, π - π EDA interaction, π -H bonding
<p>Ibuprofen (IBU) (15687-27-1), Anti-inflammatory drug, $pK_a=4.5$, $\log K_{ow}=3.5$, $\log D_{ow}= -0.3$, Acid (-),</p> 	-COOH	Column 2/ ZVI	-OH on surface of ZVI	H bonding
	Not reported		ZVI	Reduction ⁵
	Aromatic structure	Column 3/ BC	Graphene aromatic structure	π - π stacking
	-COOH		-OH, graphene aromatic structure	H bonding, π - π EDA interaction ⁶ , π -H bonding
	Aromatic structure, -COOH	Column 4/ (ZVI +BC)	-OH, graphene aromatic structure	Reduction, H bonding, π - π stacking, π - π EDA interaction, π -H bonding

Table 5.2 Continued.

Contaminant		Reactive Media		Potential interaction between contaminant and reactive media
CAS#, therapeutic use, pK_a , $\log K_{ow}$, $\log D_{ow}$, character (charge), and structure	Reactive functional group	Column/ Reactive media	Reactive functional group or agent	
<p>Gemfibrozil (GEM) (25812-30-0), Lipid regulator, $pK_a=4.8$, $\log K_{ow}=4.3$, $\log D_{ow}=0.8$, Acid (-),</p> 	-COOH	Column 2/ ZVI	-OH on surface of ZVI	H bonding
	Xylene aromatic structure	Column 3/ BC	Graphene aromatic structure	π - π stacking
	-COOH		-OH, graphene aromatic structure	H bonding, π - π EDA interaction, π -H bonding
	-COOH, xylene aromatic structure	Column 4/ (ZVI +BC)	-OH, graphene aromatic structure	H bonding, π - π stacking, π - π EDA interaction, π -H bonding
<p>Naproxen (NAP) (22204-53-1), Anti-inflammatory drug, $pK_a=4.2$, $\log K_{ow}=2.8$, $\log D_{ow}=-1.3$, Acid (-),</p> 	-COOH	Column 2/ ZVI	-OH on surface of ZVI	H bonding
	Naphthalene aromatic structure	Column 3/ BC	Graphene aromatic structure	π - π stacking
	-COOH		-OH, graphene aromatic structure	H bonding, π - π EDA interaction and high Van der Waals forces ⁷ , π -H bonding
	Naphthalene aromatic structure, -COOH	Column 4/ (ZVI +BC)	-OH, graphene aromatic structure	H bonding, π - π stacking, π - π EDA interaction, π -H bonding

References: ^a From Schaffer et al. (2012). ^b From Martínez-Hernández et al. (2014). 1. König et al. (2016); 2. Inyang and Dickenson (2015); 3. Tomizawa et al. (2016); 4. Zheng et al. (2013); 5. Machado et al. (2013); 6. (Jung et al. (2013)); 7. Jung et al. (2015a).

Table 5.3 Selected properties of target artificial sweeteners and potential interaction (removal mechanisms) between target artificial sweeteners and reactive media. N: Neutral; (+): Positive charged; (-): Negative charged.

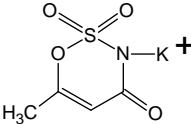
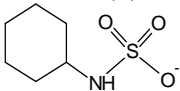
Contaminant		Reactive Media		Potential interaction between contaminant and reactive media
CAS#, pKa, log K _{ow} , log D _{ow} , character (charge), and structure	Reactive functional group	Column/ Reactive media	Reactive functional group or agent	
Acesulfame-K (ACE-K) (55589-62-3), pKa=2.0, log K _{ow} = -1.33, log D _{ow} = -1.33, Base (-), 	=O, N	Column 2/ ZVI	-OH on surface of ZVI	H bonding Reduction by ZVI
	—	Column 3/ BC	—	Not removed
	-C=O	Column 4/ (ZVI +BC)	-OH	H bonding
Cyclamate (CYC) (45951-45-9), pKa=1.7, log K _{ow} = -2.63, log D _{ow} = -2.63, Acid (-), 	—	Column 2/ ZVI	—	Not removed
	—	Column 3/ BC	—	Not removed
	—	Column 4/ (ZVI +BC)	—	Not removed

Table 5.3 Continued.

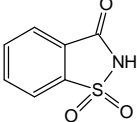
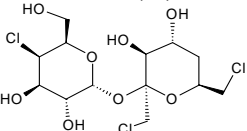
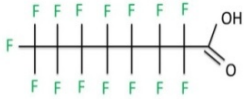
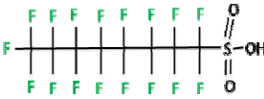
Contaminant		Reactive Media		Potential interaction between contaminant and reactive media
CAS#, pKa, log K _{ow} , log D _{ow} , character (charge), and structure	Reactive functional group	Column/ Reactive media	Reactive functional group or agent	
<p>Saccharin (SAC) (81-07-2), pKa=1.3, log K_{ow}=0.91, log D_{ow}= -5.39, Acid (-),</p> 	—	Column 2/ ZVI	—	Not removed
	Aromatic structure, sulfonamide group, C=O group	Column 3/ BC	Graphene aromatic structure	π-π stacking, π-π EDA interaction
	Aromatic structure, sulfonamide group, C=O group	Column 4/ (ZVI +BC)	Graphene aromatic structure	π-π stacking, π-π EDA interaction
<p>Sucralose (SCL) (56038-13-2) pKa=11.8, log K_{ow}= -1.0, log D_{ow}= -1.0, Acid (N),</p> 	-Cl	Column 2/ ZVI	ZVI	Dechlorination
	-OH		-OH on surface of ZVI	H bonding
	-OH	Column 3/ BC	-OH	H bonding
	-Cl, -OH	Column 4/ (ZVI +BC)	ZVI, -OH	Dechlorination, H bonding

Table 5.4 Selected properties of target perfluoroalkyl substances and potential interaction (removal mechanisms) between target perfluoroalkyl substances and reactive media. N: Neutral; (+): Positive charged; (-): Negative charged.

Contaminant		Reactive Media		Potential interaction between contaminant and reactive media
CAS#, pKa, log K _{ow} , character (charge), and structure	Reactive functional group	Column/ Reactive media	Reactive functional group or agent	
Perfluorooctanoic acid (PFOA) (335-67-1), pKa=0.5, log K _{ow} =5.11 ^a , log D _{ow} =1.58 ^a , Acid (-), 	-COOH	Column 2/ ZVI	-OH on surface of ZVI	H bonding, ion-dipole interaction
	CF ₃ (CF ₂) ₆ -	Column 3/ BC	Hydrophobicity	Hydrophobic interaction
	-COOH		-OH, graphene aromatic structure	H bonding, ion-dipole interaction
	-COOH, CF ₃ (CF ₂) ₆ -	Column 4/ (ZVI +BC)	-OH, hydrophobicity, graphene aromatic structure	H bonding, hydrophobic interaction, ion-dipole interaction
Perfluorooctane sulfonic acid (PFOS) (2795-39-3), pKa= -2.3, log K _{ow} =5.41 ^a , log D _{ow} =3.05 ^a , Acid (-), 	-SOOH	Column 2/ ZVI	-OH on surface of ZVI	H bonding, ion-dipole interaction
	CF ₃ (CF ₂) ₇ -	Column 3/ BC	Hydrophobicity	Hydrophobic interaction
	-SOOH		OH, graphene aromatic structure	H bonding, ion-dipole interaction
	-SOOH, CF ₃ (CF ₂) ₇ -	Column 4/ (ZVI +BC)	-OH, hydrophobicity, graphene aromatic structure	H bonding, hydrophobic interaction, ion-dipole interaction

^a Obtained from Chemicalize.org by ChemAxon (<http://www.chemicalize.org>)

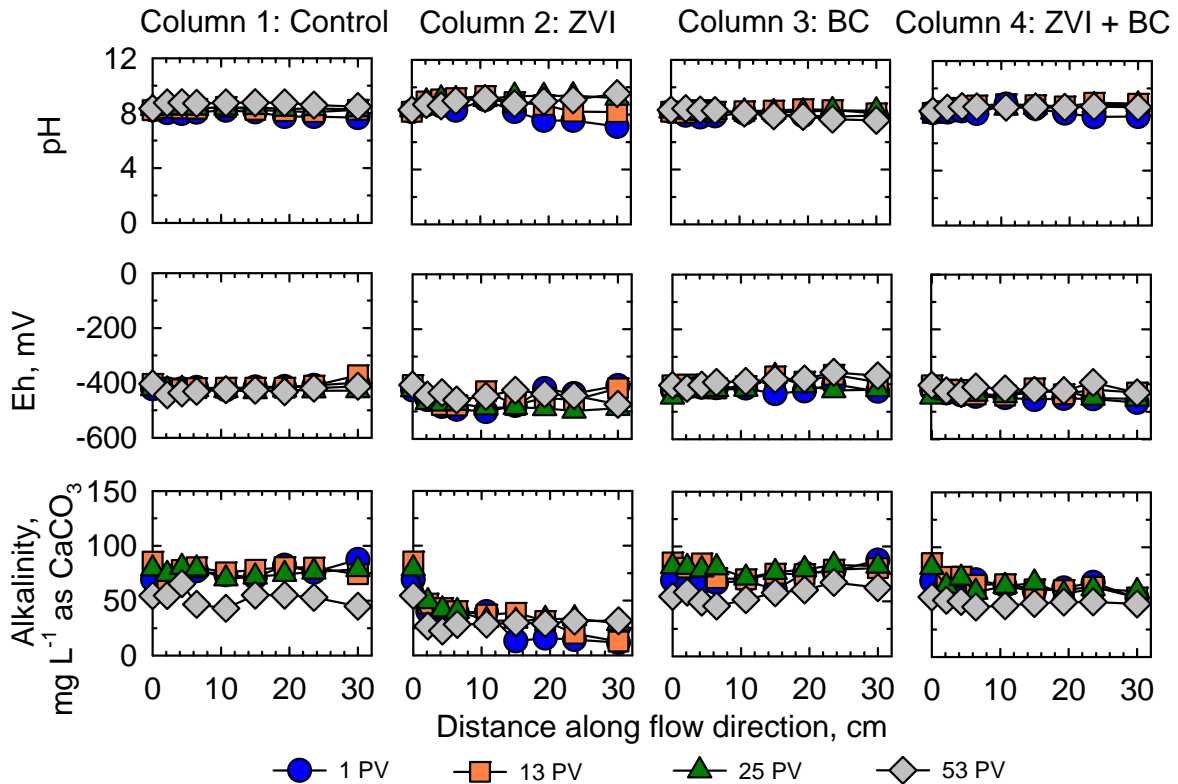


Figure 5.1 Values of pH, Eh, and concentrations of alkalinity as a function of distance along flow direction within control column and columns containing zero-valent Fe (ZVI), biochar (BC), and both. Blue circle, orange square, and green triangle symbols represent data collected during the first stage of the experiment (flow rate = 0.3 PV/d), while grey diamond symbols represent data collected during the second stage of the experiment (flow rate = 0.1 PV/d), given in terms of pore volumes (PV).

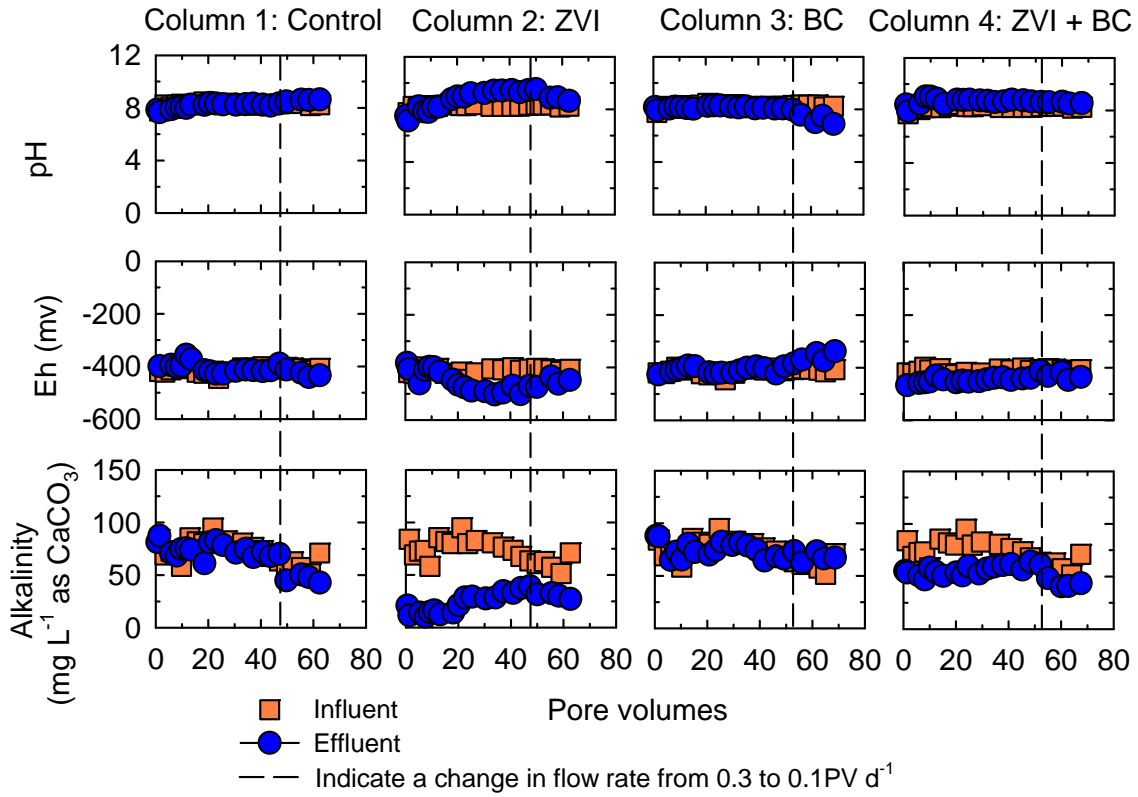


Figure 5.2 Values of pH, Eh, and concentrations of alkalinity as a function of pore volumes (PV) in effluent from control column and columns containing zero-valent Fe (ZVI), biochar (BC), and both; dash lines indicate a decrease in flow rate in each column, dividing the experiment into two stages.

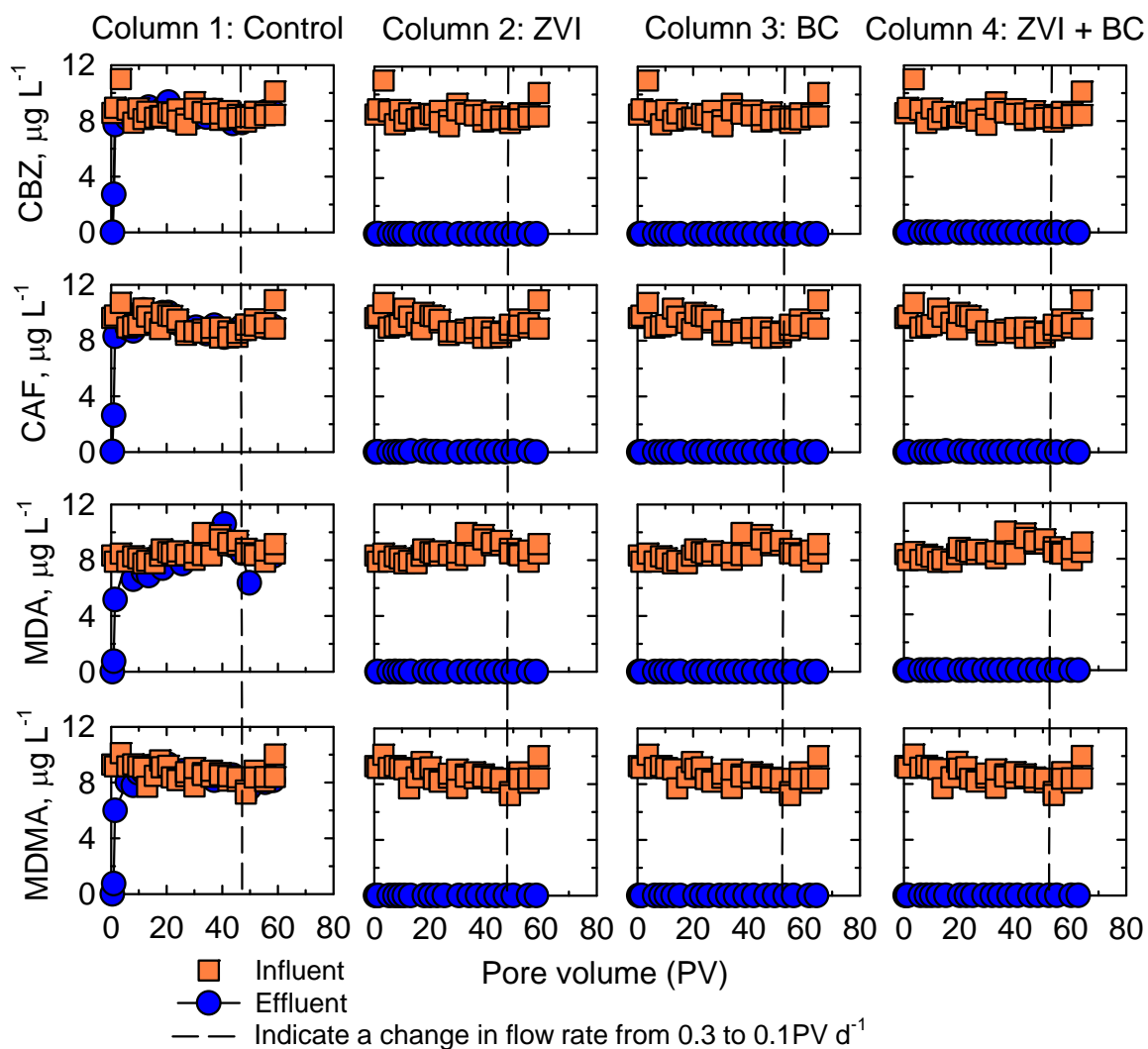


Figure 5.3 Concentrations of neutral pharmaceutical carbamazepine (CBZ) and basic pharmaceuticals caffeine (CAF), 3,4-methylenedioxyamphetamine (MDA), and 3,4-methylenedioxymethamphetamine (MDMA) as a function of pore volumes (PV) in effluent from control column and columns containing zero-valent Fe (ZVI), biochar (BC), and both; dash lines indicate a decrease in flow rate in each column, dividing the experiment into two stages.

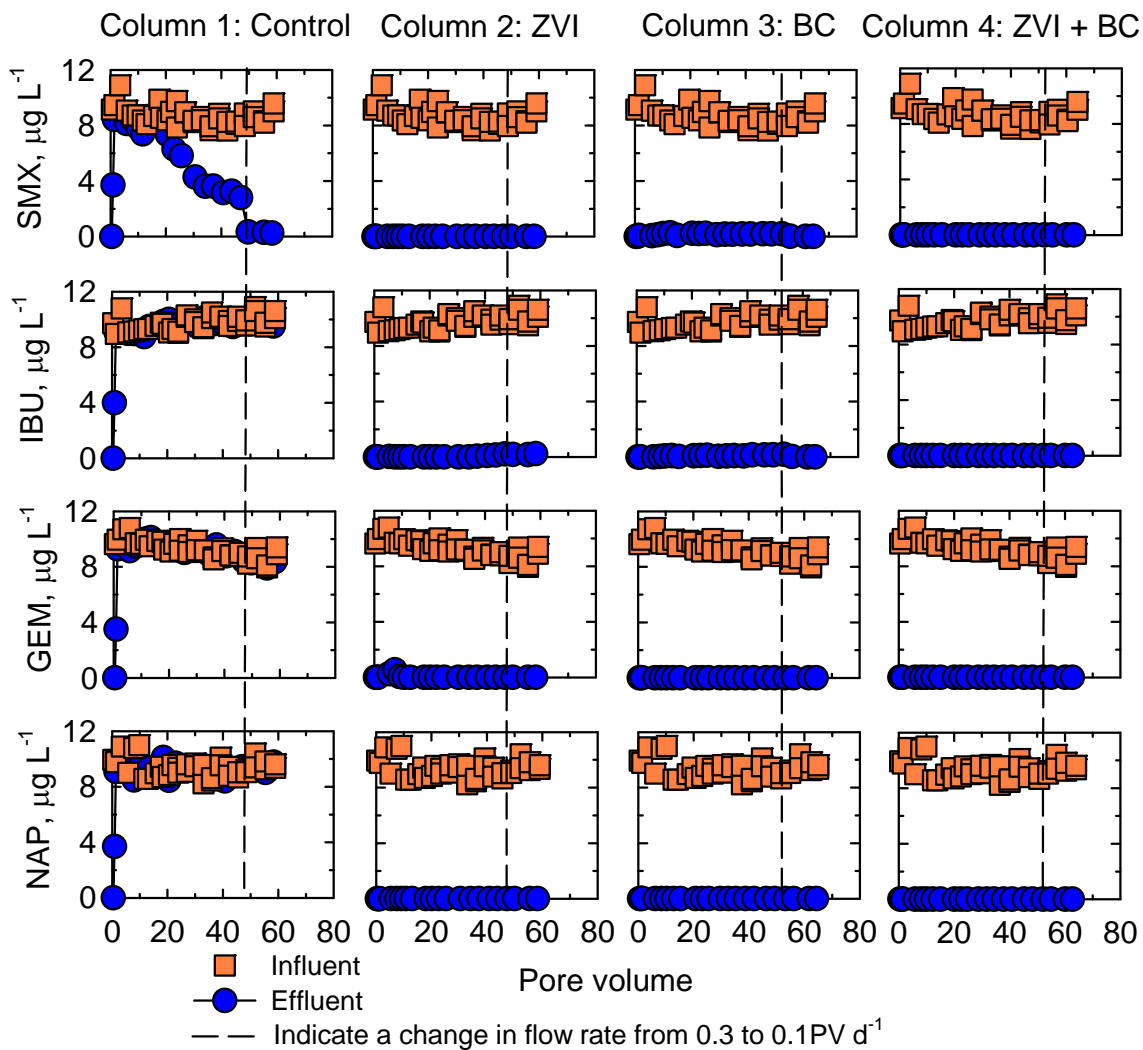


Figure 5.4 Concentrations of acidic pharmaceuticals sulfamethoxazole (SMX), ibuprofen (IBU), gemfibrozil (GEM), and naproxen (NAP) as a function of pore volumes (PV) in effluent from control column and columns containing zero-valent Fe (ZVI), biochar (BC), and both; dash lines indicate a decrease in flow rate in each column, dividing the experiment into two stages.

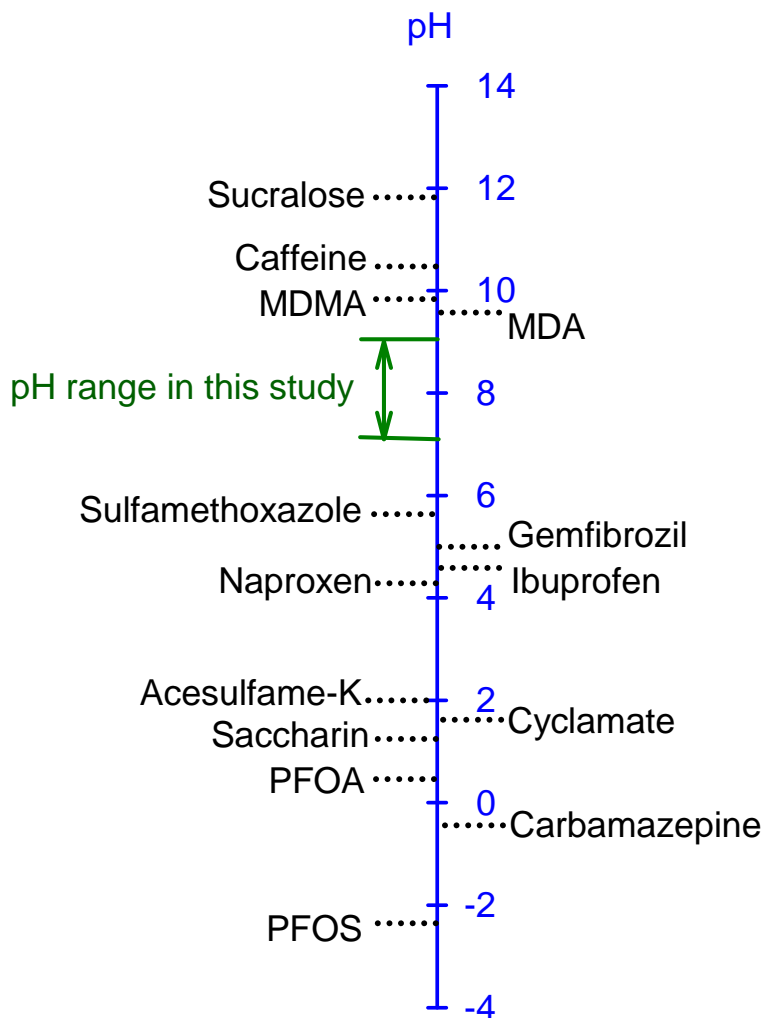


Figure 5.5 *pKa* values of target contaminants plotted on the pH scale. The pH range in Column ZVI is between 7.5–9.5; the pH range in Column BC is between 7.0–8.3; the pH range in Column (ZVI + BC) is between 7.9–8.9.

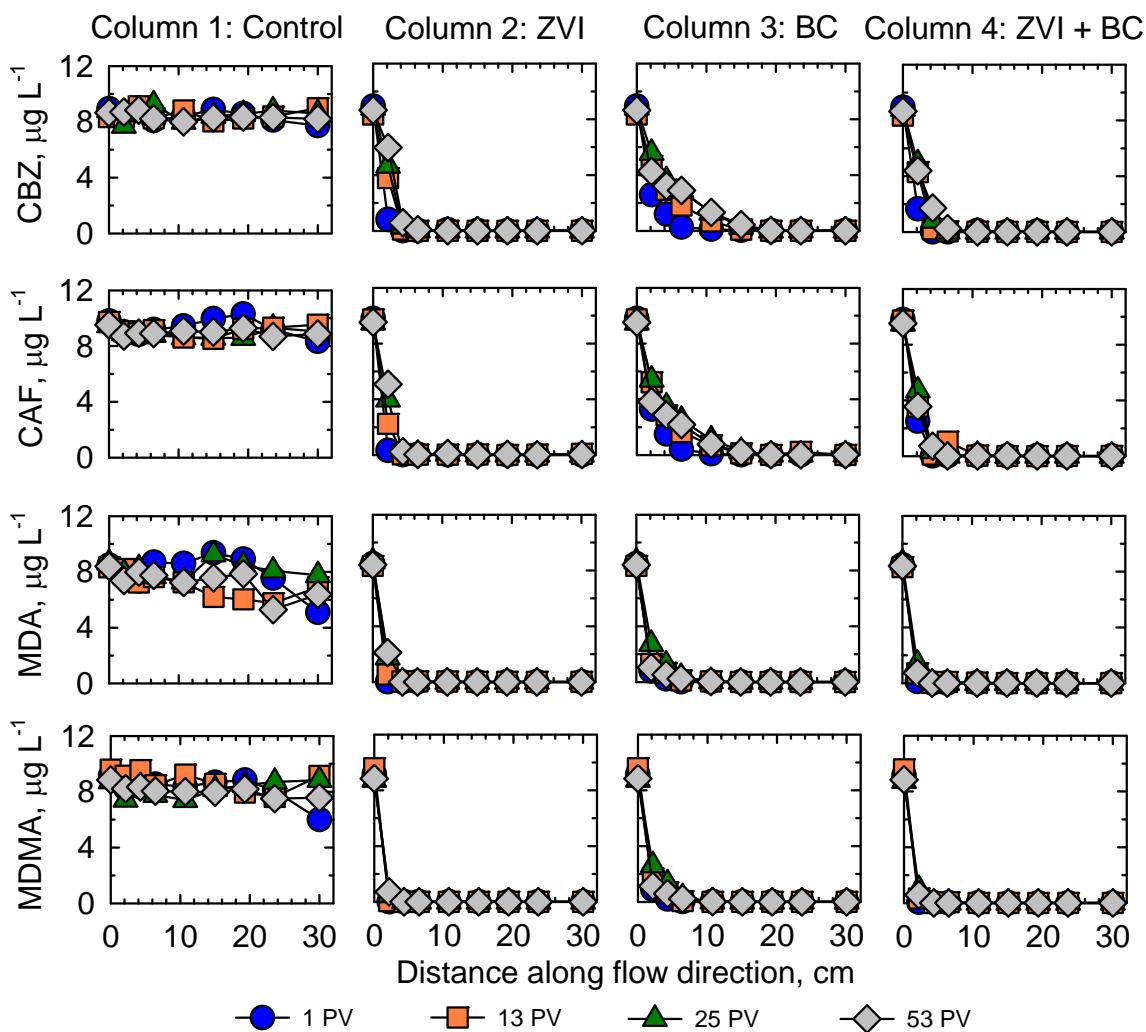


Figure 5.6 Concentrations of neutral pharmaceutical carbamazepine (CBZ) and basic pharmaceuticals caffeine (CAF), 3,4-methylenedioxyamphetamine (MDA), and 3,4-methylenedioxymethamphetamine (MDMA) as a function of distance along flow direction within control column and columns containing zero-valent Fe (ZVI), biochar (BC), and both. Blue circle, orange square, and green triangle symbols represent data collected during the first stage of the experiment (flow rate = 0.3 PV/d), while grey diamond symbols represent data collected during the second stage of the experiment (flow rate = 0.1 PV/d), given in terms of pore volumes (PV).

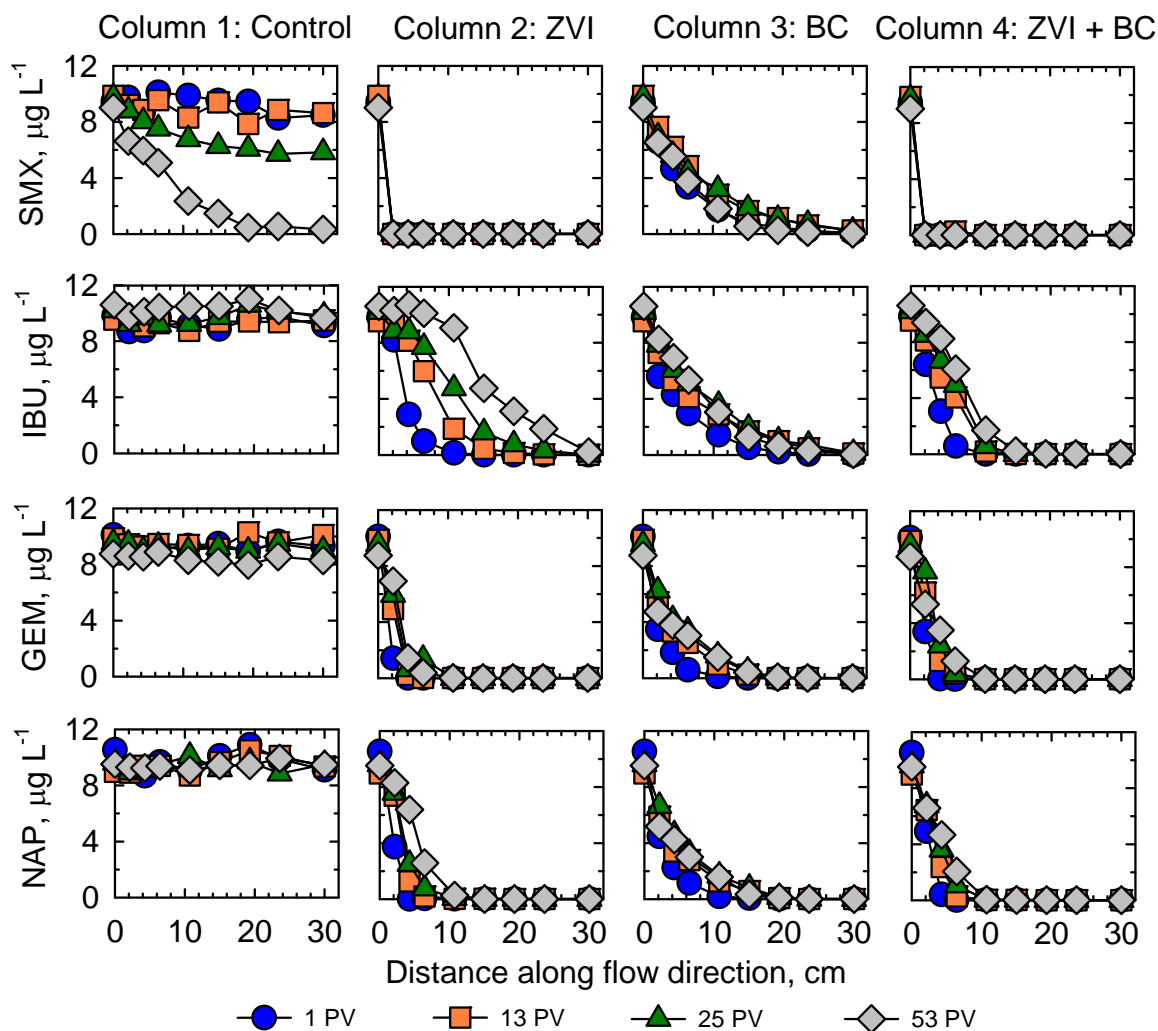


Figure 5.7 Concentrations of acidic pharmaceuticals sulfamethoxazole (SMX), ibuprofen (IBU), gemfibrozil (GEM), and naproxen (NAP) as a function of distance along flow direction within control column and columns containing zero-valent Fe (ZVI), biochar (BC), and both. Blue circle, orange square, and green triangle symbols represent data collected during the first stage of the experiment (flow rate = 0.3 PV/d), while grey diamond symbols represent data collected during the second stage of the experiment (flow rate = 0.1 PV/d), given in terms of pore volumes (PV).

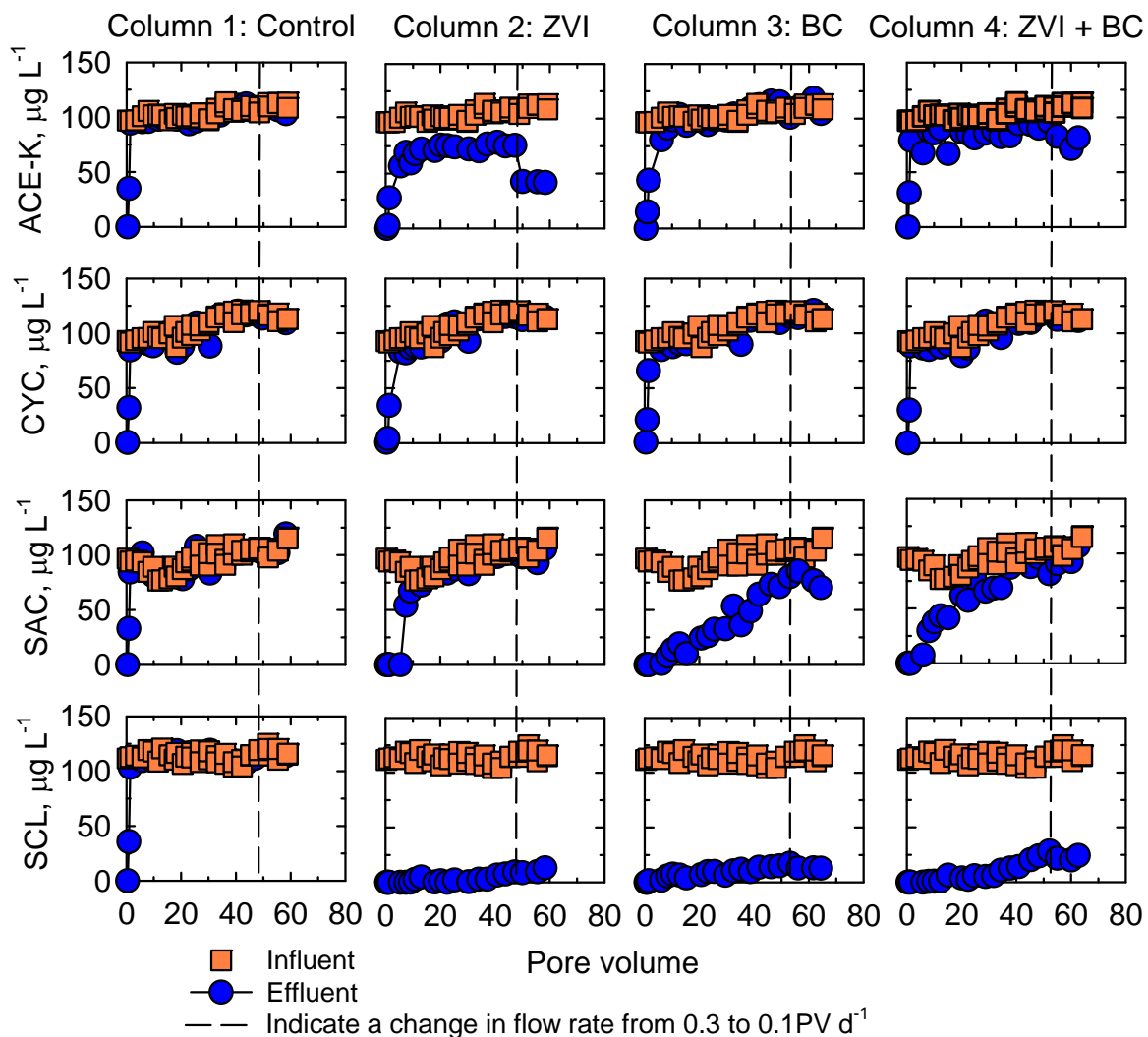


Figure 5.8 Concentrations of acefulfame-K (ACE-K), cyclamate (CYC), saccharine (SAC), and sucralose (SCL) as a function of pore volumes (PV) in effluent from control column and columns containing zero-valent Fe (ZVI), biochar (BC), and both; dash lines indicate a decrease in flow rate in each column, dividing the experiment into two stages.

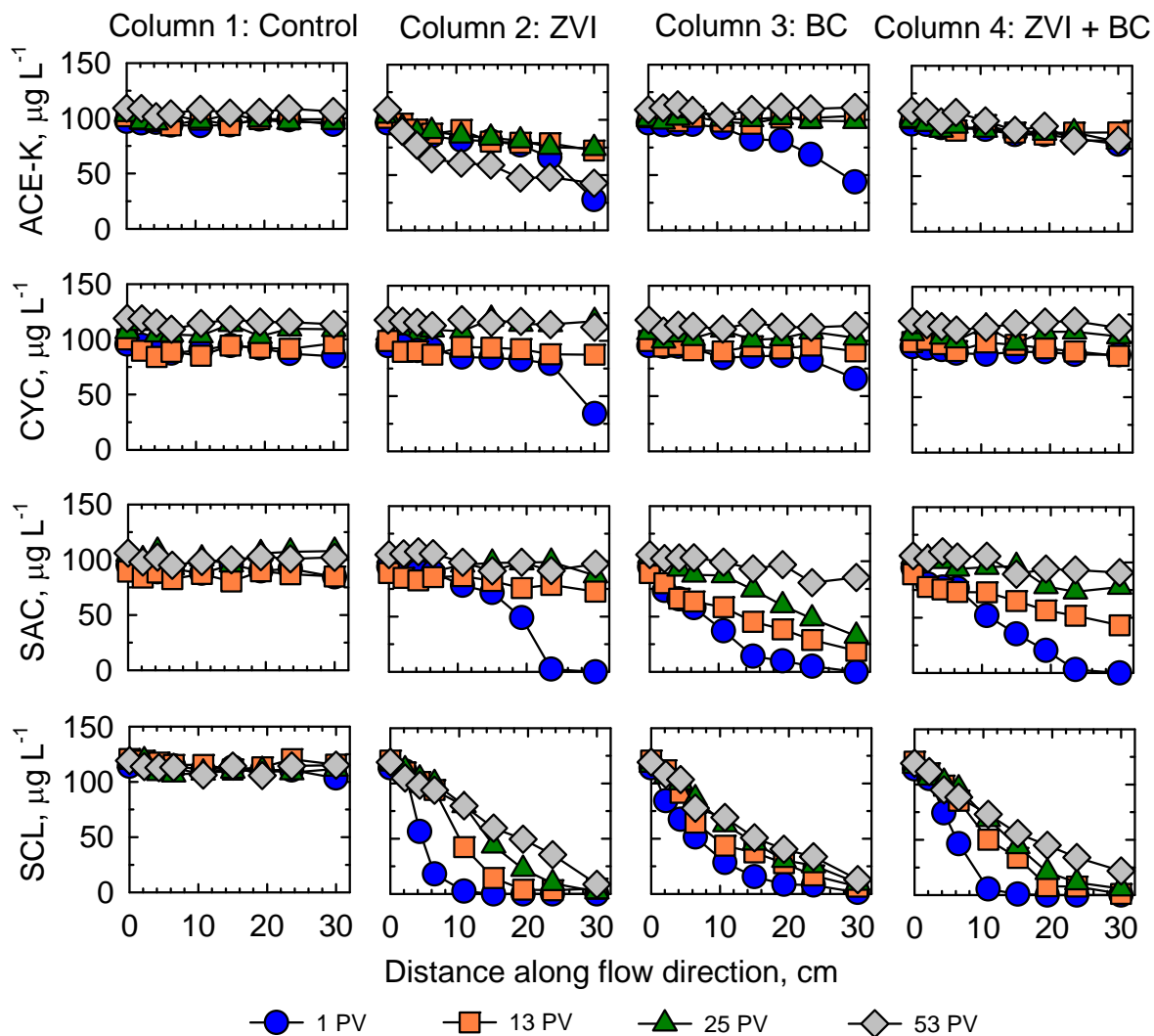


Figure 5.9 Concentrations of acefulfame-K (ACE-K), cyclamate (CYC), saccharine (SAC), and sucralose (SCL) as a function of distance along flow direction within control column and columns containing zero-valent Fe (ZVI), biochar (BC), and both. Blue circle, orange square, and green triangle symbols represent data collected during the first stage of the experiment (flow rate = 0.3 PV/d), while grey diamond symbols represent data collected during the second stage of the experiment (flow rate = 0.1 PV/d), given in terms of pore volumes (PV).

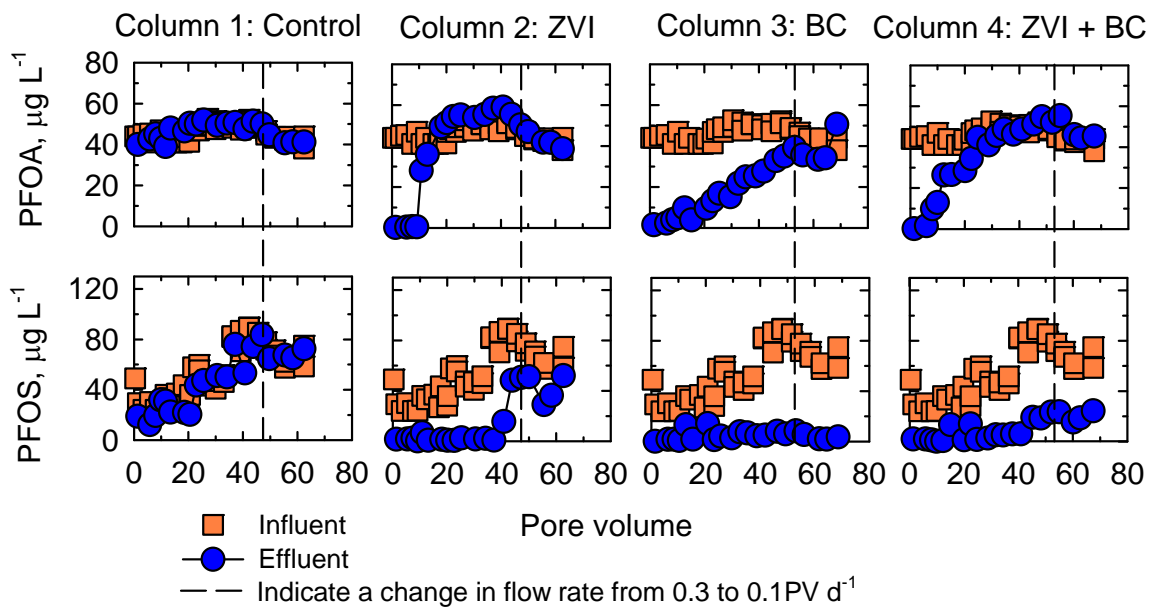


Figure 5.10 Concentrations of perfluorooctanoic acid (PFOA) and perfluorooctane sulfonic acid (PFOS) as a function of pore volumes (PV) in effluent from control column and columns containing zero-valent Fe (ZVI), biochar (BC), and both; dash lines indicate a decrease in flow rate in each column, dividing the experiment into two stages.

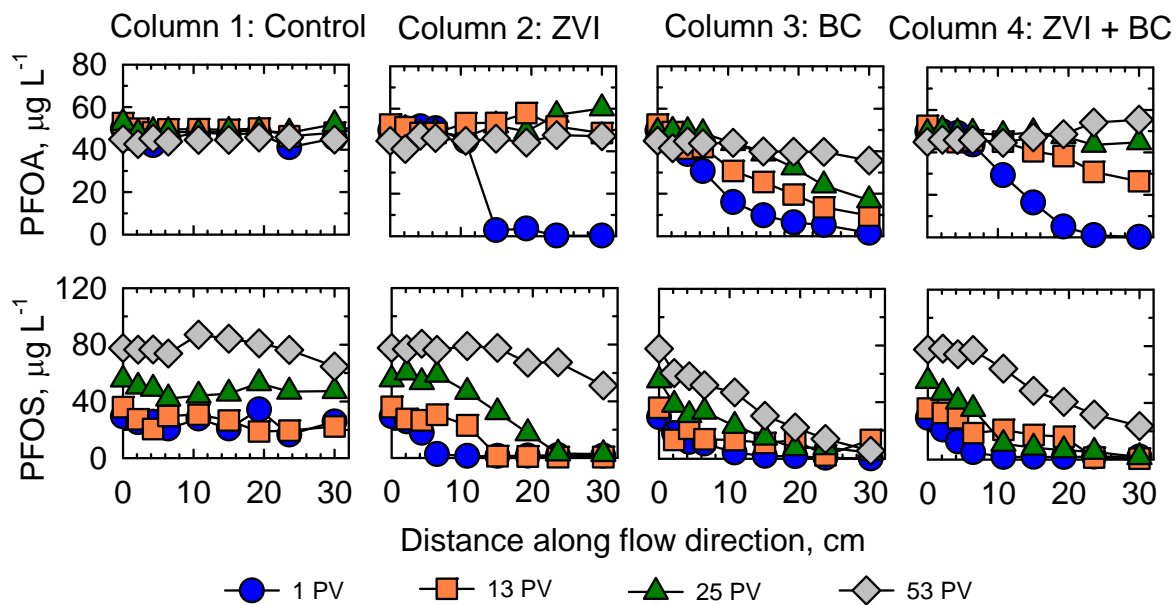


Figure 5.11 Concentrations of perfluorooctanoic acid (PFOA) and perfluorooctane sulfonic acid (PFOS) as a function of distance along flow direction within control column and columns containing zero-valent Fe (ZVI), biochar (BC), and both. Blue circle, orange square, and green triangle symbols represent data collected during the first stage of the experiment (flow rate = 0.3 PV/d), while grey diamond symbols represent data collected during the second stage of the experiment (flow rate = 0.1 PV/d), given in terms of pore volumes (PV).

Chapter 6: *Removal of Perfluoroalkyl*

Carboxylic and Sulfonic Acids from Water

Using Zero-valent Iron and Biochar

6.1 Executive Summary

Perfluoroalkyl substances (PFASs), a class of Persistent Organic Pollutants, have received a great deal of attention due to their widespread occurrences and persistence in the environment and their potential toxicity to animals and humans. Effective decomposition of PFASs usually involves advanced oxidation or reduction processes under extremely acidic pH conditions, high temperature and pressure (except for activated carbon adsorption and nanofiltration), which makes these technologies costly and less feasible for full-scale applications. In this study, a series of laboratory batch experiments was conducted to evaluate the effectiveness of zero-valent iron (ZVI) alone and a mixture of ZVI and biochar (ZVI + BC) for removal of perfluoroalkyl carboxylic acids (PFCAs) and perfluoroalkyl sulfonic acids (PFASs) from water under ambient environmental conditions. The target PFCAs include perfluorooctanoic acid (PFOA, C8-PFCA), perfluoroheptanoic acid (PFHpA, C7-PFCA), and perfluorohexanoic acid (PFHxA, C6-PFCA); the target PFASs include perfluorooctane sulfonic acid (PFOS, C8-PFSA), perfluoroheptane sulfonic acid (PFHpS, C7-PFSA), perfluorohexane sulfonic acid (PFHxS, C6-PFSA), and perfluorobutane sulfonic acid (PFBS, C4-PFSA). The results show that PFCAs were less effectively removed than PFASs when utilizing ZVI and (ZVI + BC). About 20% and 60% of input PFOA ($\sim 18,550 \mu\text{g L}^{-1}$) was removed by ZVI alone and the mixture of (ZVI + BC). Lower removal of short chain PFCAs was observed using ZVI alone and (ZVI + BC) compared to PFOA. The ZVI alone and (ZVI + BC) exhibited similar removal ($\sim 17\%$) of input PFHpA ($26 \mu\text{g L}^{-1}$); however, PFHxA was not removed by ZVI alone or (ZVI + BC). About 90% and 94% of input PFOS ($\sim 18,580 \mu\text{g L}^{-1}$) was removed by ZVI and (ZVI + BC). Similarly, the removal of short chain PFASs by reactive media was lower than PFOS. About 57% and 70% of input PFHpS ($330 \mu\text{g L}^{-1}$) were removed by ZVI and (ZVI + BC); $\sim 30\%$ and 40% of input PFHxS (13

$\mu\text{g L}^{-1}$) were removed by ZVI and (ZVI + BC); ~20% of input PFBS ($\sim 6 \mu\text{g L}^{-1}$) by ZVI or (ZVI + BC). The removal efficiencies of PFCAs and PFSAAs by ZVI and (ZVI + BC) decreased with decreasing chain length. The removal of PFCAs and PFSAAs by ZVI may be due to a combination of reductive defluorination and sorption; the removal of PFCAs and PFSAAs by BC was likely due to hydrophobic sorption. About 5 – 10 % of input PFOA and PFOS were partially defluorinated by ZVI alone as indicated by F^- release, however, the defluorination efficiency of PFCAs and PFSAAs by (ZVI + BC) may be underestimated due to sorption of F^- by the reactive media.

6.2 Introduction

Perfluoroalkyl substances (PFASs) such as perfluoroalkyl carboxylic acids (PFCAs) and perfluoroalkyl sulfonic acids (PFSAAs) are anthropogenic organic compounds that consist of a hydrophobic perfluorinated carbon (C-F) tail and a hydrophilic ionic head (carboxylic or sulfonic acid) (Rahman et al., 2014). Due to the presence of the strong C-F bond in their structure, these compounds exhibit high thermal and chemical stability. As a result, they have been widely used in a range of applications, such as polymer additives, fire retardants, pesticides, and surfactants (Kotthoff et al., 2015; Wang et al., 2014). The high stability of PFASs makes these compounds resistant to environmental degradation processes (Kissa, 2001), which results in their ubiquitous occurrence and persistence in the aquatic environment.

PFASs have been globally detected in surface water (Liu et al., 2015a; Myers et al., 2012), groundwater (Lin et al., 2015b; Schaider et al., 2014), and drinking water (Quiñones & Snyder, 2009; Yim et al., 2009) in the ng L^{-1} to $\mu\text{g L}^{-1}$ range; these compounds have also been detected in Antarctic snow (Wang et al., 2015), animals (Furdui et al., 2008), and human bodies (Von Ehrenstein et al., 2009; Wang et al., 2011). Many studies demonstrate that PFASs have adverse impacts on humans and wildlife; they are bioaccumulative and possibly carcinogenic (Goudarzi et al., 2016; Suja et al., 2009). Consequently, perfluorooctane sulfonic acid (PFOS) has been included in the Annex B of the Stockholm Convention on Persistent Organic Pollutants, resulting in global restrictions on production (United Nations Environment Programme, 2009). In addition, the U.S. Environmental Protection Agency (U.S. EPA) has proposed a drinking water health advisory for PFOA (400 ng L^{-1}) and PFOS (200 ng L^{-1}) (US EPA, 2009a).

Emerging contaminants consumed by human beings are collected in the wastewater treatment plants (WWTPs); municipal wastewater and industrial discharges are considered to be the major point source release of PFAS to surface water bodies; non-point-sources of PFAS including agricultural run-off and atmospheric transport also contribute to PFAS contamination (Fujii et al., 2007). Giesy and Kannan (2001) report the widespread distribution of perfluorooctane sulfonate (PFOS) associated with the industrial production and application of PFASs. Conventional WWTPs typically do not effectively remove PFASs from water (Arvaniti & Stasinakis, 2015), unless activated carbon (AC) sorption, nanofiltration, or reverse osmosis are utilized (Fujii et al., 2007; Rayne & Forest, 2009). Due to the wide global distribution and toxicity of PFASs, a variety of treatment methods have been studied for removing these compounds from water.

Advanced oxidation processes (using strong oxidizing radicals such as $\cdot\text{OH}$, $\text{O}_2\cdot^-$, and $\text{SO}_4\cdot^-$) have been extensively studied to degrade PFASs (Hori et al., 2005; Ochiai et al., 2011); however, low rates of PFASs degradation are typically observed under ambient temperature and environmental pH conditions due to the presence of the strong C-F bond and the electronegative fluorine atom in the structure. A combination of strong oxidizing radicals and extreme treatment conditions (such as low pH, high temperature, vacuum ultraviolet, and microwave) is more likely to lead to greater removal efficiency of PFASs. Yin et al. (2016) report 90% of input perfluorooctanoic acid (PFOA) ($\sim 20 \mu\text{M}$) was degraded by activated persulfate ($\sim 2 \text{ mM}$) at a pH of 2.0, a reaction temperature of $50 \text{ }^\circ\text{C}$, and reaction time of 100 h. Hori et al. (2008) report defluorination (78%) of $374 \mu\text{M}$ PFOA was achieved using 50 mM persulfate with $80 \text{ }^\circ\text{C}$ reaction temperature and 6 h reaction time. Moriwaki et al. (2005) demonstrate the degradation of PFOS and PFOA under ultrasonic irradiation with half-life times for PFOS of 43 min and for

PFOA of 22 min under an argon atmosphere. Similarly, reductive removal of PFASs using nanoscale zero-valent iron (ZVI) or highly reactive reducing radicals such as aqueous electrons, H^\cdot , and $SO_3^{\cdot-}$ also require extreme reaction conditions such as high pressure, ultraviolet, microwave, or ultrasound to facilitate treatment (Hori et al., 2006; Park et al., 2011; Song et al., 2013). These harsh reaction conditions (such as low pH, high temperature) and high energy consumption of the advanced oxidative and reductive treatment hamper their large-scale application to municipal water treatment plants and WWTPs.

Compared to the destructive oxidative and reductive methods, removal of PFASs by adsorption using activated carbon (AC) and filtration technologies such as nanofiltration and reverse osmosis are less energy demanding. However, the AC and membranes used for adsorption and filtration need to be frequently renewed or changed, which makes these technologies costly and less feasible for large-scale application. Zero-valent iron (ZVI) is a relatively inexpensive, abundant, and environmentally friendly reductant. ZVI has been successfully used in in-situ permeable reactive barriers (PRBs) for removing a wide range of environmental organic contaminants, including halogenated organic compounds, chlorinated methanes, and nitroaromatics (Jeen et al., 2013; Johnson et al., 1996; Lavine et al., 2001; Matheson & Tratnyek, 1994) and inorganic contaminants (such as As, Cd, Cr, Ni, Zn, V, NO_3 , PO_4 , SO_4 , and ClO_4^-) (Blowes et al., 2000; Cantrell et al., 1995; Jamieson-Hanes et al., 2014; Liu et al., 2014c; Shrimpton et al., 2015) from wastewater and groundwater. Biochar (BC) is a stable carbon-rich product synthesized through pyrolysis/carbonization of plant- and animal-based biomass under low oxygen (O_2) and at relatively low temperature ($< 700^\circ C$) condition (Lehmann & Joseph, 2009). Due to the relative low cost, abundance, and comparable sorption ability to AC, BC has been used as a potential alternative sorbent for AC for removal or

immobilization of a wide range of organic contaminants such as pharmaceutical compounds and polycyclic aromatic hydrocarbons (PAHs) (Oleszczuk et al., 2012; Rajapaksha et al., 2015) and inorganic contaminants such as heavy metals Hg, Cr, Cu, Ni, and Zn (Liu et al., 2016a; Uchimiya et al., 2010) from contaminated soil and wastewater. The combination of ZVI and BC is a promising reactive media for environmental soil and water remediation, which integrates both the strong reduction of ZVI and sorption capacity of BC. Enhanced removals of organic contaminants such as tetracycline, methyl orange, and methylene blue and inorganic contaminants such as Pb(II), Cr(VI), As(V), and phosphate (P) from contaminated water have been reported using biochar-supported ZVI (Han et al., 2015; Peng et al., 2014; Zhou et al., 2014).

In this study, a series of batch experiments was conducted to evaluate the effectiveness of the reactive media ZVI alone and a mixture of (ZVI + BC) for removal of three perfluoroalkyl carboxylic acids (PFCAs) and four perfluoroalkyl sulfonic acids (PFSAs) from water under environmental pH conditions and ambient temperature. The target PFCAs included perfluorooctanoic acid (PFOA, C8-PFCA), perfluoroheptanoic acid (PFHpA, C7-PFCA) and perfluorohexanoic acid (PFHxA, C6-PFCA). The target PFSAs included perfluorooctane sulfonic acid (PFOS, C8-PFSA), perfluoroheptane sulfonic acid (PFHpS, C7-PFSA), perfluorohexane sulfonic acid (PFHxS, C6-PFSA), and perfluorobutane sulfonic acid (PFBS, C4-PFSA).

Fluoride (F^-) is an indicative byproduct of defluorination of PFOA and PFOS. Defluorination of PFOS by ZVI has been observed in subcritical water in laboratory batch experiments with the production of F^- and CHF_3 gas (Hori et al., 2006). In column experiments using zero valent iron (Chapter 5), release of F^- associated with defluorination of PFOA and

PFOS was not observed, likely due to either lack of defluorination reactions, analytical limitations, or other factors. Concentrations of F^- in the column effluent and pore waters were below the analytical detection limit (0.02 mg L^{-1}). Simulated groundwater (CaCO_3 saturated H_2O , $\text{pH}=8.3$) was used as an input solution matrix in the column experiment to represent the ubiquitous occurrence of HCO_3^- and CO_3^{2-} in natural waters. An alternative reason for lack of F^- detection, is the potential removal of F^- through precipitation with Ca^{2+} (present in simulated groundwater) to form CaF_2 . In this study, batch experiments were conducted to evaluate potential defluorination of PFOA and PFOS by zero-valent iron (ZVI) under reducing conditions. In these experiments, NaHCO_3 was used as an input solution matrix, and not CaCO_3 (as was used in column experiments in Chapter 5) to minimize the removal of F^- generated through defluorination reactions through formation of CaF_2 precipitation. The concentrations of PFOA and PFOS in the input NaHCO_3 solution were set at 20 mg L^{-1} by assuming only one F atom defluorinated from 20 mg L^{-1} of PFOA or PFOS; the anticipated concentration of F^- defluorinated from 20 mg L^{-1} of PFOA or PFOS would be $\sim 1 \text{ mg L}^{-1}$, which is well above the analytical detection limit of F^- (0.02 mg L^{-1}) for quantification. In addition, a series of batch experiments (F^- sorption test) was conducted to evaluate the sorption of F^- (at $\sim 1 \text{ mg L}^{-1}$, the anticipated concentration of F^- defluorinated from 20 mg L^{-1} of PFOA or PFOS) by reactive media ZVI alone and the mixture of (ZVI + BC).

6.3 Materials and Methods

6.3.1 Batch Experiments for Removal of Perfluoroalkyl Carboxylic Acids (PFCAs) and Perfluoroalkyl Sulfonic Acids (PFSA) Using ZVI and Mixture of ZVI and BC

6.3.1.1 Batch Experimental Setup

Granular Fe⁰ (ZVI, 0.25–1.19 mm) was obtained from Connelly-GPM, and was washed five times using 1L of 1.2 M reagent-grade HCl acid (Fisher Scientific, Canada) to remove the iron rust and impurities, followed by ten times rinse using 1L of ultrapure H₂O (MilliQ A10, 18.2 MΩ cm @ 25 °C, Etobicoke, Canada). Hard-wood (oak) based biochar (BC, 0.5–2.36 mm) was obtained from Cowboy Charcoal Co., Brentwood, TN, USA. Dry perfluorooctanoic acid (PFOA) powder (96% purity) and perfluorooctane sulfonic acid potassium salt (PFOS) powder (98% purity) were obtained from Sigma-Aldrich, Canada. The input solution matrix consisted of a 0.8 mM NaHCO₃ in Ar_(g) purged ultrapure H₂O with pH of 8.54

The individual PFOA and PFOS stock solutions containing 10,000 mg L⁻¹ of PFOA and 10,000 mg L⁻¹ of PFOS were prepared by dissolving 0.100 g PFOA and 0.100 g PFOS dry powder in 10 mL methanol (HPLC grade, Sigma-Aldrich, Canada). Individual PFOA and PFOS input solutions contained 20 mg L⁻¹ PFOA and 20 mg L⁻¹ PFOS, which were prepared by spiking 1 L of Ar_(g) purged 0.8 mM NaHCO₃ solution with 2 mL of 10,000 mg L⁻¹ of PFOA and PFOS stock solution. Blank samples including Blank NaHCO₃, Blank ZVI, and Blank (ZVI + BC), were used to track the background concentrations of PFOA and PFOS in the NaHCO₃ solution (input solution matrix), and on the reactive media of ZVI and (ZVI + BC). Blank NaHCO₃ sample consisted of 35 mL 0.8 mM NaHCO₃ solution. Blank ZVI and Blank (ZVI + BC)

samples were prepared by adding 35 g ZVI alone or a mixture of 7 g ZVI and 3.5 g BC to 35 mL of 0.8 mM NaHCO₃ solution. The volume ratio of 3.5 g BC to 7g ZVI was approximately 4, which was similar to the volume ratio of BC to ZVI used in the column experiment (Chapter 5). Control samples were used to determine the concentration losses of input PFOA and PFOS during the reaction period due to sorption to containers or photolysis. Control PFOA and Control PFOS were 35 mL of input PFOA and 35 mL of input PFOS solution. Treatment samples were used to determine the removals of PFOA and PFOS by reactive media ZVI alone and the mixture of (ZVI + BC) during the reaction period. Treatment PFOA + ZVI and Treatment PFOA + (ZVI+BC) samples were prepared by adding 35 g ZVI or a mixture of 7 g ZVI and 3.5 g BC to 35 mL of PFOA input solutions. Treatment samples PFOS + ZVI and PFOS + (ZVI+BC) were prepared by adding 35 g ZVI or a mixture of 7 g ZVI and 3.5 g BC to 35 mL of PFOS input solutions (Table 6.1). Sampling times were set at Days 0, 20, 40, 60, 90, and 120. Duplicate batch samples were prepared at Days 40, 90, and 120. All batch mixtures were prepared in 50 mL polypropylene centrifuge tubes with screw caps (Eppendorf, Canada). All batch mixtures were manually shaken every other day in an anaerobic glove box (COY Ltd.) that contained 3.5% H₂ and 96.5% N₂. The batch mixtures were taken out of the glove box for centrifugation (6000 rpm for 15 min) and placed back in the glove box to collect samples of the supernatant and reactive media.

6.3.1.2 Collection of Supernatant Samples

Supernatant samples were collected using a needle attached to 24 mL plastic syringe. Supernatant samples for pH and Eh analyses were not filtered; samples for alkalinity analyses were filtered through 0.45- μ m cellulose acetate membranes before measurement. Supernatant PFOA and PFOS samples were not filtered and collected in polyethylene bottles. Supernatant

anion samples were filtered through 0.45- μ m cellulose acetate filters and collected in polyethylene bottles. The measurement of pH, Eh, and alkalinity were determined immediately after sampling, other samples were stored at 4 °C and analyzed within one week of collection.

6.3.1.3 Aqueous Samples Extracted from Reactive Media

Perfluoroalkyl substances (PFASs) were extracted from the reactive media (ZVI and mixture of ZVI and BC) following a previously described method (Arvaniti et al., 2014) with slight modifications to determine the amount of PFOA and PFOS adsorbed by ZVI and BC. The method reported by Arvaniti et al. (2014) was validated based on absolute analyte (target PFASs) recoveries that ranged from 78% to 115% and satisfactory precision (RSD < 15%) (N=6). An aliquot of 0.4 g of ZVI and the mixture of ZVI and BC (wet solid samples) from the Treatments PFOA + ZVI, PFOA + (ZVI + BC), PFOS + ZVI, PFOS + (ZVI + BC), Blank ZVI, and Blank (ZVI + BC) were transferred to 50 mL Eppendorf tubes. Liquid-solid extraction (LSE) was performed by adding 7.5 mL 1% (v/v) acetic acid and 1.5 mL methanol to the sample tubes. The samples were vortexed for 1 min, followed by 15 min sonication, and then centrifuged at 3500 rpm for 15 min. The supernatants were transferred to 50 mL polypropylene centrifuge tubes with screw caps (Eppendorf, Canada). The LSE process was repeated another two successive times for each sample by only adding 7.5 mL 1% acetic acid followed by the same vortex, sonication, and centrifugation steps. The supernatants from the three LSE steps were collected together in 50 mL polypropylene centrifuge tubes and stored at 4 °C for PFAS analysis. Water content of each LSE sample was determined to calculate the dry mass of the reactive media used in the LSE process.

6.3.2 Batch Experiments for Evaluating Sorption of F⁻ by Reactive Media

The F⁻ sorption test was performed to evaluate the sorption of F⁻ by ZVI alone and the mixture of ZVI and BC (Table 6.1). The F⁻ stock solution containing 500 mg L⁻¹ F⁻ was prepared by mixing 0.553 g sodium fluoride (NaF) dry powder (> 99%) (Anachemia, Canada) in 500 mL ultrapure H₂O. The F⁻ input solution containing 1 mg L⁻¹ F⁻ in 0.8 mM NaHCO₃ solution was prepared by spiking 499 mL of 0.8 mM NaHCO₃ solution with 1 mL of 500 mg L⁻¹ F⁻ stock solution. Blank samples including Blank NaHCO₃, Blank ZVI, and Blank (ZVI + BC) were used to track the background concentrations of F⁻ in the NaHCO₃ solution (input solution matrix), and on the reactive media of ZVI and (ZVI + BC). Blanks NaHCO₃, ZVI, and (ZVI + BC) samples were prepared the same way as in section 6.3.1.1. Control F⁻ samples contained 35 mL of 1 mg L⁻¹ F⁻ input solution in 50 mL polypropylene centrifuge tubes, which was used to track the loss of F⁻ due to sorption to containers during the reaction period. Sorption test samples were used to determine the sorption of F⁻ by ZVI alone and the mixture of (ZVI + BC). Sorption test samples F⁻ + ZVI and F⁻ + (ZVI + BC) were prepared by adding 35 g ZVI alone and the mixture of 7 g ZVI and 3.5 g BC to 35 mL of F⁻ input solution in 50 mL polypropylene centrifuge tubes (Table 6.1). All the batch samples were kept in the anaerobic glove box and manually shaken every other day. Samples were taken out of the glove box and centrifuged at 6000 rpm for 15 min, and placed back into the glove box for sampling at Days 0, 20, 40, 60, 90, and 120. Samples for F⁻ analysis were filtered through 0.45- μ m cellulose acetate filters and collected in 8 mL polyethylene bottles stored at 4 °C until analysis within one month of collection.

6.3.3 Analysis of Water Samples and Solid-Phase Extracts

6.3.3.1 Measurements of pH, Eh, and Alkalinity of Supernatant Samples

Measurements of pH were conducted using an Orion Ross combination electrode (model 815600) calibrated with standard buffer solutions of pH 7, 4, and 10, and checked against pH 7 and 10 buffer solutions between samples. The redox potentials (corrected to the standard hydrogen electrode and reported as Eh values) were measured using a Pt-billeted Ag-AgCl combination electrode (Orion 9678BNWP), checked against A and B solutions (redox/ORP electrode user guide, Thermo Scientific, Canada) before measurement. Measurements of alkalinity were performed using a HACH digital titrator and bromocresol green/methyl red indicator and with $0.08 \text{ mol L}^{-1} \text{ H}_2\text{SO}_4$.

6.3.3.2 Analysis of Fluoride in Supernatant Samples

The concentrations of F^- were determined by a Dionex ICS-5000 ion chromatography (IC) system (Thermo Scientific, Sunnyvale, CA, USA). The F^- was separated by an IonPac AS11-HC (2 x 250 mm) column (Thermo Scientific) using a potassium hydroxide (KOH) gradient. The EGC III KOH eluent generator cartridge (Dionex) was used to generate the KOH gradient. The KOH gradient elution initially started at 10 mM, increased to 22 mM in 12 min and increased to 40 mM in 8 min, held at 40 mM for 8 min, then decreased to 22 mM at 28.1 min and decreased to 10 mM in 5 min, and then held at 10 mM for 5 min. The flow rate was 0.25 mL min^{-1} and the injection volume was 10 μL . The system operating pressure was 139–142 bars. The retention time of F^- was around 14.0 min. The electrolytically regenerated suppressor ERS 500 (Dionex, Canada) with the applied current of 40 mA and the carbonate removal device CRD 200 (2 mm) (Dionex, Canada) were used in the system. A seven point calibration curve ($0.01\text{-}2.0 \text{ mg L}^{-1}$) was used to quantify F^- concentrations. The method detection limit (MDL) for F^- was 0.02 mg L^{-1} . To ensure the identification of F^- peak (not acetate peak which is eluted right after F^-), the supernatant samples of Treatment PFOA + ZVI and Treatment PFOS + ZVI at Days 90 and 120

were fortified with either a known amount of F⁻ or acetate or both F⁻ and acetate. The concentrations of spiked F⁻ and acetate in supernatant samples were 0.1 mg L⁻¹ (F⁻) and 1 mg L⁻¹ (acetate). The recoveries of spiked F⁻ and acetate were between 73% and 101%. The spiking strategy and IC chromatograms are provided in Appendix E (Table E.1 and Figures E.1–E.4).

6.3.3.3 Analysis of PFOA and PFOS

The diluted samples (20 mL) for PFOA and PFOS analysis were spiked with 400 µL internal standards (IS) mixture which contained 10 µg L⁻¹ [¹³C]-PFOA and 20 µg L⁻¹ [¹³C]-PFOS (Wellington Laboratories Inc., Guelph, Canada). The IS spiked PFOA and PFOS samples (20 mL) were passed through solid-phase extraction (SPE) cartridges (Oasis HLB 3 cc glass cartridges; Waters Corp., Mississauga, Canada). The cartridges were preconditioned with 2 x 1 mL methanol (HPLC grade), washed with 2 x 1 mL ultrapure H₂O, then loaded with 20 mL IS spiked PFOA and PFOS samples, washed with 2 x 1 mL ultrapure H₂O, vacuum dried for 1 min, finally eluted with 2 x 1 mL methanol (HPLC grade). The 2 mL PFOA and PFOS methanol extracts were collected in 5 mL polypropylene centrifuge tubes (Eppendorf, Canada) and kept at room temperature until analysis.

The concentrations of PFOA and PFOS in methanol extracts were determined by high performance liquid chromatography (1290 HPLC, Agilent Technologies, Mississauga, Canada) followed by tandem mass spectrometry (6460 QQQ, Agilent Technologies, Mississauga, Canada) in ESI- mode using EPA Method 537 (Shoemaker, 2013) with recommended modifications (Yamashita et al., 2004) to enhance the instrument performance. The PFOA and PFOS were separated using a Zorbax Eclipse C18 column (4.6 × 150 mm, 5 µm i.d.) (Agilent, Mississauga, Canada) at 55 °C. The mobile phase A contained 2 mM ammonium acetate (HPLC grade,

Sigma-Aldrich, Oakville, Canada) in water; the mobile phase B contained 2 mM ammonium acetate in methanol. The mobile phase elution gradient, instrument operating conditions, and preparations of the calibration curves were the same as described in section 5.3.2. The accuracy of a sample was calculated as the ratio of the measured PFOA and PFOS concentrations to the expected PFOA and PFOS concentrations. The accuracy of PFOA and PFOS calibration, determined by calibration verification (CV) and continuous calibration verification (CCV) samples was between 85% and 113%. Tap water samples and unknown samples were spiked with PFOA and PFOS analyte and IS to track the accuracy of SPE procedures. The accuracy of PFOA and PFOS for spiked tap water and unknown samples were between 87% and 114%. The absolute IS recoveries of PFOA and PFOS for the CV, CCV, tap water samples, and unknown samples (including PFOA and PFOS supernatant samples and aqueous PFOA samples extracted from the reactive media) were between 74–118%. The IS recoveries of PFOS for the aqueous samples extracted from the reactive media were likely affected by acetic acid used in LSE process, and the relative IS recoveries were between 81% and 115%. The method detection limits (MDLs) of PFOA and PFOS were 45 and 110 ng L⁻¹.

6.3.3.4 Analysis of Short Chain Perfluoroalkyl Carboxylic Acids (PFCAs) and Perfluoroalkyl Sulfonic Acids (PFSAs)

The short chain perfluoroalkyl carboxylic acids (PFCAs) and perfluoroalkyl sulfonic acids (PFSAs) samples (20 mL) were spiked with 400 µL of 20 µg L⁻¹ [1,2-¹³C₂]-PFHxA and [¹⁸O]-PFHxS (Wellington Laboratories Inc., Canada) internal standard (IS) mixture to yield 2 µg L⁻¹ of ISs in 20 mL samples. The IS spiked 20 mL diluted samples were then prepared following the same solid phase extraction (SPE) procedures with the ones for PFOA and PFOS (section 6.3.3.3). The short chain PFCAs and PFSAs extracts were analyzed by high performance liquid

chromatography (1290 HPLC, Agilent Technologies, Mississauga, Canada) followed by tandem mass spectrometry (6460 QQQ, Agilent Technologies, Mississauga, Canada) in ESI- mode following the method of Houtz and Sedlak (2012) with slight modifications to optimize the instrument performance. The analytes were separated using Poroshell 120 EC-C18, 3 x 5 mm, 2.7 μm i.d. (Agilent, Mississauga, Canada) at 55 $^{\circ}\text{C}$. The mobile phases were the same as used for PFOA and PFOS analysis. A gradient elution started at 40 % B for 1.5 min, increased linearly to 100 % B within 6 min and held at 100% for 3 min, then decreased to 40 % B at 9.5 min and held at 40 % until 13.5 min. The flow rate was 0.5 mL min^{-1} and the injection volume was 2 μL . The calibration standards prepared in 96 : 4% (v/v) methanol/water were serially diluted from the analyte standard stock (1000 $\mu\text{g L}^{-1}$) of short chain PFCAs including perfluoroheptanoic acid (PFHpA), perfluorohexanoic acid (PFHxA), perfluoropentanoic acid (PFPeA) and the short chain PFSAAs including perfluoroheptane sulfonic acid (PFHpS), perfluorohexane sulfonic acid (PFHxS), perfluorobutane sulfonic acid (PFBS) (Wellington Laboratories Inc., Canada) (Table 6.2). Seven to nine points calibration curves (PFBS: 0.1–30 $\mu\text{g L}^{-1}$; PFBA and PFHxA: 0.2–30 $\mu\text{g L}^{-1}$; PFHpA, PFPeA, PFHpS, and PFHxS: 0.5–30 $\mu\text{g L}^{-1}$) were used for PFCAs and PFSAAs quantitation with 2 $\mu\text{g L}^{-1}$ of [1,2- ^{13}C]-PFHxA and [^{18}O]-PFHxS (Wellington Laboratories Inc., Canada). The accuracy of calibration, CV, and CCV samples was between 89–120%. Tap water samples and unknown samples spiked with analyte and IS was used to track the precision of SPE procedures. The absolute IS recoveries of the CV, CCV, tap water samples, and unknown samples were 82–125%. The instrument limits of quantification (LOQ) were calculated at 10 times the signal-to-noise value. The LOQ of PFBS and PFHxS was 0.2 $\mu\text{g L}^{-1}$; the LOQ of PFHpS, PFHxA, and PFHpA were 0.5 $\mu\text{g L}^{-1}$; the LOQ of PFBA and PFPeA were 1 $\mu\text{g L}^{-1}$ and 2 $\mu\text{g L}^{-1}$.

6.4 Results and Discussion

6.4.1 Removal of Perfluoroalkyl Carboxylic Acids (PFCAs) and Perfluoroalkyl Sulfonic Acids (PFSAs) Using ZVI and Mixture of ZVI and BC

6.4.1.1 Geochemistry of Supernatant Samples

The pH values of the Treatment PFOA/PFOS + (ZVI + BC) supernatant samples were constant at ~8.5, which were consistent with that of the control samples. However, relatively higher pH values of ~10.5 (except for Day 0) were observed for the supernatant samples of Treatment PFOA/PFOS + ZVI, likely due to the corrosion of ZVI in H₂O. The Eh values of the treatment supernatant samples were consistent with the control samples, which increased slightly from -368 mV at Day 0 to -230 mV at Day 40 and maintained at -230 to -293 mV, indicating strong reducing conditions in the treatment and control samples during the 120 days of reaction time. The alkalinity of Control PFOA/PFOS and Treatment PFOA/PFOS supernatant samples exhibited a slightly increasing trend from Day 0 to Day 90, followed by a slight decrease at Day 120, with concentrations ranging from 12 to 38 mg L⁻¹ as CaCO₃ during the entire batch experiment (Figure 6.1).

6.4.1.2 Removal of Perfluoroalkyl Carboxylic Acids (PFCAs) and Perfluoroalkyl Sulfonic Acids (PFSAs) Using ZVI and Mixture of ZVI and BC in Supernatant Samples

The concentrations of perfluoroalkyl carboxylic acids (PFCAs) including PFOA (C8-PFCA), PFHpA (C7-PFCA), PFHxA (C6-PFCA), PFPeA (C5-PFCA), and PFBA (C4-PFCA) and perfluoroalkyl sulfonic acids (PFSAs) including PFOS (C8-PFSA), PFHpS (C7-PFSA), PFHxS (C6-PFSA), and PFBS (C4-PFSA) in the Blank NaHCO₃, Blank ZVI, and Blank (ZVI + BC) samples were below the MDLs or LOQs, indicating there was no background contaminations of

these compounds in the input solution or on the reactive media. The input concentrations of PFOA in the Control PFOA samples and PFOS in the Control PFOS samples were about 18,500 $\mu\text{g L}^{-1}$ (Figure 6.2). Three to four orders of magnitude lower concentrations of short chain PFCAs including PFHpA (C7-PFCA) at $\sim 26 \mu\text{g L}^{-1}$ and PFHxA (C6-PFCA) at $\sim 0.8 \mu\text{g L}^{-1}$ were detected in the Control PFOA samples compared to input PFOA; the concentrations of PFPeA (C5-PFCA) and PFBA (C4-PFCA) were below the LOQ (Figure 6.3). Similarly, two to four orders of magnitude lower concentrations of short chain PFSAs including PFHpS (C7-PFSA) at $\sim 330 \mu\text{g L}^{-1}$, PFHxS (C6-PFSA) at $\sim 13 \mu\text{g L}^{-1}$, and PFBS (C4-PFSA) at $\sim 6 \mu\text{g L}^{-1}$ were detected in the Control PFOS samples compared to input PFOS (Figure 6.4). The detections of short chains PFCAs in the Control PFOA samples and PFSAs in the Control PFOS samples were likely due to the impurity of PFOA (96%) and PFOS (98%) dry stock (see section 6.3.1.1).

The concentrations of PFOA, PFOS, and short chain PFCAs and PFSAs in the Control samples were constant over the reaction time (Figures 6.2–6.4), indicating the sorption of these compounds to the sample containers or the photolysis of these compounds under natural light was limited. The concentration of PFOA in the Treatment PFOA + ZVI supernatant samples decreased from input concentration of 18,550 $\mu\text{g L}^{-1}$ to 14,240 $\mu\text{g L}^{-1}$ at Day 20 and were maintained at $\sim 14,500 \mu\text{g L}^{-1}$ until Day 120, representing $\sim 20\%$ of input PFOA removed by ZVI alone. However, the mixture of (ZVI + BC) exhibited a greater removal of PFOA ($\sim 60\%$) than ZVI alone; the concentration of PFOA in the Treatment PFOA + (ZVI + BC) supernatant samples decreased from 20,000 $\mu\text{g L}^{-1}$ at Day 0 to 6,041 $\mu\text{g L}^{-1}$ at Day 20, but then gradually increased to 8,560 $\mu\text{g L}^{-1}$ at Day 120 (Figure 6.2). Compared to PFOA, lower removals of the short chain PFCAs were observed by ZVI and (ZVI + BC). The concentration of PFHpA (C7-PFCA) decreased from the input concentration of 26 $\mu\text{g L}^{-1}$ at Day 0 to 24.4 $\mu\text{g L}^{-1}$ in the

Treatment PFOA + ZVI supernatant sample and $18.4 \mu\text{g L}^{-1}$ in the Treatment PFOA + (ZVI + BC) supernatant sample at Day 20, and then remained at $\sim 22.0 \mu\text{g L}^{-1}$ during the rest of the experiment with an average PFHpA removal of 17%. The concentrations of PFHxA (C6-PFCA) in the Treatment PFOA + ZVI and PFOA + (ZVI + BC) supernatant samples were consistent with the control samples from Day 0 to Day 120 indicating no removals of PFHxA throughout the batch experiment (Figure 6.3).

The input PFOS ($\sim 18,580 \mu\text{g L}^{-1}$) was effectively removed by ZVI and (ZVI + BC). The concentration of PFOS rapidly decreased from $18,580 \mu\text{g L}^{-1}$ at Day 0 to $4,120 \mu\text{g L}^{-1}$ in the Treatment PFOS + ZVI supernatant sample and $1,780 \mu\text{g L}^{-1}$ in the Treatment PFOS + (ZVI + BC) supernatant sample at Day 20, then continued to decrease until Day 120 with removals of 90% and 94% (Figure 6.2). Lower removals of short chain PFSA were observed using ZVI and (ZVI + BC) compared to PFOS. Greater removals of PFHpS (C7-PFSA) and PFHxS (C6-PFSA) were observed using (ZVI + BC) than ZVI alone. The concentration of PFHpS in the Treatment PFOS + ZVI supernatant sample decreased from input concentration of $330 \mu\text{g L}^{-1}$ at Day 0 to $225 \mu\text{g L}^{-1}$ at Day 20, and then continued to decrease to $142 \mu\text{g L}^{-1}$ at Day 120 with removal of 57%. The concentration of PFHpS in the Treatment PFOS + (ZVI + BC) supernatant sample decreased from $330 \mu\text{g L}^{-1}$ at Day 0 to $91.6 \mu\text{g L}^{-1}$ at Day 20 and remained at $95 \mu\text{g L}^{-1}$ until Day 120 with removal of 70%. Similarly, the concentrations of input PFHxS ($\sim 13 \mu\text{g L}^{-1}$) in the Treatment PFOS + ZVI and PFOS + (ZVI + BC) supernatant samples gradually decreased over reaction time with removals of 30% and 40% at Day 120. Only $\sim 20\%$ of input PFBS (C4-PFSA) ($\sim 6 \mu\text{g L}^{-1}$) was removed by ZVI and (ZVI + BC) during 120 d reaction time (Figure 6.4).

6.4.1.3 Production of F⁻ in Supernatant Samples

Fluoride (F⁻) is the indicative by-product of defluorination of PFOA and PFOS; its concentration in the Blank NaHCO₃, Blank ZVI, and Blank (ZVI + BC) supernatant samples and aqueous samples extracted from the reactive media remained below the MDL (0.02 mg L⁻¹) in this study. However, increasing concentrations of F⁻ were observed in the Treatment PFOA/PFOS + ZVI supernatant samples; the concentration of F⁻ gradually increased from undetectable level at Day 0 to 0.14 mg L⁻¹ in the Treatment PFOA + ZVI supernatant samples and 0.06 mg L⁻¹ in treatment PFOS + ZVI supernatant samples at Day 120 (Figure 6.5). Similarly, the reductive defluorination of PFOA and PFOS using Mg-aminoclay coated nanoscale ZVI led to production of F⁻ but no detection of organic byproducts, with a higher removal efficiency for PFOS (95% at 20 °C) than for PFOA (40% at 20 °C) (Arvaniti et al., 2015). The measured F⁻ concentrations in the Treatment PFOA/PFOS + ZVI supernatant samples were stoichiometrically back-calculated to determine the concentrations of defluorinated PFOA and PFOS; results showed that approximately 8% of input PFOA and 4% of input PFOS were partially defluorinated by ZVI (2F defluorinated from 15F of 8% input PFOA and 17F of 4% input PFOS). These defluorination efficiencies were not corrected for the adsorption F⁻ by reactive media (discussed in section 6.4.2). The concentrations of F⁻ in the Treatment PFOA/PFOS + (ZVI + BC) supernatant samples were below the method detection limit, likely due to the sorption of F⁻ to BC.

6.4.2 Sorption of F⁻ by Reactive Media ZVI and Mixture of ZVI and BC

The concentration of F⁻ provides a direct measurement of the extent of PFAS defluorination; however, the sorption of F⁻ by the reactive media ZVI and BC will result in a lower back-calculated defluorination efficiency of PFAS. The concentration of F⁻ in the input solution for F⁻ sorption test was set at 1 mg L⁻¹ to represent only one F atom defluorinated from 20 mg L⁻¹ of the

input PFOA or PFOS during the treatment using ZVI and (ZVI +BC). The results of the F⁻ sorption test showed that ~20% and ~75% of the input F⁻ (1 mg L⁻¹) were adsorbed by ZVI and (ZVI + BC) over 120 d (Figure 6.6). The F⁻ ions produced from defluorination of PFOA, PFOS, and short chain PFCAs and PFSA were possibly partially or completely adsorbed to the reactive media ZVI and (ZVI + BC). The defluorination efficiency of PFOA and PFOS by ZVI and (ZVI + BC) were likely underestimated due to the sorption of F⁻ by reactive media.

Jeen et al. (2007) demonstrate that iron hydroxy carbonate [$\text{Fe}_2(\text{OH})_2\text{CO}_3$ or $\text{Fe}^{2+}_{2-x}\text{Fe}^{3+}_x(\text{OH})_{2+x}\text{CO}_3$] was the major iron corrosion product formed on the surface of ZVI when the ZVI were exposed in the CaCO_3 solution (pH=8.2-8.3) under reducing conditions. Similarly, the iron hydroxy carbonate (chukanovite) is observed as a secondary mineral precipitate in several granular ZVI PRBs (Lee & Wilkin, 2010). In this study, the corrosion of Fe^0 in the input NaHCO_3 solution (similar to CaCO_3 solution pH=8.3) likely resulted in the same corrosion product iron hydroxyl carbonate on ZVI surface, which may have led to sorption of F⁻ by ZVI. The sorption of F⁻ on iron hydroxide has been reported by Sujana et al. (2009), and the removal of F⁻ (20 mg L⁻¹) from aqueous solution using Fe hydroxides followed first-order kinetics with a sorption capacity of 77 mg g⁻¹, which is much higher than sorption capacity of ZVI for F⁻ (2.0 E-4 mg g⁻¹) in this study. In addition, Guan et al. (2015) report effective sorption of F⁻ using a pine tree sawdust biochar.

6.4.3 Correction of Defluorination Efficiency

The defluorination efficiencies of PFOA and PFOS were likely underestimated due to the sorption of F⁻ by reactive media; ~20% of input F⁻ was adsorbed by ZVI and ~80% of input F⁻ was in the supernatant (discussed in section 6.4.2). The defluorination efficiencies of PFOA and PFOS by ZVI were corrected (divided by 80%) to account for the amount of F⁻ adsorbed by ZVI.

Corrected results showed that approximately 10% of input PFOA and 5% of input PFOS were partially defluorinated by ZVI (2F defluorinated from 15F of 10% input PFOA and 2F defluorinated from 17F of 5% input PFOS). The defluorination efficiencies of PFOA and PFOS by (ZVI + BC) cannot be confirmed and corrected because the concentrations of F^- in the supernatant samples of PFOA/PFOS + (ZVI+BC) were below the detection limit (0.02 mgL^{-1}) due to sorption of F^- by (ZVI + BC).

6.4.4 Possible Removal Mechanisms of PFCAs and PFSAs by ZVI and BC

6.4.4.1 Possible Removal Mechanisms of PFCAs and PFSAs by ZVI

The removal mechanisms of PFCAs and PFSAs by ZVI was likely through reductive defluorination and H bonding. The potential reductive defluorination pathway for PFOA (for instance) is shown in Figure 6.7 (reproduced from Song et al., 2013). The defluorination of PFOA ($C_6F_{13}CF_2COOH$) is initiated by the cleavage of α -position C-F bond by electron transfer from ZVI, leading to the formation of increasing concentrations of $C_6F_{13}CFHCOOH$ ($m/z=395$), $C_6F_{13}CH_2COOH$ ($m/z=377$), and F^- as degradation products. The generated $C_6F_{13}CH_2COOH$ is further decomposed to $C_6F_{13}COOH$ through UV radical splitting of α -position CH_2 - and recombination; this defluorination reaction repeats to further decrease the chain length (Song et al., 2013). However, splitting of α -position CH_2 - (chain decreasing) from PFOA and PFOS with formation of short chain PFCAs and PFSAs likely was limited in this study, because the concentrations of potential α -position CH_2 - splitting products such as C7-PFCA (PFHpA, $C_6F_{13}COOH$) and C6-PFCA (PFHxA, $C_5F_{11}COOH$) remained constant throughout the experiment.

The greater defluorination efficiency of PFOA compared to PFOS (section 6.4.1.3 and Figure 6.5) is likely due to stronger C-F bonds in PFOS than PFOA. Both PFOA [$\text{CF}_3(\text{CF}_2)_6\text{COOH}$] and PFOS [$\text{CF}_3(\text{CF}_2)_7\text{SO}_3\text{H}$] have 8C in their structure; however, PFOS contains one more CF_2 moiety compared to PFOA resulting in a stronger C-F bond in PFOS. In addition, the sulfonic group in PFOS is more electronegative than the carboxylic groups in PFOA, which also contributes to the stronger C-F in PFOS than PFOA.

Formation of gaseous phase byproducts during reductive defluorination of PFOA and PFOS by ZVI was not monitored in this study. However, it should be noted that the formation of gas byproducts such as CO_2 and CHF_3 during decomposition of PFOA and PFOS is usually accompanied by an effective defluorination (complete defluorination efficiency > 50%). Hori et al. (2004) and Hori et al. (2007) report the production of CO_2 gas coupled with a high defluorination efficiency (~95% completely defluorinated) during advanced photochemical decomposition of PFOA. Similarly, a trace amount (0.7%) of volatile unstable degradation products CHF_3 was detected during advanced reductive decomposition of PFOS using ZVI in subcritical water with a complete defluorination efficiency of ~50% (Hori et al., 2006). Given the relatively low defluorination efficiency of PFOA and PFOS (5–10% was partially defluorinated or 0.5–1% was completely defluorinated) in this study compared to previously reported studies, substantial formation of these gas phase byproducts was unlikely.

Besides reductive defluorination, the target PFCAs and PFSA were also likely removed by ZVI through H bonding. The corrosion of ZVI in H_2O likely results in a complex mixture of amorphous and crystalline iron oxyhydroxides (Fe_3O_4 , Fe_2O_3 , FeOOH , $\text{Fe}(\text{OH})_2$, $\text{Fe}(\text{OH})_3$, etc.) coated on the ZVI surface (Mukesh & Panday, 2001; Sun et al., 2016; Wilson, 1923). The hydroxyl ($-\text{OH}$) groups (H donors) on the surface of ZVI likely interact with the electronegative

O atoms (H acceptors) in the functional carboxylic and sulfonic heads of PFASs through H bonding. Many researchers indicate that the H bonding formed between the O atoms in carboxylic and sulfonic heads of PFAS and H donor functional groups on the sorbents play an important role for PFASs sorption (Gao & Chorover, 2012; Karoyo & Wilson, 2013; Xiao et al., 2012).

The electrostatic interaction between PFOA and PFOS and iron oxides (hydroxides) on the surface of ZVI was likely limited in this study. The low pK_a values of PFASs (-0.2 for PFOA and -3.3 for PFOS) (Deng et al., 2012) indicate that these PFASs will predominantly exist in their dissociated, negatively charged anionic forms at environmentally relevant pH condition (or in this study pH: 8.3–10.0). The iron hydroxy carbonate as the primary iron corrosion product formed on the surface of ZVI (formation discussed in section 6.4.2) was more likely neutral or negatively charged in this study (pH: 8.3–10.5) (Guilbaud et al., 2013; Kosmulski, 2009; Parks, 1965). The electrostatic interaction between negatively charged PFASs and neutral or negatively charged iron oxides was likely not predominant in this study. However, electrostatic interaction has been proposed to be an important sorption mechanism for PFASs. Gao and Chorover (2012) report that PFOA and PFOS can be adsorbed by iron oxide (hematite) through electrostatic interaction as well as the formation of inner-sphere Fe-carboxylate complexes (for PFOA) by ligand exchange and outer-sphere complexes and hydrogen-bonds (for PFOS) at the mineral surfaces. In addition, the relatively weak ion-dipole interaction between the polar hydroxyl group on iron hydroxides and the anionic PFOA/PFOS may also contribute to the sorption of PFOA/PFOS by iron corrosion products (Punyapalukul et al., 2013). Lin et al. (2015a) observe the removal of PFCAs and PFOS by iron hydroxides generated by electrocoagulation likely as a

result of electrostatic interactions, hydrogen bonding, ion and/or ligand exchange, and possibly hydrophobic effects.

6.4.4.2 Potential Removal Mechanisms of PFCAs and PFSAs by BC

The removal of target PFCAs and PFSAs by BC was likely due to hydrophobic interaction between the C-F chains and hydrophobic sites on BC. In addition, H bonding and ion-dipole interaction may also contribute to the sorption of PFCAs and PFSAs by BC (Du et al., 2014). The hydrophobic sorption of PFOS by maize straw- and willow- derived biochars has been reported previously (Chen et al., 2011b). Overall, PFOS and short chain PFSAs were more effectively removed by (ZVI + BC) compared to the same C chain length of PFOA and short chain PFCAs, which is attributed to the greater hydrophobicity of PFSAs than PFCAs. With the same number of C in their structure, PFSA such as PFOS contain two more C-F bond than the corresponding PFCA such as PFOA, contributing to stronger hydrophobicity and enhanced sorption (Merino et al., 2016; Zhou et al., 2010). Moreover, the addition of each extra CF₂ moiety to PFCAs and PFSAs structure results in stronger hydrophobicity and increased sorption (Merino et al., 2016), which explains the greater removals of PFOA and PFOS by BC compared to the short chain PFCAs (such as PFHpA and PFHxA) and PFSAs (such as PFHpS, PFHxS, and PFBS). Higgins and Luthy (2006) demonstrate a stronger sorption potential of long chain PFASs to sediment compared to the short chain counterparts. In addition, the stronger sorption (0.71–0.76 log units higher) of PFSAs to suspended sediment particulate matter compared to the PFCA analogs has been reported by Ahrens et al. (2010).

The H bonding formed between the hydroxyl (–OH) groups (H donors) on BC (Liu et al., 2015b) and the electronegative O atoms (H acceptors) in carboxylic (2O, 2H acceptors) and

sulfonic (3O, 3H acceptors) groups of PFCAs and PFSAAs may also contribute to the sorption of target PFASs to BC. The H bonding between PFOS and BC was likely stronger than between PFOA and BC, possibly due to the presence of one more H acceptor in PFOS than PFOA. This greater H bonding between PFOS and BC may also contribute to greater removal of PFOS by BC compared to PFOA. Similar to the possible ion-dipole interaction between ZVI and PFOA/PFOS, a relatively weak ion-dipole interaction between the polar hydroxyl group on BC and the anionic PFOA/PFOS may also contribute to the sorption of PFOA/PFOS by BC (Punyapalakul et al., 2013).

Electrostatic interactions between negatively charged PFASs and BC were likely limited. The biochar used in this study is oak wood biochar pyrolyzed at 700 °C which likely had a net negative surface charge under most pH conditions (2 – 14) (Mukherjee et al., 2011). The negatively charged BC likely repulsed the negatively charged PFASs.

6.4.5 Mass Balance of PFOA (PFCAs) and PFOS (PFSAAs) in Treatment Samples

Mass balance of PFOA and PFOS during the treatment using ZVI alone and (ZVI + BC) was calculated and illustrated in Figure 6.8. Between 5% and 10% of input PFOA/PFOS was removed through reductive defluorination (partially) by ZVI, between 10% and 40% of input PFOA/PFOS was removed through sorption by ZVI or (ZVI + BC), and between 2% and 85% of input PFOA/PFOS was removed through unknown mechanisms.

Because the concentrations of PFOA and PFOS in the supernatant samples and aqueous samples extracted from the reactive media were two to five orders of magnitude higher than the concentrations of short chain PFCAs and PFSAAs, the concentrations of short chain PFCAs

(PFHpA and PFHxA) and short chains of PFSAs (PFHpS, PFHxS, and PFBS) are negligible compared to PFOA and PFOS. The change in mass balance of PFOA and PFOS as a function of reaction time in Figure 6.8 also represents the mass balance of total PFCAs (sum of PFOA, PFHpA, and PFHxA) and total PFSAs (sum of PFOS, PFHpS, PFHxS, and PFBS) over the reaction time. The percentage of PFOA/PFOS in supernatant samples represents the remaining (not removed) PFOA/PFOS. The percentage of adsorbed PFOA/PFOS was the percentage of extractable PFOA/PFOS on reactive media. The sum of adsorbed PFOA/PFOS on reactive media, partially defluorinated PFOA/PFOS, and unknown PFOA/PFOS represents the total removed PFOA/PFOS from input solution.

Mass balance results showed that ~20% of input PFOA (PFCAs) was removed by ZVI alone (Figure 6.8). Partial defluorination, sorption and unknown accounted for ~10%, ~10%, and ~2% of PFOA removal by ZVI. PFOA was more effectively removed by (ZVI + BC) compared to ZVI alone, with an average removal of ~60%, which consisted of ~24% of sorption and ~36% of unknown. About 90% and 94% of input PFOS (PFSAs) was removed using ZVI and (ZVI + BC). Partial defluorination, sorption and unknown accounted for ~5%, ~40%, and ~45% of PFOS removal (~90%) by ZVI; sorption and unknown accounted for ~8% and ~86% of PFOS (PFSAs) removal (~94%) by (ZVI + BC) (Figure 6.8).

Addition of BC to ZVI increased the removals of PFOA (PFCAs) and PFOS (PFSAs) compared to ZVI alone. The sorption percentage (24%) of PFOA (PFCAs) by (ZVI + BC) was relatively greater than that (10%) by ZVI alone. However, a smaller percentage of PFOS (PFSAs) (8%) was adsorbed by (ZVI + BC) than that (40%) by ZVI alone likely due to the stronger hydrophobic interaction between BC and PFOS (PFSAs) compared to PFOA which might not be extracted from the solid phase.

The unknown percentage of PFOA/PFOS in the mass balance calculation varied greatly from ~2% to ~85% and may include the following portions: (1) uncounted defluorinated PFOA/PFOS due to the sorption of F^- by the reactive media; (2) non-extractable PFOA/PFOS; and (3) other intermediate degradation products which were not monitored in this study. The defluorination efficiencies (5–10%) of PFOA/PFOS by ZVI was corrected to account for the sorption of F^- by ZVI; however, defluorination of PFOA/PFOS by (ZVI + BC) cannot be confirmed due to the sorption F^- by (ZVI + BC) resulting in undetectable F^- . This unaccounted defluorinated PFOA/PFOS by (ZVI + BC) likely contributed to the large unknown percentage of PFOA/PFOS in Treatment PFOA/PFOS + (ZVI+BC) samples. The non-extractable PFOA/PFOS refers to the adsorbed PFOA and PFOS which was possibly stabilized in ZVI and BC through strong hydrophobic interaction and(or) covalent bonding and cannot be extracted through the aqueous extraction process. This non-extractable PFOA/PFOS also likely increased the mass percentage of the unknown portion. In addition, other unknown intermediate PFOA/PFOS degradation products which were not analyzed in this study may also contribute to the unknown PFOA/PFOS mass percentage. Such unknown intermediate degradation products might include $C_6F_{13}CFHCOOH$ ($m/z=395$), $C_6F_{13}CH_2COOH$ ($m/z=377$) (discussed in section 6.4.4.1 and shown in Figure 6.7), and similar PFOS degradation products such as $C_7F_{15}CFHSO_3H$ and $C_7F_{15}CH_2SO_3H$.

6.5 Conclusions

Approximately 60% and 94% of input PFOA and PFOS (average input concentration: 18,600 $\mu g L^{-1}$) were removed by the combination of the reactive media (ZVI + BC). Less input PFOA (20%) and PFOS (90%) were removed using ZVI alone compared to (ZVI + BC). The short chain PFCAs (PFHpA) and PFSAs (PFHpS, PFHxS, and PFBS) were less removed (17–70%) by

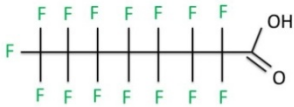

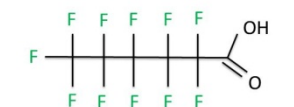
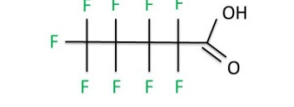
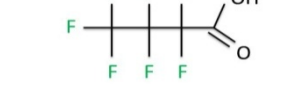
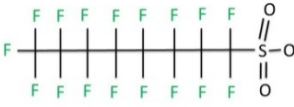
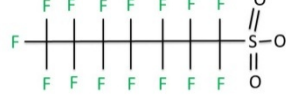

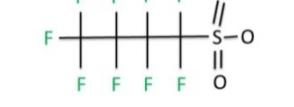
reactive media ZVI and (ZVI + BC) compared to PFOA and PFOS. The removals of short chain PFCAs and PFSAs by ZVI and (ZVI + BC) decreased with the decreasing chain length. Removals of PFOA (PFCAs) and PFOS (PFSAs) by ZVI and BC were likely through reductive defluorination and sorption. Fluoride, as the indicative product of defluorination of PFCAs and PFSAs, was used to back calculate the defluorination efficiencies of PFCAs and PFSAs; results showed that 10% of PFOA (PFCAs) and 5% of PFOS (PFSAs) were partially defluorinated by ZVI alone. The defluorination of PFOA (PFCAs) and PFOS (PFSAs) by (ZVI + BC) was likely underestimated due to sorption of F^- by the reactive media. The combination of ZVI and BC may be cost-effective for potential use in passive treatment systems and in-situ reactors for removing emerging contaminants PFASs from water under ambient environmental conditions.

Table 6.1 Batch experimental setup.

Test		Series	Mass of ZVI, g	Mass of BC, g	Input concentration
Removal of PFOA and PFOS using ZVI and BC	Blank	NaHCO ₃ solution	–	–	20 mg L ⁻¹ PFOA/PFOS
		ZVI	35	–	
		ZVI + BC	7	3.5	
	Control	PFOA	–	–	
		PFOS	–	–	
	Treatment	PFOA + ZVI	35	–	
		PFOA + (ZVI + BC)	7	3.5	
		PFOS + ZVI	35	–	
PFOS + (ZVI + BC)		7	3.5		
F ⁻ adsorption	Control	F ⁻	–	–	
	adsorption	F ⁻ + ZVI	35	–	
		F ⁻ + (ZVI + BC)	7	3.5	

Note: input solution matrix for both PFOA/PFOS removal test and F⁻ adsorption test was 35 mL of 0.8 mM NaHCO₃ in Ar_(g) purged H₂O. “–” represents not applicable.

Table 6.2 Selected properties for target perfluoroalkyl carboxylic acids (PFCAs) and perfluoroalkyl sulfonic acids (PFSA).

Compound (CAS#)	Acronym	Molecular Formula	Structure
Perfluoroalkyl carboxylic acids (PFCAs)	Perfluorooctanoic acid (335-67-1)	PFOA $C_8HF_{15}O_2$	
	Perfluoroheptanoic acid (375-85-9)	PFHpA $C_7HF_{13}O_2$	
	Perfluorohexanoic acid (307-24-4)	PFHxA $C_6HF_{11}O_2$	
	Perfluoro-n-pentanoic acid (2706-90-3)	PFPeA $C_5HF_9O_2$	
	Perfluorobutanoic acid (375-22-4)	PFBA $C_4HF_7O_2$	
Perfluoroalkyl sulfonic acids (PFSAs)	Perfluorooctane sulfonate acid (2795-39-3)	PFOS $C_8HF_{17}O_3S$	
	Perfluoroheptane sulfonic acid (375-92-8)	PFHpS $C_7HF_{15}O_3S$	
	Perfluorohexane sulfonic acid (355-46-4)	PFHxS $C_6HF_{13}O_3S$	
	Perfluorobutane sulfonic acid (375-73-5)	PFBS $C_4HF_9O_3S$	

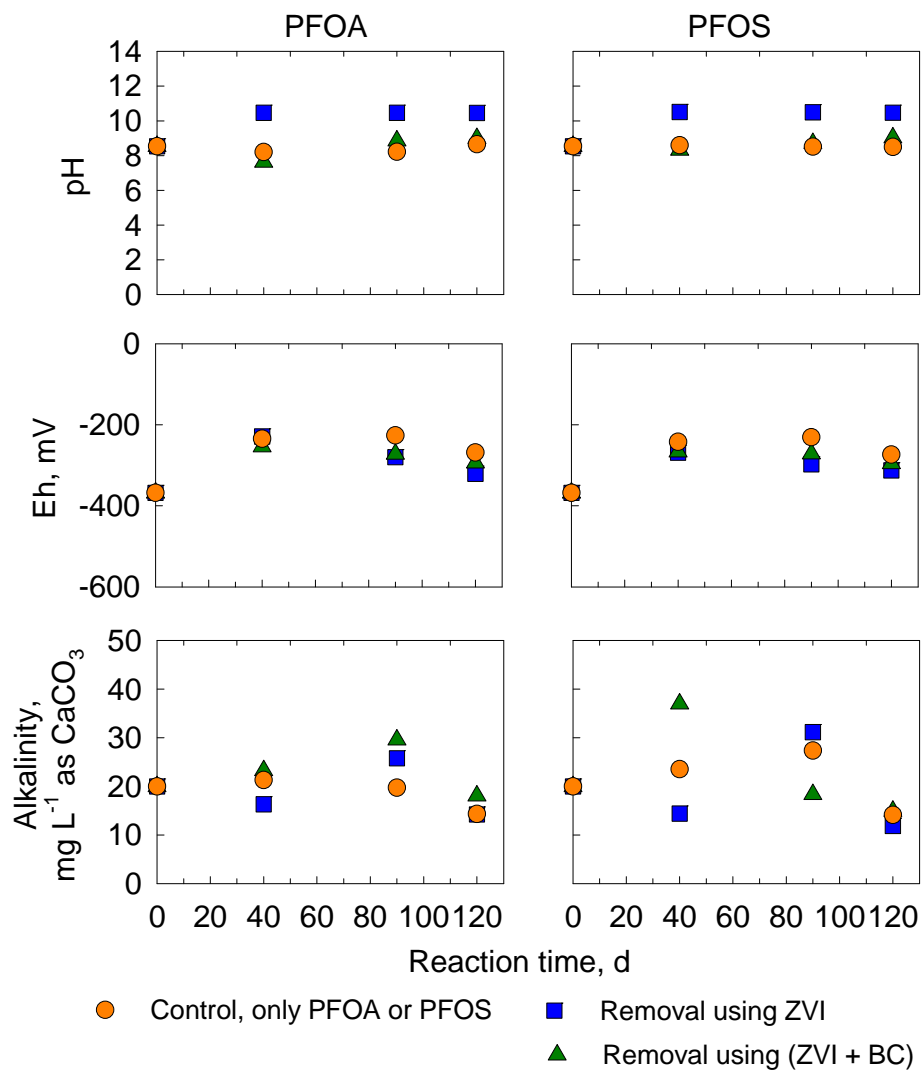


Figure 6.1 Values of pH, Eh, and concentrations of alkalinity as a function of reaction time in the supernatant samples of batch experiment for removal of PFOA and PFOS using zero-valent Fe (ZVI) alone and a 1:4 (v/v) mixture of ZVI and biochar (ZVI + BC).

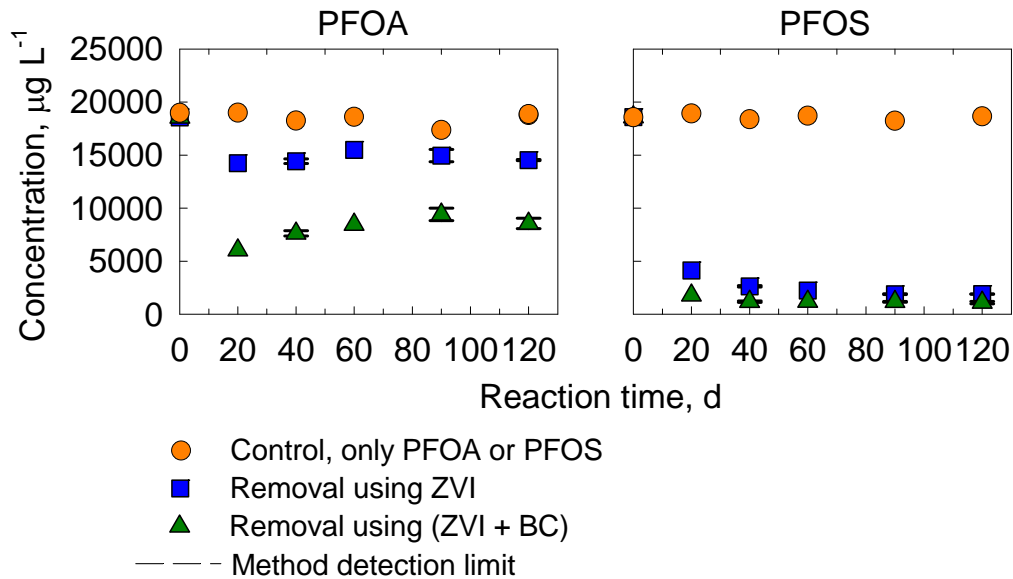


Figure 6.2 Concentrations of perfluorooctanoic acid (PFOA) and perfluorooctane sulfonic acid (PFOS) as a function of reaction time in the supernatant samples of batch experiment for removal of PFOA and PFOS using zero-valent Fe (ZVI) alone and a 1:4 (v/v) mixture of ZVI and biochar (ZVI + BC). Duplicate samples were prepared at Days 40, 90, and 120 where were indicated with error bars. The method detection limits (MDLs) of PFOA and PFOS were 45 and 110 ng L^{-1} , which were too low to appear in the figure.

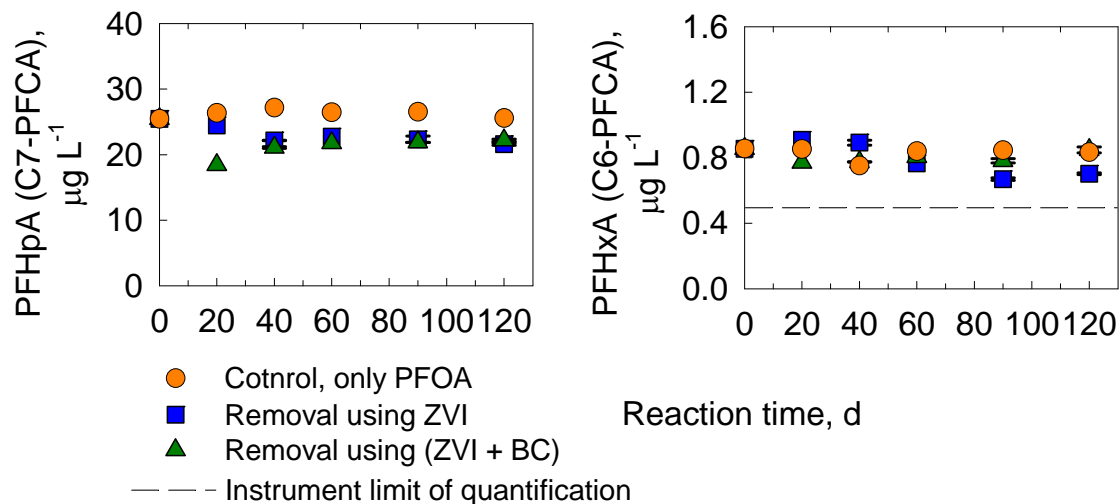


Figure 6.3 Concentrations of perfluoroheptanoic acid (PFHpA, C7-PFCA) and perfluorohexanoic acid (PFHxA, C6-PFCA) as a function of reaction time in the supernatant samples of batch experiment for removal of PFOA and PFOS using zero-valent Fe (ZVI) alone and a 1:4 (v/v) mixture of ZVI and biochar (ZVI + BC). Duplicate samples were prepared at Days 40, 90, and 120 where were indicated with error bars. The instrument limits of quantification (LOQ) of PFHpA and PFHxA were $0.5 \mu\text{g L}^{-1}$. The LOQ of PFHpA was too low to appear in the figure.

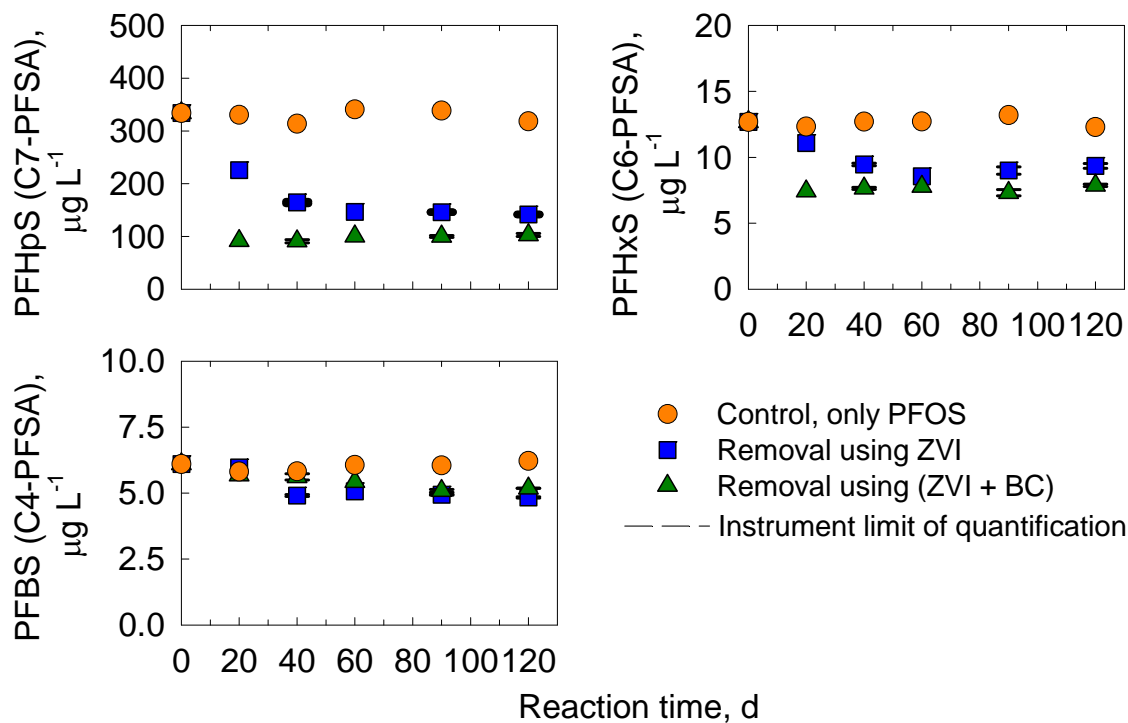


Figure 6.4 Concentrations of perfluoroheptane sulfonic acid (PFHpS, C7-PFSA), perfluorohexane sulfonic acid (PFHxS, C6-PFSA), and perfluorobutane sulfonic acid (PFBS, C4-PFSA) as a function of reaction time in the supernatant samples of batch experiment for removal of PFOA and PFOS using zero-valent Fe (ZVI) alone and a 1:4 (v/v) mixture of ZVI and biochar (ZVI + BC). Duplicate samples were prepared at Days 40, 90, and 120 where were indicated with error bars. The instrument limit of quantification (LOQ) of PFHpS was $0.5 \mu\text{g L}^{-1}$; the LOQ of PFHxS and PFBS was $0.2 \mu\text{g L}^{-1}$. The LOQ of PFHpS, PFHxS, and PFBS were too low to appear in the figure.

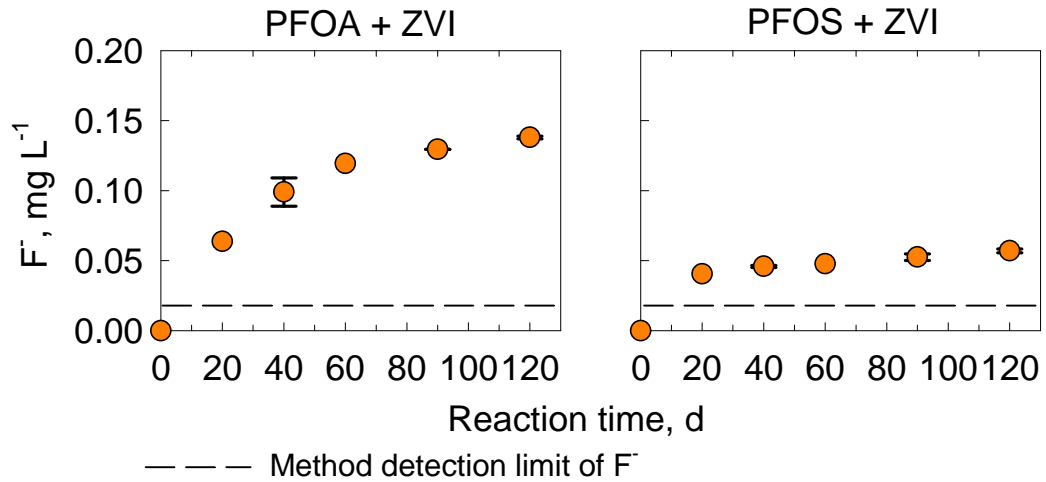


Figure 6.5 Concentrations of F⁻ as a function of reaction time in the supernatant samples of batch experiment for removal of PFOA and PFOS using zero-valent Fe (ZVI) alone and a 1:4 (v/v) mixture of ZVI and biochar (ZVI + BC). The concentrations of F⁻ in the supernatant samples PFOA/PFOS + (ZVI +BC) were below the method detection limits. Duplicate samples were prepared at Days 40, 90, and 120 where were indicated with error bars.

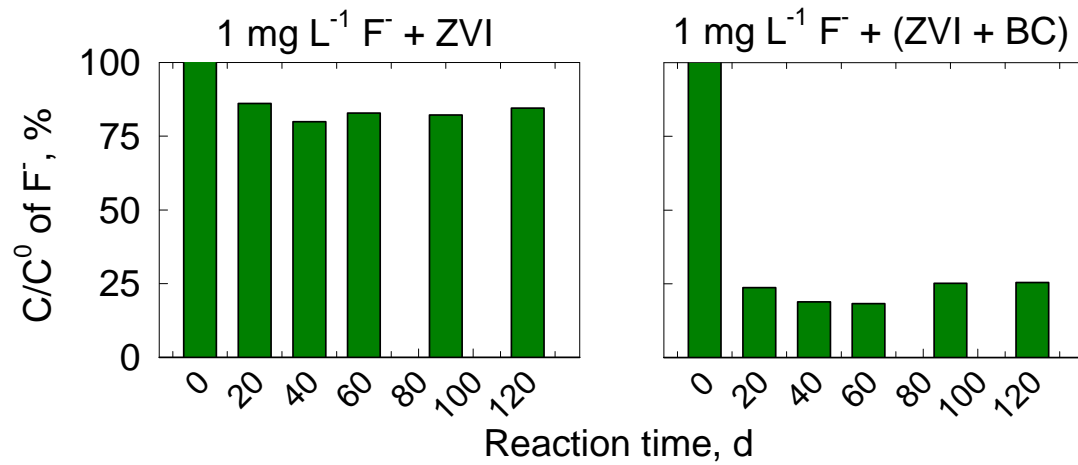


Figure 6.6 Percentage of F⁻ remaining in the supernatant samples of F⁻ sorption test as a function of reaction time.

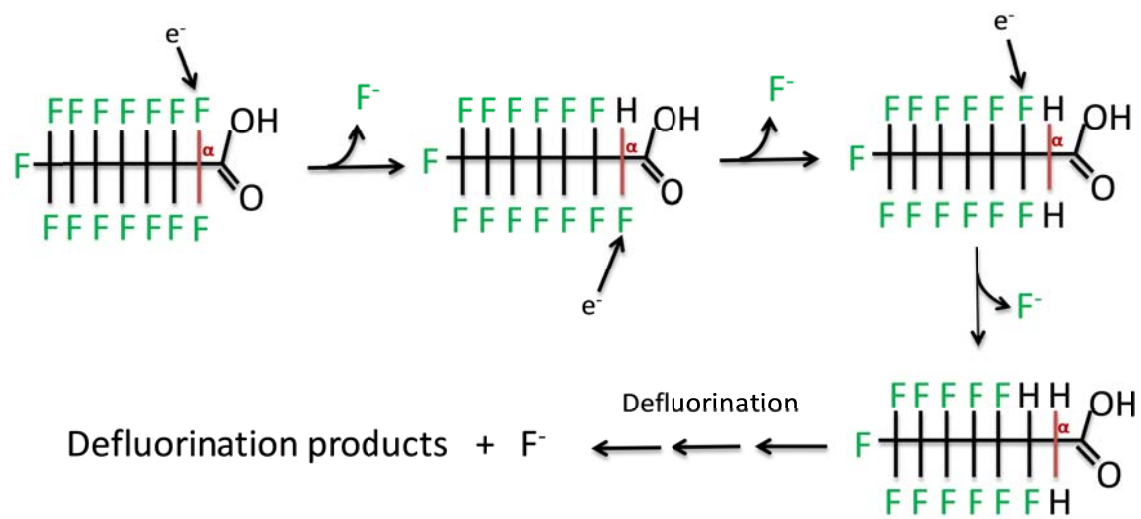


Figure 6.7 Proposed defluorination mechanisms of PFOA by ZVI (Reproduced from Song et al., 2003). The defluorination of PFOA was initiated by the cleavage of α -position C-F bond by e^- transfer from ZVI.

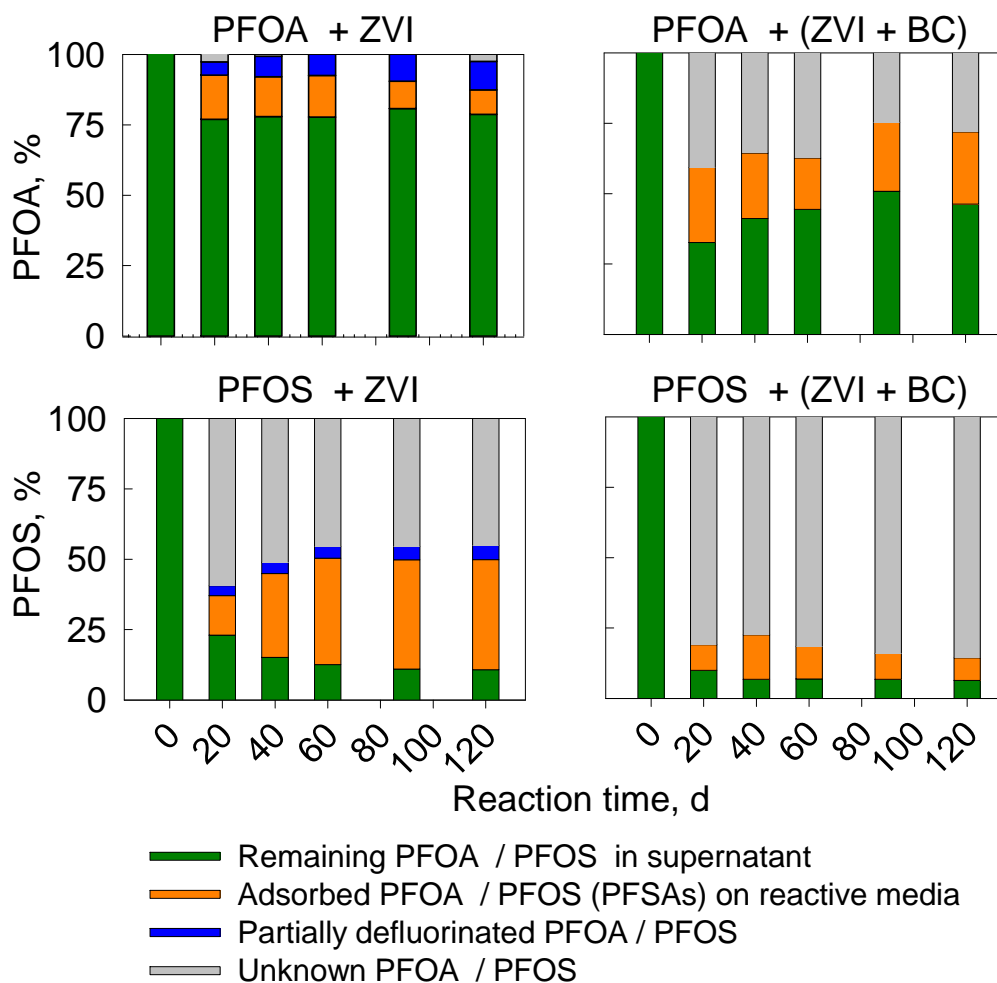


Figure 6.8 Mass balances for PFOA and PFOS in batch experiments as a function of reaction time. Because the concentrations of PFOA and PFOS were two to four orders of magnitude higher than that of the short chain PFCAs and PFSA in both supernatant samples and aqueous samples extracted from reactive media, this figure also represents the mass balances of total perfluoroalkyl carboxylic acids (PFCAs, including PFOA, PFHpA, and PFHxA) and total perfluoroalkyl sulfonic acids (PFSA, including PFOS, PFHpS, PFHxS, and PFBS) in the batch experiments as a function of reaction time. Partial defluorination percentages were stoichiometrically back-calculated based on the observed F^- concentrations in the supernatant, assuming 2F defluorinated from 15F atoms of PFOA and 2F defluorinated from 17F atoms of PFOS.

Chapter 7: *Conclusions*

7.1 Summary of Findings and Comparison of Contaminant Removals Using Photocatalytic and Passive Treatment Systems

7.1.1 Summary of Findings

Laboratory column and batch experiments were conducted to evaluate the effectiveness of passive treatment systems that contain zero-valent iron (ZVI), organic carbon (OC), and biochar (BC) for removal of NO_3^- , SO_4^{2-} and emerging contaminants perchlorate, pharmaceuticals, artificial sweeteners, and perfluoroalkyl substances from simulated groundwater. Laboratory batch experiments were conducted to evaluate the effectiveness of ultraviolet light (UV) photocatalytic treatment using magnetically recoverable TiO_2 nanoparticles for removing artificial sweetener acesulfame-K and pharmaceuticals from water. In addition, a field investigation was conducted to evaluate the use of potential multiple tracers including an artificial sweetener and several pharmaceuticals to track wastewater derived from two wastewater treatment plants (WWTPs) in a receiving river.

Water contaminated by co-mingled ClO_4^- , NO_3^- , and SO_4^{2-} are associated with sulfide-bearing mine sites when ClO_4^- and NO_3^- containing blasting agents are used in the ore extraction process. Four column experiments containing ZVI, wood chips (OC), and a mixture of (ZVI + OC) were conducted to remove ClO_4^- , NO_3^- , and SO_4^{2-} from water (described in Chapter 2). Complete removals of NO_3^- were achieved in all treatment columns ZVI, OC, and the mixture of (ZVI + OC). However, the by-product NH_4^+ was produced during NO_3^- reduction by ZVI alone (Equation 2.1). The bacterial mediated denitrification of NO_3^- by OC was observed and is consistent with thermodynamic predictions for the conversion to the environmentally innocuous N_2 gas (Equation 2.3). The extensive removal of NO_3^- in Column (ZVI + OC) likely involved both NO_3^- reduction by ZVI and denitrification by OC, following a first-order rate, with a much

more rapid NO_3^- removal rate compared to the other two treatment columns. The removal of SO_4^{2-} was only observed in Column OC (pH=7.4) through the onset of biologically mediated SO_4^{2-} reduction coupled to OC oxidation (Equation 2.4); the higher pH (8.6) in Column (ZVI + OC) likely inhibited biological sulfate reduction. Effective removal of ClO_4^- was only observed in the columns containing OC through biological degradation of ClO_4^- to Cl^- following the zeroth-order rate; however, ClO_4^- was not removed in Column ZVI. As the potential end product of ClO_4^- biological degradation, Cl^- was observed at the concentrations equivalent to the concentration of ClO_4^- removed in the effluents of Columns OC and (ZVI + OC). Complete removal of ClO_4^- occurred after the complete removal of NO_3^- due to the inhibition of NO_3^- ($> 2 \text{ mg L}^{-1} \text{ NO}_3\text{-N}$) on ClO_4^- removal. However, augmentation of OC by a small fraction of ZVI reduced the inhibition of NO_3^- ($> 2 \text{ mg L}^{-1} \text{ NO}_3\text{-N}$) on ClO_4^- removal. The more complete removals of ClO_4^- , NO_3^- and SO_4^{2-} were attributed to the decrease in flow rate from 0.5 to 0.1 pore volume (PV) d^{-1} in Columns OC and (ZVI + OC).

Chloride, nutrients, and some of the emerging contaminants such as artificial sweetener acesulfame-K (ACE-K) and pharmaceuticals carbamazepine (CBZ) and caffeine (CAF) are proposed as tracers of municipal wastewater in the aquatic environment. However, the anthropogenic sources of contamination such as road salts, fertilizer, and the natural attenuation processes make these tracers less reliable and ideal to track wastewater. Use of multiple tracers will greatly increase the confidence of tracking wastewater in the environment. A two-year study was conducted along a river downstream of two WWTPs to identify potential tracers to track the wastewater (described in Chapter 3). The results indicate that elevated concentrations of artificial sweetener ACE-K and pharmaceuticals CBZ, CAF, sulfamethoxazole (SMX), ibuprofen (IBU), gemfibrozil (GEM), and naproxen (NAP) were observed near the WWTP 1 as a result of human

excretion in the study area of the receiving river. The artificial sweetener ACE-K combined with pharmaceuticals CBZ, GEM, and NAP were strongly correlated and can be used as potential co-tracers to track the wastewater.

TiO₂ nanoparticles are effective photocatalysts used in UV photocatalytic treatment of emerging contaminants. However, the non-recoverable TiO₂ nanoparticles themselves are emerging contaminants which could cause adverse impacts on human and ecosystem health after entering the environment. The use of recoverable photocatalysts rather than the non-recoverable ones can mitigate the release of these nanoparticles to the environment. In Chapter 4, the photocatalytic ability of two magnetically recoverable TiO₂ nanoparticles (MST: magnetically separable TiO₂ nanoparticles; GO TiO₂: graphene oxide supported TiO₂ nanoparticles) were evaluated compared to the commercial non-recoverable P25 TiO₂ nanoparticles in UV photocatalysis of an artificial sweetener ACE-K and a suite of pharmaceutical compounds (CBZ, CAF, SMX, MDA, MDMA, IBU, GEM, and NAP). The results show the GO TiO₂ nanoparticles exhibited competitive or greater catalytic ability compared to P25 TiO₂ nanoparticles in assisting photocatalytic treatment of target contaminants (> 99% removal of ACE-K and > 92% removal of pharmaceuticals); however, the MST nanoparticles were less effective in inducing photocatalysis of the contaminants than P25 and GO TiO₂ nanoparticles. The UV photocatalytic treatment of target contaminants followed a pseudo-first-order rate. The recoverable GO TiO₂ nanoparticles could be a potential substitute for commercial P25 TiO₂ nanoparticles in the water treatment industry due to their high magnetic recovery (> 90%) and photocatalytic efficiency.

Four column experiments consisting of ZVI, biochar (BC), and a mixture of (ZVI + BC) were conducted for simultaneous removal of pharmaceutical compounds, artificial sweeteners, and perfluoroalkyl substances from water (described in Chapter 5). More than 97% of input

pharmaceuticals ($\sim 9 \mu\text{g L}^{-1}$) CBZ, CAF, SMX, MDA, MDMA, IBU, GEM, and NAP were removed in three treatment Columns ZVI, BC, and (ZVI + BC), and the removals of pharmaceuticals followed the first-order rate. Artificial sweetener sucralose (SUC) at input concentration of $\sim 110 \mu\text{g L}^{-1}$ were removed in three treatment columns with removals $> 76\%$. Poor removals of artificial sweetener ACE-K were observed in Column ZVI (27% removed) and Column (ZVI + BC) (14% removed) when the flow rate was maintained at 0.3 PV d^{-1} ; however, the removals of ACE-K increased to 60% in Column ZVI and 30% in Column (ZVI + BC) when the flow rate was decreased to 0.1 PV d^{-1} . ACE-K was not removed in Column BC. Artificial sweetener saccharin (SAC) was not removed in Column ZVI; removals of SAC in the columns containing BC decreased over time. Artificial sweetener cyclamate (CYC) was not removed in any column in this study. Partial removals of input perfluorooctanoic acid (PFOA) ($\sim 45 \mu\text{g L}^{-1}$) were observed in Column BC and Column (ZVI + BC) with decreasing removal efficiencies. Removals of input PFOA in Column ZVI was only observed during the early stage of the experiment. About 60–99% of input perfluorooctane sulfonic acid (PFOS) ($24\text{--}90 \mu\text{g L}^{-1}$) was removed in Columns BC and (ZVI + BC) throughout the experimental period. More than 80% of input PFOS was removed in Column ZVI during the first 37 PV of the experiment with possible conversion of PFOS to PFOA from 18 to 50 PV. The removal rates of target contaminants decreased over time; the removals of target contaminants were not enhanced by the decrease in flow rate, except for ACE-K.

A series of batch experiments were conducted to assist in the interpretation of the data derived from the column experiments (Chapter 5) to investigate the removal mechanisms of PFOA and PFOS by ZVI and BC (described in Chapter 6). The results show about 20 and 60% of the input PFOA ($\sim 18,550 \mu\text{g L}^{-1}$) was removed by ZVI and the mixture of (ZVI + BC) after

120 d. Greater removals of input PFOS ($\sim 18,580 \mu\text{g L}^{-1}$) were observed by ZVI (90% removed) and (ZVI + BC) (94% removed) compared to PFOA. The removals of PFOA and PFOS by ZVI were likely due to sorption of PFOA and PFOS to iron oxides and hydroxides through H bonding and possibly reductive defluorination (10% of PFOA and 5% of PFOS were partially defluorinated). The removals of PFOA and PFOS by BC were likely due to hydrophobic sorption. Trace concentrations of short chain perfluoroalkyl carboxylic acids (PFCAs) including perfluoroheptanoic acid (PFHpA, C7-PFCA) and perfluorohexanoic acid (PFHxA, C6-PFCA) were detected in the PFOA input solution; however, only 17% of input PFHpA ($26 \mu\text{g L}^{-1}$) was removed by ZVI and (ZVI + BC), input PFHxA ($0.8 \mu\text{g L}^{-1}$) were not removed. Similarly, trace concentrations of short chain perfluoroalkyl sulfonic acids (PFSAs) including $330 \mu\text{g L}^{-1}$ of perfluoroheptane sulfonic acid (PFHpS, C7-PFSA), $13 \mu\text{g L}^{-1}$ of perfluorohexane sulfonic acid (PFHxS, C6-PFSA) and $6 \mu\text{g L}^{-1}$ perfluorobutane sulfonic acid (PFBS, C4-PFSA) were detected in the PFOS input solution. Up to 70%, 40%, and 20% of input PFHpS, PFHxS, and PFBS were removed by the reactive media; the removal efficiency decreased with a decreasing PFSAs chain length. Fluoride (F^-) as the indicative by-product of defluorination of PFOA and PFOS was adsorbed by ZVI ($\sim 20\%$ from 1mg L^{-1}) and (ZVI + BC) ($\sim 75\%$ from 1mg L^{-1}). The defluorination of PFOA and PFOS by ZVI and (ZVI + BC) may have been underestimated due to the sorption of F^- by ZVI and BC.

The results of these studies indicate that passive treatment systems such as permeable reactive barriers or in-situ bioreactors containing ZVI and OC (wood chips and biochar) may be promising and cost-effective technologies for considerable removal of NO_3^- , SO_4^{2-} , and emerging contaminants ClO_4^- , pharmaceuticals (CBZ, CAF, SMX, MDA, MDMA, IBU, GEM, and NAP), artificial sweeteners (ACE-K, SUC, and SAC), and perfluoroalkyl substances (PFOA, PFOS, and

short chain PFSA) from simulated groundwater under ambient environmental conditions. The magnetically recoverable GO TiO₂ nanoparticles could be a potential substitute for the commercial non-recoverable P25 TiO₂ nanoparticles used in water treatment applications due to its competitive or greater photocatalytic ability and environmental benefit (high magnetic recovery) compared to P25. Artificial sweetener ACE-K and pharmaceuticals CBZ, GEM, and NAP can be used as co-tracers to track wastewater.

7.1.2 Comparison of Contaminant Removals Using Photocatalytic and Passive Treatment Systems

Effective removals (>92%) of target contaminants ACE-K and eight pharmaceuticals were observed using both oxidative treatment (photocatalytic study in Chapter 4) and passive treatment (Column study in Chapter 5, except for ACE-K with 30–60% removals); however, the removal efficiencies, rates, and mechanisms varied greatly. The average surface area normalized rate constants K_{SA} (L m⁻² d⁻¹), average removal efficiencies, and potential removal mechanisms of ACE-K and eight pharmaceuticals using photocatalytic and passive treatment systems are compared and summarized in Table 7.1.

The removal of target contaminants by UV photocatalysis was attributed to the oxidation of these contaminants by hydroxyl radical ·OH under UV irradiation. The removal of target contaminants by passive treatment systems containing ZVI and BC was likely through reduction (by ZVI), electrostatic interactions, hydrophobic interactions, $\pi - \pi$ stacking and(or) EDA interactions, and H bonding between contaminants and reactive media under reducing conditions. Effective removal of target contaminants was observed using both photocatalytic treatment (>92%) and passive treatment (>97%, except for ACE-K). Removal of ACE-K and eight

pharmaceuticals by photocatalytic and passive treatment systems (removal of ACE-K within Column ZVI) followed the first-order reaction model; however, the removal rates (or rate constants K_{SA}) of ACE-K and eight pharmaceuticals using photocatalytic treatment were approximately 5–7 orders of magnitude greater than that using the passive treatment systems (Table 7.1).

Overall, photocatalytic treatment is more effective than the passive treatment system for removing ACE-K and pharmaceuticals with higher removal efficiencies and much more rapid removal rates. However, passive treatment systems require less energy (under ambient environmental conditions) and use of relatively inexpensive reactive media compared to photocatalytic treatment system which has high energy consumption (UV irradiation) and use of expensive photocatalysts (Table 7.2). Many factors should be considered when selecting a treatment method, such as the requirement of remediation rates and efficiencies and funding available for the remediation. The remediation strategy can vary greatly as the situation dictates.

7.2 Scientific Contributions

Research presented in this thesis contributed information related to removal of emerging contaminants ClO_4^- , pharmaceuticals (CBZ, CAF, SMX, MDA, MDMA, IBU, GEM, and NAP), artificial sweeteners (ACE-K, SUC, SAC, and CYC), and perfluoroalkyl substances (PFOA, short chain PFCAs, PFOS, and short chain PFSAs) from aqueous solution using UV photocatalytic treatment and passive treatment systems, and use of emerging contaminants as co-tracers to track wastewater. New scientific contributions resulting from this thesis include:

- Demonstrating that simultaneous removal of NO_3^- , SO_4^{2-} , and ClO_4^- from water can be achieved using a passive treatment system consisting of the mixture of ZVI and OC.

- Demonstrating that complete biological degradation of ClO_4^- to Cl^- can be achieved using OC under reducing conditions.
- Illustrating that addition of ZVI to OC can reduce the inhibition of NO_3^- ($> 2 \text{ mg L}^{-1} \text{ NO}_3^-$ N) on ClO_4^- removal.
- Investigating the correlation between the conventional tracer Cl^- and the emerging contaminants as they dissipated downstream from the WWTPs in a receiving river.
- Illustrating the artificial sweetener ACE-K and pharmaceuticals CBZ, NAP, and GEM can be used as co-tracers to track wastewater.
- Demonstrating that the recoverable GO TiO_2 nanoparticles could be an alternative for commercial P25 TiO_2 nanoparticles in inducing photocatalytic treatment of emerging contaminants ACE-K and a suite of pharmaceuticals (CBZ, CAF, SMX, MDA, MDMA, IBU, GEM, and NAP) due to its photocatalytic efficiency and environmental benefit (high recovery).
- Demonstrating that simultaneous removal of pharmaceuticals (CBZ, CAF, SMX, MDA, MDMA, IBU, GEM, and NAP), artificial sweeteners (ACE-K, SUC, and SAC), and perfluoroalkyl substances (PFOA and PFOS) from water can be achieved using a passive treatment system consisting of the mixture of (ZVI + BC).
- Illustrating the removals of PFOA and PFOS by ZVI and BC were likely through sorption and possibly reductive defluorination.

- Demonstrating that the removal efficiencies of PFCAs and PFSAAs by ZVI and BC decreased with the decreasing chain length.

7.3 Recommendations

Passive treatment systems consisting of the reactive mixture of (ZVI + OC) or (ZVI + BC) are potentially a cost-effective and efficient technology for simultaneous removal of NO_3^- , SO_4^{2-} and emerging contaminants ClO_4^- , pharmaceutical compounds, artificial sweeteners, and perfluoroalkyl substances from water. In addition to the target emerging contaminants, the reactive media ZVI and OC have also been demonstrated to be effective for removals of different types of the inorganic and organic contaminants (described in Chapter 1). Due to their high removal efficiencies of different types of contaminants, cost-effectiveness, and low maintenance, these reactive mixture can be widely used to enhance the performance of various onsite wastewater and water treatment systems, such as in septic treatment systems (Figures 7.1 and 7.2), permeable reactive barriers (Figure 7.3), tile drainage treatment systems (Figure 7.4), soil aquifer treatment systems (Figure 7.5), river bank filtration systems (Figure 7.6), and polishing cells for WWTPs effluent (Figure 7.7).

On-site wastewater treatment and disposal systems are widely used in North America and elsewhere in the world to treat wastewater derived from homes or businesses in rural areas that are not served by community public sewers, often leading to release of partially treated wastewater back into the receiving environment. Septic tank/soil absorption systems are the most common used on-site wastewater treatment units in North America (website: nepis.epa.gov/Exe/ZyPURL.cgi?Dockey=9101NLXN.TXT). In septic tanks, most of the settleable solids are separated from wastewater to allow for digestion of organic matter. The

clarified wastewater is then fed to the soil absorption system to further filter and treat the effluent before it enters the groundwater zone. However, emerging contaminants in wastewater often are not effectively removed by soil adsorption process (Carrara et al., 2008; Onesios & Bouwer, 2012; Patterson et al., 2011; Robertson et al., 2013; Scheurer et al., 2009) which likely results in the broader distribution of emerging contaminants to the environment (described in Chapter 1). The augmentation of soil adsorption systems with reactive mixtures (ZVI + OC) or (ZVI + BC) can potentially improve water quality by reducing the flux of emerging contaminants entering groundwater. A horizontal layer containing the reactive media can be installed beneath the drain field to enhance the performance of soil absorption systems (Figure 7.1). A passive flow-through reactor packed with the reactive media can be installed after the primary wastewater treatment unit to remove the emerging contaminants before discharging to soil (Figure 7.2). A vertical permeable reactive barrier containing reactive media can be installed downgradient of the septic drainage tile to remove emerging contaminants from the wastewater before it discharges to receiving surface waters (Figure 7.3).

The reactive mixture can also be utilized in subsurface tile drainage systems to remove contaminants derived from agricultural lands. Tile drainage systems are designed to collect excess water from the soil zone to lower the water table and increase crop yields. However, the application of fertilizer (containing NO_3^- and ClO_4^- described in Chapter 2), pesticides such as atrazine, liquid manure (containing veterinary drugs and nutrients), and municipal biosolids (containing human pharmaceuticals, artificial sweeteners, and nutrients) to farm lands causes the release of these contaminants to soil and soil water. As a result of the tile systems, soluble contaminants will end up in the drainage system. An in-line reactor containing ZVI, OC, and BC

mixtures can be installed in the effluent drainage pipe to remove the contaminants collected from the farm lands before they enter receiving waters (Figure 7.4).

Another potential application of the passive treatment systems is in the managed aquifer recharge (MAR) process where reactive media can be used to improve the quality of the recovered water. In a soil aquifer treatment system, the pre-treated wastewater is introduced to a recharge basin (infiltration basin); the contaminants in the wastewater can be partially removed through different natural processes (such as physical, chemical and biological processes) as the wastewater moves through soil and aquifer. The treated wastewater will be stored in the aquifer for future use. In this case, a horizontal layer containing reactive media can be placed at the base of the recharge basin to enhance the removal of emerging contaminants from the wastewater before it enters groundwater (Figure 7.5). In a river bank filtration system, a vertical permeable reactive barrier packed with the reactive mixture can be installed between the river and the production well to enhance the removal of emerging contaminants from the recovery river water before end uses (Figure 7.6). In addition, when emerging contaminants cannot be removed in WWTPs (described in Chapter 1); a flow-through reactor packed with the reactive mixture or facilitated with UV photocatalytic treatment using recoverable GO TiO₂ nanoparticles can be installed to polish treated water before discharge (Figure 7.7).

Passive treatment systems consisting of (ZVI + OC) or (ZVI + BC) could be an economical and practical technology for augmentation of the current and future on-site wastewater treatment and disposal systems, tile drainage systems, and managed aquifer recharge systems, and WWTPs for enhanced removal of the emerging contaminants. The application of these passive treatment technologies can reduce the amount of NO₃⁻, SO₄²⁻ and emerging contaminants ClO₄⁻, pharmaceutical compounds, artificial sweeteners, and perfluoroalkyl

substances entering the natural waters through wastewater disposal and water reuse, providing environmental benefits in heavily populated and water shortage (reuse) areas.

In this study, there were no obvious signs of system clogging or decrease in hydraulic conductivity when 50% (v/v) of silica sand was used as supporting material in the experiments. When passive treatment systems are used in field applications, mixing of the reactive mixture with sand or gravel (e.g., 50%, v/v) is recommended to maintain the hydraulics of the system. Furthermore, addition of a small fraction (e.g., 10%, v/v) of ZVI to wood chips or biochar (e.g., 40%, v/v) is recommended based on findings from this study. Higher ZVI amendment rates not only increase the remedy cost (because ZVI is more expensive compared to wood chips and biochar), but may also increase the pH values of the wastewater which will potentially inhibit the microbial degradation of the contaminants (such as biological degradation of SO_4^{2-} , described in Chapter 2). The flow rates used in the column experiments were set at 0.1, 0.3, or 0.5 PV d⁻¹ (linear velocities: 3, 9, or 15 cm d⁻¹), which is in the range of typical groundwater velocities. However, when passive treatment systems are used in field applications, an increase in flow rate may lead to decreases in removal efficiencies. In addition, the concurrence of other organic constituents such as organic carbon and inorganic components in the wastewater may also affect the performance of passive treatment systems. Similarly, the presence of dissolved organic carbon (DOC) and inorganic constituents in the wastewater will also likely affect the performance of active treatment systems, such as UV photocatalytic treatment and WWTPs. The effect of changes in flow rates and constituents of influent wastewater on the treatment performance should be considered when passive treatment systems are applied to the field applications.

7.4 Future Research

Samples of Grand River water were only collected once in the summers of 2012 and 2013, and in the winter of 2014 (Appendix B; Chapter 3). These three sampling events only reflect the distribution of the target emerging contaminants in the Grand River during the sampling days in 2012, 2013, and 2014, and do not represent the entire year. More frequent sampling such as sampling on daily or monthly basis should be considered in future studies to enhance the understanding of variability in the Grand River. In addition, alternative sampling device such as the passive polar organic chemical integrative samplers (Li et al., 2010a) should be considered to collect time-integrated samples and determine time-weighted average concentrations of emerging contaminants from water in future studies.

The removal mechanisms of artificial sweetener ACE-K and pharmaceuticals by UV photo- and photocatalytic treatment were not investigated in this thesis, but can be considered when planning future experiments. In addition, the application of recoverable GO TiO₂ nanoparticles to water treatment industry requires additional information, including optimizing UV photocatalytic reactor design to maximize both the removal of the target contaminants and recovery of the GO TiO₂ nanoparticles, and to evaluate the influence of water chemistry changes on the removal efficiency of contaminants and reaction kinetics. The UV intensity of the UVP CL-1000 Ultraviolet Crosslinker reactor used in this study was 66.7 W m⁻² and the UV irradiation time was 1 h (3600 s), which gave the target contaminants a UV dose of 24 J cm⁻². The UV dose used in this study was much higher than the typical UV dose applied for disinfection systems in water treatment plants (e.g., Trojan UV bulbs with UV intensity of ~33 mW cm⁻² and UV dose of 40 mJ cm⁻²). The removal efficiency of the target contaminants under typical UV disinfection dose would likely be reduced. Future batch experiments can be

performed to evaluate the effectiveness of common UV bulbs in facilitating the photocatalysis of the target contaminants using recoverable GO TiO₂ nanoparticles.

Passive treatment systems containing (ZVI + OC) or (ZVI + BC) have shown promising removals of NO₃⁻, SO₄²⁻ and emerging contaminants ClO₄⁻, pharmaceutical compounds, artificial sweeteners, and perfluoroalkyl substances from the water under reducing anaerobic conditions. The removal efficiency of the target contaminants might be different when the passive treatment system is applied to the mildly anoxic or oxic wastewater treatment conditions. In addition, simulated groundwater (CaCO₃ saturated solution) was used as input solution matrix (Chapter 1 and Chapter 5); the velocity of the column experiments was set at 3–15 cm d⁻¹ to represent typical average groundwater velocities in shallow aquifers. Future laboratory experiments should be conducted to evaluate the removal of target contaminants by reactive mixtures under mildly anoxic or oxic conditions, at higher flow rates, and with spiked wastewater as an input matrix to simulate potential field conditions. The ZVI is more expensive than wood chips and biochar; the cost of the passive treatment system could be reduced by decreasing the amount of ZVI used. Lower amendment rates of ZVI to OC and BC such as (5%, v/v) could be evaluated to determine whether similar removals of the target contaminants can be achieved using less ZVI.

Removal of PFOA and PFOS by ZVI and BC was likely through sorption in this study (described in Chapters 5 and 6); however, the sorption mechanism was not confirmed. Application of Attenuated Total Reflection (ATR)-Fourier Transform Infrared (FTIR) spectroscopy could be considered in future research to determine the functionalities on the surface of ZVI (iron oxides and hydroxides) and BC. The results of ATR-FTIR might assist in the explanation of the sorption mechanism of PFCAs and PFSA by ZVI (iron oxides and hydroxides) and BC. In addition, the defluorination efficiency of PFOA and PFOS was not confirmed in the

PFAS column study and was likely underestimated in the PFAS batch study due to the potential sorption of F^- by the reactive media. Extraction of F^- from the reactive media should be considered in future studies to confirm the defluorination of PFOA and PFOS.

Table 7.1 Comparison of average surface area normalized rate constants (K_{SA} , $L m^{-2} d^{-1}$), average removal efficiencies, and potential removal mechanisms of target contaminants during UV photocatalytic treatment using GO TiO₂ nanoparticles (Chapter 4) and passive treatment using ZVI and BC (Chapter 5).

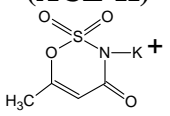
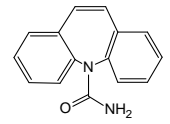
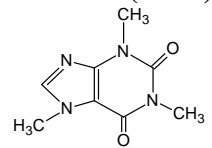
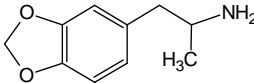
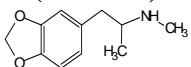
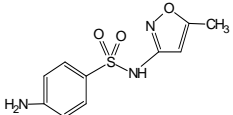
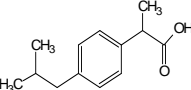
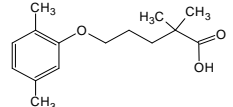
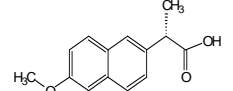
Contaminant	UV Photocatalytic Treatment			Passive Treatment		
	Average K_{SA}	Removal efficiency	Potential removal mechanisms	Average K_{SA}	Removal efficiency	Potential removal mechanisms
Acesulfame-K (ACE-K) 	5.3E+01	99%	Ring breakage and ·OH radical cleavage of S-N in sulfonamide group ^{1,2}	3.3E-06 ^a	30-60% in Column ZVI	Reduction by ZVI, H bonding
Carbamazepine (CBZ) 	1.7E+01	97%	Multi-step and interconnected pathway involving ·OH radical cleavage of C=C bonds ^{3,4}	1.1E-04	99%	Catalytic hydrogenation ¹⁷ , hydrophobic interaction ¹⁸ , π-π interaction, H bonding
Caffeine (CAF) 	3.8E+01	99%	Hydroxylation of C4=C8 double bond and demethylation ^{5,6}	1.3E-04	99%	Reduction and adsorption ¹⁹ , π-π EDA interaction, H bonding, electrostatic interaction
3,4-methylenedioxyamphetamine (MDA) 	1.3E+02	99%	·OH radical cleavage of methylenedioxy group ⁷	6.0E-04	99%	Electrostatic interaction, π-π stacking, π-π EDA interaction, π-H bonding, H bonding

Table 7.1 Continued.

3,4-methylenedioxy-methamphetamine (MDMA) 	1.4E+02	98%	·OH radical cleavage of methylenedioxy group ⁷	1.6E-03	99%	Electrostatic interaction, π - π stacking, π - π EDA interaction, π -H bonding, H bonding
Sulfamethoxazole (SMX) 	1.1E+02	99%	·OH radical cleavage of S-N in sulfonamide group, ·OH radical addition to open carbon position of isoxazole ring and aromatic ring ^{8,9}	6.5E-03	>97%	π - π stacking, π - π EDA interaction ²⁰ , π -H bonding, H bonding
Ibuprofen (IBU) 	2.6E+01	92%	Decarboxylation, ·OH radicals addition to the alkane Cs ^{10,11}	3.8E-05	>97%	Reduction ²¹ , H bonding, π - π stacking, π - π EDA interaction ²² , π -H bonding
Gemfibrozil (GEM) 	7.1E+01	99%	·OH radicals addition to benzene ring and breakage of ethereal bond ^{12,13}	9.2E-05	99%	π - π stacking, π - π EDA interaction, π -H bonding, H bonding
Naproxen (NAP) 	6.8E+01	99%	Decarboxylation, demethylation, photoionization ^{14,15,16}	7.1E-05	99%	π - π stacking, π - π EDA interaction ²³ , π -H bonding, H bonding

References: 1. Scheurer et al. (2014); 2. Li et al. (2016); 3. Jelic et al. (2013); 4. Doll and Frimmel (2005); 5. Dalmázio et al. (2005); 6. Chuang et al. (2011); 7. Kumagai et al. (1991); 8. Hu et al. (2007); 9. Abellán et al. (2007); 10. Méndez-Arriaga et al. (2008a); 11. Jacobs et al. (2011). 12. Razavi et al. (2009); 13. Yurdakal et al. (2007); 14. Méndez-Arriaga et al. (2008b); 15. Boscá et al. (2001); 16. Moore and Chappuis (1988). 17. König et al. (2016); 18. Inyang and Dickenson (2015); 19. Tomizawa et al. (2016); 20. Zheng et al. (2013); 21. Machado et al. (2013); 22. Jung et al. (2013); 23. Jung et al. (2015a).

^a The average first order removal rate constant of ACE-K within Column ZVI.

Table 7.2 Comparison of removal efficiency and removal rate (surface area normalized rate constant, K_{SA} , L m⁻² d⁻¹), treatment conditions, energy consumption, and required catalysts/reactive media during photocatalytic and passive treatment systems for removing ACE-K and eight pharmaceuticals.

	Photocatalytic Treatment	Passive Treatment
Removal efficiency	High: 92–99%	Moderate to high: 30–60% for ACE-K 97–99% for pharmaceuticals
Removal rate (K_{SA})	Rapid (E+1 – E+2)	Slow (E-3 – E-6)
Treatment conditions	UV irradiation conditions	Ambient T, reducing conditions
Energy consumption	High	Low
Use of reactive media/catalysts	Use of high-cost photocatalysts	Use of relatively low-cost reactive media

Enhanced Septic Treatment System

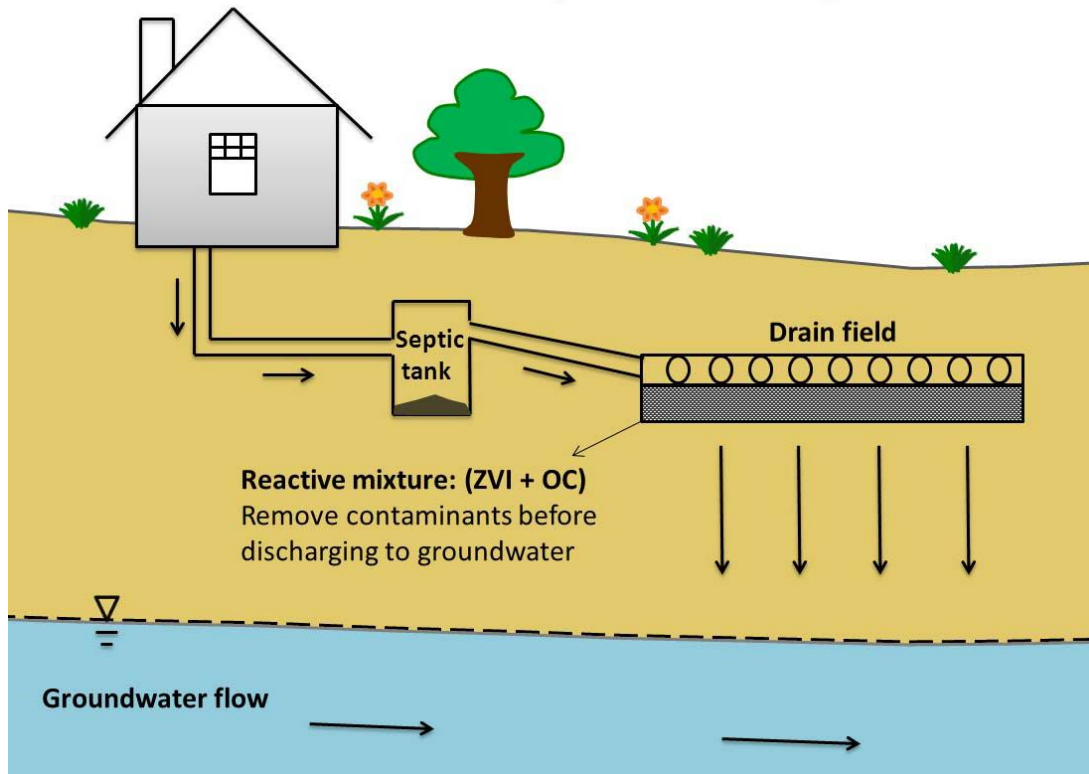


Figure 7.1 Schematic cross-section showing application of reactive mixture of zero-valent iron (ZVI) and organic carbon (OC) as a horizontal reactive layer underneath the septic drain tiles. The reactive layer is expected to remove NO_3^- , SO_4^{2-} and emerging contaminants from wastewater before it reaches groundwater.

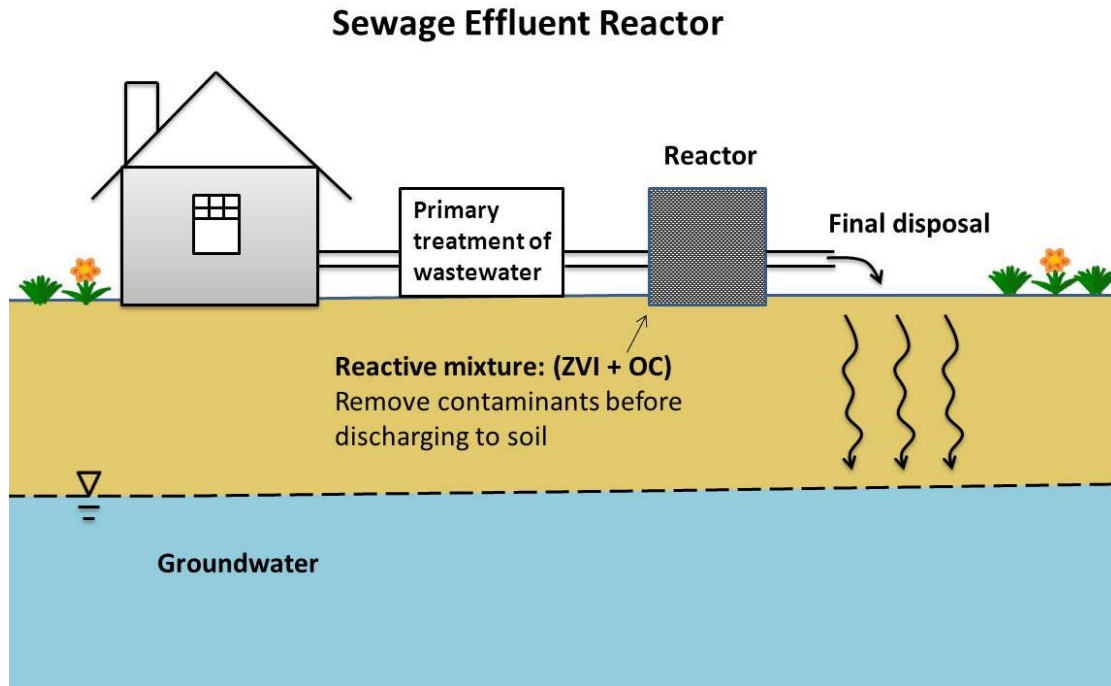


Figure 7.2 Schematic cross-section showing application of reactive mixture of zero-valent iron (ZVI) and organic carbon (OC) in a reactor attached to the effluent pipe derived from the primary treatment unit of the facility. The reactor is expected to remove NO_3^- , SO_4^{2-} and emerging contaminants in the sewage wastewater after primary treatment.

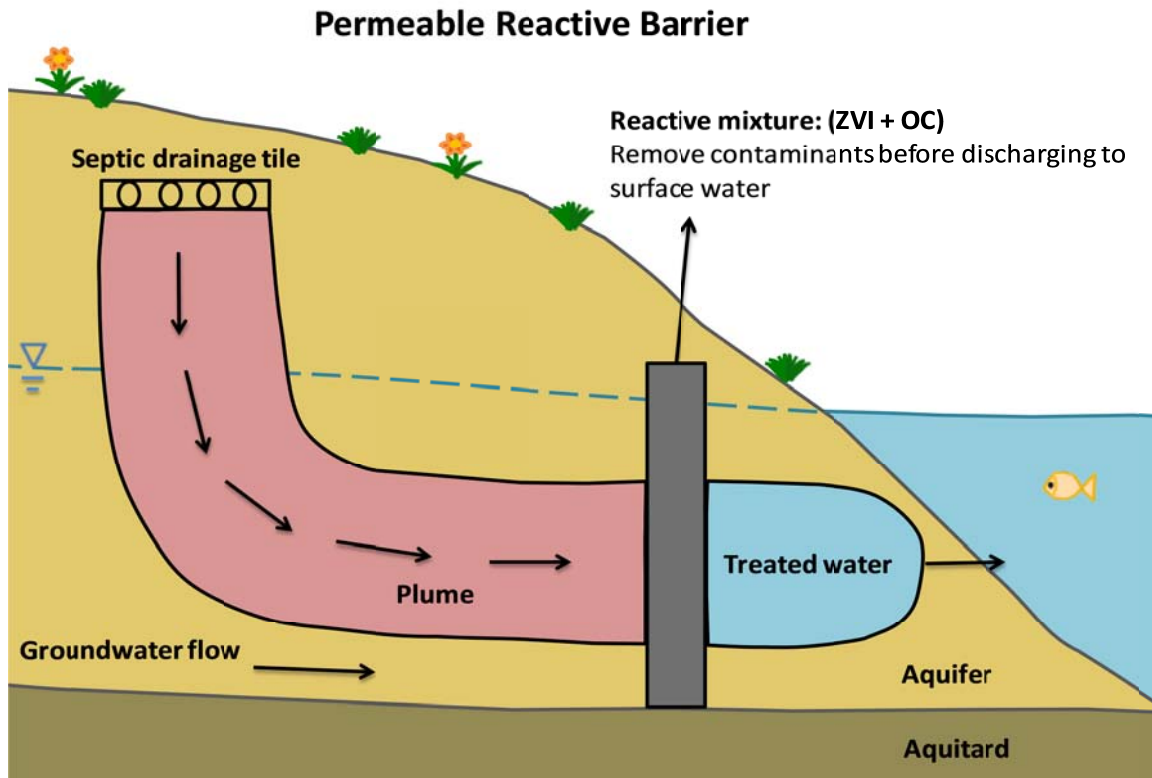


Figure 7.3 Schematic cross-section showing application of reactive mixture of zero-valent iron (ZVI) and organic carbon (OC) in a vertical permeable reactive barrier (PRB). The reactive mixture in the PRB is expected to remove NO_3^- , SO_4^{2-} and emerging contaminants in the plume before it discharges to surface water.

Enhanced Tile Drainage System

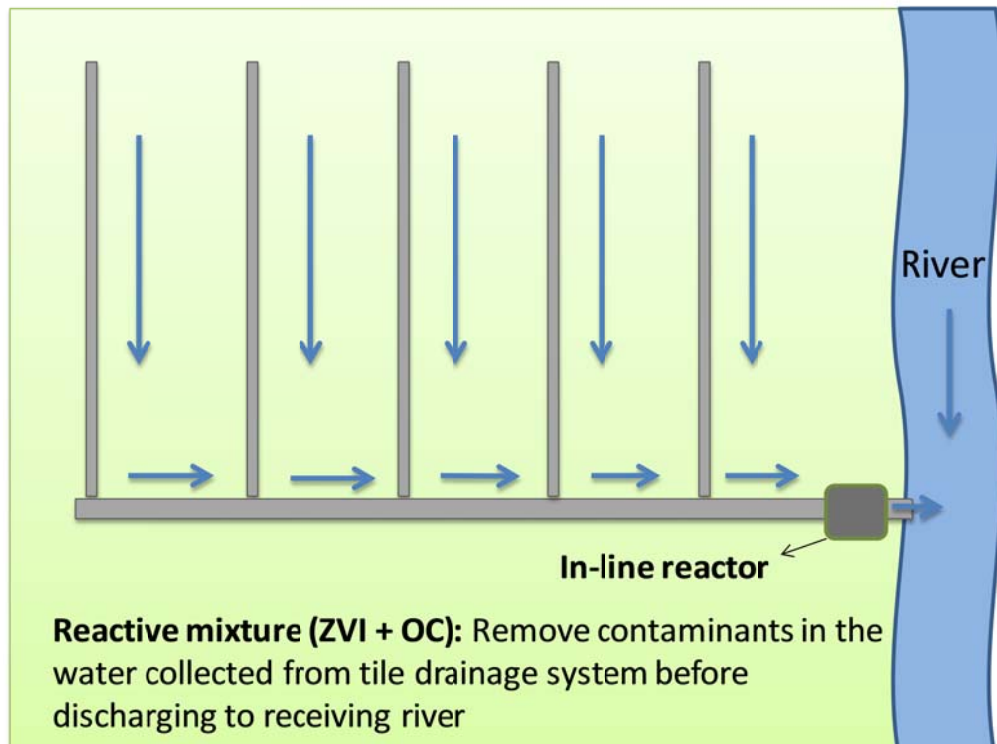


Figure 7.4 Schematic areal map showing in-line reactor containing reactive mixture of zero-valent iron (ZVI) and organic carbon (OC) to remove NO_3^- , SO_4^{2-} and emerging contaminants from water collected from the tile drainage system before it discharges to receiving water body.

Enhanced Soil Aquifer Treatment

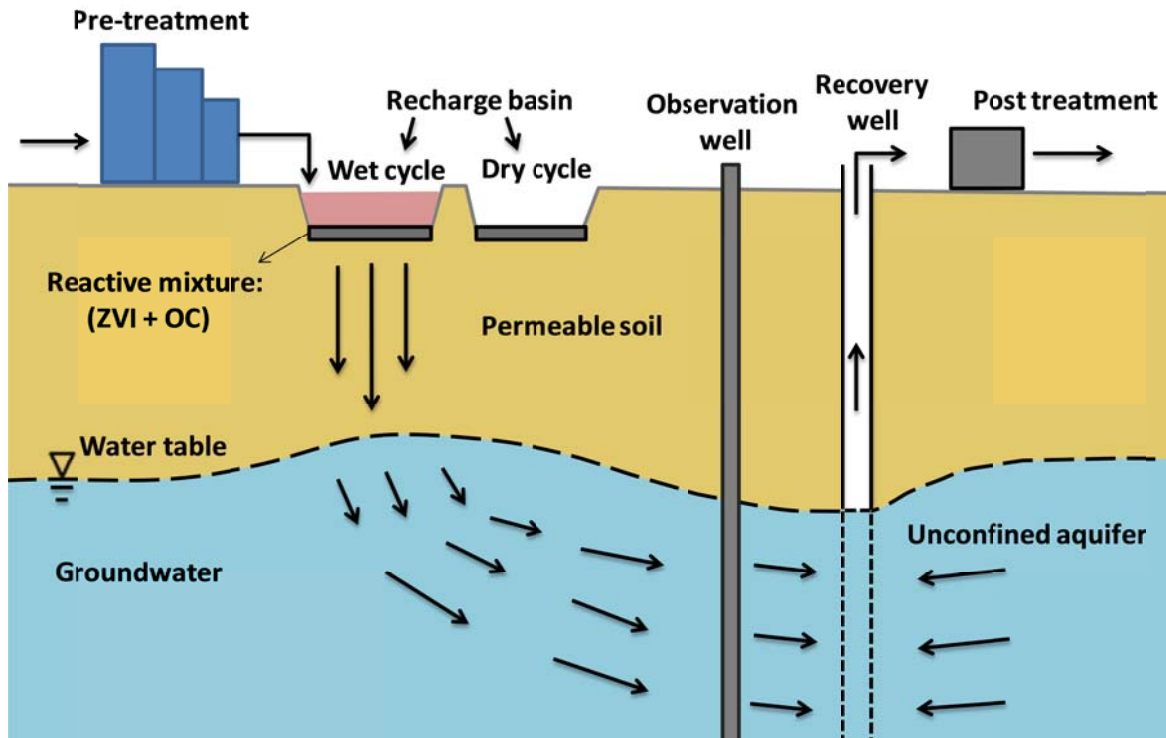


Figure 7.5 Schematic cross-section showing application of reactive mixture of zero-valent iron (ZVI) and organic carbon (OC) in a horizontal reactive layer underneath the recharge basin of a soil aquifer treatment. The reactive layer is expected to remove NO_3^- , SO_4^{2-} and emerging contaminants in the wastewater before it infiltrates to groundwater.

Enhanced River Bank Filtration

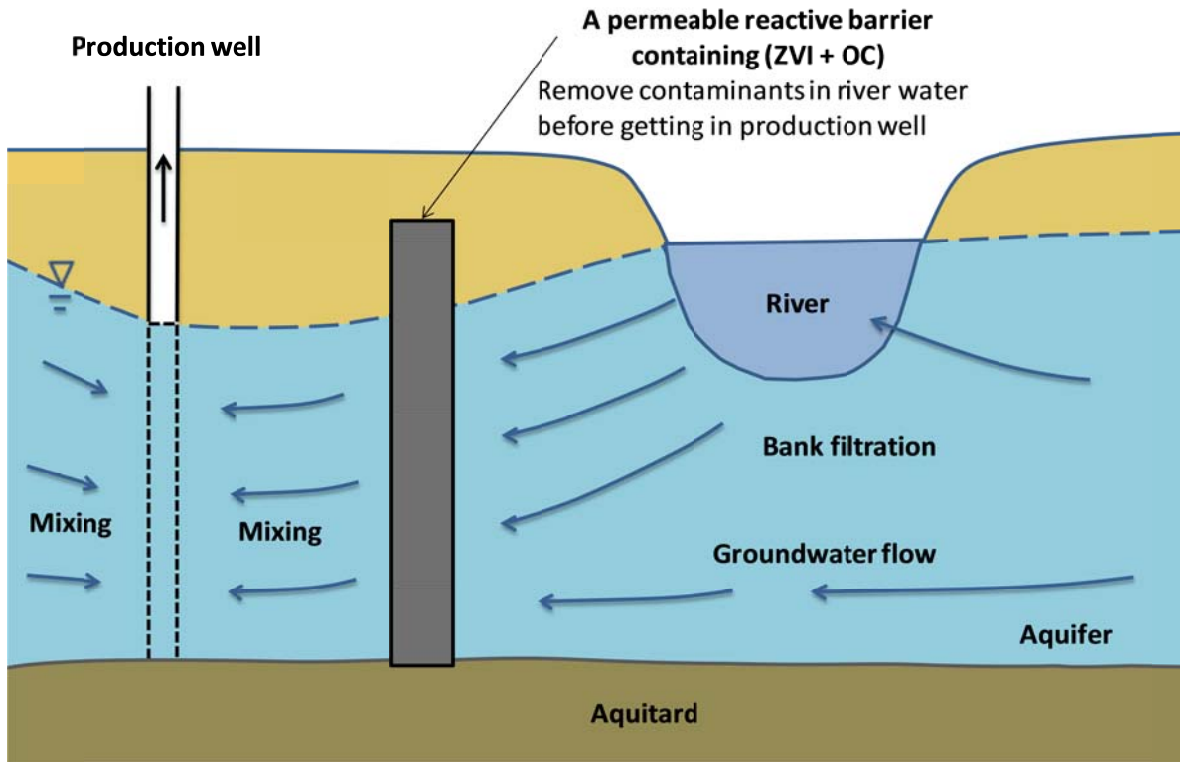


Figure 7.6 Schematic cross-section showing application of reactive mixture of zero-valent iron (ZVI) and organic carbon (OC) in a permeable reactive barrier (PRB) installed between the river and the production well in a river bank filtration process. The reactive mixture packed in the PRB is expected to remove NO_3^- , SO_4^{2-} and emerging contaminants in the recovery river water before end uses.

Polishing Cell of WWTPs Effluents

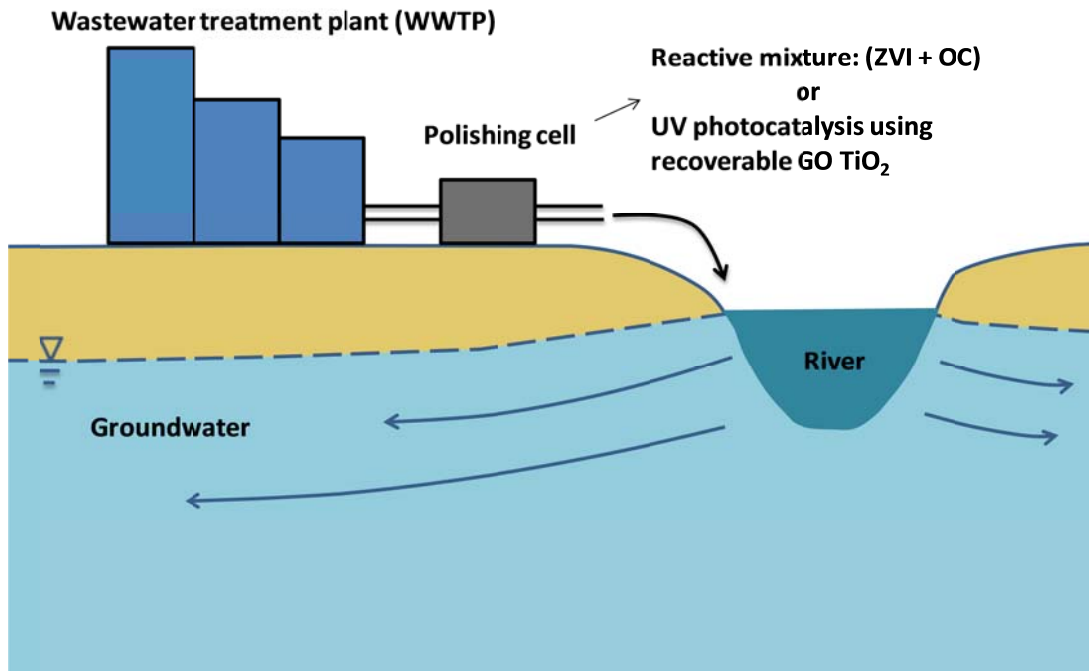


Figure 7.7 Schematic diagram showing application of reactive mixture of zero-valent iron (ZVI) and organic carbon (OC) or UV photocatalytic treatment using recoverable GO TiO₂ nanoparticles in a polishing cell (reactor) attached to the effluent of a wastewater treatment plant (WWTP). The emerging contaminants which cannot be removed in WWTPs are expected to be removed in the reactor before entering the receiving river.

References

- Abellán, M.N., Bayarri, B., Giménez, J., Costa, J., 2007. Photocatalytic degradation of sulfamethoxazole in aqueous suspension of TiO₂. *Appl. Catal. , B.* 74(3-4), 233-241.
- Achilleos, A., Hapeshi, E., Xekoukoulotakis, N.P., Mantzavinos, D., Fatta-Kassinos, D., 2010. UV-A and solar photodegradation of ibuprofen and carbamazepine catalyzed by TiO₂. *Sep. Sci. Technol.* 45(11), 1564-1570.
- Agrawal, A., Ferguson, W.J., Gardner, B.O., Christ, J.A., Bandstra, J.Z., Tratnyek, P.G., 2002. Effects of carbonate species on the kinetics of dechlorination of 1,1,1-trichloroethane by zero-valent iron. *Environ. Sci. Technol.* 36(20), 4326-4333.
- Ahmad, M., Lee, S.S., Dou, X., Mohan, D., Sung, J.-K., Yang, J.E., Ok, Y.S., 2012. Effects of pyrolysis temperature on soybean stover- and peanut shell-derived biochar properties and TCE adsorption in water. *Bioresour. Technol.* 118, 536-544.
- Ahmed, M.B., Zhou, J.L., Ngo, H.H., Guo, W., Thomaidis, N.S., Xu, J., 2016. Progress in the biological and chemical treatment technologies for emerging contaminant removal from wastewater: A critical review. *J. Hazard. Mater.* 323, Part A, 274-298.
- Ahrens, L., 2011. Polyfluoroalkyl compounds in the aquatic environment: A review of their occurrence and fate. *J. Environ. Monit.* 13(1), 20-31.
- Ahrens, L., Bundschuh, M., 2014. Fate and effects of poly- and perfluoroalkyl substances in the aquatic environment: A review. *Environ. Toxicol. Chem.* 33(9), 1921-1929.
- Ahrens, L., Taniyasu, S., Yeung, L.W.Y., Yamashita, N., Lam, P.K.S., Ebinghaus, R., 2010. Distribution of polyfluoroalkyl compounds in water, suspended particulate matter and sediment from Tokyo Bay, Japan. *Chemosphere.* 79(3), 266-272.
- Álvarez, P.M., Jaramillo, J., López-Piñero, F., Plucinski, P.K., 2010. Preparation and characterization of magnetic TiO₂ nanoparticles and their utilization for the degradation of emerging pollutants in water. *Appl. Catal. , B.* 100(1-2), 338-345.
- Ambashta, R.D., Sillanpää, M., 2010. Water purification using magnetic assistance: A review. *J. Hazard. Mater.* 180(1-3), 38-49.
- Andersson, M., Österlund, L., Ljungström, S., Palmqvist, A., 2002. Preparation of nanosize anatase and rutile TiO₂ by hydrothermal treatment of microemulsions and their activity for photocatalytic wet oxidation of phenol. *J. Phys. Chem. B.* 106(41), 10674-10679.
- Andreozzi, R., Campanella, L., Frayse, B., Garric, J., Gonnella, A., Lo Giudice, R., Marotta, R., Pinto, G., Pollio, A., 2004. Effects of advanced oxidation processes (AOPs) on the toxicity of a mixture of pharmaceuticals. *Water Sci. Technol.* 50(5), 23-28.
- Andreozzi, R., Marotta, R., Pinto, G., Pollio, A., 2002. Carbamazepine in water: Persistence in the environment, ozonation treatment and preliminary assessment on algal toxicity. *Water Res.* 36(11), 2869-2877.
- APHA. 1992. in: Method 2320 B: alkalinity, American Public Health Association. Washington, D.C.
- APHA. 2005a. Method 4500-NH₃. in: Method 4500-NH₃, American Public Health Association. Washington, D.C.
- APHA. 2005b. Method 4500-P:E. in: Method 4500-P:E, American Public Health Association. Washington, D.C.
- Appelo, C.A.J., Postma, D., 2005. *Geochemistry, Groundwater and Pollution.* AA Balkema,

Rotterdam.

Appleman, T.D., Dickenson, E.R.V., Bellona, C., Higgins, C.P., 2013. Nanofiltration and granular activated carbon treatment of perfluoroalkyl acids. *J. Hazard. Mater.* 260, 740-746.

Application Note, Agilent Technology. www.agilent.com/chem.

Arvaniti, O.S., Asimakopoulos, A.G., Dasenaki, M.E., Ventouri, E.I., Stasinakis, A.S., Thomaidis, N.S., 2014. Simultaneous determination of eighteen perfluorinated compounds in dissolved and particulate phases of wastewater, and in sewage sludge by liquid chromatography-tandem mass spectrometry. *Anal. Methods*. 6(5), 1341-1349.

Arvaniti, O.S., Hwang, Y., Andersen, H.R., Stasinakis, A.S., Thomaidis, N.S., Aloupi, M., 2015. Reductive degradation of perfluorinated compounds in water using Mg-aminoclay coated nanoscale zero valent iron. *Chem. Eng. J.* 262, 133-139.

Arvaniti, O.S., Stasinakis, A.S., 2015. Review on the occurrence, fate and removal of perfluorinated compounds during wastewater treatment. *Sci. Total Environ.* 524-525, 81-92.

Bailey, B.L., Smith, L.J.D., Blowes, D.W., Ptacek, C.J., Smith, L., Seago, D.C., 2013. The Diavik Waste Rock Project: Persistence of contaminants from blasting agents in waste rock effluent. *Appl. Geochem.* 36, 256-270.

Barndöck, H., Peláez, M., Han, C., Platten Iii, W.E., Campo, P., Hermosilla, D., Blanco, A., Dionysiou, D.D., 2013. Photocatalytic degradation of contaminants of concern with composite NF-TiO₂ films under visible and solar light. *Environ. Sci. Pollut. R.* 20(6), 3582-3591.

Barnes, K.K., Kolpin, D.W., Furlong, E.T., Zaugg, S.D., Meyer, M.T., Barber, L.B., 2008. A national reconnaissance of pharmaceuticals and other organic wastewater contaminants in the United States - I) Groundwater. *Sci. Total Environ.* 402(2-3), 192-200.

Barry, V., Winquist, A., Steenland, K., 2013. Perfluorooctanoic acid (PFOA) exposures and incident cancers among adults living near a chemical plant. *Environ. Health Perspect.* 121(11-12), 1313-1318.

Bautitz, I.R., Velosa, A.C., Nogueira, R.F.P., 2012. Zero valent iron mediated degradation of the pharmaceutical diazepam. *Chemosphere.* 88(6), 688-692.

Beesley, L., Moreno-Jiménez, E., Gomez-Eyles, J.L., Harris, E., Robinson, B., Sizmur, T., 2011. A review of biochars' potential role in the remediation, revegetation and restoration of contaminated soils. *Environ. Pollut.* 159(12), 3269-3282.

Bell, L.S., Devlin, J.F., Gillham, R.W., Binning, P.J., 2003. A sequential zero valent iron and aerobic biodegradation treatment system for nitrobenzene. *J. Contam. Hydrol.* 66(3-4), 201-217.

Beltrán, F.J., Aguinaco, A., García-Araya, J.F., 2009. Mechanism and kinetics of sulfamethoxazole photocatalytic ozonation in water. *Water Res.* 43(5), 1359-1369.

Bendz, D., Paxéus, N.A., Ginn, T.R., Loge, F.J., 2005. Occurrence and fate of pharmaceutically active compounds in the environment, a case study: Höje River in Sweden. *J. Hazard. Mater.* 122(3), 195-204.

Benner, S.G., Blowes, D.W., Ptacek, C.J., 1997. A full-scale porous reactive wall for prevention of acid mine drainage. *Ground Water Monit. R.* 17(4), 99-107.

Benotti, M.J., Brownawell, B.J., 2009. Microbial degradation of pharmaceuticals in estuarine and coastal seawater. *Environ. Pollut.* 157(3), 994-1002.

Bertelkamp, C., Reungoat, J., Cornelissen, E.R., Singhal, N., Reynisson, J., Cabo, A.J., van der Hoek, J.P., Verliefe, A.R.D., 2014. Sorption and biodegradation of organic micropollutants during river bank filtration: A laboratory column study. *Water Res.* 52, 231-241.

Blowes, D.W., Ptacek, C.J., Benner, S.G., McRae, C.W.T., Bennett, T.A., Puls, R.W., 2000. Treatment of inorganic contaminants using permeable reactive barriers. *J. Contam. Hydrol.* 45(1-

2), 123-137.

Blowes, D.W., Ptacek, C.J., Cherry, J.A., Gillham, R.W., Robertson, W.D. 1995. Passive remediation of groundwater using in situ treatment curtains. *Geotech. Sp.*46/2. pp. 1588-1607.

Blowes, D.W., Ptacek, C.J., Jambor, J.L., 1997. In-situ remediation of Cr(VI)-contaminated groundwater using permeable reactive walls: Laboratory studies. *Environ. Sci. Technol.* 31(12), 3348-3357.

Blowes, D.W., Reardon, E.J., Jambor, J.L., Cherry, J.A., 1991. The formation and potential importance of cemented layers in inactive sulfide mine tailings. *Geochim. Cosmochim. Acta.* 55(4), 965-978.

Blowes, D.W., Robertson, W.D., Ptacek, C.J., Merkley, C., 1994. Removal of agricultural nitrate from tile-drainage effluent water using in-line bioreactors. *J. Contam. Hydrol.* 15(3), 207-221.

Bo, L., Shengen, Z., Chang, C.C., Zhanfeng, D., Hongxiang, L., 2015. Emerging pollutants-Part II: Treatment. *Water Environ. Res.* 87(10), 1873-1900.

Borden, R.C., 2007. Concurrent bioremediation of perchlorate and 1,1,1-trichloroethane in an emulsified oil barrier. *J. Contam. Hydrol.* 94(1-2), 13-33.

Boscá, F., Marín, M.L., Miranda, M.A., 2001. Photoreactivity of the nonsteroidal anti-inflammatory 2-arylpropionic acids with photosensitizing side effects. *Photochem. Photobiol.* 74(5), 637-655.

Boyd, G.R., Reemtsma, H., Grimm, D.A., Mitra, S., 2003. Pharmaceuticals and personal care products (PPCPs) in surface and treated waters of Louisiana, USA and Ontario, Canada. *Sci. Total Environ.* 311(1-3), 135-149.

Brown, J.C., Snoeyink, V.L., Kirisits, M.J., 2002. Abiotic and biotic perchlorate removal in an activated carbon filter. *Am Water Works Assoc.* 94(2), 70-79.

Bueno, M.J.M., Gomez, M.J., Herrera, S., Hernando, M.D., Agüera, A., Fernández-Alba, A.R., 2012. Occurrence and persistence of organic emerging contaminants and priority pollutants in five sewage treatment plants of Spain: Two years pilot survey monitoring. *Environ. Pollut.* 164, 267-273.

Buerge, I.J., Buser, H.R., Kahle, M., Müller, M.D., Poiger, T., 2009. Ubiquitous occurrence of the artificial sweetener acesulfame in the aquatic environment: An ideal chemical marker of domestic wastewater in groundwater. *Environ. Sci. Technol.* 43(12), 4381-4385.

Buerge, I.J., Keller, M., Buser, H.R., Müller, M.D., Poiger, T., 2011. Saccharin and other artificial sweeteners in soils: Estimated inputs from agriculture and households, degradation, and leaching to groundwater. *Environ. Sci. Technol.* 45(2), 615-621.

Buerge, I.J., Poiger, T., Müller, M.D., Buser, H.R., 2003. Caffeine, an anthropogenic marker for wastewater contamination of surface waters. *Environ. Sci. Technol.* 37(4), 691-700.

California Department of Health Services (CDHS), 2004. Perchlorate in California drinking water.

Caliman, F.A., Gavrilescu, M., 2009. Pharmaceuticals, personal care products and endocrine disrupting agents in the environment - A review. *Clean - Soil, Air, Water.* 37(4-5), 277-303.

Calisto, V., Domingues, M.R.M., Esteves, V.I., 2011. Photodegradation of psychiatric pharmaceuticals in aquatic environments - Kinetics and photodegradation products. *Water Res.* 45(18), 6097-6106.

Calza, P., Sakkas, V.A., Medana, C., Vlachou, A.D., Dal Bello, F., Albanis, T.A., 2013. Chemometric assessment and investigation of mechanism involved in photo-Fenton and TiO₂ photocatalytic degradation of the artificial sweetener sucralose in aqueous media. *Appl. Catal. , B.* 129, 71-79.

Cantrell, K.J., Kaplan, D.I., Wietsma, T.W., 1995. Zero-valent iron for the in situ remediation of

selected metals in groundwater. *J. Hazard. Mater.* 42(2), 201-212.

Carrara, C., Ptacek, C.J., Robertson, W.D., Blowes, D.W., Moncur, M.C., Sverko, E., Backus, S., 2008. Fate of pharmaceutical and trace organic compounds in three septic system plumes, Ontario, Canada. *Environ. Sci. Technol.* 42(8), 2805-2811.

Chefetz, B., Mualem, T., Ben-Ari, J., 2008. Sorption and mobility of pharmaceutical compounds in soil irrigated with reclaimed wastewater. *Chemosphere.* 73(8), 1335-1343.

Chen, B., Chen, Z., Lv, S., 2011a. A novel magnetic biochar efficiently sorbs organic pollutants and phosphate. *Bioresour. Technol.* 102(2), 716-723.

Chen, W., Cannon, F.S., Rangel-Mendez, J.R., 2005. Ammonia-tailoring of GAC to enhance perchlorate removal. II: Perchlorate adsorption. *Carbon.* 43(3), 581-590.

Chen, X., Xia, X., Wang, X., Qiao, J., Chen, H., 2011b. A comparative study on sorption of perfluorooctane sulfonate (PFOS) by chars, ash and carbon nanotubes. *Chemosphere.* 83(10), 1313-1319.

Cheng, W., Tang, K., Qi, Y., Sheng, J., Liu, Z., 2010. One-step synthesis of superparamagnetic monodisperse porous Fe₃O₄ hollow and core-shell spheres. *J. Mater. Chem.* 20(9), 1799-1805.

Cho, I.H., 2011. Degradation and reduction of acute toxicity of environmentally persistent perfluorooctanoic acid (PFOA) using VUV photolysis and TiO₂ photocatalysis in acidic and basic aqueous solutions. *Toxicol. Environ. Chem.* 93(5), 925-940.

Choina, J., Duwensee, H., Flechsig, G.U., Kosslick, H., Morawski, A.W., Tuan, V.A., Schulz, A., 2010. Removal of hazardous pharmaceutical from water by photocatalytic treatment. *Cent. Eur. J. Chem.* 8(6), 1288-1297.

Chong, M.N., Jin, B., Chow, C.W.K., Saint, C., 2010. Recent developments in photocatalytic water treatment technology: A review. *Water Res.* 44(10), 2997-3027.

Chuang, L.C., Luo, C.H., Huang, S.W., Wu, Y.C., Huang, Y.C., 2011. Photocatalytic degradation mechanism and kinetics of caffeine in aqueous suspension of nano-TiO₂. *Adv. Mat. Res.* 214, 97-102.

Chung, J., Shin, S., Oh, J., 2010. Influence of nitrate, sulfate and operational parameters on the bioreduction of perchlorate using an up-flow packed bed reactor at high salinity. *Environ. Technol.* 31(6), 693-704.

Clara, M., Strenn, B., Gans, O., Martinez, E., Kreuzinger, N., Kroiss, H., 2005. Removal of selected pharmaceuticals, fragrances and endocrine disrupting compounds in a membrane bioreactor and conventional wastewater treatment plants. *Water Res.* 39(19), 4797-4807.

Clara, M., Strenn, B., Kreuzinger, N., 2004. Carbamazepine as a possible anthropogenic marker in the aquatic environment: Investigations on the behaviour of carbamazepine in wastewater treatment and during groundwater infiltration. *Water Res.* 38(4), 947-954.

Coiffard, C.A.C., Coiffard, L.J.M., De Roeck-Holtzhauer, Y.M.R., 1999. Photodegradation kinetics of acesulfame-K solutions under UV light: Effect of pH. *Eur. Food Res. Technol.* 208(1), 6-9.

Conder, J.M., Hoke, R.A., De Wolf, W., Russell, M.H., Buck, R.C., 2008. Are PFCAs bioaccumulative? A critical review and comparison with regulatory criteria and persistent lipophilic compounds. *Environ. Sci. Technol.* 42(4), 995-1003.

Conkle, J.L., White, J.R., Metcalfe, C.D., 2008. Reduction of pharmaceutically active compounds by a lagoon wetland wastewater treatment system in Southeast Louisiana. *Chemosphere.* 73(11), 1741-1748.

Cooke, S., 2006. Water quality in the Grand River: a summary of current conditions (2000–2004) and long term trends. Grand River Conservation Authority, Cambridge, Ontario.

- Crawford, R.J., Harding, I.H., Mainwaring, D.E., 1993. Adsorption and coprecipitation of multiple heavy metal ions onto the hydrated oxides of iron and chromium. *Langmuir*. 9(11), 3057-3062.
- Cundy, A.B., Hopkinson, L., Whitby, R.L.D., 2008. Use of iron-based technologies in contaminated land and groundwater remediation: A review. *Sci. Total Environ.* 400(1-3), 42-51.
- D'Eon, J.C., Crozier, P.W., Furdui, V.I., Reiner, E.J., Libelo, E.L., Mabury, S.A., 2009. Perfluorinated phosphonic acids in Canadian surface waters and wastewater treatment plant effluent: Discovery of a new class of perfluorinated acids. *Environ. Toxicol. Chem.* 28(10), 2101-2107.
- Dalmázio, I., Santos, L.S., Lopes, R.P., Eberlin, M.N., Augusti, R., 2005. Advanced oxidation of caffeine in water: On-line and real-time monitoring by electrospray ionization mass spectrometry. *Environ. Sci. Technol.* 39(16), 5982-5988.
- Daughton, C.G., 2005. "Emerging" chemicals as pollutants in the environment: A 21st century perspective. *Renewable Resour. J.* 23(4), 6-23.
- De la Cruz, N., Giménez, J., Esplugas, S., Grandjean, D., De Alencastro, L.F., Pulgarín, C., 2012. Degradation of 32 emergent contaminants by UV and neutral photo-fenton in domestic wastewater effluent previously treated by activated sludge. *Water Res.* 46(6), 1947-1957.
- Deng, S., Zhang, Q., Nie, Y., Wei, H., Wang, B., Huang, J., Yu, G., Xing, B., 2012. Sorption mechanisms of perfluorinated compounds on carbon nanotubes. *Environ. Pollut.* 168, 138-144.
- Devlin, J.F., Klausen, J., Schwarzenbach, R.P., 1998. Kinetics of nitroaromatic reduction on granular iron in recirculating batch experiments. *Environ. Sci. Technol.* 32(13), 1941-1947.
- Dimitrakopoulou, D., Rethemiotaki, I., Frontistis, Z., Xekoukoulotakis, N.P., Venieri, D., Mantzavinos, D., 2012. Degradation, mineralization and antibiotic inactivation of amoxicillin by UV-A/TiO₂ photocatalysis. *J. Environ. Manage.* 98(1), 168-174.
- Ding, G., Peijnenburg, W.J.G.M., 2013. Physicochemical properties and aquatic toxicity of poly- and perfluorinated compounds. *Crit. Rev. Environ. Sci. Technol.* 43(6), 598-678.
- Doll, T.E., Frimmel, F.H., 2004. Kinetic study of photocatalytic degradation of carbamazepine, clofibric acid, iomeprol and iopromide assisted by different TiO₂ materials - Determination of intermediates and reaction pathways. *Water Res.* 38(4), 955-964.
- Doll, T.E., Frimmel, F.H., 2005. Removal of selected persistent organic pollutants by heterogeneous photocatalysis in water. *Catal. Today*. 101(3-4 SPEC. ISS.), 195-202.
- Du, J., Lai, X., Yang, N., Zhai, J., Kisailus, D., Su, F., Wang, D., Jiang, L., 2011. Hierarchically ordered macro-mesoporous TiO₂-graphene composite films: Improved mass transfer, reduced charge recombination, and their enhanced photocatalytic activities. *ACS Nano*. 5(1), 590-596.
- Du, Z., Deng, S., Bei, Y., Huang, Q., Wang, B., Huang, J., Yu, G., 2014. Adsorption behavior and mechanism of perfluorinated compounds on various adsorbents-A review. *J. Hazard. Mater.* 274, 443-454.
- Durán-álvarez, J.C., Prado-Pano, B., Jiménez-Cisneros, B., 2012. Sorption and desorption of carbamazepine, naproxen and triclosan in a soil irrigated with raw wastewater: Estimation of the sorption parameters by considering the initial mass of the compounds in the soil. *Chemosphere*. 88(1), 84-90.
- Ek, M., Baresel, C., Magnér, J., Bergström, R., Harding, M., 2014. Activated carbon for the removal of pharmaceutical residues from treated wastewater. *Water Sci. Technol.* 69(11), 2372-2380.
- El-Bassat, R.A., Touliabah, H.E., Harisa, G.I., 2012. Toxicity of four pharmaceuticals from different classes to isolated plankton species. *Afr. J. Aquat. Sci.* 37(1), 71-80.

Elsner, M., Schwarzenbach, R.P., Haderlein, S.B., 2004. Reactivity of Fe(II)-bearing minerals toward reductive transformation of organic contaminants. *Environ. Sci. Technol.* 38(3), 799-807.

Environment Canada, 2013. Hydrometric Data. Environment Canada, Water Survey of Canada.

Evans, P.J., Trute, M.M., 2006. In situ bioremediation of nitrate and perchlorate in vadose zone soil for groundwater protection using gaseous electron donor injection technology. *Water Environ. Res.* 78(13), 2436-2446.

Farré, M.I., Pérez, S., Kantiani, L., Barceló, D., 2008. Fate and toxicity of emerging pollutants, their metabolites and transformation products in the aquatic environment. *TrAC - Trends Anal. Chem.* 27(11), 991-1007.

Feng, X., Guo, H., Patel, K., Zhou, H., Lou, X., 2014. High performance, recoverable Fe₃O₄-ZnO nanoparticles for enhanced photocatalytic degradation of phenol. *Chem. Eng. J.* 244, 327-334.

Fent, K., Weston, A.A., Caminada, D., 2006. Ecotoxicology of human pharmaceuticals. *Aquat. Toxicol.* 76(2), 122-159.

Ferrer, I., Thurman, E.M., 2010. Analysis of sucralose and other sweeteners in water and beverage samples by liquid chromatography/time-of-flight mass spectrometry. *J. Chromatogr. A.* 1217(25), 4127-4134.

Focazio, M.J., Kolpin, D.W., Barnes, K.K., Furlong, E.T., Meyer, M.T., Zaugg, S.D., Barber, L.B., Thurman, M.E., 2008. A national reconnaissance for pharmaceuticals and other organic wastewater contaminants in the United States - II) Untreated drinking water sources. *Sci. Total Environ.* 402(2-3), 201-216.

Fono, L.J., Kolodziej, E.P., Sedlak, D.L., 2006. Attenuation of wastewater-derived contaminants in an effluent-dominated river. *Environ. Sci. Technol.* 40(23), 7257-7262.

Ford, K.L., 2003. Passive treatment systems for acid mine drainage. Bureau of Land Management, National Science and Technology Center, Technical Note 409.

Fujii, S., Polprasert, C., Tanaka, S., Lien, N.P.H., Qiu, Y., 2007. New POPs in the water environment: Distribution, bioaccumulation and treatment of perfluorinated compounds - A review paper. *J. Water Supply Res. T. - AQUA.* 56(5), 313-326.

Fukahori, S., Fujiwara, T., Ito, R., Funamizu, N., 2012. Photocatalytic decomposition of crotamiton over aqueous TiO₂ suspensions: Determination of intermediates and the reaction pathway. *Chemosphere.* 89(3), 213-220.

Furdui, V.I., Helm, P.A., Crozier, P.W., Lucaciu, C., Reiner, E.J., Marvin, C.H., Whittle, D.M., Mabury, S.A., Tomy, G.T., 2008. Temporal trends of perfluoroalkyl compounds with isomer analysis in lake trout from Lake Ontario (1979-2004). *Environ. Sci. Technol.* 42(13), 4739-4744.

Gagnon, C., Lajeunesse, A., Cejka, P., Gagné, F., Hausler, R., 2008. Degradation of selected acidic and neutral pharmaceutical products in a primary-treated wastewater by disinfection processes. *Ozone Sci. Eng.* 30(5), 387-392.

Gal, H., Ronen, Z., Weisbrod, N., Dahan, O., Nativ, R., 2008. Perchlorate biodegradation in contaminated soils and the deep unsaturated zone. *Soil Biol. and Biochem.* 40(7), 1751-1757.

Gan, Z., Sun, H., Wang, R., Hu, H., Zhang, P., Ren, X., 2014. Transformation of acesulfame in water under natural sunlight: Joint effect of photolysis and biodegradation. *Water Res.* 64, 113-122.

Ganzenko, O., Oturan, N., Huguenot, D., Van Hullebusch, E.D., Esposito, G., Oturan, M.A., 2015. Removal of psychoactive pharmaceutical caffeine from water by electro-Fenton process using BDD anode: Effects of operating parameters on removal efficiency. *Sep.Purif, Technol.* 156, 987-995.

Gao, X., Chorover, J., 2012. Adsorption of perfluorooctanoic acid and perfluorooctanesulfonic acid to iron oxide surfaces as studied by flow-through ATR-FTIR spectroscopy. *Envir. Chem.* 9(2), 148-157.

Gaya, U.I., Abdullah, A.H., 2008. Heterogeneous photocatalytic degradation of organic contaminants over titanium dioxide: A review of fundamentals, progress and problems. *J. Photochem. Photobiol. C: Photochem. Rev.* 9(1), 1-12.

Ghatak, H.R., 2014. Advanced oxidation processes for the treatment of biorecalcitrant organics in wastewater. *Crit. Rev. Environ. Sci. Technol.* 44(11), 1167-1219.

Giblin, T., Frankenberger W.T, Jr., 2001. Perchlorate and nitrate reductase activity in the perchlorate-respiring bacterium *perclace*. *Microbiol. Res.* 156(4), 311-315.

Giblin, T.L., Herman, D.C., Deshusses, M.A., Frankenberger Jr., W.T., 2000. Removal of perchlorate in ground water with a flow-through bioreactor. *J. Environ. Qual.* 29(2), 578-583.

Giesy, J.P., Kannan, K., 2001. Global distribution of perfluorooctane sulfonate in wildlife. *Environ. Sci. Technol.* 35(7), 1339-1342.

Gillham, R.W., O'Hannesin, S.F., 1994. Enhanced degradation of halogenated aliphatics by zero-valent iron. *Groundwater.* 32(6), 958-967.

Gillis, P.L., McInnis, R., Salerno, J., de Solla, S.R., Servos, M.R., Leonard, E.M., 2017. Freshwater mussels in an urban watershed: Impacts of anthropogenic inputs and habitat alterations on populations. *Sci. Total Environ.* 574, 671-679.

González, S., López-Roldán, R., Cortina, J.L., 2012. Presence and biological effects of emerging contaminants in Llobregat River basin: A review. *Environ. Pollut.* 161, 83-92.

Goudarzi, H., Nakajima, S., Ikeno, T., Sasaki, S., Kobayashi, S., Miyashita, C., Ito, S., Araki, A., Nakazawa, H., Kishi, R., 2016. Prenatal exposure to perfluorinated chemicals and neurodevelopment in early infancy: The Hokkaido study. *Sci. Total Environ.* 541, 1002-1010.

Grover, D.P., Zhou, J.L., Frickers, P.E., Readman, J.W., 2011. Improved removal of estrogenic and pharmaceutical compounds in sewage effluent by full scale granular activated carbon: Impact on receiving river water. *J. Hazard. Mater.* 185(2-3), 1005-1011.

Guan, X., Zhou, J., Ma, N., Chen, X., Gao, J., Zhang, R., 2015. Studies on modified conditions of biochar and the mechanism for fluoride removal. *Desalin. Water Treat.* 55(2), 440-447.

Guilbaud, R., White, M.L., Poulton, S.W., 2013. Surface charge and growth of sulphate and carbonate green rust in aqueous media. *Geochim. Cosmochim. Acta.* 108, 141-153.

Gullick, R.W., Lechevallier, M.W., Barhorst, T.S., 2001. Occurrence of perchlorate in drinking water sources. *J. Am. Water Works Ass.* 93(1), 66-77.

Han, L., Xue, S., Zhao, S., Yan, J., Qian, L., Chen, M., 2015. Biochar supported nanoscale iron particles for the efficient removal of methyl orange dye in aqueous solutions. *PLoS ONE.* 10(7).

Harraz, F.A., Mohamed, R.M., Rashad, M.M., Wang, Y.C., Sigmund, W., 2014. Magnetic nanocomposite based on titania-silica/cobalt ferrite for photocatalytic degradation of methylene blue dye. *Ceram. Int.* 40(1 PART A), 375-384.

Hatzinger, P.B., Greene, M.R., Frisch, S., Togna, A.P., Manning, J., Guarini, W.J. 2000. Biological Treatment of Perchlorate-contaminated Groundwater Using Fluidized Bed Reactors. 2nd International Conference on Remediation of Chlorinated and Recalcitrant Compounds, May 22 - 25, 2000, Monterey, California.

Health Canada, 2005. Perchlorate and human health. Available online: http://www.hc-sc.gc.ca/ewh-semt/water-eau/drink-potab/perchlorate_e.html.

Heberer, T., 2002. Occurrence, fate, and removal of pharmaceutical residues in the aquatic environment: A review of recent research data. *Toxicology Letters.* 131(1-2), 5-17.

- Her, N., Kim, J., Yoon, Y., 2010. Perchlorate in dairy milk and milk-based powdered infant formula in South Korea. *Chemosphere*. 81(6), 732-737.
- Higgins, C.P., Luthy, R.G., 2006. Sorption of perfluorinated surfactants on sediments. *Environ. Sci. Technol.* 40(23), 7251-7256.
- Hirsch, R., Ternes, T., Haberer, K., Kratz, K.L., 1999. Occurrence of antibiotics in the aquatic environment. *Sci. Total Environ.* 225(1-2), 109-118.
- Hori, H., Hayakawa, E., Einaga, H., Kutsuna, S., Koike, K., Ibusuki, T., Kiatagawa, H., Arakawa, R., 2004. Decomposition of environmentally persistent perfluorooctanoic acid in water by photochemical approaches. *Environ. Sci. Technol.* 38(22), 6118-6124.
- Hori, H., Nagaoka, Y., Murayama, M., Kutsuna, S., 2008. Efficient decomposition of perfluorocarboxylic acids and alternative fluorochemical surfactants in hot water. *Environ. Sci. Technol.* 42(19), 7438-7443.
- Hori, H., Nagaoka, Y., Yamamoto, A., Sano, T., Yamashita, N., Taniyasu, S., Kutsuna, S., Osaka, I., Arakawa, R., 2006. Efficient decomposition of environmentally persistent perfluorooctanesulfonate and related fluorochemicals using zerovalent iron in subcritical water. *Environ. Sci. Technol.* 40(3), 1049-1054.
- Hori, H., Yamamoto, A., Hayakawa, E., Taniyasu, S., Yamashita, N., Kutsuna, S., Kiatagawa, H., Arakawa, R., 2005. Efficient decomposition of environmentally persistent perfluorocarboxylic acids by use of persulfate as a photochemical oxidant. *Environ. Sci. Technol.* 39(7), 2383-2388.
- Hori, H., Yamamoto, A., Koike, K., Kutsuna, S., Osaka, I., Arakawa, R., 2007. Photochemical decomposition of environmentally persistent short-chain perfluorocarboxylic acids in water mediated by iron(II)/(III) redox reactions. *Chemosphere*. 68(3), 572-578.
- Houde, M., De Silva, A.O., Muir, D.C.G., Letcher, R.J., 2011. Monitoring of perfluorinated compounds in aquatic biota: An updated review. *Environ. Sci. Technol.* 45(19), 7962-7973.
- Houtz, E.F., Sedlak, D.L., 2012. Oxidative conversion as a means of detecting precursors to perfluoroalkyl acids in urban runoff. *Environ. Sci. Technol.* 46(17), 9342-9349.
- Hsiao, I.L., Huang, Y.J., 2011. Effects of various physicochemical characteristics on the toxicities of ZnO and TiO₂ nanoparticles toward human lung epithelial cells. *Sci. Total Environ.* 409(7), 1219-1228.
- Hu, L., Flanders, P.M., Miller, P.L., Strathmann, T.J., 2007. Oxidation of sulfamethoxazole and related antimicrobial agents by TiO₂ photocatalysis. *Water Res.* 41(12), 2612-2626.
- Huang, Q., Yu, Y., Tang, C., Zhang, K., Cui, J., Peng, X., 2011. Occurrence and behavior of non-steroidal anti-inflammatory drugs and lipid regulators in wastewater and urban river water of the Pearl River Delta, South China. *J. Environ. Monit.* 13(4), 855-863.
- Hund-Rinke, K., Simon, M., 2006. Ecotoxic effect of photocatalytic active nanoparticles (TiO₂) on algae and daphnids. *Environ. Sci. Pollut. R.* 13(4), 225-232.
- Hunter, W.J., 2002. Bioremediation of chlorate or perchlorate contaminated water using permeable barriers containing vegetable oil. *Curr. Microbiol.* 45(4), 287-292.
- Hurley, K.D., Shapley, J.R., 2007. Efficient heterogeneous catalytic reduction of perchlorate in water. *Environ. Sci. Technol.* 41(6), 2044-2049.
- Hurtado, C., Cañameras, N., Domínguez, C., Price, G.W., Comas, J., Bayona, J.M., 2016. Effect of soil biochar concentration on the mitigation of emerging organic contaminant uptake in lettuce. *J. Hazard. Mater.* 323, Part A, 386-393.
- Hurum, D.C., Agrios, A.G., Gray, K.A., Rajh, T., Thurnauer, M.C., 2003. Explaining the enhanced photocatalytic activity of Degussa P25 mixed-phase TiO₂ using EPR. *J. Phys. Chem. B.* 107(19), 4545-4549.

- Iannece, P., Motta, O., Tedesco, R., Carotenuto, M., Proto, A., 2013. Determination of perchlorate in bottled water from Italy. *Water (Switzerland)*. 5(2), 767-779.
- Inyang, M., Dickenson, E., 2015. The potential role of biochar in the removal of organic and microbial contaminants from potable and reuse water: A review. *Chemosphere*. 134, 232-240.
- Ismail, A.A., Bahnemann, D.W., 2011. Mesoporous titania photocatalysts: Preparation, characterization and reaction mechanisms. *J. Mater. Chem.* 21(32), 11686-11707.
- Izbicki, J.A., Teague, N.F., Hatzinger, P.B., Böhlke, J.K., Sturchio, N.C., 2015. Groundwater movement, recharge, and perchlorate occurrence in a faulted alluvial aquifer in California (USA). *Hydrogeol. J.* 23(3), 467-491.
- Jacobs, L.E., Fimmen, R.L., Chin, Y.P., Mash, H.E., Weavers, L.K., 2011. Fulvic acid mediated photolysis of ibuprofen in water. *Water Res.* 45(15), 4449-4458.
- James, C.A., Miller-Schulze, J.P., Ultican, S., Gipe, A.D., Baker, J.E., 2016. Evaluating Contaminants of Emerging Concern as tracers of wastewater from septic systems. *Water Res.* 101, 241-251.
- Jamieson-Hanes, J.H., 2012. Characterizing Chromium Isotope Fractionation During Reduction of Cr(VI): Batch and Column Experiments. (Master of Science). University of Waterloo, Waterloo, Ontario, Canada.
- Jamieson-Hanes, J.H., Lentz, A.M., Amos, R.T., Ptacek, C.J., Blowes, D.W., 2014. Examination of Cr(VI) treatment by zero-valent iron using in situ, real-time X-ray absorption spectroscopy and Cr isotope measurements. *Geochim. Cosmochim. Acta.* 142, 299-313.
- Jeen, S.W., Gillham, R.W., Blowes, D.W., 2006. Effects of carbonate precipitates on long-term performance of granular iron for reductive dechlorination of TCE. *Environ. Sci. Technol.* 40(20), 6432-6437.
- Jeen, S.W., Jambor, J.L., Blowes, D.W., Gillham, R.W., 2007. Precipitates on granular iron in solutions containing calcium carbonate with trichloroethene and hexavalent chromium. *Environ. Sci. Technol.* 41(6), 1989-1994.
- Jeen, S.W., Yang, Y., Gui, L., Gillham, R.W., 2013. Treatment of trichloroethene and hexavalent chromium by granular iron in the presence of dissolved CaCO₃. *J. Contam. Hydrol.* 144, 108-121.
- Jelic, A., Michael, I., Achilleos, A., Hapeshi, E., Lambropoulou, D., Perez, S., Petrovic, M., Fatta-Kassinos, D., Barcelo, D., 2013. Transformation products and reaction pathways of carbamazepine during photocatalytic and sonophotocatalytic treatment. *J. Hazard. Mater.* 263, 177-186.
- Johnson, D.B., Hallberg, K.B., 2005. Acid mine drainage remediation options: A review. *Sci. Total Environ.* 338(1-2 SPEC. ISS.), 3-14.
- Johnson, T.L., Scherer, M.M., Tratnyek, P.G., 1996. Kinetics of halogenated organic compound degradation by iron metal. *Environ. Sci. Technol.* 30(8), 2634-2640.
- Jones, O.A., Lester, J.N., Voulvoulis, N., 2005. Pharmaceuticals: A threat to drinking water? *Trends Biotechnol.* 23(4), 163-167.
- José, H.J., Gebhardt, W., Moreira, R.F.P.M., Pinnekamp, J., Schröder, H.F., 2010. Advanced oxidation processes for the elimination of drugs resisting biological membrane treatment. *Ozone Sci. Eng.* 32(5), 305-312.
- Joss, A., Keller, E., Alder, A.C., Göbel, A., McArdell, C.S., Ternes, T., Siegrist, H., 2005. Removal of pharmaceuticals and fragrances in biological wastewater treatment. *Water Res.* 39(14), 3139-3152.
- Jung, C., Boateng, L.K., Flora, J.R.V., Oh, J., Braswell, M.C., Son, A., Yoon, Y., 2015a. Competitive adsorption of selected non-steroidal anti-inflammatory drugs on activated biochars:

Experimental and molecular modeling study. *Chem. Eng. J.* 264, 1-9.

Jung, C., Oh, J., Yoon, Y., 2015b. Removal of acetaminophen and naproxen by combined coagulation and adsorption using biochar: Influence of combined sewer overflow components. *Environ. Sci. Pollut. R.* 22(13), 10058-10069.

Jung, C., Park, J., Lim, K.H., Park, S., Heo, J., Her, N., Oh, J., Yun, S., Yoon, Y., 2013. Adsorption of selected endocrine disrupting compounds and pharmaceuticals on activated biochars. *J. Hazard. Mater.* 263, 702-710.

Jung, C., Son, A., Her, N., Zoh, K.D., Cho, J., Yoon, Y., 2015c. Removal of endocrine disrupting compounds, pharmaceuticals, and personal care products in water using carbon nanotubes: A review. *J. Ind. Eng. Chem.* 27, 1-11.

Jurado, A., Mastroianni, N., Vázquez-Suñé, E., Carrera, J., Tubau, I., Pujades, E., Postigo, C., de Alda, M.L., Barceló, D., 2012. Drugs of abuse in urban groundwater. A case study: Barcelona. *Sci. Total Environ.* 424, 280-288.

Kaniou, S., Pitarakis, K., Barlagianni, I., Poullos, I., 2005. Photocatalytic oxidation of sulfamethazine. *Chemosphere.* 60(3), 372-380.

Karoyo, A.H., Wilson, L.D., 2013. Tunable macromolecular-based materials for the adsorption of perfluorooctanoic and octanoic acid anions. *J. Colloid Interface Sci.* 402, 196-203.

Karthikeyan, K.G., Meyer, M.T., 2006. Occurrence of antibiotics in wastewater treatment facilities in Wisconsin, USA. *Sci. Total Environ.* 361(1-3), 196-207.

Kasprzyk-Hordern, B., Dinsdale, R.M., Guwy, A.J., 2009. Illicit drugs and pharmaceuticals in the environment - Forensic applications of environmental data, Part 2: Pharmaceuticals as chemical markers of faecal water contamination. *Environ. Pollut.* 157(6), 1778-1786.

Keen, O.S., Baik, S., Linden, K.G., Aga, D.S., Love, N.G., 2012. Enhanced biodegradation of carbamazepine after UV/H₂O₂ advanced oxidation. *Environ. Sci. Technol.* 46(11), 6222-6227.

Keen, O.S., Linden, K.G., 2013. Re-engineering an artificial sweetener: Transforming sucralose residuals in water via advanced oxidation. *Environ. Sci. Technol.* 47(13), 6799-6805.

Khetan, S.K., Collins, T.J., 2007. Human pharmaceuticals in the aquatic environment: A challenge to green chemistry. *Chem. Rev.* 107(6), 2319-2364.

Kim, E., Jung, C., Han, J., Her, N., Park, C.M., Jang, M., Son, A., Yoon, Y., 2016. Sorptive removal of selected emerging contaminants using biochar in aqueous solution. *J. Ind. Eng. Chem.* 36, 364-371.

Kim, H.K., Kim, J.H., Lee, B.C., Yu, S.J., Kim, H.J., 2009a. Occurrence of perchlorate in drinking water sources in Korea. *Wa. Sci. Technol.* 9, 133-139.

Kim, I., Tanaka, H., 2009. Photodegradation characteristics of PPCPs in water with UV treatment. *Environ. Int.* 35(5), 793-802.

Kim, I., Yamashita, N., Tanaka, H., 2009b. Performance of UV and UV/H₂O₂ processes for the removal of pharmaceuticals detected in secondary effluent of a sewage treatment plant in Japan. *J. Hazard. Mater.* 166(2-3), 1134-1140.

Kim, I.H., Yamashita, N., Kato, Y., Tanaka, H., 2009c. Discussion on the application of UV/H₂O₂, O₃ and O₃/UV processes as technologies for sewage reuse considering the removal of pharmaceuticals and personal care products. *Water Sci. Technol.* 59, 945-955.

Kissa, E., 2001. Fluorinated surfactants and repellents. CRC Press.

Klaine, S.J., Alvarez, P.J.J., Batley, G.E., Fernandes, T.F., Handy, R.D., Lyon, D.Y., Mahendra, S., McLaughlin, M.J., Lead, J.R., 2008. Nanomaterials in the environment: Behavior, fate, bioavailability, and effects. *Environ. Toxicol. Chem.* 27(9), 1825-1851.

Kleinmann, R.L.P., Hedin, R.S., 1993. Treat mine water using passive methods. *Pollut. Eng.*

25(13), 20-22.

Kleywegt, S., Pileggi, V., Yang, P., Hao, C., Zhao, X., Rocks, C., Thach, S., Cheung, P., Whitehead, B., 2011. Pharmaceuticals, hormones and bisphenol A in untreated source and finished drinking water in Ontario, Canada - Occurrence and treatment efficiency. *Sci. Total Environ.* 409(8), 1481-1488.

Kolpin, D.W., Furlong, E.T., Meyer, M.T., Thurman, E.M., Zaugg, S.D., Barber, L.B., Buxton, H.T., 2002. Pharmaceuticals, hormones, and other organic wastewater contaminants in U.S. streams, 1999-2000: A national reconnaissance. *Environ. Sci. Technol.* 36(6), 1202-1211.

König, A., Weidauer, C., Seiwert, B., Reemtsma, T., Unger, T., Jekel, M., 2016. Reductive transformation of carbamazepine by abiotic and biotic processes. *Water Res.* 101, 272-280.

Konstantinou, I.K., Albanis, T.A., 2004. TiO₂-assisted photocatalytic degradation of azo dyes in aqueous solution: Kinetic and mechanistic investigations: A review. *Appl. Catal. , B.* 49(1), 1-14.

Kosmulski, M., 2009. pH-dependent surface charging and points of zero charge. IV. Update and new approach. *J. Colloid Interface Sci.* 337(2), 439-448.

Kotthoff, M., Müller, J., Jüriling, H., Schlummer, M., Fiedler, D., 2015. Perfluoroalkyl and polyfluoroalkyl substances in consumer products. *Environ. Sci. Pollut. R.* 22(19), 14546-14559.

Kroger, M., Meister, K., Kava, R., 2006. Low-calorie sweeteners and other sugar substitutes: A review of the safety issues. *Compr. Rev. Food Sci. Food Saf.* 5(2), 35-47.

Kumagai, Y., Lin, L.Y., Schmitz, D.A., Cho, A.K., 1991. Hydroxyl radical mediated demethylenation of (methylenedioxy)phenyl compounds. *Chem. Res. Toxicol.* 4(3), 330-334.

Kupryianchuk, D., Hale, S.E., Breedveld, G.D., Cornelissen, G., 2016. Treatment of sites contaminated with perfluorinated compounds using biochar amendment. *Chemosphere.* 142, 35-40.

Kurissery, S., Kanavillil, N., Verenitch, S., Mazumder, A., 2012. Caffeine as an anthropogenic marker of domestic waste: A study from Lake Simcoe watershed. *Ecol. Indic.* 23, 501-508.

Lai, F.Y., Bruno, R., Leung, H.W., Thai, P.K., Ort, C., Carter, S., Thompson, K., Lam, P.K.S., Mueller, J.F., 2013. Estimating daily and diurnal variations of illicit drug use in Hong Kong: A pilot study of using wastewater analysis in an Asian metropolitan city. *Forensic Sci. Int.* 233(1-3), 126-132.

Lam, M.W., Mabury, S.A., 2005. Photodegradation of the pharmaceuticals atorvastatin, carbamazepine, levofloxacin, and sulfamethoxazole in natural waters. *Aquat. Sci.* 67(2), 177-188.

Lange, F.T., Scheurer, M., Brauch, H.J., 2012. Artificial sweeteners-A recently recognized class of emerging environmental contaminants: A review. *Anal. Bioanal. Chem.* 403(9), 2503-2518.

Lapworth, D.J., Baran, N., Stuart, M.E., Ward, R.S., 2012. Emerging organic contaminants in groundwater: A review of sources, fate and occurrence. *Environ. Pollut.* 163, 287-303.

Larcher, S., Yargeau, V., 2012. Biodegradation of sulfamethoxazole: Current knowledge and perspectives. *Appl. Microbiol. Biot.* 96(2), 309-318.

Lavine, B.K., Auslander, G., Ritter, J., 2001. Polarographic studies of zero valent iron as a reductant for remediation of nitroaromatics in the environment. *Microchem. J.* 70(2), 69-83.

Lee, J.-W., Kong, S., Kim, W.-S., Kim, J., 2007. Preparation and characterization of SiO₂/TiO₂ core-shell particles with controlled shell thickness. *Mater. Chem. Phys.* 106(1), 39-44.

Lee, T.R., Wilkin, R.T., 2010. Iron hydroxy carbonate formation in zerovalent iron permeable reactive barriers: Characterization and evaluation of phase stability. *J. Contam. Hydrol.* 116(1-4), 47-57.

Lee, W., Batchelor, B., 2002. Abiotic reductive dechlorination of chlorinated ethylenes by iron-bearing soil minerals. 2. Green rust. *Environ. Sci. Technol.* 36(24), 5348-5354.

- Lee, Y.C., Lo, S.L., Chiueh, P.T., Chang, D.G., 2009. Efficient decomposition of perfluorocarboxylic acids in aqueous solution using microwave-induced persulfate. *Water Res.* 43(11), 2811-2816.
- Lehmann, J., Joseph, S., 2009. *Biochar for Environmental Management: Science and Technology*. Earthscan, London, UK.
- Leshuk, T., Everett, P., Krishnakumar, H., Wong, K., Linley, S., Gu, F., 2013. Mesoporous magnetically recyclable photocatalysts for water treatment. *J. Nanosci. Nanotechnol.* 13, 3127-3132.
- Leung, A.M., Pearce, E.N., Braverman, L.E., 2010. Perchlorate, iodine and the thyroid. *Best. Pract. Res. Cl. En.* 24(1), 133-141.
- Li, A.J., Schmitz, O.J., Stephan, S., Lenzen, C., Yue, P.Y.K., Li, K., Li, H., Leung, K.S.Y., 2016. Photocatalytic transformation of acesulfame: Transformation products identification and embryotoxicity study. *Water Res.* 89, 68-75.
- Li, H., Helm, P.A., Metcalfe, C.D., 2010a. Sampling in the great lakes for pharmaceuticals, personal care products, and endocrine-disrupting substances using the passive polar organic chemical integrative sampler. *Environ. Toxicol. Chem.* 29(4), 751-762.
- Li, X.Q., Elliott, D.W., Zhang, W.X., 2006. Zero-valent iron nanoparticles for abatement of environmental pollutants: Materials and engineering aspects. *Crit. Rev. Solid State Mater. Sci.* 31(4), 111-122.
- Li, Z.H., Li, P., Rodina, M., Randak, T., 2010b. Effect of human pharmaceutical carbamazepine on the quality parameters and oxidative stress in common carp (*Cyprinus carpio* L.) spermatozoa. *Chemosphere.* 80(5), 530-534.
- Light, T., 1972. Standard solution for redox potential measurements. *Anal. Chem.* 44(6), 1038-1039.
- Lin, A.Y.C., Plumlee, M.H., Reinhard, M., 2006. Natural attenuation of pharmaceuticals and alkylphenol polyethoxylate metabolites during river transport: Photochemical and biological transformation. *Environ. Toxicol. Chem.* 25(6), 1458-1464.
- Lin, A.Y.C., Reinhard, M., 2005. Photodegradation of common environmental pharmaceuticals and estrogens in river water. *Environ. Toxicol. Chem.* 24(6), 1303-1309.
- Lin, H., Wang, Y., Niu, J., Yue, Z., Huang, Q., 2015a. Efficient sorption and removal of perfluoroalkyl acids (PFAAs) from aqueous solution by metal hydroxides generated in situ by electrocoagulation. *Environ. Sci. Technol.* 49(17), 10562-10569.
- Lin, H., Wu, J., Oturan, N., Zhang, H., Oturan, M.A., 2016. Degradation of artificial sweetener saccharin in aqueous medium by electrochemically generated hydroxyl radicals. *Environ. Sci. Pollut. R.* 23(5), 4442-4453.
- Lin, K., Gan, J., 2011. Sorption and degradation of wastewater-associated non-steroidal anti-inflammatory drugs and antibiotics in soils. *Chemosphere.* 83(3), 240-246.
- Lin, S.Y., Chen, W.F., Cheng, M.T., Li, Q., 2013. Investigation of factors that affect cationic surfactant loading on activated carbon and perchlorate adsorption. *Colloids Surf. A Physicochem. Eng. Asp.* 434, 236-242.
- Lin, Y.C., Lai, W.W.P., Tung, H.H., Lin, A.Y.C., 2015b. Occurrence of pharmaceuticals, hormones, and perfluorinated compounds in groundwater in Taiwan. *Environ. Monit. Assess.* 187(5).
- Lindsay, M.B.J., Wakeman, K.D., Rowe, O.F., Grail, B.M., Ptacek, C.J., Blowes, D.W., Johnson, D.B., 2011. Microbiology and geochemistry of mine tailings amended with organic carbon for passive treatment of pore water. *Geomicrobiol. J.* 28(3), 229-241.

- Lindsay, S.S., Baedecker, M.J. 1988. Determination of aqueous sulfide in contaminated and natural water using the methylene blue method. in: *Ground-water Contamination: Field Methods*, (Ed.) Collins, A.G., Johnson, A. I., American Society for Testing and Materials. Philadelphia, pp. 349-357.
- Linley, S., Leshuk, T., Gu, F., 2013. Synthesis of magnetic rattle-type nanostructures for use in water treatment. *ACS Appl. Mater. Interfaces*. 5(7), 2540-2548.
- Linley, S., Liu, Y., Ptacek, C.J., Blowes, D.W., Gu, F.X., 2014. Recyclable graphene oxide-supported titanium dioxide photocatalysts with tunable properties. *ACS Appl. Mater. Interfaces*. 6(7), 4658-4668.
- Lishman, L., Smyth, S.A., Sarafin, K., Kleywegt, S., Toito, J., Peart, T., Lee, B., Servos, M., Beland, M., Seto, P., 2006. Occurrence and reductions of pharmaceuticals and personal care products and estrogens by municipal wastewater treatment plants in Ontario, Canada. *Sci. Total Environ*. 367(2-3), 544-558.
- Liu, B., Zhang, H., Xie, L., Li, J., Wang, X., Zhao, L., Wang, Y., Yang, B., 2015a. Spatial distribution and partition of perfluoroalkyl acids (PFAAs) in rivers of the Pearl River Delta, southern China. *Sci. Total Environ*. 524-525, 1-7.
- Liu, C., Liu, J., 2016. Aerobic biotransformation of polyfluoroalkyl phosphate esters (PAPs) in soil. *Environ. Pollut*. 212, 230-237.
- Liu, H., Bruton, T.A., Doyle, F.M., Sedlak, D.L., 2014a. In situ chemical oxidation of contaminated groundwater by persulfate: Decomposition by Fe(III)- and Mn(IV)-containing oxides and aquifer materials. *Environ. Sci. Technol*. 48(17), 10330-10336.
- Liu, J., Mejia Avendaño, S., 2013. Microbial degradation of polyfluoroalkyl chemicals in the environment: A review. *Environ. Int*. 61, 98-114.
- Liu, P., 2016. *Stabilization of Mercury in River Water and Sediment Using Biochars*. (Doctor of Philosophy). University of Waterloo, Waterloo, Ontario, Canada.
- Liu, P., Ptacek, C.J., Blowes, D.W., Berti, W.R., Landis, R.C., 2015b. Aqueous leaching of organic acids and dissolved organic carbon from various biochars prepared at different temperatures. *J. Environ. Qual*. 44(2), 684-695.
- Liu, P., Ptacek, C.J., Blowes, D.W., Landis, R.C., 2016a. Mechanisms of mercury removal by biochars produced from different feedstocks determined using X-ray absorption spectroscopy. *J. Hazard. Mater*. 308, 233-242.
- Liu, X., Zhang, X., Shao, K., Lin, C., Li, C., Ge, F., Dong, Y., 2016b. Fe⁰-activated persulfate-assisted mechanochemical destruction of expired compound sulfamethoxazole tablets. *RSC Advances*. 6(25), 20938-20948.
- Liu, Y., Chen, S., Quan, X., Yu, H., Zhao, H., Zhang, Y., 2015c. Efficient mineralization of perfluorooctanoate by electro-fenton with H₂O₂ electro-generated on hierarchically porous carbon. *Environ. Sci. Technol*. 49(22), 13528-13533.
- Liu, Y., Wang, J., 2013. Degradation of sulfamethazine by gamma irradiation in the presence of hydrogen peroxide. *J. Hazard. Mater*. 250-251, 99-105.
- Liu, Y.Y., Blowes, D.W., Groza, L., Sabourin, M.J., Ptacek, C.J., 2014b. Acesulfame-K and pharmaceuticals as co-tracers of municipal wastewater in a receiving river. *Environ. Sci.: Processes Impacts*. 16(12), 2789-2795.
- Liu, Y.Y., Ptacek, C.J., Blowes, D.W., 2014c. Treatment of dissolved perchlorate, nitrate, and sulfate using zero-valent iron and organic carbon. *J. Environ. Qual*. 43(3), 842-850.
- Logan, B.E., LaPoint, D., 2002. Treatment of perchlorate- and nitrate-contaminated groundwater in an autotrophic, gas phase, packed-bed bioreactor. *Water Res*. 36(14), 3647-3653.

- Lopez-Espinosa, M.J., Fletcher, T., Armstrong, B., Genser, B., Dhataraya, K., Mondal, D., Ducatman, A., Leonardi, G., 2011. Association of perfluorooctanoic acid (PFOA) and perfluorooctane sulfonate (PFOS) with age of puberty among children living near a chemical plant. *Environ. Sci. Technol.* 45(19), 8160-8166.
- Lubick, N., 2008. Artificial sweetener persists in the environment. *Environ. Sci. Technol.* 42(9), 3125.
- Lubick, N., 2009. Artificial sweetener makes ideal tracer. *Environ. Sci. Technol.* 43(12), 4220.
- Machado, S., Stawiński, W., Slonina, P., Pinto, A.R., Grosso, J.P., Nouws, H.P.A., Albergaria, J.T., Delerue-Matos, C., 2013. Application of green zero-valent iron nanoparticles to the remediation of soils contaminated with ibuprofen. *Sci. Total Environ.* 461-462, 323-329.
- Mackulák, T., Birošová, L., Bodík, I., Grabic, R., Takáčová, A., Smolinská, M., Hanusová, A., Híveš, J., Gál, M., 2016. Zerovalent iron and iron(VI): Effective means for the removal of psychoactive pharmaceuticals and illicit drugs from wastewaters. *Sci. Total Environ.* 539, 420-426.
- Mahmudov, R., Huang, C.P., 2010. Perchlorate removal by activated carbon adsorption. *Sep. Purif. Technol.* 70(3), 329-337.
- Mailler, R., Gasperi, J., Coquet, Y., Deshayes, S., Zedek, S., Cren-Olivé, C., Cartiser, N., Eudes, V., Bressy, A., Caupos, E., Moilleron, R., Chebbo, G., Rocher, V., 2014. Study of a large scale powdered activated carbon pilot: Removals of a wide range of emerging and priority micropollutants from wastewater treatment plant effluents. *Water Res.* 72, 315-330.
- Mailler, R., Gasperi, J., Coquet, Y., Deshayes, S., Zedek, S., Cren-Olivé, C., Cartiser, N., Eudes, V., Bressy, A., Caupos, E., Moilleron, R., Chebbo, G., Rocher, V., 2015. Study of a large scale powdered activated carbon pilot: Removals of a wide range of emerging and priority micropollutants from wastewater treatment plant effluents. *Water Res.* 72, 315-330.
- Makovec, D., Sajko, M., Selišnik, A., Drogenik, M., 2011. Magnetically recoverable photocatalytic nanocomposite particles for water treatment. *Mater. Chem. Phys.* 129(1-2), 83-89.
- Malarvizhi, A., Kavitha, C., Saravanan, M., Ramesh, M., 2012. Carbamazepine (CBZ) induced enzymatic stress in gill, liver and muscle of a common carp, *Cyprinus carpio*. *J. King Saud Univ. Sci.* 24(2), 179-186.
- Malato, S., Fernández-Ibáñez, P., Maldonado, M.I., Blanco, J., Gernjak, W., 2009. Decontamination and disinfection of water by solar photocatalysis: Recent overview and trends. *Catal. Today.* 147(1), 1-59.
- Margot, J., Kienle, C., Magnet, A., Weil, M., Rossi, L., de Alencastro, L.F., Abegglen, C., Thonney, D., Chèvre, N., Schäfer, M., Barry, D.A., 2013. Treatment of micropollutants in municipal wastewater: Ozone or powdered activated carbon? *Sci. Total Environ.* 461-462, 480-498.
- Marques, R.R.N., Sampaio, M.J., Carrapiço, P.M., Silva, C.G., Morales-Torres, S., Dražić, G., Faria, J.L., Silva, A.M.T., 2013. Photocatalytic degradation of caffeine: Developing solutions for emerging pollutants. *Catal. Today.* 209, 108-115.
- Martín, J., Camacho-Muñoz, D., Santos, J.L., Aparicio, I., Alonso, E., 2011. Monitoring of pharmaceutically active compounds on the Guadalquivir River basin (Spain): Occurrence and risk assessment. *J. Environ. Monit.* 13(7), 2042-2049.
- Martin, J.W., Mabury, S.A., Solomon, K.R., Muir, D.C.G., 2003. Dietary accumulation of perfluorinated acids in juvenile rainbow trout (*Oncorhynchus mykiss*). *Environ. Toxicol. Chem.* 22(1), 189-195.
- Martínez-Hernández, V., Meffe, R., Herrera López, S., de Bustamante, I., 2016. The role of

sorption and biodegradation in the removal of acetaminophen, carbamazepine, caffeine, naproxen and sulfamethoxazole during soil contact: A kinetics study. *Sci. Total Environ.* 559, 232-241.

Martínez-Hernández, V., Meffe, R., Herrera, S., Arranz, E., de Bustamante, I., 2014. Sorption/desorption of non-hydrophobic and ionisable pharmaceutical and personal care products from reclaimed water onto/from a natural sediment. *Sci. Total Environ.* 472, 273-281.

Matamoros, V., Duhec, A., Albaigés, J., Bayona, J.M., 2009. Photodegradation of carbamazepine, ibuprofen, ketoprofen and 17 α -ethinylestradiol in fresh and seawater. *Water Air Soil Pollut.* 196(1-4), 161-168.

Matheson, L.J., Tratnyek, P.G., 1994. Reductive dehalogenation of chlorinated methanes by iron metal. *Environ. Sci. Technol.* 28(12), 2045-2053.

Mawhinney, D.B., Young, R.B., Vanderford, B.J., Borch, T., Snyder, S.A., 2011. Artificial sweetener sucralose in U.S. drinking water systems. *Environ. Sci. Technol.* 45(20), 8716-8722.

Melse-Boonstra, A., Jaiswal, N., 2010. Iodine deficiency in pregnancy, infancy and childhood and its consequences for brain development. *Best. Pract. Res. Cl. En.* 24(1), 29-38.

Méndez-Arriaga, F., Esplugas, S., Giménez, J., 2008a. Photocatalytic degradation of non-steroidal anti-inflammatory drugs with TiO₂ and simulated solar irradiation. *Water Res.* 42(3), 585-594.

Méndez-Arriaga, F., Gimenez, J., Esplugas, S., 2008b. Photolysis and TiO₂ photocatalytic treatment of naproxen: Degradation, mineralization, intermediates and toxicity. *J. Adv. Oxid. Technol.* 11(3), 435-444.

Mendez, W., Dederick, E., Cohen, J., 2010. Drinking water contribution to aggregate perchlorate intake of reproductive-age women in the United States estimated by dietary intake simulation and analysis of urinary excretion data. *J. Expo. Sci. Environ. Epidemiol.* 20(3), 288-297.

Merino, N., Qu, Y., Deeb, R.A., Hawley, E.L., Hoffmann, M.R., Mahendra, S., 2016. Degradation and removal methods for perfluoroalkyl and polyfluoroalkyl substances in water. *Environ. Eng. Sci.* 33(9), 615-649.

Metcalf, C., Tindale, K., Li, H., Rodayan, A., Yargeau, V., 2010a. Illicit drugs in Canadian municipal wastewater and estimates of community drug use. *Environ. Pollut.* 158(10), 3179-3185.

Metcalf, C.D., Chu, S., Judt, C., Li, H., Oakes, K.D., Servos, M.R., Andrews, D.M., 2010b. Antidepressants and their metabolites in municipal wastewater, and downstream exposure in an urban watershed. *Environ. Toxicol. Chem.* 29(1), 79-89.

Metcalf, C.D., Koenig, B.G., Bennie, D.T., Servos, M., Ternes, T.A., Hirsch, R., 2003a. Occurrence of neutral and acidic drugs in the effluents of Canadian sewage treatment plants. *Environ. Toxicol. Chem.* 22(12), 2872-2880.

Metcalf, C.D., Miao, X.S., Koenig, B.G., Struger, J., 2003b. Distribution of acidic and neutral drugs in surface waters near sewage treatment plants in the lower Great Lakes, Canada. *Environ. Toxicol. Chem.* 22(12), 2881-2889.

Miao, X.S., Bishay, F., Chen, M., Metcalfe, C.D., 2004. Occurrence of antimicrobials in the final effluents of wastewater treatment plants in Canada. *Environ. Sci. Technol.* 38(13), 3533-3541.

Miao, X.S., Yang, J.J., Metcalfe, C.D., 2005. Carbamazepine and its metabolites in wastewater and in biosolids in a municipal wastewater treatment plant. *Environ. Sci. Technol.* 39(19), 7469-7475.

Milić, N., Milanović, M., Letić, N.G., Sekulić, M.T., Radonić, J., Mihajlović, I., Miloradov, M.V., 2013. Occurrence of antibiotics as emerging contaminant substances in aquatic environment. *Int.*

J. Environ. Heal. R. 23(4), 296-310.

Mimeault, C., Woodhouse, A.J., Miao, X.S., Metcalfe, C.D., Moon, T.W., Trudeau, V.L., 2005. The human lipid regulator, gemfibrozil bioconcentrates and reduces testosterone in the goldfish, *Carassius auratus*. *Aquat. Toxicol.* 73(1), 44-54.

Min, B., Evans, P.J., Chu, A.K., Logan, B.E., 2004. Perchlorate removal in sand and plastic media bioreactors. *Water Res.* 38(1), 47-60.

Min, L., 2012. *Organic Chemistry of Drug Degradation*. The Royal Society of Chemistry, Cambridge, UK.

Minten, J., Adolfsson-Erici, M., Björleinius, B., Alsberg, T., 2011. A method for the analysis of sucralose with electrospray LC/MS in recipient waters and in sewage effluent subjected to tertiary treatment technologies. *Int. J. Environ. Anal. Chem.* 91(4), 357-366.

Moore, D.E., Chappuis, P.P., 1988. A comparative study of the photochemistry of the non-steroidal anti-inflammatory drugs, naproxen, benoxaprofen and indomethacin. *Photochem. Photobiol.* 47(2), 173-180.

Moreira, F.C., Soler, J., Alpendurada, M.F., Boaventura, R.A.R., Brillas, E., Vilar, V.J.P., 2016. Tertiary treatment of a municipal wastewater toward pharmaceuticals removal by chemical and electrochemical advanced oxidation processes. *Water Res.* 105, 251-263.

Moriwaki, H., Takagi, Y., Tanaka, M., Tsuruho, K., Okitsu, K., Maeda, Y., 2005. Sonochemical decomposition of perfluorooctane sulfonate and perfluorooctanoic acid. *Environ. Sci. Technol.* 39(9), 3388-3392.

Morley, N.J., 2009. Environmental risk and toxicology of human and veterinary waste pharmaceutical exposure to wild aquatic host-parasite relationships. *Environ. Toxicol. Pharmacol.* 27(2), 161-175.

Mu, R., Xu, Z., Li, L., Shao, Y., Wan, H., Zheng, S., 2010. On the photocatalytic properties of elongated TiO₂ nanoparticles for phenol degradation and Cr(VI) reduction. *J. Hazard. Mater.* 176(1-3), 495-502.

Mukesh, K., Panday, Y.D., 2001. Chemical corrosion in cast iron in soil-water medium. *Environ. Technol.* 22(2), 137-150.

Mukherjee, A., Zimmerman, A.R., Harris, W., 2011. Surface chemistry variations among a series of laboratory-produced biochars. *Geoderma.* 163(3-4), 247-255.

Müller, C.E., Gerecke, A.C., Alder, A.C., Scheringer, M., Hungerbühler, K., 2011. Identification of perfluoroalkyl acid sources in Swiss surface waters with the help of the artificial sweetener acesulfame. *Environ. Pollut.* 159(5), 1419-1426.

Murnyak, G., Vandenberg, J., Yaroschak, P.J., Williams, L., Prabhakaran, K., Hinz, J., 2011. Emerging contaminants: Presentations at the 2009 Toxicology and Risk Assessment Conference. *Toxicol. Appl. Pharmacol.* 254(2), 167-169.

Myers, A.L., Crozier, P.W., Helm, P.A., Brimacombe, C., Furdui, V.I., Reiner, E.J., Burniston, D., Marvin, C.H., 2012. Fate, distribution, and contrasting temporal trends of perfluoroalkyl substances (PFASs) in Lake Ontario, Canada. *Environ. Int.* 44(1), 92-99.

Naddeo, V., Meriç, S., Kassinos, D., Belgiorno, V., Guida, M., 2009. Fate of pharmaceuticals in contaminated urban wastewater effluent under ultrasonic irradiation. *Water Res.* 43(16), 4019-4027.

Naddeo, V., Uyguner-Demirel, C.S., Prado, M., Cesaro, A., Belgiorno, V., Ballesteros, F., 2015. Enhanced ozonation of selected pharmaceutical compounds by sonolysis. *Environ. Technol. (United Kingdom)*. 36(15), 1876-1883.

Nefau, T., Karolak, S., Castillo, L., Boireau, V., Levi, Y., 2013. Presence of illicit drugs and

metabolites in influents and effluents of 25 sewage water treatment plants and map of drug consumption in France. *Sci. Total Environ.* 461-462, 712-722.

Ngouyap Mouamfon, M.V., Li, W., Lu, S., Chen, N., Qiu, Z., Lin, K., 2011. Photodegradation of sulfamethoxazole applying UV- and VUV-based processes. *Water Air Soil Pollut.* 218(1-4), 265-274.

Ngouyap Mouamfon, M.V., Li, W., Lu, S., Qiu, Z., Chen, N., Lin, K., 2010. Photodegradation of sulphamethoxazole under UV-light irradiation at 254 nm. *Environ. Technol.* 31(5), 489-494.

Nordstrom, D.K., 1977. Thermochemical redox equilibria of ZoBell's solution. *Geochim. Cosmochim. Acta.* 41(12), 1835-1841.

Oaks, J.L., Gilbert, M., Virani, M.Z., Watson, R.T., Meteyer, C.U., Rideout, B.A., Shivaprasad, H.L., Ahmed, S., Chaudhry, M.J.I., Arshad, M., Mahmood, S., Ali, A., Khan, A.A., 2004. Diclofenac residues as the cause of vulture population decline in Pakistan. *Nature.* 427(6975), 630-633.

Ochiai, T., Iizuka, Y., Nakata, K., Murakami, T., Tryk, D.A., Koide, Y., Morito, Y., Fujishima, A., 2011. Efficient decomposition of perfluorocarboxylic acids in aqueous suspensions of a TiO₂ photocatalyst with medium-pressure ultraviolet lamp irradiation under atmospheric pressure. *Ind. Eng. Chem. Res.* 50(19), 10943-10947.

Ochoa-Herrera, V., Field, J.A., Luna-Velasco, A., Sierra-Alvarez, R., 2016. Microbial toxicity and biodegradability of perfluorooctane sulfonate (PFOS) and shorter chain perfluoroalkyl and polyfluoroalkyl substances (PFASs). *Environ. Sci.: Processes Impacts.* 18(9), 1236-1246.

Odziemkowski, M.S., Simpraga, R.P., 2004. Distribution of oxides on iron materials used for remediation of organic groundwater contaminants - Implications for hydrogen evolution reactions. *Can. J. Chem.* 82(10), 1495-1506.

Okeke, B.C., Frankenberger Jr., W.T., 2003. Molecular analysis of a perchlorate reductase from a perchlorate-respiring bacterium *Perclace*. *Microbiol. Res.* 158(4), 337-344.

Okeke, B.C., Frankenberger Jr., W.T., 2005. Use of starch and potato peel waste for perchlorate bioreduction in water. *Sci. Total Environ.* 347(1-3), 35-45.

Okeke, B.C., Giblin, T.L., Frankenberger Jr., W.T., 2002. Reduction of perchlorate and nitrate by salt tolerant bacteria. *Environ. Pollut.* 118(3), 357-363.

Oleszczuk, P., Hale, S.E., Lehmann, J., Cornelissen, G., 2012. Activated carbon and biochar amendments decrease pore-water concentrations of polycyclic aromatic hydrocarbons (PAHs) in sewage sludge. *Bioresour. Technol.* 111, 84-91.

Onesios, K.M., Bouwer, E.J., 2012. Biological removal of pharmaceuticals and personal care products during laboratory soil aquifer treatment simulation with different primary substrate concentrations. *Water Res.* 46(7), 2365-2375.

Orth, W.S., Gillham, R.W., 1996. Dechlorination of trichloroethene in aqueous solution using Fe⁰. *Environ. Sci. Technol.* 30(1), 66-71.

Pal, R., Megharaj, M., Kirkbride, K.P., Naidu, R., 2013. Illicit drugs and the environment - A review. *Sci. Total Environ.* 463-464, 1079-1092.

Pan, C.G., Liu, Y.S., Ying, G.G., 2016. Perfluoroalkyl substances (PFASs) in wastewater treatment plants and drinking water treatment plants: Removal efficiency and exposure risk. *Water Res.* 106, 562-570.

Park, H., Vecitis, C.D., Cheng, J., Choi, W., Mader, B.T., Hoffmann, M.R., 2009. Reductive defluorination of aqueous perfluorinated alkyl surfactants: Effects of ionic headgroup and chain length. *J. Phys. Chem. A.* 113(4), 690-696.

Park, H., Vecitis, C.D., Cheng, J., Dalleska, N.F., Mader, B.T., Hoffmann, M.R., 2011. Reductive

degradation of perfluoroalkyl compounds with aquated electrons generated from iodide photolysis at 254 nm. *Photochem. Photobiol. Sci.* 10(12), 1945-1953.

Parks, G.A., 1965. The isoelectric points of solid oxides, solid hydroxides, and aqueous hydroxo complex systems. *Chem. Rev.* 65(2), 177-198.

Patterson, B.M., Shackleton, M., Furness, A.J., Bekele, E., Pearce, J., Linge, K.L., Busetti, F., Spadek, T., Toze, S., 2011. Behaviour and fate of nine recycled water trace organics during managed aquifer recharge in an aerobic aquifer. *J. Contam. Hydrol.* 122(1-4), 53-62.

Paul, A.G., Jones, K.C., Sweetman, A.J., 2009. A first global production, emission, and environmental inventory for perfluorooctane sulfonate. *Environ. Sci. Technol.* 43(2), 386-392.

Peng, L., Ren, Y., Gu, J., Qin, P., Zeng, Q., Shao, J., Lei, M., Chai, L., 2014. Iron improving bio-char derived from microalgae on removal of tetracycline from aqueous system. *Environ. Sci. Pollut. R.* 21(12), 7631-7640.

Periša, M., Babić, S., Škorić, I., Frömel, T., Knepper, T.P., 2013. Photodegradation of sulfonamides and their N4-acetylated metabolites in water by simulated sunlight irradiation: Kinetics and identification of photoproducts. *Environ. Sci. Pollut. R.* 20(12), 8934-8946.

Perkola, N., Vaalgamaa, S., Jernberg, J., Vähätalo, A.V., 2016. Degradation of artificial sweeteners via direct and indirect photochemical reactions. *Environ. Sci. Pollut. R.* 23(13), 13288-13297.

Post, G.B., Louis, J.B., Lippincott, R.L., Procopio, N.A., 2013. Occurrence of perfluorinated compounds in raw water from New Jersey public drinking water systems. *Environ. Sci. Technol.* 47(23), 13266-13275.

Prieto-Rodriguez, L., Miralles-Cuevas, S., Oller, I., Agüera, A., Puma, G.L., Malato, S., 2012. Treatment of emerging contaminants in wastewater treatment plants (WWTP) effluents by solar photocatalysis using low TiO₂ concentrations. *J. Hazard. Mater.* 211-212, 131-137.

Punyapalakul, P., Suksomboon, K., Prarat, P., Khaodhiar, S., 2013. Effects of surface functional groups and porous structures on adsorption and recovery of perfluorinated compounds by inorganic porous silicas. *Separ. Sci. Technol. (Philadelphia)*. 48(5), 775-788.

Quiñones, O., Snyder, S.A., 2009. Occurrence of perfluoroalkyl carboxylates and sulfonates in drinking water utilities and related waters from the United States. *Environ. Sci. Technol.* 43(24), 9089-9095.

Rahman, A., Agrawal, A. 1997. Reduction of nitrate and nitrite by iron metal: Implications for ground water remediation. in: Extended abstract, Division of Environmental Chemistry, ACS National Meeting, American Chemical Society. San Francisco, CA, pp. 13-17.

Rahman, M.F., Peldszus, S., Anderson, W.B., 2014. Behaviour and fate of perfluoroalkyl and polyfluoroalkyl substances (PFASs) in drinking water treatment: A review. *Water Res.* 50, 318-340.

Rahman, M.F., Yanful, E.K., Jasim, S.Y., Bragg, L.M., Servos, M.R., Ndongue, S., Borikar, D., 2010. Advanced oxidation treatment of drinking water: Part I. occurrence and removal of pharmaceuticals and endocrine-disrupting compounds from Lake Huron water. *Ozone Sci. Eng.* 32(4), 217-229.

Rajagopalan, S., Anderson, T.A., Fahlquist, L., Rainwater, K.A., Ridley, M., Jackson, W.A., 2006. Widespread presence of naturally occurring perchlorate in high plains of Texas and New Mexico. *Environ. Sci. Technol.* 40(10), 3156-3162.

Rajapaksha, A.U., Vithanage, M., Ahmad, M., Seo, D.C., Cho, J.S., Lee, S.E., Lee, S.S., Ok, Y.S., 2015. Enhanced sulfamethazine removal by steam-activated invasive plant-derived biochar. *J. Hazard. Mater.* 290, 43-50.

- Rankin, K., Mabury, S.A., Jenkins, T.M., Washington, J.W., 2016. A North American and global survey of perfluoroalkyl substances in surface soils: Distribution patterns and mode of occurrence. *Chemosphere*. 161, 333-341.
- Rayne, S., Forest, K., 2009. Perfluoroalkyl sulfonic and carboxylic acids: A critical review of physicochemical properties, levels and patterns in waters and wastewaters, and treatment methods. *J. Environ. Sci. Health. A Tox. Hazard. Subst. Environ. Eng.* 44(12), 1145-1199.
- Razavi, B., Song, W., Cooper, W.J., Greaves, J., Jeong, J., 2009. Free-radical-induced oxidative and reductive degradation of fibrate pharmaceuticals: Kinetic studies and degradation mechanisms. *J. Phys. Chem. A*. 113(7), 1287-1294.
- Reungoat, J., Escher, B.I., Macova, M., Argand, F.X., Gernjak, W., Keller, J., 2012. Ozonation and biological activated carbon filtration of wastewater treatment plant effluents. *Water Res.* 46(3), 863-872.
- Richardson, S.D., Ternes, T.A., 2011. Water analysis: Emerging contaminants and current issues. *Anal. Chem.* 83(12), 4616-4648.
- Rikken, G.B., Kroon, A.G.M., Van Ginkel, C.G., 1996. Transformation of (per)chlorate into chloride by a newly isolated bacterium: Reduction and dismutation. *Appl. Microbiol. Biot.* 45(3), 420-426.
- Robertson, W.D., Blowes, D.W., Ptacek, C.J., Cherry, J.A., 2000. Long-term performance of in situ reactive barriers for nitrate remediation. *Ground Water*. 38(5), 689-695.
- Robertson, W.D., Ptacek, C.J., Brown, S.J., 2007. Geochemical and hydrogeological impacts of a wood particle barrier treating nitrate and perchlorate in ground water. *Ground Water Monit. R.* 27(2), 85-95.
- Robertson, W.D., Van Stempvoort, D.R., Solomon, D.K., Homewood, J., Brown, S.J., Spoelstra, J., Schiff, S.L., 2013. Persistence of artificial sweeteners in a 15-year-old septic system plume. *J. Hydrol.* 477, 43-54.
- Rodil, R., Quintana, J.B., Concha-Graña, E., López-Mahía, P., Muniategui-Lorenzo, S., Prada-Rodríguez, D., 2012. Emerging pollutants in sewage, surface and drinking water in Galicia (NW Spain). *Chemosphere*. 86(10), 1040-1049.
- Rodríguez, S., Santos, A., Romero, A., 2016. Oxidation of priority and emerging pollutants with persulfate activated by iron: Effect of iron valence and particle size. *Chem. Eng. J.* 318, 197-205.
- Roldan, M.D., Reyes, F., Moreno-Vivian, C., Castillo, F., 1994. Chlorate and nitrate reduction in the phototrophic bacteria *Rhodobacter capsulatus* and *Rhodobacter sphaeroides*. *Curr. Microbiol.* 29(4), 241-245.
- Rosal, R., Rodríguez, A., Gonzalo, M.S., García-Calvo, E., 2008. Catalytic ozonation of naproxen and carbamazepine on titanium dioxide. *Appl. Catal. , B.* 84(1-2), 48-57.
- Rosario-Ortiz, F.L., Wert, E.C., Snyder, S.A., 2010. Evaluation of UV/H₂O₂ treatment for the oxidation of pharmaceuticals in wastewater. *Water Res.* 44(5), 1440-1448.
- Rusanova, M.Y., Polášková, P., Muzikař, M., Fawcett, W.R., 2006. Electrochemical reduction of perchlorate ions on platinum-activated nickel. *Electrochim. Acta.* 51(15), 3097-3101.
- Safe, S.H., 2000. Endocrine disruptors and human health - Is there a problem? An update. *Environ. Health Perspect.* 108(6), 487-493.
- Sahu, A.K., Conneely, T., Nüsslein, K.R., Ergas, S.J., 2009. Biological perchlorate reduction in packed bed reactors using elemental sulfur. *Environ. Sci. Technol.* 43(12), 4466-4471.
- Sanchez, W., Sremski, W., Piccini, B., Palluel, O., Maillot-Maréchal, E., Betoulle, S., Jaffal, A., Aït-Aïssa, S., Brion, F., Thybaud, E., Hinfray, N., Porcher, J.M., 2011. Adverse effects in wild fish living downstream from pharmaceutical manufacture discharges. *Environ. Int.* 37(8), 1342-

1348.

Sang, Z., Jiang, Y., Tsoi, Y.K., Leung, K.S.Y., 2014a. Evaluating the environmental impact of artificial sweeteners: A study of their distributions, photodegradation and toxicities. *Water Res.* 52, 260-264.

Sang, Z., Jiang, Y., Tsoi, Y.K., Leung, K.S.Y., 2014b. Evaluating the environmental impact of artificial sweeteners: A study of their distributions, photodegradation and toxicities. *Water Res.* 52, 260-264.

Santos, L.H.M.L.M., Araújo, A.N., Fachini, A., Pena, A., Delerue-Matos, C., Montenegro, M.C.B.S.M., 2010. Ecotoxicological aspects related to the presence of pharmaceuticals in the aquatic environment. *J. Hazard. Mater.* 175(1-3), 45-95.

Scanlon, D.O., Dunnill, C.W., Buckeridge, J., Shevlin, S.A., Logsdail, A.J., Woodley, S.M., Catlow, C.R.A., Powell, M.J., Palgrave, R.G., Parkin, I.P., Watson, G.W., Keal, T.W., Sherwood, P., Walsh, A., Sokol, A.A., 2013. Band alignment of rutile and anatase TiO₂. *Nat. Mater.* 12, 798-801.

Schaffer, M., Boxberger, N., Börnick, H., Licha, T., Worch, E., 2012. Sorption influenced transport of ionizable pharmaceuticals onto a natural sandy aquifer sediment at different pH. *Chemosphere.* 87(5), 513-520.

Schaidler, L.A., Rudel, R.A., Ackerman, J.M., Dunagan, S.C., Brody, J.G., 2014. Pharmaceuticals, perfluorosurfactants, and other organic wastewater compounds in public drinking water wells in a shallow sand and gravel aquifer. *Sci. Total Environ.* 468-469, 384-393.

Scherer, M.M., Richter, S., Valentine, R.L., Alvarez, P.J.J., 2000. Chemistry and microbiology of permeable reactive barriers for in situ groundwater clean up. *Crit. Rev. Environ. Sci. Technol.* 30(3), 363-411.

Scheurer, M., Brauch, H.J., Lange, F.T., 2009. Analysis and occurrence of seven artificial sweeteners in German waste water and surface water and in soil aquifer treatment (SAT). *Anal. Bioanal. Chem.* 394(6), 1585-1594.

Scheurer, M., Godejohann, M., Wick, A., Happel, O., Ternes, T.A., Brauch, H.J., Ruck, W.K.L., Lange, F.T., 2012. Structural elucidation of main ozonation products of the artificial sweeteners cyclamate and acesulfame. *Environ. Sci. Pollut. R.* 19(4), 1107-1118.

Scheurer, M., Schmutz, B., Happel, O., Brauch, H.J., Wülser, R., Storck, F.R., 2014. Transformation of the artificial sweetener acesulfame by UV light. *Sci. Total Environ.* 481(1), 425-432.

Scheurer, M., Storck, F.R., Brauch, H.J., Lange, F.T., 2010. Performance of conventional multi-barrier drinking water treatment plants for the removal of four artificial sweeteners. *Water Res.* 44(12), 3573-3584.

Scheurer, M., Storck, F.R., Graf, C., Brauch, H.J., Ruck, W., Lev, O., Lange, F.T., 2011. Correlation of six anthropogenic markers in wastewater, surface water, bank filtrate, and soil aquifer treatment. *J. Environ. Monit.* 13(4), 966-973.

Schwarzenbach, R.P., Escher, B.I., Fenner, K., Hofstetter, T.B., Johnson, C.A., Von Gunten, U., Wehrli, B., 2006. The challenge of micropollutants in aquatic systems. *Science.* 313(5790), 1072-1077.

Schwarzenbach, R.P., Gschwend, P.M., Imboden, D.M., 2002. *Environmental Organic Chemistry.* John Wiley & Sons, Inc., New Jersey.

Schwarzenbach, R.P., Gschwend, P.M., Imboden, D.M., 2003. *Environmental Organic Chemistry.* John Wiley & Sons, Inc., New Jersey, USA.

Scott, B.F., Spencer, C., Lopez, E., Muir, D.C.G., 2009. Perfluorinated alkyl acid concentrations

in Canadian rivers and creeks. *Water Qual. Res. J. Can.* 44(3), 263-277.

Segura, Y., Martínez, F., Melero, J.A., 2014. Pharmaceutical wastewater degradation: Effective and economical treatment using waste-metallic iron shavings. *Int. J. Environ. Stud.* 71(2), 200-208.

Seiler, R.L., Zaugg, S.D., Thomas, J.M., Howcroft, D.L., 1999. Caffeine and pharmaceuticals as indicators of waste water contamination in wells. *Ground Water.* 37(3), 405-410.

Seo, P.W., Khan, N.A., Hasan, Z., Jhung, S.H., 2016. Adsorptive removal of artificial sweeteners from water using metal-organic frameworks functionalized with urea or melamine. *ACS Appl. Mater. Interfaces.* 8(43), 29799-29807.

Sharifi, S., Behzadi, S., Laurent, S., Laird Forrest, M., Stroeve, P., Mahmoudi, M., 2012. Toxicity of nanomaterials. *Chem. Soc. Rev.* 41(6), 2323-2343.

Sharma, V.K., Oturan, M., Kim, H., 2014. Oxidation of artificial sweetener sucralose by advanced oxidation processes: A review. *Environ. Sci. Pollut. R.* 21(14), 8525-8533.

Sharma, V.K., Sohn, M., Anquandah, G.A.K., Nesnas, N., 2012. Kinetics of the oxidation of sucralose and related carbohydrates by ferrate(VI). *Chemosphere.* 87(6), 644-648.

Sharpe, R.M., Irvine, D.S., 2004. How strong is the evidence of a link between environmental chemicals and adverse effects on human reproductive health? *Br. Med. J.* 328(7437), 447-451.

Shirazi, E., Torabian, A., Nabi-Bidhendi, G., 2013. Carbamazepine removal from groundwater: Effectiveness of the TiO₂/UV, nanoparticulate zero-valent iron, and fenton (NZVI/H₂O₂) processes. *Clean - Soil, Air, Water.* 41(11), 1062-1072.

Shoemaker, J.A., Grimmett, P. E., & Boutin, B. K. . 2013. Method 537. Determination of selected perfluorinated alkyl acids in drinking water by solid phase extraction and liquid chromatography/tandem mass spectrometry (LC/MS/MS), Vol. EPA/ 600/ R-08/092, U.S. Environmental Protection Agency, Office of Research and Development, National Exposure Research Laboratory. Cincinnati, OH., USA.

Shrimpton, H.K., Blowes, D.W., Ptacek, C.J., 2015. Fractionation of selenium during selenate reduction by granular zerovalent iron. *Environ. Sci. Technol.* 49(19), 11688-11696.

Sijimol, M.R., Jyothy, S., Pradeepkumar, A.P., Chandran, M.S.S., Ghose, S.S., Mohan, M., 2015. Review on fate, toxicity, and remediation of perchlorate. *Environ. Forensics.* 16(2), 125-134.

Smith, L.J.D., Ptacek, C.J., Blowes, D.W., Groza, L.G., Moncur, M.C., 2015. Perchlorate in lake water from an operating diamond mine. *Environ. Sci. Technol.* 49(13), 7589-7596.

Snyder, S.A., Vanderford, B.J., Rexing, D.J., 2005. Trace analysis of bromate, chlorate, iodate, and perchlorate in natural and bottled waters. *Environ. Sci. Technol.* 39(12), 4586-4593.

Song, Z., Tang, H., Wang, N., Zhu, L., 2013. Reductive defluorination of perfluorooctanoic acid by hydrated electrons in a sulfite-mediated UV photochemical system. *J. Hazard. Mater.* 262, 332-338.

Sonthiphand, P., Cejudo, E., Schiff, S.L., Neufeld, J.D., 2013. Wastewater effluent impacts ammonia-oxidizing prokaryotes of the Grand River, Canada. *Appl. Environ. Microbiol.* 79(23), 7454-7465.

Sorensen, J.P.R., Lapworth, D.J., Nkhuwa, D.C.W., Stuart, M.E., Gooddy, D.C., Bell, R.A., Chirwa, M., Kabika, J., Liemisa, M., Chibesa, M., Pedley, S., 2015. Emerging contaminants in urban groundwater sources in Africa. *Water Res.* 72, 51-63.

Sotelo, J.L., Ovejero, G., Rodríguez, A., Álvarez, S., Galán, J., García, J., 2014. Competitive adsorption studies of caffeine and diclofenac aqueous solutions by activated carbon. *Chem. Eng. J.* 240, 443-453.

- Spoelstra, J., Schiff, S.L., Brown, S.J., 2013. Artificial sweeteners in a large Canadian river reflect human consumption in the watershed. *PloS one*. 8(12), e82706.
- Srinivasan, A., Viraraghavan, T., 2009. Perchlorate: Health effects and technologies for its removal from water resources. *Int. J. Environ. Res. Public Health*. 6(4), 1418-1442.
- Srinivasan, R., Sorial, G.A., 2009. Treatment of perchlorate in drinking water: A critical review. *Sep. Purif. Technol.* 69(1), 7-21.
- Stackelberg, P.E., Gibs, J., Furlong, E.T., Meyer, M.T., Zaugg, S.D., Lippincott, R.L., 2007. Efficiency of conventional drinking-water-treatment processes in removal of pharmaceuticals and other organic compounds. *Sci. Total Environ.* 377(2-3), 255-272.
- Stafiej, A., Pyrzynska, K., Regan, F., 2007. Determination of anti-inflammatory drugs and estrogens in water by HPLC with UV detection. *J. Sep. Sci.* 30(7), 985-991.
- Stöber, W., Fink, A., Bohn, E., 1968. Controlled growth of monodisperse silica spheres in the micron size range. *J. Colloid Interface Sci.* 26(1), 62-69.
- Sturini, M., Speltini, A., Maraschi, F., Profumo, A., Pretali, L., Irastorza, E.A., Fasani, E., Albini, A., 2012. Photolytic and photocatalytic degradation of fluoroquinolones in untreated river water under natural sunlight. *Appl. Catal., B*. 119-120, 32-39.
- Suja, F., Pramanik, B.K., Zain, S.M., 2009. Contamination, bioaccumulation and toxic effects of perfluorinated chemicals (PFCs) in the water environment: A review paper. *Water Sci. Technol.* 60(6), 1533-1554.
- Sujana, M.G., Soma, G., Vasumathi, N., Anand, S., 2009. Studies on fluoride adsorption capacities of amorphous Fe/Al mixed hydroxides from aqueous solutions. *J. Fluorine Chem.* 130(8), 749-754.
- Sumpter, J.P., 2005. Endocrine disrupters in the aquatic environment: An overview. *Acta Hydrochim. Hydrobiol.* 33(1), 9-16.
- Sun, Y., Li, J., Huang, T., Guan, X., 2016. The influences of iron characteristics, operating conditions and solution chemistry on contaminants removal by zero-valent iron: A review. *Water Res.* 100, 277-295.
- Suttiaponarnit, K., Jiang, J., Sahu, M., Suvachittanont, S., Charinpanitkul, T., Biswas, P., 2011. Role of surface area, primary particle size, and crystal phase on titanium dioxide nanoparticle dispersion properties. *Nanoscale Res. Lett.* 6(1), 1-8.
- Tan, K., Anderson, T.A., Jackson, W.A., 2004. Degradation kinetics of perchlorate in sediments and soils. *Water Air Soil Pollut.* 151(1-4), 245-259.
- Tay, K.S., Madehi, N., 2015. Ozonation of ofloxacin in water: By-products, degradation pathway and ecotoxicity assessment. *Sci. Total Environ.* 520, 23-31.
- Ternes, T.A., 1998. Occurrence of drugs in German sewage treatment plants and rivers. *Water Res.* 32(11), 3245-3260.
- Tikkanen, M.W., 2006. Development of a drinking water regulation for perchlorate in California. *Anal. Chim. Acta.* 567(1 SPEC. ISS.), 20-25.
- Till, B.A., Weathers, L.J., Alvarez, P.J.J., 1998. Fe(0)-supported autotrophic denitrification. *Environ. Sci. Technol.* 32(5), 634-639.
- Tomizawa, M., Kurosu, S., Kobayashi, M., Kawase, Y., 2016. Zero-valent iron treatment of dark brown colored coffee effluent: Contributions of a core-shell structure to pollutant removals. *J. Environ. Manage.* 183, 478-487.
- Tong, A.Y.C., Braund, R., Warren, D.S., Peake, B.M., 2012. TiO₂-assisted photodegradation of pharmaceuticals - A review. *Cent. Eur. J. Chem.* 10(4), 989-1027.
- Toride, N., Leij, F.J., Van Genuchten, M.T. 1995. The CXTFIT code for estimating transport

parameters from laboratory or field tracer experiments. U.S. Salinity Laboratory, Agricultural Research Service. 137.

Toth, J.E., Rickman, K.A., Venter, A.R., Kiddle, J.J., Mezyk, S.P., 2012. Reaction kinetics and efficiencies for the hydroxyl and sulfate radical based oxidation of artificial sweeteners in water. *J. Phys. Chem. A*. 116(40), 9819-9824.

Tungudomwongsa, H., Leckie, J., Mill, T., 2006. Photocatalytic oxidation of emerging contaminants: Kinetics and pathways for photocatalytic oxidation of pharmaceutical compounds. *J. Adv. Oxid. Technol.* 9(1), 59-64.

Uchimiya, M., Lima, I.M., Thomas Klasson, K., Chang, S., Wartelle, L.H., Rodgers, J.E., 2010. Immobilization of heavy metal ions (Cu^{II} , Cd^{II} , Ni^{II} , and Pb^{II}) by broiler litter-derived biochars in water and soil. *J. Agric. Food Chem.* 58(9), 5538-5544.

Underwood, J.C., Harvey, R.W., Metge, D.W., Repert, D.A., Baumgartner, L.K., Smith, R.L., Roane, T.M., Barber, L.B., 2011. Effects of the antimicrobial sulfamethoxazole on groundwater bacterial enrichment. *Environ. Sci. Technol.* 45(7), 3096-3101.

United Nations Environment Programme, 2009. Stockholm convention persistent organic pollutants.SC-4/17: listing of perfluorooctane sulfonic acid, its salts and perfluorooctane sulfonyl fluoride.

Urbansky, E., 2002. Perchlorate as an environmental contaminant. *Environ. Sci. Pollut. R.* 9(3), 187-192.

Urbansky, E.T., Brown, S.K., Magnuson, M.L., Kelty, C.A., 2001. Perchlorate levels in samples of sodium nitrate fertilizer derived from Chilean caliche. *Environ. Pollut.* 112(3), 299-302.

US EPA, 2005. Integrated Risk Information System (IRIS). 2005. "Perchlorate and Perchlorate Salts." www.epa.gov/iris/subst/1007.htm.

US EPA, 2006. Drinking water contaminant candidate list (CCL) and regulatory determination.

US EPA, 2009a. Provisional health advisories for perfluorooctanoic acid (PFOA) and perfluorooctane sulfonate (PFOS).

US EPA, 2009b. "Revised Assessment Guidance for Perchlorate." www.epa.gov/fedfac/documents/perchlorate_memo_01-08-09.pdf.

US EPA, 2012. "2012 Edition of the Drinking Water Standards and Health Advisories." EPA 822-S-12-001.

Van Nuijs, A.L.N., Castiglioni, S., Tarcomnicu, I., Postigo, C., de Alda, M.L., Neels, H., Zuccato, E., Barcelo, D., Covaci, A., 2011. Illicit drug consumption estimations derived from wastewater analysis: A critical review. *Sci. Total Environ.* 409(19), 3564-3577.

Van Stempvoort, D.R., Roy, J.W., Brown, S.J., Bickerton, G., 2011. Artificial sweeteners as potential tracers in groundwater in urban environments. *J. Hydrol.* 401(1-2), 126-133.

Van Stempvoort, D.R., Roy, J.W., Grabuski, J., Brown, S.J., Bickerton, G., Sverko, E., 2013. An artificial sweetener and pharmaceutical compounds as co-tracers of urban wastewater in groundwater. *Sci. Total Environ.* 461-462, 348-359.

Vandenberg, L.N., Colborn, T., Hayes, T.B., Heindel, J.J., Jacobs, D.R., Lee, D.H., Shioda, T., Soto, A.M., vom Saal, F.S., Welshons, W.V., Zoeller, R.T., Myers, J.P., 2012. Hormones and endocrine-disrupting chemicals: Low-dose effects and nonmonotonic dose responses. *Endocr. Rev.* 33(3), 378-455.

Vanderford, B.J., Pearson, R.A., Rexing, D.J., Snyder, S.A., 2003. Analysis of endocrine disruptors, pharmaceuticals, and personal care products in water using liquid chromatography/tandem mass spectrometry. *Anal. Chem.* 75(22), 6265-6274.

Vanderford, B.J., Snyder, S.A., 2006. Analysis of pharmaceuticals in water by isotope dilution

liquid chromatography/tandem mass spectrometry. *Environ. Sci. Technol.* 40(23), 7312-7320.

Vellanki, B.P., Batchelor, B., Abdel-Wahab, A., 2013. Advanced reduction processes: A new class of treatment processes. *Environ. Eng. Sci.* 30(5), 264-271.

Verlicchi, P., Zambello, E., 2014. How efficient are constructed wetlands in removing pharmaceuticals from untreated and treated urban wastewaters? A review. *Sci. Total Environ.* 470-471, 1281-1306.

Verliefde, A.R.D., Heijman, S.G.J., Cornelissen, E.R., Amy, G.L., Van Der Bruggen, B., Van Dijk, J.C., 2008. Rejection of trace organic pollutants with high pressure membranes (NF/RO). *Environ. Prog.* 27(2), 180-188.

Von Ehrenstein, O.S., Fenton, S.E., Kato, K., Kuklenyik, Z., Calafat, A.M., Hines, E.P., 2009. Polyfluoroalkyl chemicals in the serum and milk of breastfeeding women. *Reprod. Toxicol.* 27(3-4), 239-245.

Vymazal, J., Dvořáková Březinová, T., 2016. Removal of saccharin from municipal sewage: The first results from constructed wetlands. *Chem. Eng. J.* 306, 1067-1070.

Wang, B., Zhang, W., Li, H., Fu, H., Qu, X., Zhu, D., 2016. Micropore clogging by leachable pyrogenic organic carbon: A new perspective on sorption irreversibility and kinetics of hydrophobic organic contaminants to black carbon. *Environ. Pollut.* 220, Part B, 1349-1358.

Wang, F., Shih, K., 2011. Adsorption of perfluorooctanesulfonate (PFOS) and perfluorooctanoate (PFOA) on alumina: Influence of solution pH and cations. *Water Res.* 45(9), 2925-2930.

Wang, J., Wang, S., 2016. Removal of pharmaceuticals and personal care products (PPCPs) from wastewater: A review. *J. Environ. Manage.* 182, 620-640.

Wang, L., Li, J., Jiang, Q., Zhao, L., 2012. Water-soluble Fe₃O₄ nanoparticles with high solubility for removal of heavy-metal ions from waste water. *Dalton Trans.* 41(15), 4544-4551.

Wang, Y., Beesoon, S., Benskin, J.P., De Silva, A.O., Genuis, S.J., Martin, J.W., 2011. Enantiomer fractions of chiral perfluorooctanesulfonate (PFOS) in human sera. *Environ. Sci. Technol.* 45(20), 8907-8914.

Wang, Y., Jin, L., Deshusses, M.A., Matsumoto, M.R., 2013. The effects of various amendments on the biostimulation of perchlorate reduction in laboratory microcosm and flowthrough soil columns. *Chem. Eng. J.* 232, 388-396.

Wang, Z., Cousins, I.T., Scheringer, M., Buck, R.C., Hungerbühler, K., 2014. Global emission inventories for C4-C14 perfluoroalkyl carboxylic acid (PFCA) homologues from 1951 to 2030, Part I: Production and emissions from quantifiable sources. *Environ. Int.* 70, 62-75.

Wang, Z., Xie, Z., Mi, W., Möller, A., Wolschke, H., Ebinghaus, R., 2015. Neutral poly/perfluoroalkyl substances in air from the Atlantic to the southern ocean and in Antarctic snow. *Environ. Sci. Technol.* 49(13), 7770-7775.

Ward, C.H., 2008. *In Situ Bioremediation of Perchlorate in Groundwater*. Springer, New York.

Watson, S., Scott, J., Beydoun, D., Amal, R., 2005. Studies on the preparation of magnetic photocatalysts. *J. Nanopart. Res.* 7(6), 691-705.

Watts, C.D., Crathorne, B., Fielding, M., Steel, C.P., 1983. Identification of non-volatile organics in water using field desorption mass spectrometry and high performance liquid chromatography, in: Angeletti, G., Bjorseth, A.(Eds.), *Analysis of Organic Micropollutants in Water*. D.D. Reidel Publishing Co, Oslo, Norway,, pp. 120-131.

Westerhoff, P., Yoon, Y., Snyder, S., Wert, E., 2005. Fate of endocrine-disruptor, pharmaceutical, and personal care product chemicals during simulated drinking water treatment processes. *Environ. Sci. Technol.* 39(17), 6649-6663.

Wilkin, R.T., Fine, D.D., Burnett, N.G., 2007. Perchlorate behavior in a municipal lake following

fireworks displays. *Environ. Sci. Technol.* 41(11), 3966-3971.

Williams, C.F., Adamsen, F.J., 2006. Sorption-desorption of carbamazepine from irrigated soils. *J. Environ. Qual.* 35(5), 1779-1783.

Williams, M., Kumar, A., Ort, C., Lawrence, M.G., Hambly, A., Khan, S.J., Kookana, R., 2013. The use of multiple tracers for tracking wastewater discharges in freshwater systems. *Environ. Monit. Assess.* 185(11), 9321-9332.

Williams, M., Martin, S., Kookana, R.S., 2015. Sorption and plant uptake of pharmaceuticals from an artificially contaminated soil amended with biochars. *Plant Soil.* 395(1-2), 75-86.

Wilson, R.E., 1923. The mechanism of the corrosion of iron and steel in natural waters and the calculation of specific rates of corrosion. *Ind. Eng. Chem.* 15(2), 127-133.

Wolff, J., 1998. Perchlorate and the thyroid gland. *Pharmacol. Rev.* 50(1), 89-105.

Wunder, D.B., Bosscher, V.A., Cok, R.C., Hozalski, R.M., 2011. Sorption of antibiotics to biofilm. *Water Res.* 45(6), 2270-2280.

Xiang, G., Wang, Y.G., Wu, D., Li, T., He, J., Li, J., Wang, X., 2012. Size-dependent surface activity of rutile and anatase TiO₂ nanocrystals: Facile surface modification and enhanced photocatalytic performance. *Chem. Eur. J.* 18(15), 4759-4765.

Xiao, F., Davidsavor, K.J., Park, S., Nakayama, M., Phillips, B.R., 2012. Batch and column study: Sorption of perfluorinated surfactants from water and cosolvent systems by Amberlite XAD resins. *J. Colloid Interface Sci.* 368(1), 505-511.

Xu, J., Song, Y., Min, B., Steinberg, L., Logan, B.E., 2003a. Microbial degradation of perchlorate: Principles and applications. *Environ. Eng. Sci.* 20(5), 405-422.

Xu, J.L., Song, Y.G., Min, B.K., Steinberg, L., Logan, B.E., 2003b. Microbial degradation of perchlorate: principles and applications. *Environ. Eng. Sci.* 20(5), 405-422.

Xu, X., Cao, X., Zhao, L., Wang, H., Yu, H., Gao, B., 2012. Removal of Cu, Zn, and Cd from aqueous solutions by the dairy manure-derived biochar. *Environ. Sci. Pollut. R.* 20(1), 358-368.

Yamashita, N., Kannan, K., Taniyasu, S., Horii, Y., Okazawa, T., Petrick, G., Gamo, T., 2004. Analysis of perfluorinated acids at parts-per-quadrillion levels in seawater using liquid chromatography-tandem mass spectrometry. *Environ. Sci. Technol.* 38(21), 5522-5528.

Yan, S., Song, W., 2014. Photo-transformation of pharmaceutically active compounds in the aqueous environment: A review. *Environ. Sci.: Processes Impacts.* 16(4), 697-720.

Yang, G.C.C., Tang, P.L., 2016. Removal of phthalates and pharmaceuticals from municipal wastewater by graphene adsorption process. *Water Sci. Technol.* 73(9), 2268-2274.

Yang, Q., Yao, F., Zhong, Y., Wang, D., Chen, F., Sun, J., Hua, S., Li, S., Li, X., Zeng, G., 2016. Catalytic and electrocatalytic reduction of perchlorate in water – A review. *Chem. Eng. J.* 306, 1081-1091.

Yargeau, V., Lopata, A., Metcalfe, C., 2007. Pharmaceuticals in the Yamaska River, Quebec, Canada. *Water Qual. Res. J. Can.* 42(4), 231-239.

Yavuz, C.T., Prakash, A., Mayo, J.T., Colvin, V.L., 2009. Magnetic separations: From steel plants to biotechnology. *Chem. Eng. Sci.* 64(10), 2510-2521.

Ye, L., Wang, S., You, H., Yao, J., Kang, X., 2013. Photocatalytic reduction of perchlorate in aqueous solutions in UV/Cu-TiO₂/SiO₂ system. *Chem. Eng. J.* 226, 434-443.

Ye, L., You, H., Yao, J., Su, H., 2012. Water treatment technologies for perchlorate: A review. *Desalination.* 298, 1-12.

Yim, L.M., Taniyasu, S., Yeung, L.W.Y., Lu, G., Jin, L., Yang, Y., Lam, P.K.S., Kannan, K., Yamashita, N., 2009. Perfluorinated compounds in tap water from china and several other countries. *Environ. Sci. Technol.* 43(13), 4824-4829.

- Yin, P., Hu, Z., Song, X., Liu, J., Lin, N., 2016. Activated persulfate oxidation of perfluorooctanoic acid (PFOA) in groundwater under acidic conditions. *Int. J. Environ. Res. Public Health*. 13(6), 602.
- Yu, J., Lv, L., Lan, P., Zhang, S., Pan, B., Zhang, W., 2012. Effect of effluent organic matter on the adsorption of perfluorinated compounds onto activated carbon. *J. Hazard. Mater.* 225-226, 99-106.
- Yu, X., Amrhein, C., Deshusses, M.A., Matsumoto, M.R., 2006. Perchlorate reduction by autotrophic bacteria in the presence of zero-valent iron. *Environ. Sci. Technol.* 40(4), 1328-1334.
- Yurdakal, S., Loddo, V., Augugliaro, V., Berber, H., Palmisano, G., Palmisano, L., 2007. Photodegradation of pharmaceutical drugs in aqueous TiO₂ suspensions: Mechanism and kinetics. *Catal. Today*. 129(1-2 SPEC. ISS.), 9-15.
- Zhang, C., Wang, L., Li, J., Su, P., Peng, C., 2015. Removal of perfluorinated compounds in wastewater treatment plant effluents by electrochemical oxidation. *Water Sci. Technol.* 71(12), 1783-1789.
- Zhang, D., Luo, Q., Gao, B., Chiang, S.Y.D., Woodward, D., Huang, Q., 2016. Sorption of perfluorooctanoic acid, perfluorooctane sulfonate and perfluoroheptanoic acid on granular activated carbon. *Chemosphere*. 144, 2336-2342.
- Zhang, H., Lv, X., Li, Y., Wang, Y., Li, J., 2010. P25-graphene composite as a high performance photocatalyst. *ACS Nano*. 4(1), 380-386.
- Zhang, Y., Geißen, S.U., Gal, C., 2008. Carbamazepine and diclofenac: Removal in wastewater treatment plants and occurrence in water bodies. *Chemosphere*. 73(8), 1151-1161.
- Zhang, Y., Hurley, K.D., Shapley, J.R., 2011. Heterogeneous catalytic reduction of perchlorate in water with Re-Pd/C catalysts derived from an oxorhenium(V) molecular precursor. *Inorg. Chem.* 50(4), 1534-1543.
- Zheng, B.G., Zheng, Z., Zhang, J.B., Luo, X.Z., Wang, J.Q., Liu, Q., Wang, L.H., 2011. Degradation of the emerging contaminant ibuprofen in aqueous solution by gamma irradiation. *Desalination*. 276(1-3), 379-385.
- Zheng, H., Wang, Z., Zhao, J., Herbert, S., Xing, B., 2013. Sorption of antibiotic sulfamethoxazole varies with biochars produced at different temperatures. *Environ. Pollut.* 181, 60-67.
- Zhou, Q., Deng, S., Zhang, Q., Fan, Q., Huang, J., Yu, G., 2010. Sorption of perfluorooctane sulfonate and perfluorooctanoate on activated sludge. *Chemosphere*. 81(4), 453-458.
- Zhou, Y., Gao, B., Zimmerman, A.R., Chen, H., Zhang, M., Cao, X., 2014. Biochar-supported zerovalent iron for removal of various contaminants from aqueous solutions. *Bioresour. Technol.* 152, 538-542.
- Ziylan, A., Ince, N.H., 2015. Catalytic ozonation of ibuprofen with ultrasound and Fe-based catalysts. *Catal. Today*. 240, 2-8.

Appendix A: *Supplementary Information in*
Chapter 2

Table A.1 Data used for regression fits of NO₃-N removal as a function of residence time in columns containing zero-valent Fe (ZVI), organic C (OC), or both. PV: pore volumes; RT: residence time. “< DL” indicates the concentrations < detection limits (DL).

Distance from the input, cm	Column 2 (ZVI)				Column 3 (OC)				Column 4 (ZVI + OC)			
	Stage 1: 95 PV		Stage 2: 115 PV		Stage 1: 108 PV		Stage 2: 132 PV		Stage 1: 106 PV		Stage 2: 128 PV	
	RT, d	NO ₃ -N, mg L ⁻¹	RT, d	NO ₃ -N, mg L ⁻¹	RT, d	NO ₃ -N, mg L ⁻¹	RT, d	NO ₃ -N, mg L ⁻¹	RT, d	NO ₃ -N, mg L ⁻¹	RT, d	NO ₃ -N, mg L ⁻¹
0	0	11.0	0	11.0	0	11.0	0	11.0	0	11.0	0	11.0
4.3	0.4	6.4	1.3	4.2	0.3	8.7	1.0	5.8	0.3	7.9	1.0	3.8
8.6	0.8	4.8	2.7	2.0	0.6	7.3	1.9	3.6	0.7	4.7	2.0	< DL
13	1.2	3.8	4.0	0.7	1.0	6.3	2.9	2.1	1.0	1.7	3.0	< DL
17	1.6	2.8	5.3	0.3	1.3	5.4	3.8	0.9	1.3	0.1	4.1	< DL
21	1.9	1.8	6.7	0.1	1.6	3.8	4.8	0.4	1.7	< DL	5.1	< DL
26	2.3	1.1	8.0	< DL	1.9	3.2	5.8	0.1	2.0	< DL	6.1	< DL
30	2.7	0.4	9.4	< DL	2.2	2.6	6.7	< DL	2.4	< DL	7.1	< DL

Table A. 2 Data used for regression fits of ClO_4^- removal as a function of residence time in columns containing organic C (OC) and both zero-valent Fe (ZVI) and OC. PV: pore volumes; RT: residence time. “–” indicates the samples were not available or analyzed.

Distance from the input (cm)	Column 3 (OC)				Column 4 (ZVI + OC)			
	Stage 1: 108 PV		Stage 2: 132 PV		Stage 1: 106 PV		Stage 2: 128 PV	
	RT, d	ClO_4^- , $\mu\text{g L}^{-1}$	RT, d	ClO_4^- , $\mu\text{g L}^{-1}$	RT, d	ClO_4^- , $\mu\text{g L}^{-1}$	RT, d	ClO_4^- , $\mu\text{g L}^{-1}$
0	0	919	0	857	0	919	0	857
4.3	0.3	830	1.0	798	0.3	831	1.0	747
8.6	0.6	833	1.9	745	0.7	848	2.0	668
13	1.0	790	2.9	679	1.0	827	3.0	564
17	1.3	783	3.8	506	1.3	–	4.1	475
21	1.6	751	4.8	309	1.7	739	5.1	398
26	1.9	651	5.8	104	2.0	717	6.1	200
30	2.2	547	6.7	0.2	2.4	679	7.1	0.1

Appendix B: *Supplementary Information*
in Chapter 3

Table B.1 Spearman rank correlation coefficients (ρ)[†] of the target compounds and Cl⁻ over the sampling distance in the Grand River in December 2014.

	SUC	SAC	CBZ	IBU	GEM	NAP	Cl
ACE	0.90	0.54	0.81	0.74	0.74	0.71	0.55
SUC		0.48	0.88	0.74	0.74	0.90	0.48
SAC			0.57	0.80	0.80	0.45	0.73
CBZ				0.74	0.74	0.93	0.55
IBU					1.00	0.74	0.74
GEM						0.74	0.74
NAP							0.43

Note: [†] Positive values were interpreted as follows: 0.8-1.0 = very strong; 0.6-0.8 = strong; 0.4-0.6 = moderate; 0.2-0.4 = weak; 0.0-0.2 = weak or no relationship.

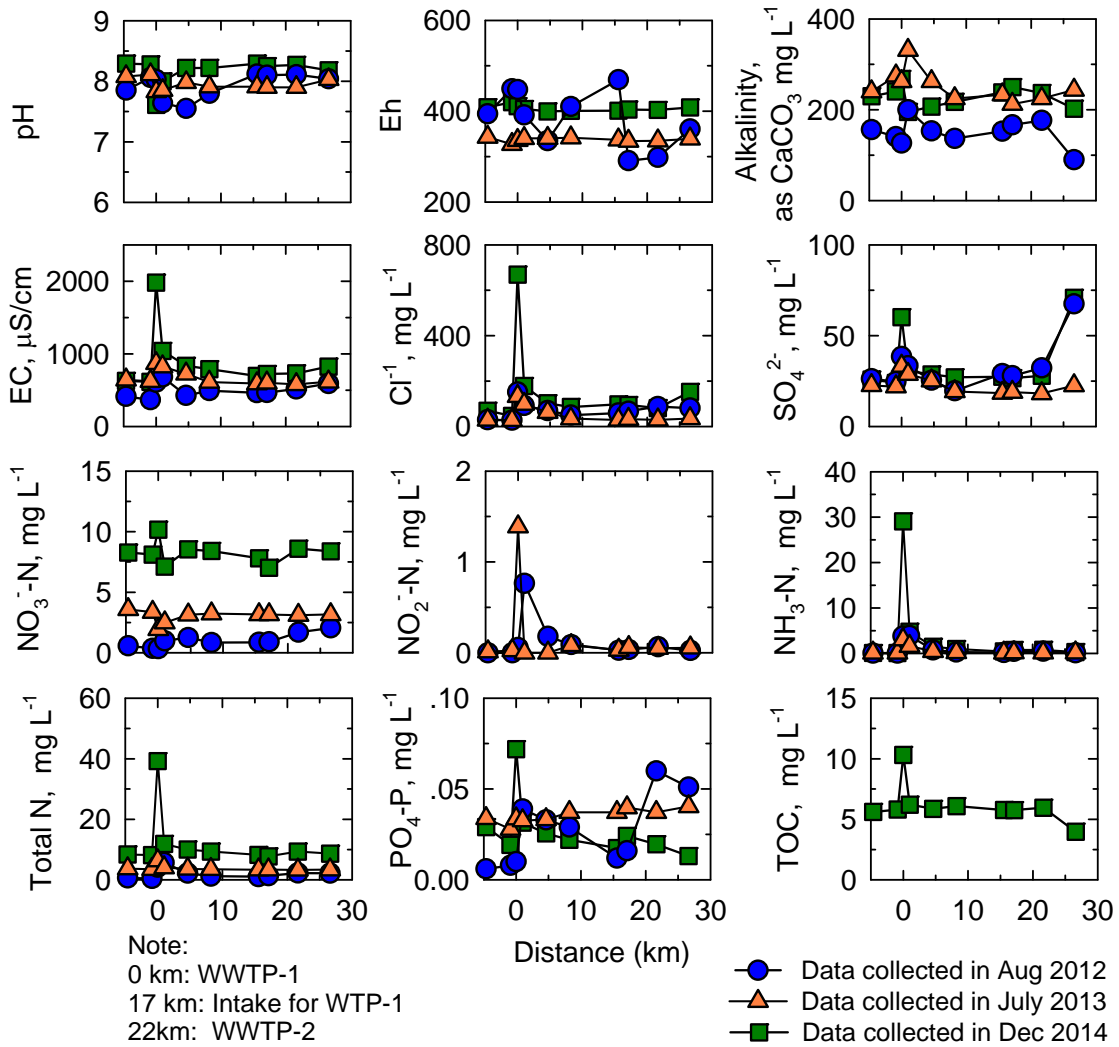


Figure B.1 Concentrations of pH, Eh, alkalinity, EC, Cl^- , SO_4^{2-} , NO_3^- -N, NO_2^- -N, NH_3 -N, total N, PO_4 -P, and TOC as a function of sampling distance.

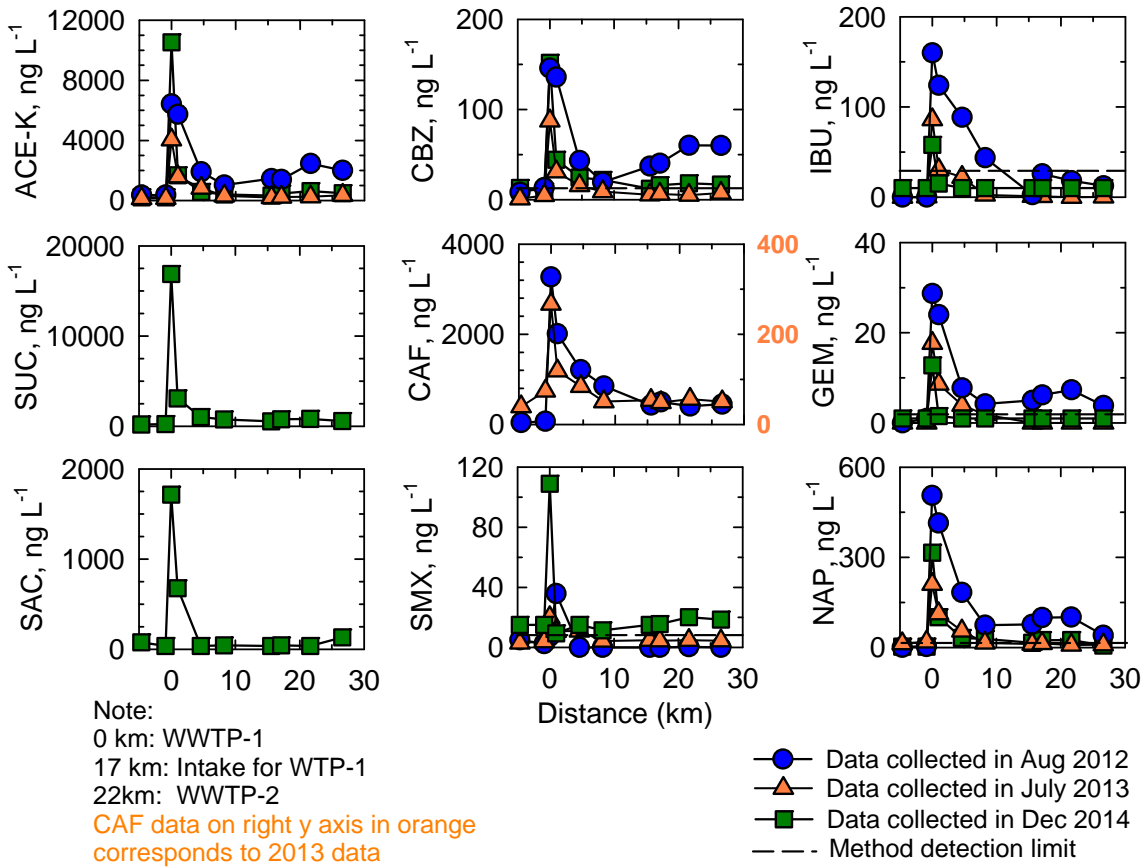


Figure B.2 Concentrations of acesulfame-K (ACE-K), sucralose (SUC), saccharine (SAC), carbamazepine (CBZ), caffeine (CAF), sulfamethoxazole (SMX), ibuprofen (IBU), gemfibrozil (GEM) and naproxen (NAP) as a function of sampling distance. The method detection limits of ACE-K, SUC, SAC and CAF were too low to appear in the figure.

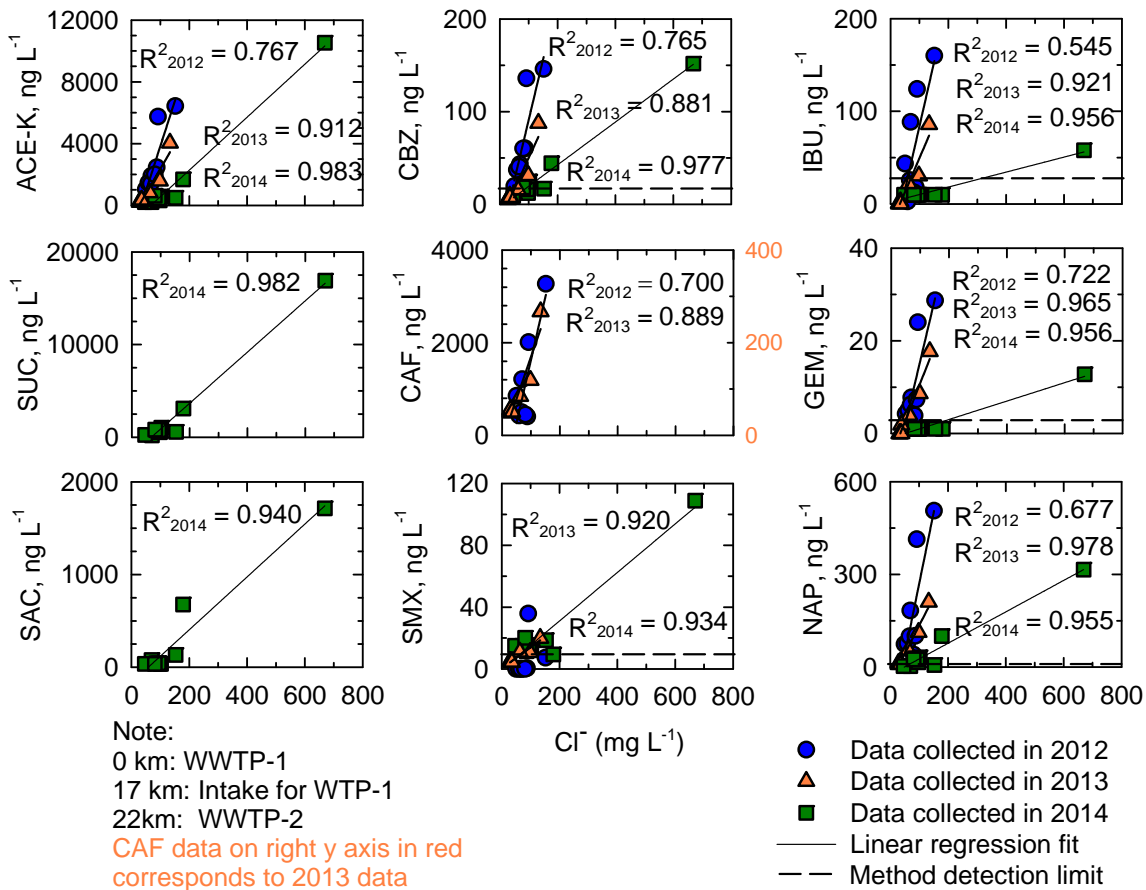


Figure B.3 Concentrations of acesulfame-K (ACE-K), sucralose (SUC), saccharine (SAC), carbamazepine (CBZ), caffeine (CAF), sulfamethoxazole (SMX), ibuprofen (IBU), gemfibrozil (GEM), and naproxen (NAP) as a function of Cl^- concentration. The method detection limits of ACE-K, SUC, SAC, and CAF were too low to appear in the figure.

Appendix C: *Supplementary Information in*
Chapter 4

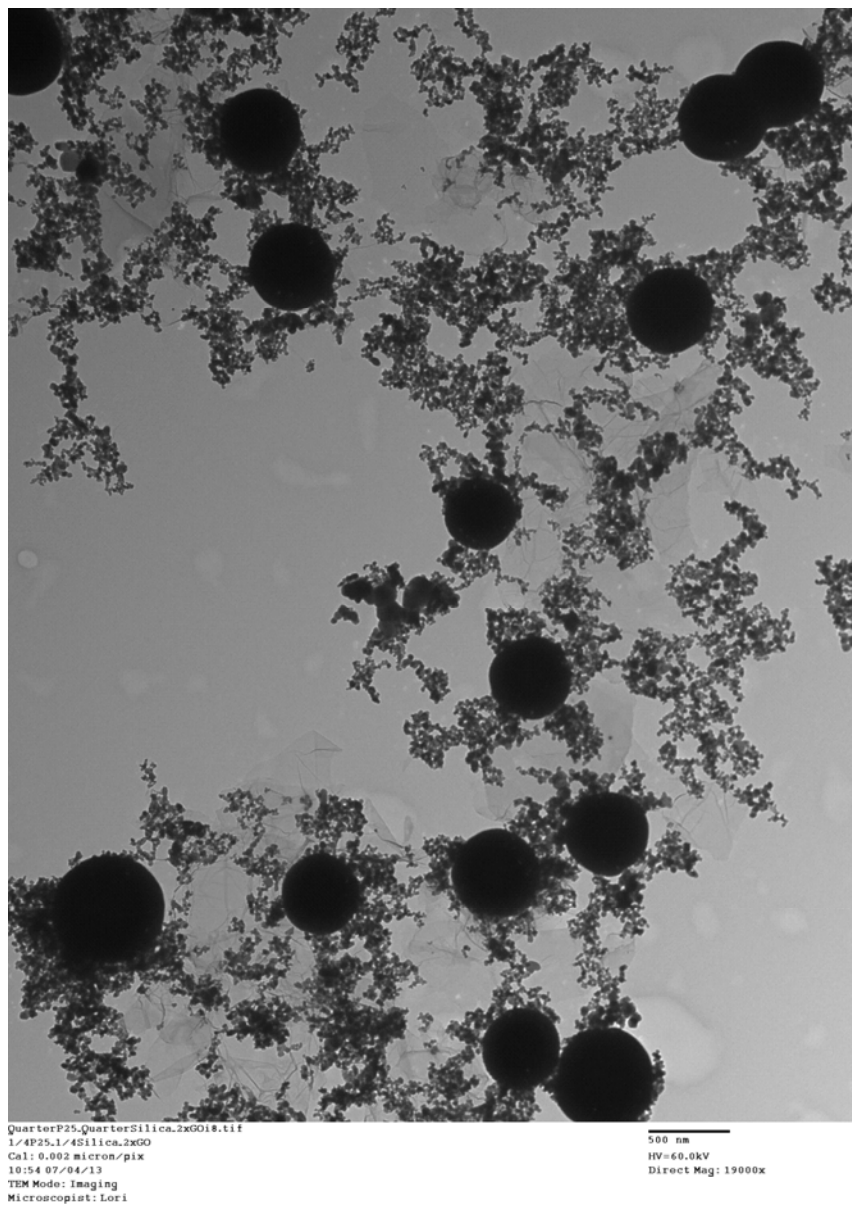


Figure C.1 The TEM image of GO/TiO₂/CSA nanoparticles.

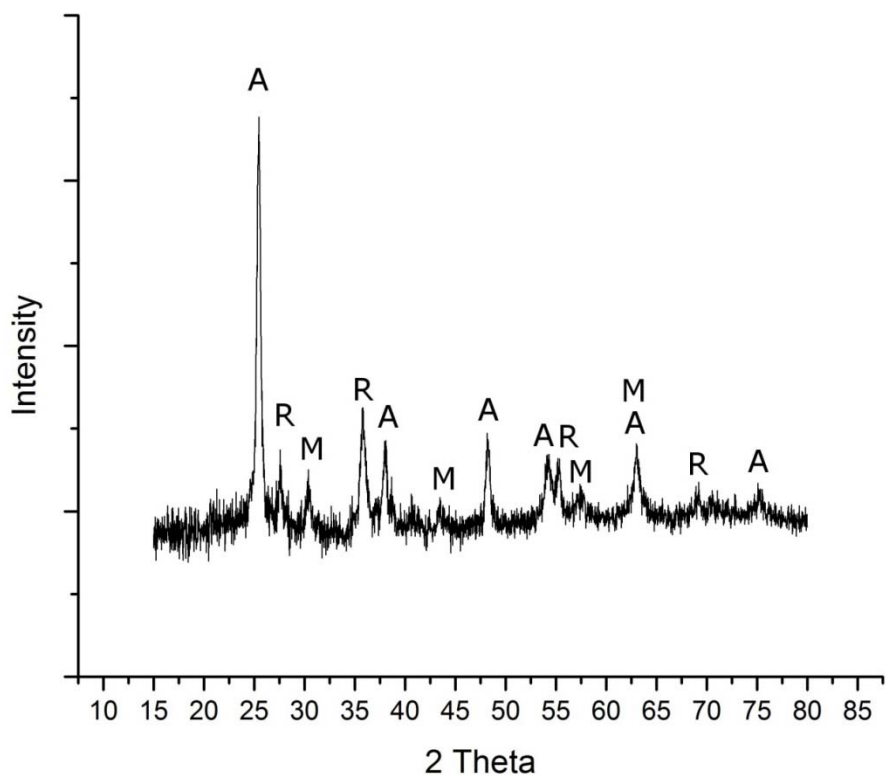


Figure C.2 The XRD patterns of GO/TiO₂/CSA nanoparticles. Peaks labelled with A match anatase phase TiO₂ (JCPDS No. 21-1272), R matches rutile phase TiO₂ (JCPDS No. 21-1276), and those labeled with M match Magnetite (Fe₃O₄) iron oxide (JCPDS No. 19-629).

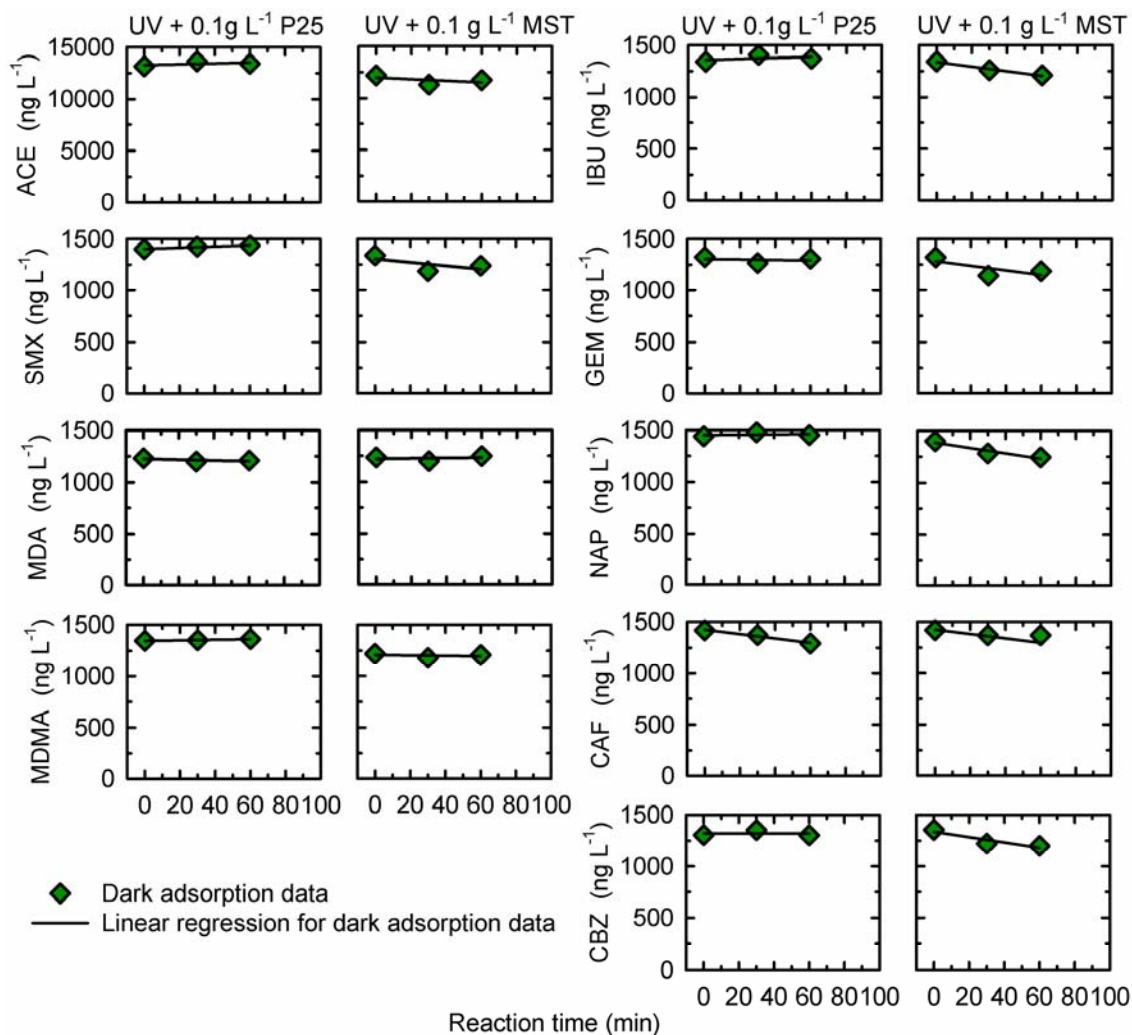
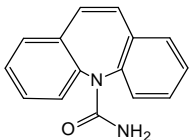


Figure C.3 Concentration of ACE-K, SMX, MDA, MDMA, IBU, GEM, NAP, CAF, and CBZ as a function of reaction time during the 60 min dark adsorption test.

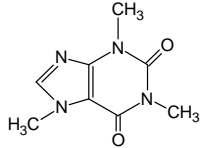
Appendix D: *Supplementary Information in*
Chapter 5

Table D.1 First order removal rate constant (k_{obs} , d^{-1}), mass normalized rate constant (k_M , $L g^{-1} d^{-1}$), and surface area normalized rate constant (k_{SA} , $L m^{-2} d^{-1}$) of carbamazepine. k_{obs} is calculated using least-squares regression during two experimental stages. 1C is the input contaminant concentration.

Contaminant (CAS#), pKa, log Kow, and structure	Column	Stage	PV	Removal rate ¹ , $\mu mol L^{-1} d^{-1}$ ($\mu g L^{-1} d^{-1}$)	k_{obs} , d^{-1}	k_M , $L g^{-1} d^{-1}$	k_{SA} , $L m^{-2} d^{-1}$	Half-life, d	R ²	
Carbamazepine (CBZ) (298-46-4) pKa= -0.49, log K _{ow} =2.25 	Column 2 (ZVI)	1	1	$1.1E+01 \times C$	1.1E+01	2.6E-03	2.8E-04	0.06	0.999	
			13	$4.9 \times C$	4.9	1.1E-03	1.2E-04	0.14	0.975	
			25	$4.4 \times C$	4.4	1.0E-03	1.1E-04	0.16	0.965	
		Column 3 (BC)	2	53	$1.2 \times C$	1.2	2.9E-04	3.0E-05	0.56	0.931
				1	$5.4 \times C$	5.4	1.2E-02	1.8E-04	0.19	0.998
				13	$2.5 \times C$	2.5	5.3E-03	8.2E-05	0.28	0.998
	Column 4 (ZVI + BC)	1	25	$1.9 \times C$	1.9	4.2E-03	6.4E-05	0.36	0.996	
			2	53	$0.7 \times C$	0.7	1.5E-03	2.3E-05	1.0	0.970
			1	$8.2 \times C$	8.2	7.2E-03	2.1E-04	0.09	0.999	
		2	13	$4.5 \times C$	4.5	3.9E-03	1.2E-04	0.16	0.966	
			25	$4.0 \times C$	4.0	3.5E-03	1.0E-04	0.17	0.970	
			53	$1.3 \times C$	1.3	1.1E-03	3.3E-05	0.55	0.992	

K_M and K_{SA} were calculated following the expression $K_M = K_{obs}/\rho_m$; $K_{SA} = K_{obs}/\rho_a = K_M/a_s$ (Johnson et al., 1996). ρ_m is the mass concentrations of reactive media ($g L^{-1}$ of solution). ρ_a is the surface area concentrations of reactive media ($m^2 L^{-1}$ of solution). a_s is the specific surface area of reactive media ($m^2 g^{-1}$). Specific surface areas of ZVI, BC, and (ZVI + BC) are 9.5, 64.5, and 33.6 $m^2 g^{-1}$.

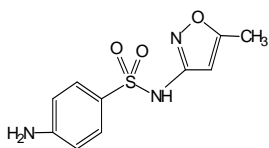
Table D.2 First order removal rate constant (k_{obs} , d^{-1}), mass normalized rate constant (k_M , $L g^{-1} d^{-1}$), and surface area normalized rate constant (k_{SA} , $L m^{-2} d^{-1}$) of caffeine. k_{obs} is calculated using least-squares regression during two experimental stages. tC is the input contaminant concentration.

Contaminant (CAS#), pKa, log K_{ow} , and structure	Column	Stage	PV	Removal rate ^t , $\mu mol L^{-1} d^{-1}$ ($\mu g L^{-1} d^{-1}$)	k_{obs} , d^{-1}	k_M , $L g^{-1} d^{-1}$	k_{SA} , $L m^{-2} d^{-1}$	Half-life, d	R ²		
Caffeine (CAF) (58-08-2) pKa=10.4, log K_{ow} = -0.07 	Column 2 (ZVI)	1	1	$1.6E+01 \times C$	1.6E+01	3.7E-03	3.9E-04	0.04	0.999		
			13	$7.2 \times C$	7.2	1.7E-03	1.8E-04	0.10	0.998		
			25	$5.1 \times C$	5.1	1.2E-03	1.2E-04	0.14	0.982		
		2	53	$1.5 \times C$	1.5	3.5E-04	3.6E-05	0.47	0.961		
			Column 3 (BC)	1	1	$4.8 \times C$	4.8	1.0E-02	1.6E-04	0.14	0.999
					13	$2.8 \times C$	2.8	6.0E-03	9.4E-05	0.25	0.999
	Column 4 (ZVI + BC)	1	13	25	$2.2 \times C$	2.2	4.8E-03	7.4E-05	0.31	0.996	
				53	$1.0 \times C$	1.0	2.1E-03	3.3E-05	0.70	0.973	
				1	$6.9 \times C$	6.9	6.0E-03	1.8E-04	0.10	0.996	
		2	53	13	$5.5 \times C$	5.5	4.8E-03	1.4E-04	0.13	0.989	
				25	$4.5 \times C$	4.5	3.9E-03	1.2E-04	0.15	0.973	
				53	$1.7 \times C$	1.7	1.5E-03	4.5E-05	0.40	0.996	

K_M and K_{SA} were calculated following the expression $K_M = K_{obs}/\rho_m$; $K_{SA} = K_{obs}/\rho_a = K_M/a_s$ (Johnson et al., 1996). ρ_m is the mass concentrations of reactive media ($g L^{-1}$ of solution). ρ_a is the surface area concentrations of reactive media ($m^2 L^{-1}$ of solution). a_s is the specific surface area of reactive media ($m^2 g^{-1}$). Specific surface areas of ZVI, BC, and (ZVI + BC) are 9.5, 64.5, and 33.6 $m^2 g^{-1}$.

Table D.3 First order removal rate constant (k_{obs} , d^{-1}), mass normalized rate constant (k_M , $L g^{-1} d^{-1}$), and surface area normalized rate constant (k_{SA} , $L m^{-2} d^{-1}$) of sulfamethoxazole. k_{obs} is calculated using least-squares regression during two experimental stages. 1C is the input contaminant concentration. “–” represents not applicable.

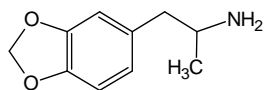
Contaminant (CAS#), pKa, log K_{ow} , and structure	Column	Stage	PV	Removal rate ¹ , $\mu mol L^{-1} d^{-1}$ ($\mu g L^{-1} d^{-1}$)	k_{obs} , d^{-1}	k_M , $L g^{-1} d^{-1}$	k_{SA} , $L m^{-2} d^{-1}$	Half-life, d	R^2
Sulfamethoxazole (SMX) (723-46-6) pKa ₁ =1.7, pKa ₂ =5.6, log K_{ow} =0.89	Column 1 (Control)	1	25	$0.2 \times C$	0.2	–	–	3.6	0.877
		2	53	$0.4 \times C$	0.4	–	–	1.8	0.984
	Column 2 (ZVI)	1	13	$4.5E+02 \times C$	$4.5E+02$	$1.1E-01$	$1.1E-02$	0.002	1.000
			25	$4.7E+02 \times C$	$4.7E+02$	$1.1E-01$	$1.1E-02$	0.001	1.000
		2	53	$4.6E+02 \times C$	$4.6E+02$	$1.1E-01$	$1.1E-02$	0.001	1.000
			53	$1.5E+02 \times C$	$1.5E+02$	$3.5E-02$	$3.7E-03$	0.005	1.000
	Column 3 (BC)	1	13	$1.6 \times C$	1.6	$3.5E-03$	$5.4E-05$	0.43	0.999
			25	$1.2 \times C$	1.2	$2.5E-03$	$3.8E-05$	0.60	0.999
		2	25	$1.1 \times C$	1.1	$2.4E-03$	$3.8E-05$	0.61	0.993
			53	$0.5 \times C$	0.5	$1.1E-03$	$1.7E-05$	1.4	0.991
	Column 4 (ZVI + BC)	1	13	$4.5E+02 \times C$	$4.5E+02$	$4.0E-01$	$1.2E-02$	0.002	1.000
			25	$4.7E+02 \times C$	$4.7E+02$	$4.1E-01$	$1.2E-02$	0.001	1.000
2		53	$4.6E+02 \times C$	$4.6E+02$	$4.1E-01$	$1.2E-02$	0.001	1.000	
		53	$1.5E+02 \times C$	$1.5E+02$	$1.3E-01$	$3.9E-03$	0.005	1.000	



K_M and K_{SA} were calculated following the expression $K_M = K_{obs}/\rho_m$; $K_{SA} = K_{obs}/\rho_a = K_M/a_s$ (Johnson et al., 1996). ρ_m is the mass concentrations of reactive media ($g L^{-1}$ of solution). ρ_a is the surface area concentrations of reactive media ($m^2 L^{-1}$ of solution). a_s is the specific surface area of reactive media ($m^2 g^{-1}$). Specific surface areas of ZVI, BC, and (ZVI + BC) are 9.5, 64.5, and 33.6 $m^2 g^{-1}$.

Table D.4 First order removal rate constant (k_{obs} , d^{-1}), mass normalized rate constant (k_M , $L g^{-1} d^{-1}$), and surface area normalized rate constant (k_{SA} , $L m^{-2} d^{-1}$) of MDA. k_{obs} is calculated using least-squares regression during two experimental stages. 1C is the input contaminant concentration.

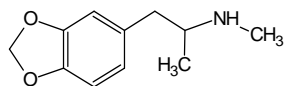
Contaminant (CAS#), pK_a , $\log K_{ow}$, and structure	Column	Stage	PV	Removal rate ¹ , $\mu mol L^{-1} d^{-1}$, ($\mu g L^{-1} d^{-1}$)	k_{obs} , d^{-1}	k_M , $L g^{-1} d^{-1}$	k_{SA} , $L m^{-2} d^{-1}$	Half-life, d	R^2		
3,4- methylenedioxyamphetamine (MDA) (4764-17-4), $pK_a=9.7$, $\log K_{ow}=1.64$	Column 2 (ZVI)	1	1	$1.9E+02 \times C$	1.9E+02	4.3E-02	4.6E-03	0.004	1.000		
			13	$1.3E+01 \times C$	1.3E+01	3.0E-03	3.1E-04	0.06	0.999		
			25	$7.8 \times C$	7.8	1.8E-03	1.9E-04	0.09	0.998		
		2	53	$2.4 \times C$	2.4	5.5E-04	5.8E-05	0.29	0.996		
			Column 3 (BC)	1	1	$1.1E+01 \times C$	1.1E+01	2.4E-02	3.7E-04	0.06	0.999
					13	$8.1 \times C$	8.1	1.7E-02	2.7E-04	0.09	0.997
	25	$5.1 \times C$			5.1	1.1E-02	1.7E-04	0.14	0.998		
	2	53		$3.2 \times C$	3.2	6.8E-03	1.1E-04	0.22	0.997		
		Column 4 (ZVI + BC)		1	1	$2.0E+01 \times C$	2.0E+01	1.8E-02	5.3E-04	0.03	1.000
					13	$1.2E+01 \times C$	1.2E+01	1.0E-02	3.0E-04	0.06	0.999
	25		$8.7 \times C$		8.7	7.6E-03	2.3E-04	0.08	0.999		
	2		53	$3.9 \times C$	3.9	3.4E-03	1.0E-04	0.18	0.999		



K_M and K_{SA} were calculated following the expression $K_M = K_{obs}/\rho_m$; $K_{SA} = K_{obs}/\rho_a = K_M/a_s$ (Johnson et al., 1996). ρ_m is the mass concentrations of reactive media ($g L^{-1}$ of solution). ρ_a is the surface area concentrations of reactive media ($m^2 L^{-1}$ of solution). a_s is the specific surface area of reactive media ($m^2 g^{-1}$). Specific surface areas of ZVI, BC, and (ZVI + BC) are 9.5, 64.5, and 33.6 $m^2 g^{-1}$.

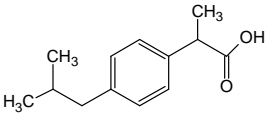
Table D.5 First order removal rate constant (k_{obs} , d^{-1}), mass normalized rate constant (k_M , $L g^{-1} d^{-1}$), and surface area normalized rate constant (k_{SA} , $L m^{-2} d^{-1}$) of MDMA. k_{obs} is calculated using least-squares regression during two experimental stages. 1C is the input contaminant concentration.

Contaminant (CAS#), pKa, log K_{ow} , and structure	Column	Stage	PV	Removal rate ¹ , $\mu mol L^{-1} d^{-1}$ ($\mu g L^{-1} d^{-1}$)	k_{obs} , d^{-1}	k_M , $L g^{-1} d^{-1}$	k_{SA} , $L m^{-2} d^{-1}$	Half-life, d	R^2	
3,4-methylenedioxyamphetamine (MDMA) (42542-10-9), pKa=9.9, log K_{ow} =2.28	Column 2 (ZVI)	1	1	$3.0E+02 \times C$	3.0E+02	6.9E-02	7.3E-03	0.002	1.000	
			13	$3.5E+02 \times C$	3.5E+02	8.2E-02	8.7E-03	0.002	1.000	
			25	$1.4E+01 \times C$	1.4E+01	3.2E-03	3.4E-04	0.05	1.000	
	Column 3 (BC)	1	2	53	$4.0 \times C$	4.0	9.3E-04	9.8E-05	0.17	1.000
			1	13	$1.1E+01 \times C$	1.1E+01	2.3E-02	3.6E-04	0.07	0.999
			25	53	$7.7 \times C$	7.7	1.7E-02	2.6E-04	0.09	0.998
	Column 4 (ZVI + BC)	1	2	53	$5.2 \times C$	5.2	1.1E-02	1.7E-04	0.13	0.997
			1	13	$3.1 \times C$	3.1	6.7E-03	1.0E-04	0.22	0.997
			25	53	$2.5E+01 \times C$	2.5E+01	2.2E-02	6.6E-04	0.03	1.000
	Column 4 (ZVI + BC)	1	2	53	$1.6E+01 \times C$	1.6E+01	1.4E-02	4.1E-04	0.04	1.000
			25	53	$1.0E+01 \times C$	1.0E+01	9.0E-03	2.7E-04	0.07	0.999
			2	53	$4.3 \times C$	4.3	3.8E-03	1.1E-04	0.16	1.000



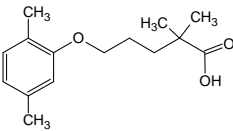
K_M and K_{SA} were calculated following the expression $K_M = K_{obs}/\rho_m$; $K_{SA} = K_{obs}/\rho_a = K_M/a_s$ (Johnson et al., 1996). ρ_m is the mass concentrations of reactive media ($g L^{-1}$ of solution). ρ_a is the surface area concentrations of reactive media ($m^2 L^{-1}$ of solution). a_s is the specific surface area of reactive media ($m^2 g^{-1}$). Specific surface areas of ZVI, BC, and (ZVI + BC) are 9.5, 64.5, and 33.6 $m^2 g^{-1}$.

Table D.6 First order removal rate constant (k_{obs} , d^{-1}), mass normalized rate constant (k_M , $L g^{-1} d^{-1}$), and surface area normalized rate constant (k_{SA} , $L m^{-2} d^{-1}$) of ibuprofen. k_{obs} is calculated using least-squares regression during two experimental stages. 1C is the input contaminant concentration.

Contaminant (CAS#), pKa, log K_{ow} , and structure	Column	Stage	PV	Removal rate [†] , $\mu mol L^{-1} d^{-1}$ ($\mu g L^{-1} d^{-1}$)	k_{obs} , d^{-1}	k_M , $L g^{-1} d^{-1}$	k_{SA} , $L m^{-2} d^{-1}$	Half-life, d	R ²	
Ibuprofen (IBU) (15687-27-1), pKa=4.5, log K_{ow} =3.5 	Column 2 (ZVI)	1	1	$2.6 \times C$	2.6	6.0E-04	6.3E-05	0.27	0.943	
			13	$1.2 \times C$	1.2	2.9E-04	3.0E-05	0.56	0.926	
			25	$0.9 \times C$	0.9	2.2E-04	2.3E-05	0.74	0.932	
	Column 3 (BC)	2	1	53	$0.2 \times C$	0.2	4.7E-05	4.9E-06	3.5	0.864
				13	$1.9 \times C$	1.9	4.2E-03	6.5E-05	0.36	0.992
				25	$1.2 \times C$	1.2	2.6E-03	4.0E-05	0.57	0.997
	Column 4 (ZVI + BC)	1	2	53	$1.1 \times C$	1.1	2.4E-03	3.7E-05	0.63	0.996
				1	$2.9 \times C$	2.9	2.5E-03	7.6E-05	0.24	0.978
				13	$1.7 \times C$	1.7	1.5E-03	4.5E-05	0.41	0.958
	Column 4 (ZVI + BC)	2	1	25	$1.6 \times C$	1.6	1.4E-03	4.1E-05	0.44	0.952
				53	$0.5 \times C$	0.5	4.0E-04	1.2E-05	1.5	0.941

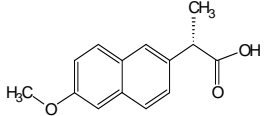
K_M and K_{SA} were calculated following the expression $K_M = K_{obs}/\rho_m$; $K_{SA} = K_{obs}/\rho_a = K_M/a_s$ (Johnson et al., 1996). ρ_m is the mass concentrations of reactive media ($g L^{-1}$ of solution). ρ_a is the surface area concentrations of reactive media ($m^2 L^{-1}$ of solution). a_s is the specific surface area of reactive media ($m^2 g^{-1}$). Specific surface areas of ZVI, BC, and (ZVI + BC) are 9.5, 64.5, and $33.6 m^2 g^{-1}$.

Table D.7 First order removal rate constant (k_{obs} , d^{-1}), mass normalized rate constant (k_M , $L g^{-1} d^{-1}$), and surface area normalized rate constant (k_{SA} , $L m^{-2} d^{-1}$) of gemfibrozil. k_{obs} is calculated using least-squares regression during two experimental stages. 1C is the input contaminant concentration.

Contaminant (CAS#), pKa, log Kow, and structure	Column	Stage	PV	Removal rate [†] , $\mu mol L^{-1} d^{-1}$ ($\mu g L^{-1} d^{-1}$)	k_{obs} , d^{-1}	k_M , $L g^{-1} d^{-1}$	k_{SA} , $L m^{-2} d^{-1}$	Half-life, d	R ²		
Gemfibrozil (GEM) (25812-30-0), pKa=4.8, log K _{ow} =4.3 	Column 2 (ZVI)	1	1	$9.3 \times C$	9.3	2.2E-03	2.3E-04	0.07	0.999		
			13	$4.6 \times C$	4.6	1.1E-03	1.1E-04	0.15	0.969		
			25	$3.5 \times C$	3.5	8.2E-04	8.6E-05	0.20	0.954		
		2	53	$1.0 \times C$	1.0	2.4E-04	2.5E-05	0.67	0.927		
			Column 3 (BC)	1	1	$4.5 \times C$	4.5	9.7E-03	1.5E-04	0.15	0.997
					13	$2.4 \times C$	2.4	5.1E-03	8.0E-05	0.29	0.995
	25	$1.8 \times C$			1.8	3.8E-03	5.9E-05	0.39	0.996		
	2	53		$0.6 \times C$	0.6	1.4E-03	2.1E-05	1.1	0.981		
		Column 4 (ZVI + BC)		1	1	$5.9 \times C$	5.9	5.1E-03	1.5E-04	0.12	0.990
					13	$3.5 \times C$	3.5	3.1E-03	9.2E-05	0.20	0.967
	25		$2.8 \times C$		2.8	2.5E-03	7.4E-05	0.24	0.935		
	2		53	$0.9 \times C$	0.9	7.6E-04	2.3E-05	0.80	0.989		

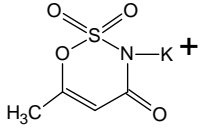
K_M and K_{SA} were calculated following the expression $K_M = K_{obs}/\rho_m$; $K_{SA} = K_{obs}/\rho_a = K_M/a_s$ (Johnson et al., 1996). ρ_m is the mass concentrations of reactive media ($g L^{-1}$ of solution). ρ_a is the surface area concentrations of reactive media ($m^2 L^{-1}$ of solution). a_s is the specific surface area of reactive media ($m^2 g^{-1}$). Specific surface areas of ZVI, BC, and (ZVI + BC) are 9.5, 64.5, and 33.6 $m^2 g^{-1}$.

Table D.8 First order removal rate constant (k_{obs} , d⁻¹), mass normalized rate constant (k_M , L g⁻¹ d⁻¹), and surface area normalized rate constant (k_{SA} , L m⁻² d⁻¹) of naproxen. k_{obs} is calculated using least-squares regression during two experimental stages. ¹C is the input contaminant concentration.

Contaminant (CAS#), pKa, log K _{ow} , and structure	Column	Stage	PV	Removal rate ¹ , μmol L ⁻¹ d ⁻¹ (μg L ⁻¹ d ⁻¹)	k_{obs} , d ⁻¹	k_M , L g ⁻¹ d ⁻¹	k_{SA} , L m ⁻² d ⁻¹	Half-life, d	R ²	
Naproxen (NAP) (22204-53-1), pKa=4.2, log K _{ow} =2.8 	Column 2 (ZVI)	1	1	$5.7 \times C$	5.7	1.3E-03	1.4E-04	0.12	0.988	
			13	$3.1 \times C$	3.1	7.2E-04	7.6E-05	0.22	0.908	
			25	$2.8 \times C$	2.8	6.4E-04	6.8E-05	0.25	0.949	
	Column 3 (BC)	1	2	53	$0.6 \times C$	0.6	1.4E-04	1.5E-05	1.2	0.941
				1	$3.7 \times C$	3.7	8.0E-03	1.2E-04	0.19	0.999
				13	$2.0 \times C$	2.0	4.2E-03	6.6E-05	0.35	0.996
	Column 4 (ZVI + BC)	1	2	53	$1.7 \times C$	1.7	3.6E-03	5.6E-05	0.41	0.999
				1	$4.7 \times C$	4.7	4.1E-03	1.2E-04	0.15	0.978
				13	$3.0 \times C$	3.0	2.6E-03	7.7E-05	0.23	0.959
	Column 4 (ZVI + BC)	1	2	25	$2.6 \times C$	2.6	2.2E-03	6.7E-05	0.27	0.977
				53	$0.7 \times C$	0.7	6.5E-04	1.9E-05	0.94	0.980

K_M and K_{SA} were calculated following the expression $K_M = K_{obs}/\rho_m$; $K_{SA} = K_{obs}/\rho_a = K_M/a_s$ (Johnson et al., 1996). ρ_m is the mass concentrations of reactive media (g L⁻¹ of solution). ρ_a is the surface area concentrations of reactive media (m² L⁻¹ of solution). a_s is the specific surface area of reactive media (m² g⁻¹). Specific surface areas of ZVI, BC, and (ZVI + BC) are 9.5, 64.5, and 33.6 m² g⁻¹.

Table D.9 Removal rate constant k_{obs} , mass normalized rate constant k_M , and surface area normalized rate constant k_{SA} of acesulfame-K. Removal rate constant k_{obs} is calculated using least-squares regression during two experimental stages. 1C is the input contaminant concentration. “–” represents no removal of contaminant was observed.

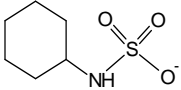
Contaminant (CAS#), pKa, log K_{ow} , and structure	Column	Stage	PV	Removal rate [†] , $\mu\text{mol L}^{-1} \text{d}^{-1}$ ($\mu\text{g L}^{-1} \text{d}^{-1}$)	k_{obs}	k_M	k_{SA}	Half-life, d	R ²	
Acesulfame-K (ACE-K) (55589-62-3), pKa=2.0, log K_{ow} = -1.3 	Column 2 (ZVI)	1	1	$2.3\text{E-}01 \times C^a$	$2.3\text{E-}01^a$	$5.3\text{E-}05^a$	$5.6\text{E-}06^a$	3.1	0.749	
			13	$1.0\text{E-}01 \times C^a$	$1.0\text{E-}01^a$	$2.4\text{E-}05^a$	$2.6\text{E-}06^a$	6.6	0.906	
			25	$9.8\text{E-}02 \times C^a$	$9.8\text{E-}02^a$	$2.3\text{E-}05^a$	$2.4\text{E-}06^a$	7.0	0.874	
	Column 3 (BC)	2	53	1	$1.1\text{E-}01 \times C^a$	$1.1\text{E-}01^a$	$2.7\text{E-}05^a$	$2.8\text{E-}06^a$	6.1	0.870
				1	$1.6 \text{E+}01^b$	$1.6 \text{E+}01^b$	$3.4\text{E-}02^b$	$5.3\text{E-}04^b$	3.2	0.864
				13	–	–	–	–	–	–
	Column 4 (ZVI + BC)	1	13	25	–	–	–	–	–	–
				53	–	–	–	–	–	–
				1	5.9^b	5.8^b	$5.1\text{E-}03^b$	$1.5\text{E-}04^b$	8.3	0.976
	Column 4 (ZVI + BC)	2	53	13	4.2^b	4.2^b	$3.7\text{E-}03^b$	$1.1\text{E-}04^b$	12	0.634
				25	4.9^b	4.9^b	$4.3\text{E-}03^b$	$1.3\text{E-}04^b$	10	0.835
				53	3.2^b	3.2^b	$2.8\text{E-}03^b$	$8.3\text{E-}05^b$	17	0.866

^a Removal of ACE-K followed a first order reaction rate, unit of k_{obs} is d^{-1} , unit of k_M is $\text{L g}^{-1} \text{d}^{-1}$, unit of k_{SA} is $\text{L m}^{-2} \text{d}^{-1}$.

^b Removal of ACE-K followed a zero order reaction rate, unit of k is $\mu\text{mol ACE-K L}^{-1} \text{d}^{-1}$ ($\mu\text{g ACE-K L}^{-1} \text{d}^{-1}$), unit of k_M is $\mu\text{mol ACE-K d}^{-1} \text{g (reactive media)}^{-1}$ [$\mu\text{g ACE-K d}^{-1} \text{g (reactive media)}^{-1}$], unit of k_{SA} is $\mu\text{mol ACE-K d}^{-1} \text{m}^{-2}$ ($\mu\text{g ACE-K d}^{-1} \text{m}^{-2}$).

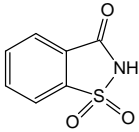
K_M and K_{SA} were calculated following the expression $K_M = K_{obs}/\rho_m$; $K_{SA} = K_{obs}/\rho_a = K_M/a_s$ (Johnson et al., 1996). ρ_m is the mass concentrations of reactive media (g L^{-1} of solution). ρ_a is the surface area concentrations of reactive media ($\text{m}^2 \text{L}^{-1}$ of solution). a_s is the specific surface area of reactive media ($\text{m}^2 \text{g}^{-1}$). Specific surface areas of ZVI, BC, and (ZVI + BC) are 9.5, 64.5, and $33.6 \text{ m}^2 \text{g}^{-1}$.

Table D.10 Zero-order removal rate constant k_{obs} ($\mu\text{mol CYC L}^{-1} \text{d}^{-1}$ or $\mu\text{g CYC L}^{-1} \text{d}^{-1}$), mass normalized rate constant k_M [$\mu\text{mol CYC g (reactive media)}^{-1} \text{d}^{-1}$ or $\mu\text{g CYC g (reactive media)}^{-1} \text{d}^{-1}$], and surface area normalized rate constant k_{SA} ($\mu\text{mol CYC m}^{-2} \text{d}^{-1}$ or $\mu\text{g CYC m}^{-2} \text{d}^{-1}$) of cyclamate. Removal rate constant k_{obs} is calculated using least-squares regression during two experimental stages. 1C is the input contaminant concentration. “–” represents no removal of contaminant was observed.

Contaminant (CAS#), pKa, log K_{ow} , and structure	Column	Stage	PV	Removal rate ¹ , $\mu\text{mol L}^{-1} \text{d}^{-1}$ ($\mu\text{g L}^{-1} \text{d}^{-1}$)	k_{obs} , $\mu\text{mol L}^{-1} \text{d}^{-1}$ ($\mu\text{g L}^{-1} \text{d}^{-1}$)	k_M , $\mu\text{mol g}^{-1} \text{d}^{-1}$ ($\mu\text{g g}^{-1} \text{d}^{-1}$)	k_{SA} , $\mu\text{mol m}^{-2} \text{d}^{-1}$ ($\mu\text{g m}^{-2} \text{d}^{-1}$)	Half-life, d	R ²	
Cyclamate (CYC) (45951-45-9), pKa=1.7, log K_{ow} = -2.6 	Column 2 (ZVI)	1	1	1.5E+01	1.5E+01	3.6E-03	3.8E-04	3.3	0.697	
			13	–	–	–	–	–	–	
			25	–	–	–	–	–	–	
	Column 3 (BC)	2	53	1	8.4	8.4	1.8E-02	2.8E-04	5.8	0.839
				13	–	–	–	–	–	–
				25	–	–	–	–	–	–
	Column 4 (ZVI+BC)	1	53	1	2.0	2.0	1.8E-03	5.2E-05	23	0.624
				13	–	–	–	–	–	–
				25	–	–	–	–	–	–
				2	53	–	–	–	–	–

K_M and K_{SA} were calculated following the expression $K_M = K_{obs}/\rho_m$; $K_{SA} = K_{obs}/\rho_a = K_M/a_s$ (Johnson et al., 1996). ρ_m is the mass concentrations of reactive media (g L^{-1} of solution). ρ_a is the surface area concentrations of reactive media ($\text{m}^2 \text{L}^{-1}$ of solution). a_s is the specific surface area of reactive media ($\text{m}^2 \text{g}^{-1}$). Specific surface areas of ZVI, BC, and (ZVI + BC) are 9.5, 64.5, and 33.6 $\text{m}^2 \text{g}^{-1}$.

Table D.11 Removal rate constant k_{obs} , mass normalized rate constant k_M , and surface area normalized rate constant k_{SA} of saccharin. Removal rate constant k_{obs} is calculated using least-squares regression during two experimental stages. ${}^1\text{C}$ is the input contaminant concentration. “–” represents no removal of contaminant was observed.

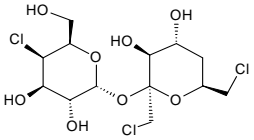
Contaminant (CAS#), p <i>K</i> _a , log <i>K</i> _{ow} , and structure	Column	Stage	PV	Removal rate [†] , μmol L ⁻¹ d ⁻¹ (μg L ⁻¹ d ⁻¹)	k_{obs}	k_M	k_{SA}	Half-life, d	R ²	
Saccharin (SAC) (81-07-2), p <i>K</i> _a =1.3, log <i>K</i> _{ow} =0.9 	Column 2 (ZVI)	1	1	3.5E+01 ^b	3.5E+01 ^b	8.1E-03 ^b	8.6E-04 ^b	1.5	0.898	
			13	4.7 ^b	4.7 ^b	1.1E-03 ^b	1.2E-04 ^b	9.3	0.804	
			25	–	–	–	–	–	–	
	Column 3 (BC)	1	2	53	1.7 ^b	1.7 ^b	3.9E-04 ^b	4.1E-05 ^b	32	0.583
				1	1.0 × C ^a	1.0 ^a	2.2E-03 ^a	3.4E-05 ^a	0.7	0.978
				13	0.5 × C ^a	0.5 ^a	9.8E-04 ^a	1.5E-05 ^a	1.5	0.981
	Column 4 (ZVI + BC)	1	2	25	2.4E+01 ^b	2.4E+01 ^b	5.2E-02 ^b	8.0E-04 ^b	2.2	0.983
				53	2.6 ^b	2.6 ^b	5.6E-03 ^b	8.6E-05 ^b	21	0.828
				1	3.4E+01 ^b	3.4E+01 ^b	3.0E-02 ^b	8.9E-04 ^b	1.3	0.969
	Column 4 (ZVI + BC)	1	2	13	1.4E+01 ^b	1.4E+01 ^b	1.2E-02 ^b	3.6E-04 ^b	3.1	0.960
				25	1.1E+01 ^b	1.1E+01 ^b	9.4E-03 ^b	2.8E-04 ^b	4.9	0.845
				53	2.1 ^b	2.1 ^b	1.9E-03 ^b	5.6E-05 ^b	25	0.701

^a Removal of SAC followed a first order reaction rate, unit of k_{obs} is d⁻¹, unit of k_M is L g⁻¹ d⁻¹, unit of k_{SA} is L m⁻² d⁻¹.

^b Removal of SAC followed a zero order reaction rate, unit of k is μmol SAC L⁻¹ d⁻¹ (μg SAC L⁻¹ d⁻¹), unit of k_M is μmol SAC d⁻¹ g (reactive media)⁻¹ [μg SAC d⁻¹ g (reactive media)⁻¹], unit of k_{SA} is μmol SAC d⁻¹ m⁻² (μg SAC d⁻¹ m⁻²).

K_M and K_{SA} were calculated following the expression $K_M = K_{obs}/\rho_m$; $K_{SA} = K_{obs}/\rho_a = K_M/a_s$ (Johnson et al., 1996). ρ_m is the mass concentrations of reactive media (g L⁻¹ of solution). ρ_a is the surface area concentrations of reactive media (m² L⁻¹ of solution). a_s is the specific surface area of reactive media (m² g⁻¹). Specific surface areas of ZVI, BC, and (ZVI + BC) are 9.5, 64.5, and 33.6 m² g⁻¹.

Table D.12 Removal rate constant k_{obs} , mass normalized rate constant k_M , and surface area normalized rate constant k_{SA} of sucralose. Removal rate constant k_{obs} is calculated using least-squares regression during two experimental stages. 1C is the input contaminant concentration. “–” represents no removal of contaminant was observed.

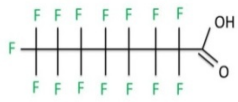
Contaminant (CAS#), pKa, log Kow, and structure	Column	Stage	PV	Removal rate [†] , $\mu\text{mol L}^{-1} \text{d}^{-1}$ ($\mu\text{g L}^{-1} \text{d}^{-1}$)	k_{obs}	k_M	k_{SA}	Half-life, d	R ²	
Sucralose (SCL) (56038-13-2) pKa=11.8, log K _{ow} = -1.0 	Column 2 (ZVI)	1	1	$2.1 \times C^a$	2.1 ^a	4.8E-04 ^a	5.1E-05 ^a	0.3	0.922	
			13	$1.0 \times C^a$	1.0 ^a	2.4E-04 ^a	2.5E-05 ^a	0.7	0.927	
			25	$4.4\text{E}+01^b$	$4.4\text{E}+01^b$	1.0E-02 ^b	1.1E-03 ^b	1.4	0.963	
		2	53	1	$1.3 \times C^a$	1.3 ^a	2.7E-03 ^a	4.2E-05 ^a	0.5	0.999
				13	$0.9 \times C^a$	0.9 ^a	1.9E-03 ^a	2.9E-05 ^a	0.8	0.983
				25	$0.7 \times C^a$	0.7 ^a	1.4E-03 ^a	2.2E-05 ^a	1.1	0.983
	Column 3 (BC)	1	13	1	$1.3 \times C^a$	1.3 ^a	2.7E-03 ^a	4.2E-05 ^a	0.5	0.999
				25	$0.7 \times C^a$	0.7 ^a	1.4E-03 ^a	2.2E-05 ^a	1.1	0.983
				53	$0.2 \times C^a$	0.2 ^a	4.3E-04 ^a	6.6E-06 ^a	3.5	0.981
		2	53	1	$1.6 \times C^a$	1.6 ^a	1.4E-03 ^a	4.2E-05 ^a	0.4	0.948
				13	$0.9 \times C^a$	0.9 ^a	8.1E-04 ^a	2.4E-05 ^a	0.8	0.961
				25	$0.7 \times C^a$	0.7 ^a	6.4E-04 ^a	1.9E-05 ^a	1.0	0.942
Column 4 (ZVI + BC)	1	13	1	$1.6 \times C^a$	1.6 ^a	1.4E-03 ^a	4.2E-05 ^a	0.4	0.948	
			25	$0.7 \times C^a$	0.7 ^a	6.4E-04 ^a	1.9E-05 ^a	1.0	0.942	
			53	$0.2 \times C^a$	0.2 ^a	1.6E-04 ^a	4.7E-06 ^a	3.9	0.995	

^a Removal of SCL followed a first order reaction rate, unit of k_{obs} is d^{-1} , unit of k_M is $\text{L g}^{-1} \text{d}^{-1}$, unit of k_{SA} is $\text{L m}^{-2} \text{d}^{-1}$.

^b Removal of SCL followed a zero order reaction rate, unit of k is $\mu\text{mol SCL L}^{-1} \text{d}^{-1}$ ($\mu\text{g SCL L}^{-1} \text{d}^{-1}$), unit of k_M is $\mu\text{mol SCL d}^{-1} \text{g}$ (reactive media)⁻¹ [$\mu\text{g SCL d}^{-1} \text{g}$ (reactive media)⁻¹], unit of k_{SA} is $\mu\text{mol SCL d}^{-1} \text{m}^{-2}$ ($\mu\text{g SCL d}^{-1} \text{m}^{-2}$).

K_M and K_{SA} were calculated following the expression $K_M = K_{obs}/\rho_m$; $K_{SA} = K_{obs}/\rho_a = K_M/a_s$ (Johnson et al., 1996). ρ_m is the mass concentrations of reactive media (g L^{-1} of solution). ρ_a is the surface area concentrations of reactive media ($\text{m}^2 \text{L}^{-1}$ of solution). a_s is the specific surface area of reactive media ($\text{m}^2 \text{g}^{-1}$). Specific surface areas of ZVI, BC, and (ZVI + BC) are 9.5, 64.5, and 33.6 $\text{m}^2 \text{g}^{-1}$.

Table D.13 Removal rate constant k_{obs} , mass normalized rate constant k_M , and surface area normalized rate constant k_{SA} of perfluorooctanoic acid (PFOA). Removal rate constant k_{obs} is calculated using least-squares regression during two experimental stages. ¹C is the input contaminant concentration. “–” represents no removal of contaminant was observed.

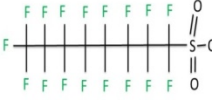
Contaminant (CAS#), pKa, log Kow, and structure	Column	Stage	PV	Removal rate ¹ , $\mu\text{mol L}^{-1} \text{d}^{-1}$ ($\mu\text{g L}^{-1} \text{d}^{-1}$)	k_{obs}	k_M	k_{SA}	Half- life, d	R ²		
Perfluorooctanoic acid (PFOA) (335-67-1), pKa=0.5, log Kow=5.11 	Column 2 (ZVI)	1	1	2.2E+01 ^b	2.2E+01 ^b	5.2E-03 ^b	5.5E-04 ^b	1.3	0.821		
			13	–	–	–	–	–	–		
			25	–	–	–	–	–	–		
		2	53	–	–	–	–	–	–	–	
			Column 3 (BC)	1	1	1.0 × C ^a	1.0 ^a	2.1E-03 ^a	3.3E-05 ^a	0.7	0.980
					13	0.5 × C ^a	0.5 ^a	1.1E-03 ^a	1.8E-05 ^a	1.3	0.987
	25	1.2E+01 ^b			1.2E+01 ^b	2.5E-02 ^b	3.9E-04 ^b	2.3	0.956		
	2	53		0.9 ^b	0.9 ^b	1.9E-03 ^b	3.0E-05 ^b	25	0.780		
		Column 4 (ZVI + BC)		1	1	2.0E+01 ^b	2.0E+01 ^b	1.8E-02 ^b	5.3E-04 ^b	1.3	0.935
					13	7.7 ^b	7.7 ^b	6.7E-03 ^b	2.0E-04 ^b	3.3	0.933
	25		2.0 ^b		2.0 ^b	1.7E-03 ^b	5.1E-05 ^b	13	0.725		
	2		53	–	–	–	–	–	–		

^a Removal of PFOA followed a first order reaction rate, unit of k_{obs} is d^{-1} , unit of k_M is $\text{L g}^{-1} \text{d}^{-1}$, unit of k_{SA} is $\text{L m}^{-2} \text{d}^{-1}$.

^b Removal of PFOA followed a zero order reaction rate, unit of k is $\mu\text{mol PFOA L}^{-1} \text{d}^{-1}$ ($\mu\text{g PFOA L}^{-1} \text{d}^{-1}$), unit of k_M is $\mu\text{mol PFOA d}^{-1} \text{g (reactive media)}^{-1}$ [$\mu\text{g PFOA d}^{-1} \text{g (reactive media)}^{-1}$], unit of k_{SA} is $\mu\text{mol PFOA d}^{-1} \text{m}^{-2}$ ($\mu\text{g PFOA d}^{-1} \text{m}^{-2}$).

K_M and K_{SA} were calculated following the expression $K_M = K_{obs}/\rho_m$; $K_{SA} = K_{obs}/\rho_a = K_M/a_s$ (Johnson et al., 1996). ρ_m is the mass concentrations of reactive media (g L^{-1} of solution). ρ_a is the surface area concentrations of reactive media ($\text{m}^2 \text{L}^{-1}$ of solution). a_s is the specific surface area of reactive media ($\text{m}^2 \text{g}^{-1}$). Specific surface areas of ZVI, BC, and (ZVI + BC) are 9.5, 64.5, and 33.6 $\text{m}^2 \text{g}^{-1}$.

Table D.14 Removal rate constant k_{obs} , mass normalized rate constant k_M , and surface area normalized rate constant k_{SA} of perfluorooctane sulfonic acid (PFOS). Removal rate constant k_{obs} is calculated using least-squares regression during two experimental stages. 1C is the input contaminant concentration. “–” represents no removal of contaminant was observed.

Contaminant (CAS#), pKa, log Kow, and structure	Column	Stage	PV	Removal rate [†] , $\mu\text{mol L}^{-1} \text{d}^{-1}$ ($\mu\text{g L}^{-1} \text{d}^{-1}$)	k_{obs}	k_M	k_{SA}	Half- life, d	R ²		
Perfluorooctane sulfonic acid (PFOS) (2795-39-3), pKa= -2.3, log K_{ow} =5.41 	Column 2 (ZVI)	1	1	$2.0 \times C^a$	2.0^a	$4.6\text{E-}04^a$	$4.9\text{E-}05^a$	0.4	0.911		
			13	$0.9 \times C^a$	0.9^a	$2.1\text{E-}04^a$	$2.3\text{E-}05^a$	0.8	0.834		
			25	$2.2\text{E+}01^b$	$2.2\text{E+}01^b$	$5.1\text{E-}03^b$	$5.4\text{E-}04^b$	1.5	0.929		
		2	53	2.6^b	2.6^b	$6.2\text{E-}04^b$	$6.5\text{E-}05^b$	16	0.734		
			Column 3 (BC)	1	1	$1.8 \times C^a$	1.8^a	$3.9\text{E-}03^a$	$6.0\text{E-}05^a$	0.4	0.989
					13	$0.5 \times C^a$	0.5^a	$1.2\text{E-}03^a$	$1.8\text{E-}05^a$	1.3	0.511
	Column 4 (ZVI + BC)	1	13	25	$0.9 \times C^a$	0.9^a	$1.8\text{E-}03^a$	$2.8\text{E-}05^a$	0.8	0.961	
				2	53	$0.2 \times C^a$	0.2^a	$4.6\text{E-}04^a$	$7.2\text{E-}06^a$	3.2	0.967
				2	53	1	$2.2 \times C^a$	2.2^a	$1.9\text{E-}03^a$	$5.7\text{E-}05^a$	0.3
		13	$0.7 \times C^a$			0.7^a	$5.8\text{E-}04^a$	$1.7\text{E-}05^a$	1.1	0.881	
		2	53	25	$1.1 \times C^a$	1.1^a	$9.6\text{E-}04^a$	$2.9\text{E-}05^a$	0.6	0.962	
				7.0 ^b	$7.0\text{E+}01^b$	$6.1\text{E-}03^b$	$1.8\text{E-}04^b$	5.9	0.966		

^a Removal of PFOS followed a first order reaction rate, unit of k_{obs} is d^{-1} , unit of k_M is $\text{L g}^{-1} \text{d}^{-1}$, unit of k_{SA} is $\text{L m}^{-2} \text{d}^{-1}$.

^b Removal of PFOS followed a zero order reaction rate, unit of k is $\mu\text{mol PFOS L}^{-1} \text{d}^{-1}$ ($\mu\text{g PFOS L}^{-1} \text{d}^{-1}$), unit of k_M is $\mu\text{mol PFOS d}^{-1} \text{g}$ (reactive media)⁻¹ [$\mu\text{g PFOS d}^{-1} \text{g}$ (reactive media)⁻¹], unit of k_{SA} is $\mu\text{mol PFOS d}^{-1} \text{m}^{-2}$ ($\mu\text{g PFOS d}^{-1} \text{m}^{-2}$).

K_M and K_{SA} were calculated following the expression $K_M = K_{obs}/\rho_m$; $K_{SA} = K_{obs}/\rho_a = K_M/a_s$ (Johnson et al., 1996). ρ_m is the mass concentrations of reactive media (g L^{-1} of solution). ρ_a is the surface area concentrations of reactive media ($\text{m}^2 \text{L}^{-1}$ of solution). a_s is the specific surface area of reactive media ($\text{m}^2 \text{g}^{-1}$). Specific surface areas of ZVI, BC, and (ZVI + BC) are 9.5, 64.5, and 33.6 $\text{m}^2 \text{g}^{-1}$.

Appendix E: *Supplementary Information in*
Chapter 6

Table E.1 Concentrations of F⁻ and acetate in treatment samples (PFOA+ ZVI, Day 90; PFOA+ ZVI, Day 120; PFOS+ ZVI, Day 90; PFOS+ ZVI, Day 120) and recoveries of F⁻ and acetate in the same sample fortified with F⁻ and acetate. Each sample was fortified with either 0.1mg L⁻¹ F⁻ or 1mg L⁻¹ acetate or both of 0.1mg L⁻¹ F⁻ and 1mg L⁻¹ acetate. The IC chromatograms for the detection of fluoride (F⁻) ions are presented in Figures E.1 – E.4. “–” indicates the samples were not available or analyzed.

Sample name	Con. of F ⁻ , mg L ⁻¹	Con. of acetate, mg L ⁻¹	Recovery of fortified F ⁻ , %	Recovery of fortified acetate, %
PFOA + ZVI, Day 90	0.14	0.91	–	–
PFOA + ZVI, Day 90_fortified with F ⁻	0.23	0.90	0.86	–
PFOA + ZVI, Day 90_fortified with acetate	0.13	1.71	–	0.79
PFOA + ZVI, Day 90_fortified with F ⁻ and acetate	0.22	1.76	0.80	0.85
PFOA + ZVI, Day 120	0.14	1.35	–	–
PFOA + ZVI, Day 120_fortified with F ⁻	0.22	1.26	0.79	–
PFOA + ZVI, Day 120_fortified with acetate	0.15	2.26	–	0.91
PFOA + ZVI, Day 120_fortified with F ⁻ and acetate	0.22	2.20	0.79	0.86
PFOS + ZVI, Day 90	0.06	1.38	–	–
PFOS + ZVI, Day 90_fortified with F ⁻	0.13	1.22	0.75	–
PFOS + ZVI, Day 90_fortified with acetate	0.05	2.04	–	0.76
PFOS + ZVI, Day 90_fortified with F ⁻ and acetate	0.14	2.11	0.83	0.73
PFOS + ZVI, Day 120	0.06	1.49	–	–
PFOS + ZVI, Day 120_fortified with F ⁻	0.15	1.54	0.83	–
PFOS + ZVI, Day 120_fortified with acetate	0.06	2.50	–	1.01
PFOS + ZVI, Day 120_fortified with F ⁻ and acetate	0.14	2.28	0.73	0.79

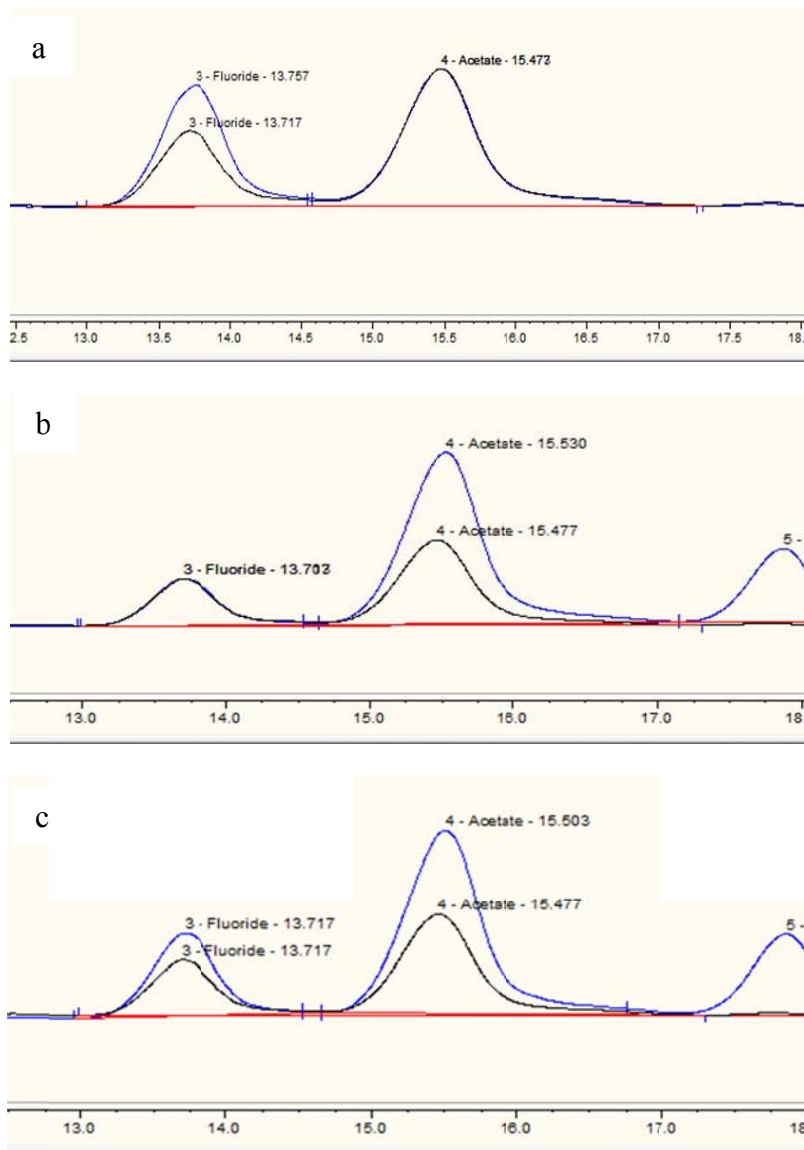


Figure E.1 IC chromatograms for the detection of fluoride (F^-) ions ($T_R = 13.70\text{--}13.76$ min) in treatment samples (PFOA + ZVI, Day 90): a) straight sample fortified with $0.1\text{ mg L}^{-1} F^-$; b) straight sample fortified with 1 mg L^{-1} acetate ($T_R = 15.48\text{--}15.53$ min); c) straight sample fortified with both $0.1\text{ mg L}^{-1} F^-$ and 1 mg L^{-1} acetate.

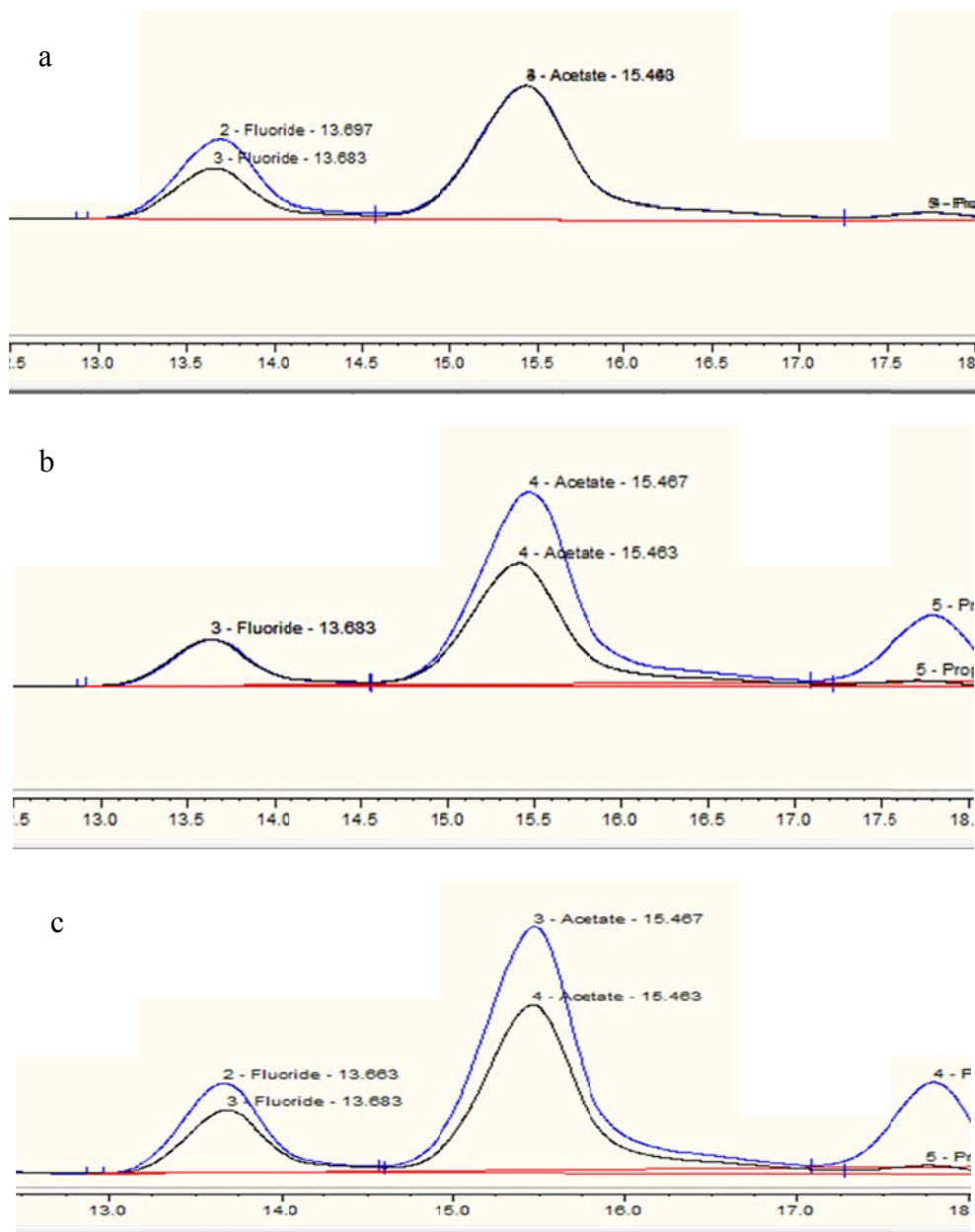


Figure E.2 IC chromatograms for the detection of fluoride (F^-) ions ($T_R = 13.66\text{--}13.70$ min) in treatment samples (PFOA + ZVI, Day 120): a) straight sample fortified with $0.1\text{ mg L}^{-1} F^-$; b) straight sample fortified with 1 mg L^{-1} acetate ($T_R = 15.46\text{--}15.47$ min); c) straight sample fortified with both $0.1\text{ mg L}^{-1} F^-$ and 1 mg L^{-1} acetate.

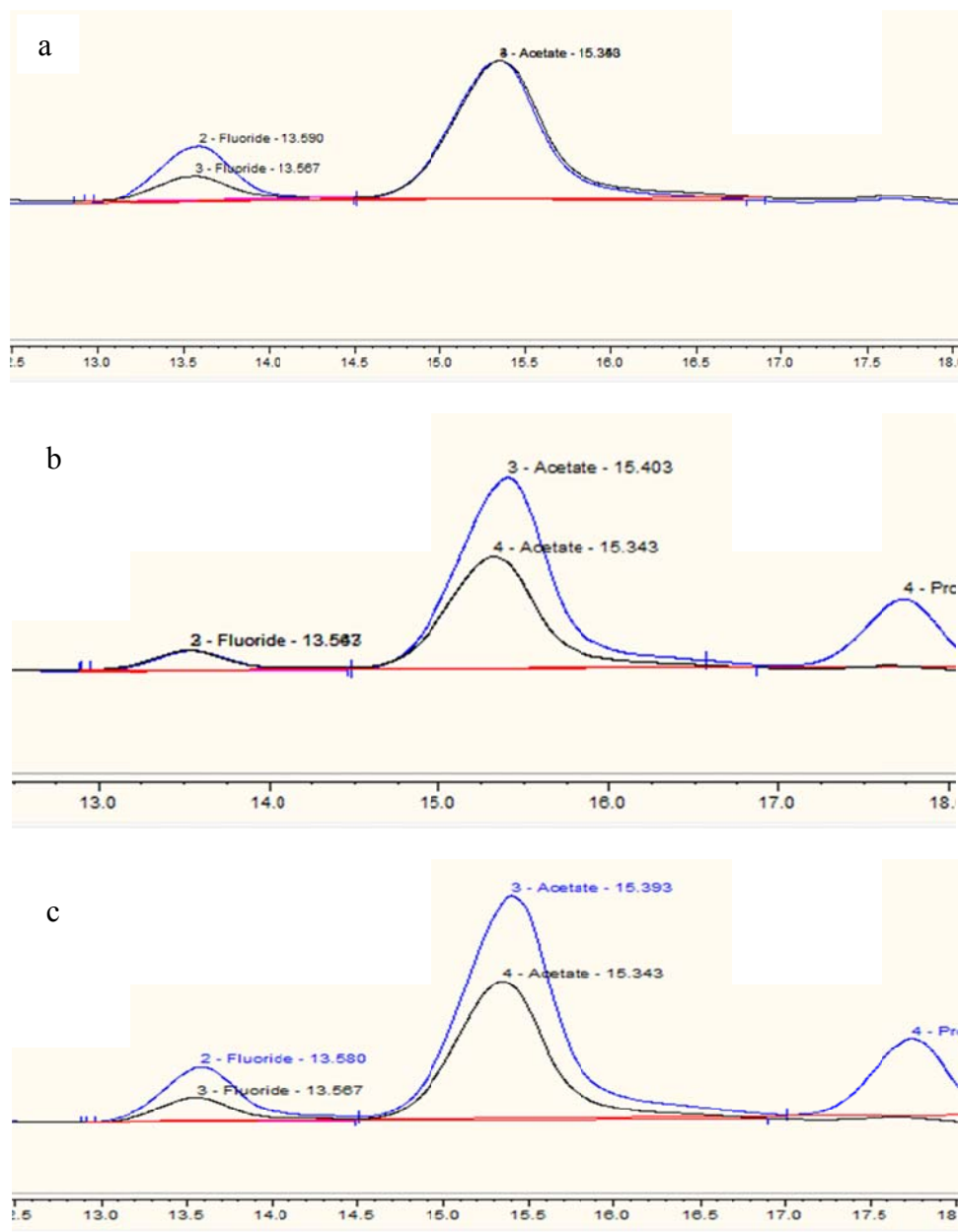


Figure E.3 IC chromatograms for the detection of fluoride (F^-) ions ($T_R = 13.54\text{--}13.59$ min) in treatment samples (PFOS + ZVI, Day 90): a) straight sample fortified with $0.1\text{ mg L}^{-1} F^-$; b) straight sample fortified with 1 mg L^{-1} acetate ($T_R = 15.34\text{--}15.40$ min); c) straight sample fortified with both $0.1\text{ mg L}^{-1} F^-$ and 1 mg L^{-1} acetate.

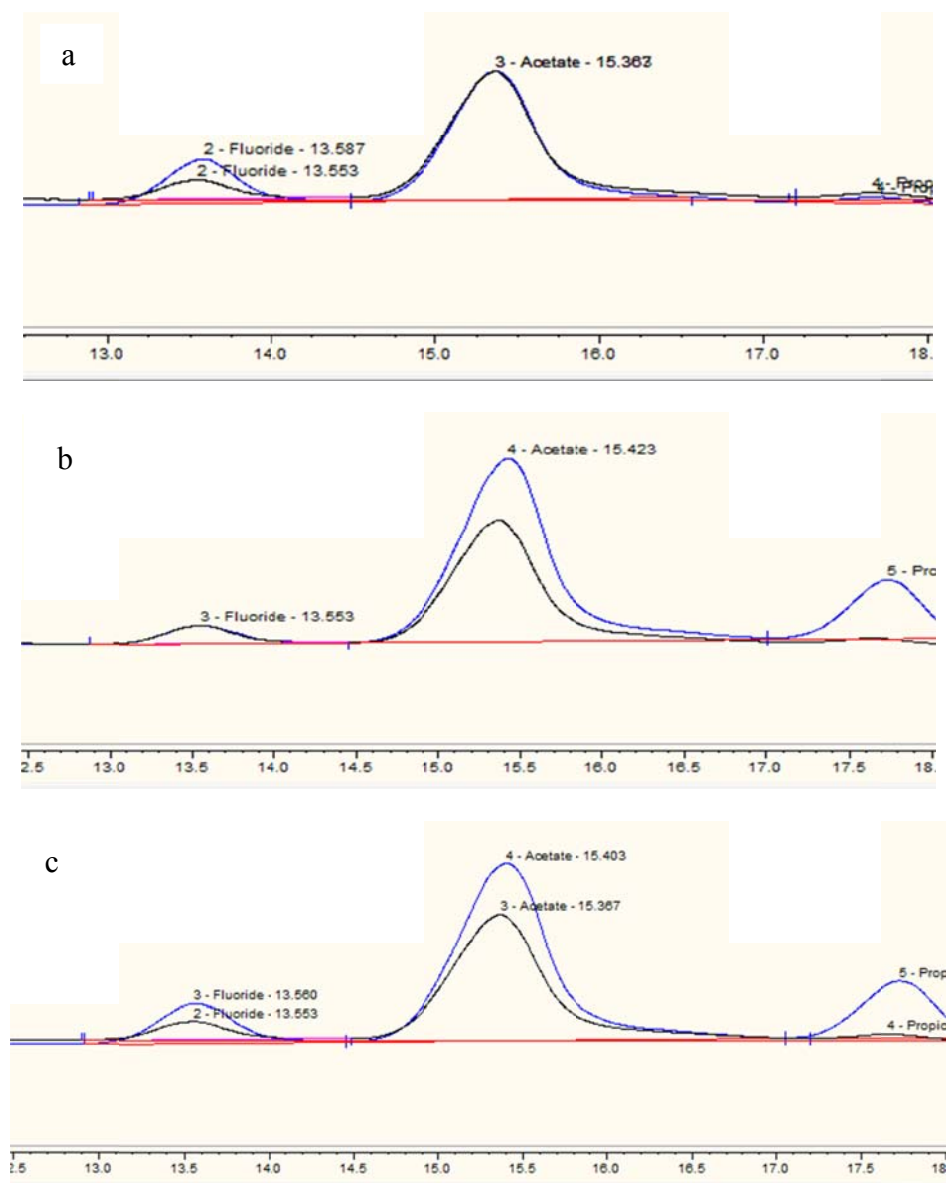


Figure E.4 IC chromatograms for the detection of fluoride (F^-) ions ($T_R = 13.55\text{--}13.58$ min) in treatment samples (PFOS + ZVI, Day 120): a) straight sample fortified with $0.1\text{ mg L}^{-1} F^-$; b) straight sample fortified with 1 mg L^{-1} acetate ($T_R = 15.36\text{--}15.42\text{min}$); c) straight sample fortified with both $0.1\text{ mg L}^{-1} F^-$ and 1 mg L^{-1} acetate.